SEDIMENTARY MODELLING AND PETROPHYSICAL CHARACTERISATION OF A PERMIAN DELTAIC SEQUENCE (*KOOKFONTEIN FORMATION*), TANQUA DEPOCENTRE, SW KAROO BASIN, SOUTH AFRICA

by

Wasiu Adedayo SONIBARE

Thesis submitted in partial fulfilment of the requirements for the degree of Master of Science in the Department of Earth Sciences, University of Stellenbosch

December 2011

STUDY LEADER: Dr Daniel MIKEŠ

DECLARATION

I, the undersigned, do solemnly declare that this thesis is my own original work and that I have not previously in its entirety or in part submitted it at any university for a degree or examination. Where use was made of the work of others it has been acknowledged properly in the text.

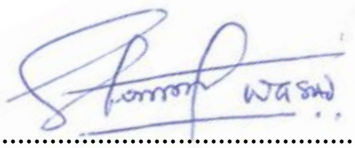

Signature: ..... Dated: 2nd February, 2011

Wasiu Adedayo SONIBARE

ABSTRACT

This study presents an outcrop characterisation and modelling of the excellently exposed Permian Kookfontein Formation of the Ecca Group in the Tanqua-Karoo sub-Basin. The sedimentary modelling (i.e. facies architecture and geometry) and petrophysical characterisation followed a hierarchical and deterministic approach. Quantitative outcrop data were based on the thirteen sedimentary cycles that characterise this stratigraphic succession at the Pienaarsfontein se Berg locality; and these data were analysed using a combination of detailed sedimentary log, gamma ray log and photopanel analysis, as well as petrographic thin-section and grain size-based petrophysical analysis.

Based on texture and sedimentary structures, twelve depofacies are recognised which are broadly grouped into four lithofacies associations i.e. sandstone facies, heterolithic facies, mudstone facies and soft-sediment deformation facies; these depofacies and lithofacies form the basic building blocks for the flooding surface-bounded facies succession (i.e. cycle). Also, based on sediment stacking and cycle thickness patterns as well as relative position to the shelf break, the succession is sub-divided into: (1) the lower Kookfontein member (i.e. cycles 1 to 5) exhibiting overall upward thickening and coarsening succession with progradational stacking pattern; representing deposition of mid-slope to top-slope/shelf-margin succession, and (2) the upper Kookfontein member (i.e. cycles 6 to 13) exhibiting overall upward thickening and coarsening succession with aggradational stacking pattern; representing deposition of top-slope/shelf-margin to outer shelf succession. Lateral juxtaposition of observed vertical facies variations across each cycle in an inferably basinwards direction exhibits upward change in features, i.e. decrease in gravity effects, increase in waves and decrease in slope gradient of subsequent cycles. This systematic upward transition in features, grading vertically from distal to proximal, with an overall upward thickening and coarsening progradational to aggradational stacking pattern indicates a normal regressive prograding delta. However, in detail, cycles 1-3 show some anomalies from a purely thickening and coarsening upward succession.

Deposition of each cycle is believed to result from: (1) primary deposition by periodic and probably sporadic mouthbar events governed by stream flow dynamics, and (2) secondary remobilisation of sediments under gravity. The facies distribution, architecture and geometry which governs the sedimentary heterogeneity within the deltaic succession is therefore mainly a consequence of the series of mouthbar flooding events governed by sediment supply and base-level changes. These series of flooding events resulted in the

delineation of the studied stratigraphic interval into two main parasequence sets, i.e. transgressive sequence set and the overlying regressive sequence set. This delineation was aided through the identification of a maximum flooding surface (i.e. maximum landwards shift in facies) above Cycle 3 in the field. The architecture and geometry of the ensuing depo-system is interpreted to have been a river-dominated, gravitationally reworked and wave-influenced shelf edge Gilbert-type delta. Widespread distribution of soft-sediment deformation structures, their growth-style and morphology within the studied succession are empirically related to progradation of Gilbert-type mouthbars over the shelf break as well as the slope gradients of the Kookfontein deltaic clinoformal geometry. Analysis of hypothetical facies stacking and geometrical models suggests that the Kookfontein sedimentary cyclicity might not be accommodation-driven but rather sediment supply-driven.

The workflow employed for petrophysical evaluation reveals that the distribution of reservoir properties within the Kookfontein deltaic sandbody geometries is strongly influenced both by depositional processes and by diagenetic factors, the latter being more important with increased burial depth. The reservoir quality of the studied sandstones decreases from proximal mouthbar sands, intermediate delta front to distal delta front facies. The major diagenetic factors influencing the reservoir quality of the studied sandstones are mechanical compaction, chemical compaction (pressure solution) and authigenic pore-filling cements (quartz cement, feldspar alteration and replacement, calcite cement, chlorite and illite). Mechanical compaction was a significant porosity reducing agent while cementation by authigenic quartz and clay minerals (i.e. illite and chlorite) might play a major role in permeability distribution. The porosity-permeability relationship trends obtained for the studied sandstones show that there is a linear relationship between porosity and permeability. The relative timing of diagenetic events as well as the percentages of porosity reduction by compaction and cementation indicates that compaction is much more responsible for porosity reduction than cementation.

The described internal heterogeneity in this work is below the resolution (i.e. mm-scale) of most conventional well-logs, and therefore could supplement well-log data especially where there is no borehole image and core data. The combination of ‘descriptive’ facies model and schematic geological model for this specific delta, and petrophysical characterisation make the results of this study applicable to any other similar ancient depo-system and particularly subsurface reservoir analogue.

OPSOMMING

Hierdie studie bied ’n dagsoomkarakterisering en -modellering van die duidelik blootgelegde Permiese Kookfontein-formasie van die Ecca-groep in die Tankwa-Karoo-subkom. Wat die sedimentêre modellering (d.w.s. fasiesargitektuur en -geometrie) en petrofisiese karakterisering betref is ’n hiërargiese en deterministiese benadering gevolg. Kwantitatiewe dagsoomdata is gebaseer op dertien sedimentêre siklusse wat hierdie stratigrafiese opeenvolging in die Pienaarsfontein se Berg-lokaliteit kenmerk; en die data is geanaliseer met behulp van ’n kombinasie van gedetailleerde sedimentêre seksie, gammastraal-profiel en fotopaneelanalises, asook petrografiese slypplaatjie- en korrelgrootte-gebaseerde petrofisiese analises.

Op grond van tekstuur en sedimentêre strukture is twaalf afsettingsfasies onderskei wat rofweg in vier assosiasies van litofasies gegroepeer kan word: sandsteenfasies, heterolitiese fasies, moddersteenfasies en sagtesediment-deformasiefasies. Hierdie afsettingsfasies en litofasies vorm die basiese boustene vir die fasiesopeenvolging (d.w.s. siklus) wat oorstromingsoppervlakgebonde is. Verder word die opeenvolging aan die hand van sedimentstapeling en skilusdiktepatrone, asook relatiewe posisie tot die rakbreuk, in die volgende onderverdeel: (1) die benede-Kookfontein-deel (d.w.s. siklus 1 tot 5), wat in die geheel ’n opwaartse verdikkings- en vergrowwingsopeenvolging met ’n progradasiestapelpatroon vertoon en die afsetting van middelhelling-tot-boonstehelling- of rakrand-opeenvolging verteenwoordig, en (2) die benede-Kookfontein-deel (d.w.s. siklus 6 tot 13) wat in die geheel ’n opwaartse verdikkings- en vergrowwingsopeenvolging met ’n aggradasiestapelpatroon vertoon en die afsetting van boonste helling- of rakrand-tot-buiterak-opeenvolging verteenwoordig. Die laterale jukstaposisie van waargenome vertikale fasiesvariasies oor elke siklus heen, in ’n afleibare komwaartse rigting, vertoon opwaartse verandering wat kenmerke betref, naamlik afname in gravitasiegevolge, toename in golwe en afname in die hellinggradiënt van daaropvolgende siklusse. Hierdie stelselmatige opwaartse oorgang van kenmerke, wat vertikaal van distaal tot proksimaal gradiënteer en in die geheel opwaartse verdikking en vergrowwing in ’n progradasie-tot-aggradasie-stapelpatroon vertoon, dui op ’n normale regressiewe progradasiedelta. Van naby beskou, vertoon siklus 1-3 egter bepaalde afwykings van ’n suiwer opwaartse verdikkings- en vergrowwingsopeenvolging.

Die afsettings van elke siklus is vermoedelik die gevolg van: (1) primêre afsetting deur periodieke en waarskynlik sporadiese mondversperringsgebeure wat deur stroomvloeidinamika beheer word, en (2) sekondêre hermobilisering van sedimente deur

gravitasie. Die fasiesverspreiding, -argitektuur en -geometrie wat die sedimentêre heterogeniteit in die deltaïese opeenvolging beheer, is dus hoofsaaklik ’n gevolg van die reeks oorstromingsgebeure by die mondversperring, wat deur sedimentvoorsiening en basisvlakveranderings beheer word. Hierdie reeks oorstromingsgebeure het gelei tot die delineasie van die bestudeerde stratigrafiese interval volgens twee hoofparasekwensie stelle, naamlik die transgressiewe opeenvolgings- en die oordekkende, regressiewe opeenvolgingsgroep. Dié delineasie word ondersteun deur die feit dat ’n maksimum oorstromingsoppervlak (d.w.s. maksimum landwaartse verskuiwing in fasies) bo siklus 3 in die veld uitgeken is. Die argitektuur en geometrie van die daaropvolgende afsettingstelsel word geïnterpreteer as behorende tot ’n Gilbert-rakranddelta wat deur ’n rivier gedomineer, deur gravitasie herbewerk en deur golfwerking beïnvloed is. Die wye verspreiding van sagtesediment-deformasiestrukture, en die groeiwyse en morfologie daarvan binne die bestudeerde opeenvolging, is empiries verwant aan die progradasie van Gilbert-mondversperrings oor die rakbreuk heen, asook aan die hellinggradiënte van die Kookfontein- deltaïese, klinoformele geometrie. Die analise van hipotetiese fasiesstapeling en geometriese modelle dui daarop dat die Kookfontein- sedimentêre siklisiteit dalk nie deur akkommodasieruimte gedryf word nie, maar deur sedimentvoorsiening.

Die werkvloei wat vir petrofisiese evaluering gebruik is dui daarop dat die verspreiding van reservoir-eienskappe in die Kookfontein- deltaïese sandliggaam geometries sterk beïnvloed word deur afsettingsprosesse en diagenetiese faktore. Die diagenetiese faktore word belangriker op groter begrawing diepte. Die reservoir-aard van die bestudeerde sandgesteentes neem algaande af van proksimale mondversperring-sandsoorte tot intermediêre deltafront tot distale deltafrontfasies. Die hoof- diagenetiese faktore wat die reservoir-kenmerke van die bestudeerde sandsteensoorte beïnvloed is meganiese verdigting, chemiese verdigting (oplossingsdruk) en outigeniese porievullingsement (kwartssement, veldspaatomsetting en -vervanging, kalsietsement, chloriet en illiet). Meganiese verdigting is ’n beduidende poreusheidreduseermiddel, terwyl sementering deur outigeniese kwarts- en kleiminerale (d.w.s. illiet en chloriet) moontlik ’n belangrike rol by permeabiliteitsverspreiding kan speel. Die poreusheid-permeabiliteit-verhoudingstendense wat bekom is vir die bestudeerde sandsteensoorte dui daarop dat daar ’n lineêre verhouding tussen poreusheid en permeabiliteit bestaan. Die relatiewe tydberekening van diagenetiese gebeure, asook die persentasie poreusheidvermindering deur verdigting en sementering, dui daarop dat verdigting baie meer as sementering tot poreusheidvermindering bydra.

Die interne heterogeniteit wat in hierdie werk beskryf word, is onder die resolusie (d.w.s. mm-skaal) van die meeste konvensionele boorgatopnames, en kan dus boorgatopnamedata aanvul, veral waar daar geen boorgatafbeelding en kerndata bestaan nie. Die kombinasie van die ‘deskriptiewe’ fasiesmodel en skematiese geologiese model vir hierdie spesifieke delta, asook petrofisiese karakterisering, beteken dat die resultate van hierdie studie op enige ander soortgelyke antieke afsettingstelsels toegepas kan word, maar veral op suboppervlakreservoir-analoogstelsels.

ACKNOWLEDGEMENTS

Firstly, I would like to thank my supervisor Dr Daniel Mikeš, who painstakingly supervised this work, offered useful suggestions and made relentless effort which contributed in no small way to the timely and successful completion of this project. Once again, thank you for your mentorship, support, guidance and encouragement at every stage of my academic and research pursuit at the "*Matieland"*.

My sincere thanks are due to the Inkaba yeAfrica Phase II Project for providing the full financial support for this research project.

Thank you also to the teaching and administrative staff at the Department of Earth Sciences, University of Stellenbosch for technical and logistical supports.

Thank you to my Karoo project colleagues at the Department of Earth Sciences, University of Stellenbosch (Bose, Malikah, Alfred, Andy, Renitia and Donovan) for helpful academic and non-academic discussions. Thank you Alfred for many hours in the field under Pienaarsfontein cold falls of rain measuring and describing sedimentary features despite your background being geophysics. Your support and understanding during the fieldwork for this project is highly appreciated.

I would also like to thank my parents and family for their kindness, prayers and moral support since 2009 that I embarked on academic sojourn outside the shore of my home country, Nigeria. Special thanks are due to my beloved mother Abisat Titilayo Sonibare and my eldest brother Engr. Abdul-Aziz to whom I dedicate this thesis. Thank you so much Zainab for your love, care, prayers, friendship and understanding.

Finally and above all, I am humbly grateful to my creator- Almighty Allah, for all His bountiful grace and blessings over me. I acknowledge Your aid, Oh God!! Without Your guidance and love, this humble contribution would not have been possible.

TABLE OF CONTENTS

LIST OF FIGURES

CHAPTER TWO

CHAPTER THREE

CHAPTER FOUR

CHAPTER FIVE

LIST OF TABLES

CHAPTER ONE

INTRODUCTION

1.1 Background

1.1.1 Geological problem identification

In recent years, the use of three-dimensional digital geological models has become a widely accepted technique within the oil industry for characterising and managing subsurface hydrocarbon reservoirs, increasing recovery and optimizing drainage strategy (e.g. Matheron et al., 1987; Weber et al., 1991; Krum and Johnson, 1993; Deutsch, 1999; Dubrule and Damsleth, 2001; Labourdette et al., 2008). The modelling workflow generally involves: (1) the construction of a facies-dependent geological model that depicts facies architecture and geometry; (2) the transformation of the geological model into a reservoir model consisting of flow units which are sub-divided into grid blocks and grid cells; and (3) the population of those grid blocks and cells with petrophysical properties i.e. porosity, permeability and fluid saturation (e.g. Mikeš et al., 2006; Keogh et al., 2007; Yu et al., 2008; Cabello et al., 2010).

Reservoir characterisation was defined by Lake and Caroll (1986) as a "process for quantitatively assigning reservoir properties, recognising geological information and uncertainties in spatial variability". They argued that geo-statistics and stochastic (i.e. probabilistic) modelling provide the methods and tools to integrate all the available geological data from different sources and scales into a common and consistent framework and to generate multiple realisations that can account for the uncertainty and spatial variability of the key reservoir properties. The stochastic reservoir models are often based on sparse subsurface datasets with poor vertical and lateral resolution (Figure 1.1) (Flint and Bryant, 1993; Macdonald, 1995; Keogh et al., 2007). They also lack the ability to properly incorporate all scales of heterogeneity particularly small-scale heterogeneities (Mikeš and

Geel, 2006; Phillips and Wen, 2007). The ensuing models will come short in terms of realistic geological and sedimentological information. As such, it can be argued that central to the success of any reservoir management technique (be it net-to-gross reservoir estimation for resource evaluation or upscaling of petrophysical properties in a reservoir simulator to predict an oilfield-scale fluid flow behaviour) is the accurate construction of a facies-dependent geological model.

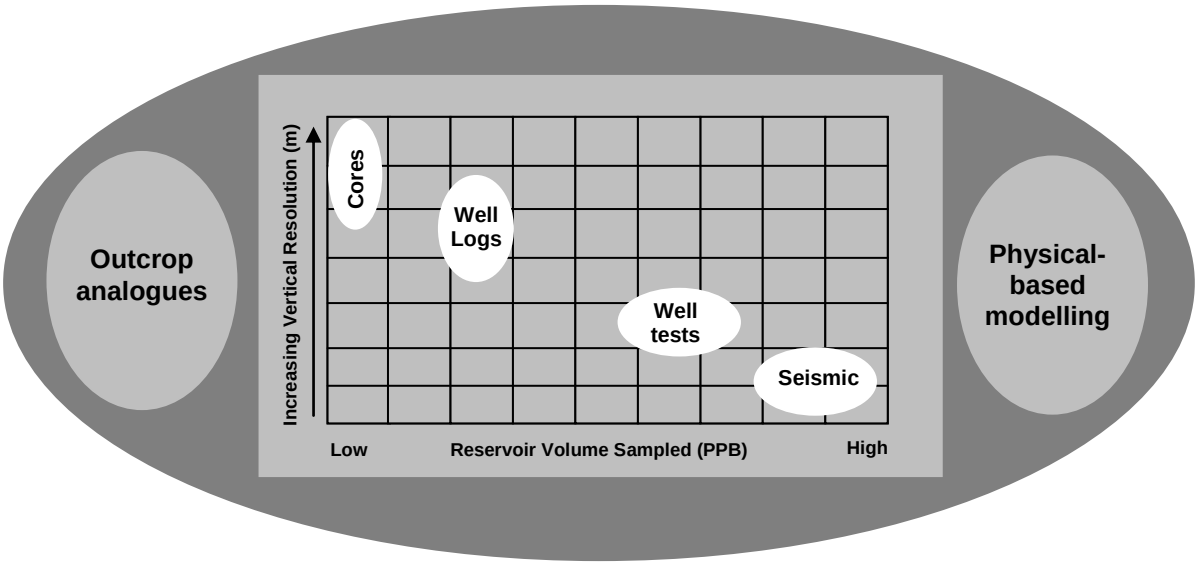

Figure 1.1. Chart showing the various subsurface data types that sample the reservoir volume plotted against the corresponding vertical resolution of the data type. Both outcrop analogue studies and physical-based modelling studies can help bridge the gaps between the different subsurface data types (adapted from Keogh et al., 2007).

Some previous reservoir characterisation studies (Kortekass, 1985; Honarpour et al., 1995; Mikeš and Geel, 2006; Phillips and Wen, 2007) have demonstrated the effect of small-scale heterogeneities (i.e. cross-bedding and laminae) on reservoir properties. These studies noted that modelling sedimentary deposits as totally homogenous bodies, with regards to both their sedimentological and structural heterogeneities is a gross simplification of their reservoir potential.

Phillips and Wen (2007) suggest that the incorporation of small-scale heterogeneities into reservoir modelling techniques will ensure a better facies-dependent distribution of porosity and permeability; thereby improving net-to-gross reservoir estimation. Moreover, Mikeš and Geel (2006) and Mikeš et al. (2006) also demonstrate the interdependence between porosity and permeability distribution i.e. inter- and intra- facies distribution and their three-dimensional temporal and spatial distribution. They propose a hierarchical-based geological modelling workflow with three-dimensional facies modelling as a critical point in the entire workflow in order to accurately predict facies geometries and their internal architecture.

Facies models incorporating the conceptual geological models are commonly built from traditional facies analysis on sediment-body geometries and sedimentary structures in outcrops (e.g. Flint and Bryant, 1993; Falivene et al., 2006; Cabello et al., 2010). Outcrop-based facies analysis has shown better spatial resolution because it gives adequate insights into process sedimentology and reveals three-dimensional control on facies geometry and architecture (e.g. Mayer and Chapin, 1991; Keogh et al., 2007; Catuneanu et al., 2009). Mayer and Chapin (1991) made a comparison of the reservoir properties and geological characteristics of sandstone bodies observed in outcrops and in cores from the Peoria Field in Colorado. They observed that outcrops were found to have grain sizes, sedimentary structures, and facies successions within channel deposits similar to those in the subsurface rocks in the

Peoria Field, and affirmed that these outcrop observations were useful in the construction of fluid flow models for the Peoria Field reservoir facies.

The characterisation and modelling of outcrop analogues allow: (1) the documentation of quantitative key reservoir parameters which can be applied to similar subsurface depositional setting (Mayer and Chapin, 1991; Satur et al., 2005; Cabello et al., 2010), (2) the testing and validation of subsurface facies-dependent geological modelling approaches (Falivene et al., 2006; Keogh et al., 2007), (3) better constraining of subsurface facies and reservoir modelling approaches so as to be more deterministic rather than entirely probabilistic and (4) reduction of uncertainties in predicting sand-body geometries, hence better and more accurate net-to-gross estimation and fluid flow prediction.

Within the oil industry and petroleum geosciences disciplines, the last two decades have witnessed the wide application of sequence stratigraphy for interpreting facies architecture and geometries of sand-body and intercalated shally baffles and barriers from data collected in outcrops, quarries and in densely drilled oilfields. The limitation of this method for proper three-dimensional process-sedimentological interpretation of most sedimentary depositional settings and its inability to be applicable in all sedimentary environments have resulted in its constructive criticism by some sedimentary stratigraphic workers (e.g. Martinsen and Helland-Hansen, 1996; Miall and Miall, 2001; Helland-Hansen and Hampson, 2009; Helland-Hansen, 2009). The recent modifications of the sequence stratigraphic workflow by the “sequence stratigraphy” school of thoughts (e.g. Catuneanu et al., 2009 and 2010) to include model-independent (i.e. a universal approach to the choice of terms for genetically related stratigraphic units and their bounding surfaces irrespective of depositional setting) and model-dependent (i.e. choice of sequence stratigraphic terms are specific to depositional setting) aspects is perhaps a commendable effort at finding a common point among differing

opinions as well as improving its applicability in constructing a geologically realistic reservoir model.

1.1.2 Upscaling: an integral part of reservoir modelling workflow

The large scale descriptive part of a routine reservoir modelling workflow is the construction of a detailed geological model that realistically distributes sedimentary facies both temporally and spatially within a depositional setting. Thus the ideal geological model represents a large-scale description of a hydrocarbon reservoir in three-dimensions honouring all scales of heterogeneity. The next step is the transformation of this geological model using sophisticated modelling software into a reservoir model that is compartmentalised into either flow units (i.e. facies scale) (e.g. Labourdette et al., 2008; Cabello et al., 2010) or flow units (i.e. facies scale) and flow cells (i.e. sub-facies/lamina scale) (Mikeš and Geel, 2006; Mikeš et al., 2006) consisting of geocellular grid blocks. These geocellular grid blocks in the reservoir model represent different facies associations with different petrophysical properties (i.e. porosity, permeability, pore geometry, pore size and pore throat, fluid saturation and sedimentological characteristics). As a result, the distribution of petrophysical properties in a reservoir is a reflection of the temporal and spatial facies distribution in the geological model. It is at this point that the method of constructing a facies-dependent geological model to capture all scales of sedimentary heterogeneity (Figure 1.2) becomes crucial to the success of any reservoir modelling approach.

In the last two decades, scaling-up or upscaling of petrophysical properties especially porosity and permeability fields from a geological model (i.e. consisting of fine-scale geocellular grids) into a commercial reservoir simulator (i.e. consisting of a fewer number of coarse-scale geocellular grids) to predict an oilfield-scale fluid flow behaviour has become an integral part of the routine reservoir modelling workflow. In general, a true representation of the oilfield-scale situation is the large scale geological model. But the limitation of the

present computer technology to accommodate the large number of grid cells generated for the large scale geological model does not permit simulation at this scale and hence the need for upscaling. The utilisation of upscaling technique as a forecasting tool by reservoir geologists and engineers for oilfield exploration, development and production strategy thereby makes it an important step in reservoir modelling workflow.

The essential step in upscaling procedure is how best to represent all the observed scales of sedimentary heterogeneity in the reservoir simulator. This leads to the development of a sampling concept i.e. representative elementary volume (REV) to reflect all observed facies and sub-facies associations in the reservoir simulator (Lasseter et al., 1986). In order to simplify the complex nature of upscaling procedure in reservoir simulation, each REV is assumed to be homogenous and isotropic, and it is assigned porosity and relative permeability values. Central to most commonly used conventional upscaling techniques (e.g. power law averaging, renormalisation, pressure-solver and pseudo-function) in establishing REV is the concept of averaging- though not in that strict sense for all cases. Averaging done without realistically honouring all scales of heterogeneity will come short in capturing effective permeability distribution. Many investigators have emphasised the relationships between sedimentary heterogeneities and inter- and intra- facies permeability anisotropy; as well as the direct effects of these relationships on REV sampling for reservoir simulation (e.g. Qi and Hesketh, 2004; Mikeš et al., 2006; Phillips and Wen, 2007; Cabello et al., 2010). For example, Mikeš et al., (2006) proposed an upscaling procedure that is based on a hierarchical-based

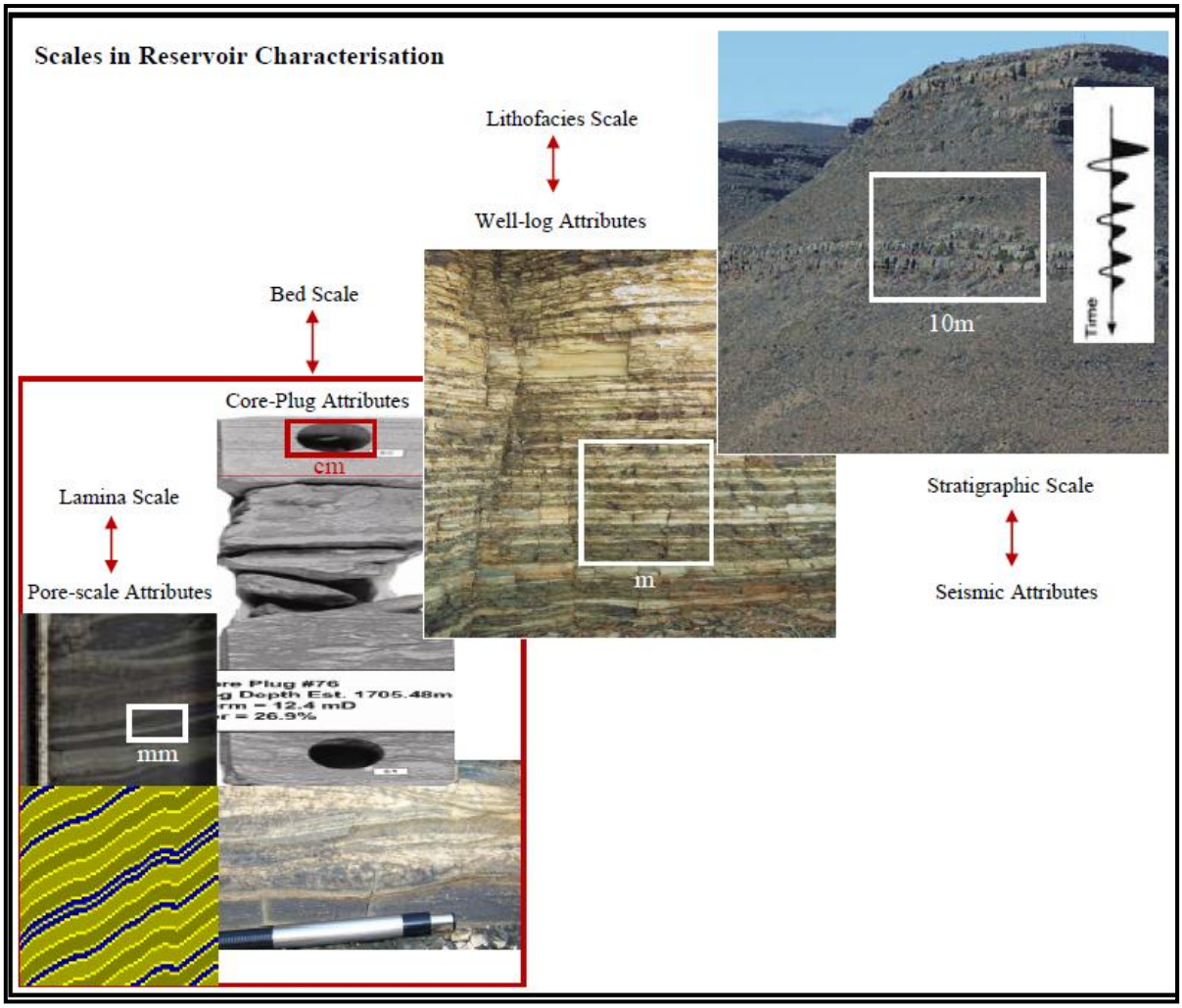

Figure 1.2. Multi-scale heterogeneities from mm- scale (i.e. Lamina scale) to m- scale (i.e. stratigraphic scale) in reservoir characterisation.

facies-dependent geological model in which the reservoir model is sub-divided into flow units (facies/sub-facies scale) and flow cells (lamina scale). They tested the effect of small-scale heterogeneities on flow behaviour by performing a two-phase simulation procedure i.e. macro-phase (i.e. flow unit simulation) and micro-phase (i.e. flow cell simulation). In their procedure, laminae are the REVs for flow cell simulation while flow cell results then automatically become the REVs for the flow unit simulation.

1.1.3 Outcrop analogue studies and deltaic sandstone reservoir bodies

Oil and gas reservoirs within ancient deltaic sediments constitute a significant proportion of world known hydrocarbon reserves (Roberts and Sydow, 2003; Samuel et al., 2007). These reserves are located in the subsurface both onshore and offshore. Most of the world's major deltas (e.g. Beaufort-Mackenzie, Canada; Gulf of Mexico, USA; Niger, Nigeria; Nile, Egypt; Rhone, France; Amur-Darya, Russia; Baram, Malaysia; Mahakam, Indonesia) with known hydrocarbon resources are shown in Figure 1.3. Consequently owing to their economic importance, they have been the focus of many sedimentological and reservoir characterisation studies in outcrops (e.g. Besley and Williams, 1989; Syvitski and Farrow, 1989; Kostic et al., 2005; Sonibare, 2009; Cabello et al., 2010) as well as in the subsurface (e.g. Scotchman and Johnes, 1990; Mayer and Chapin, 1991; Ainsworth, 2005; Labourdette et al., 2008; Zhang et al., 2008).

Conceptual sedimentary models of deltaic depositional setting have advanced through field and laboratory observations as well as digital computer simulation. However, lacking in many of these models is the accurate prediction of three-dimensional geometric behaviour of deltaic sedimentary bodies. The complexity of deltaic regimes is largely due to its position at the transitional zone between continental and marine influences (Figure 1.4). Hence the need to develop standard facies models that attempt to simplify this complexity, and at the same time reflect the temporal and spatial variability of facies and their three-dimensional

architecture. Moreover, despite the potential use of outcrop-derived measurements of deltaic systems to supplement sparse subsurface datasets for better characterisation of equivalent subsurface reservoirs, their applicability is "up to date" not well quantified.

Many previous studies (e.g. Elliot, 1989; Postma, 1990; Longhitano, 2008; Wild et al., 2009) have attempted to explain in detail the various dominant sedimentological factors such as climate, sediment supply rate, tectonic subsidence and uplift, global eustasy, deltaic lobe switching, relative sea-level changes, sediment transport and nature of discharge systems that govern the evolution of deltaic regime. The interplay between these factors and base-level changes (i.e. creation of accommodation space) determines the morphology, relative position, sediment stacking pattern and texture of deltas in both recent and ancient settings. For instance, Postma (1990)'s prototype deltaic classification into: 1) Gilbert-type or mouthbar-type based on the nature of the active growth front of the delta at the mouth of the river; 2) Gravely or alluvial fan delta based on the nature of river feeder system; 3) shelf or shelf edge delta based on the position of the basin with respect to shoreline or roll-over point; 4) shallow-water or deep-water deltas based on the water depth at the receiving basin. The understanding of this interplay is crucial to three-dimensional reconstruction of facies geometric elements in outcrops and in subsurface petroleum reservoirs.

1.1.4 Tanqua-Karoo Sub-basin: Previous work

The earliest studies on the Tanqua-Karoo depocentre (Figure 1.5) (e.g. Bouma and Wickens, 1991; Wickens 1994; Johnson et al., 2001 and Van der Werff and Johnson, 2003) concentrated on the fine-grained sand-rich submarine fan systems of the Skoorsteenberg Formation which underlie the Kookfontein deltaic sequence. Most of these studies including some recent ones (e.g. Andersson et al., 2004; Hodgson et al., 2006; Wild, 2005) are being conducted so that detailed observations and measurements from these outcrops could be documented for applications to similar deepwater reservoir analogues. At the moment, the

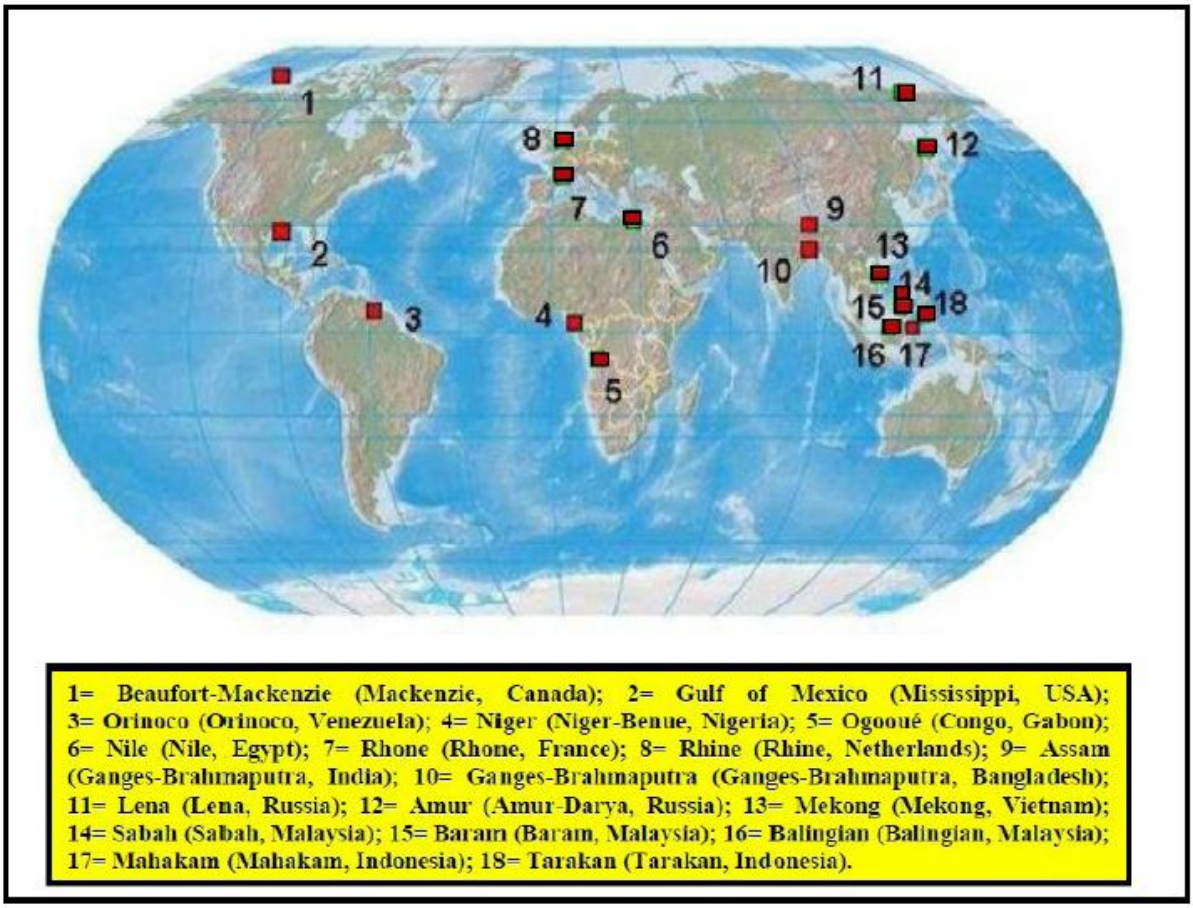

Figure 1.3. World map showing the global distribution of Tertiary deltaic basins with known hydrocarbon potential. In brackets are the respective names of the draining river and location (modified from Samuel et al., 2007; additional source from Roberts and Sydow, 2003).

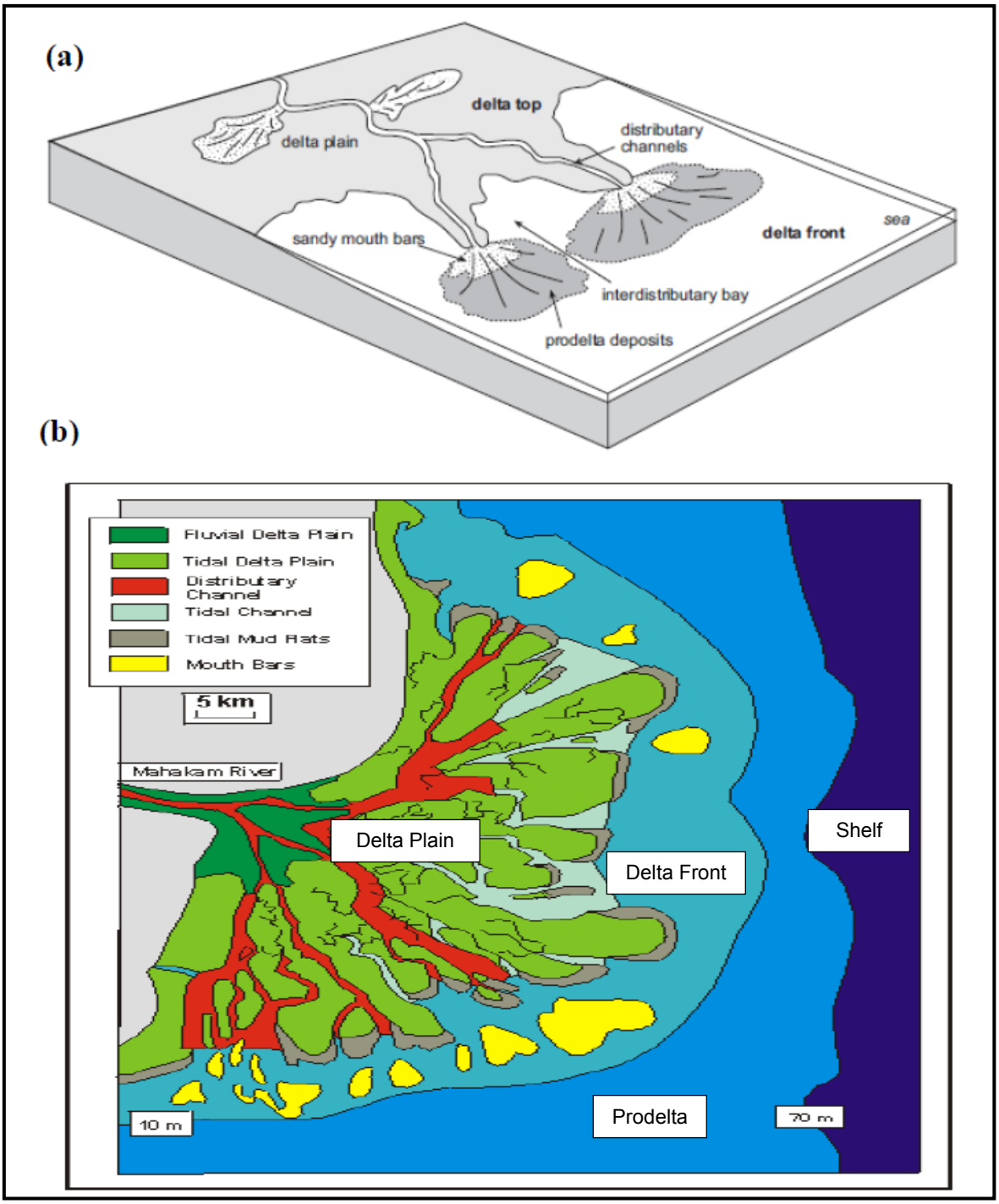

Figure 1.4. (a) Diagram of deltaic depositional environment showing deltaic reservoir facies i.e. distributary channel and mouth bar deposits (modified from Nichols, 2009); (b) deltaic facies distribution of onshore and offshore modern Mahakam Delta (adapted from Darman et al., 1999).

extent of their contribution to reservoir characterisation of such examples is yet to be fully quantified and documented.

The overlying ~250 m thick deltaic sequence of the Kookfontein Formation (Wickens, 1994) with a north to south lateral extent of about 72 km (Figure 1.6) in seven type localities i.e. Katjiesberg, Syfer, Skoorsteenberg, Bitterberg, Vaalberg, Pienaarsfontein and Roosterberg (Wild et al., 2009) has not been previously studied in detail. Presently, there is neither a detailed lithostratigraphic map nor a robust facies-dependent geological model that describes facies relationships of the Tanqua-Karoo deltaic succession in terms of their spatial and temporal distribution, geometry and internal architecture. Moreover, the Kookfontein deltaic sequence has not been studied and documented as an outcrop analogue to subsurface examples. The studies by Wild (2005) and Wild et al. (2009) appear to be the first attempt to describe the sedimentology, stratigraphic evolution and depositional setting of the Kookfontein deltaic succession. However, these studies do not incorporate enough detail typical of an outcrop analogue study.

Wild (2005) and Wild et al. (2009) describe thirteen sedimentary cycles for the Kookfontein deltaic sequence observed at the Pienaarsfontein locality, and employ sequence stratigraphic approach to interpret their sedimentological and stratigraphic evolutionary trend. They use depositional terms typical of passive margin shelf-slope-basin floor profile despite the fact that Karoo stratigraphy was deposited in an active margin intra-cratonic basin. Within these 13 cycles, they identify twelve flooding surfaces separated by two erosional sequence boundaries as the sequence stratigraphic surfaces that bound the sedimentary cycles of Kookfontein Formation. They also use terms like sediment accretion (i.e. deposition and shelf construction) and bypass (erosion and slope failure) to describe the sedimentological and stratigraphic evolution of the Kookfontein deltaic succession and their relationships to the underlying basin-floor fan systems of the Skoorsteenberg Formation. However, the

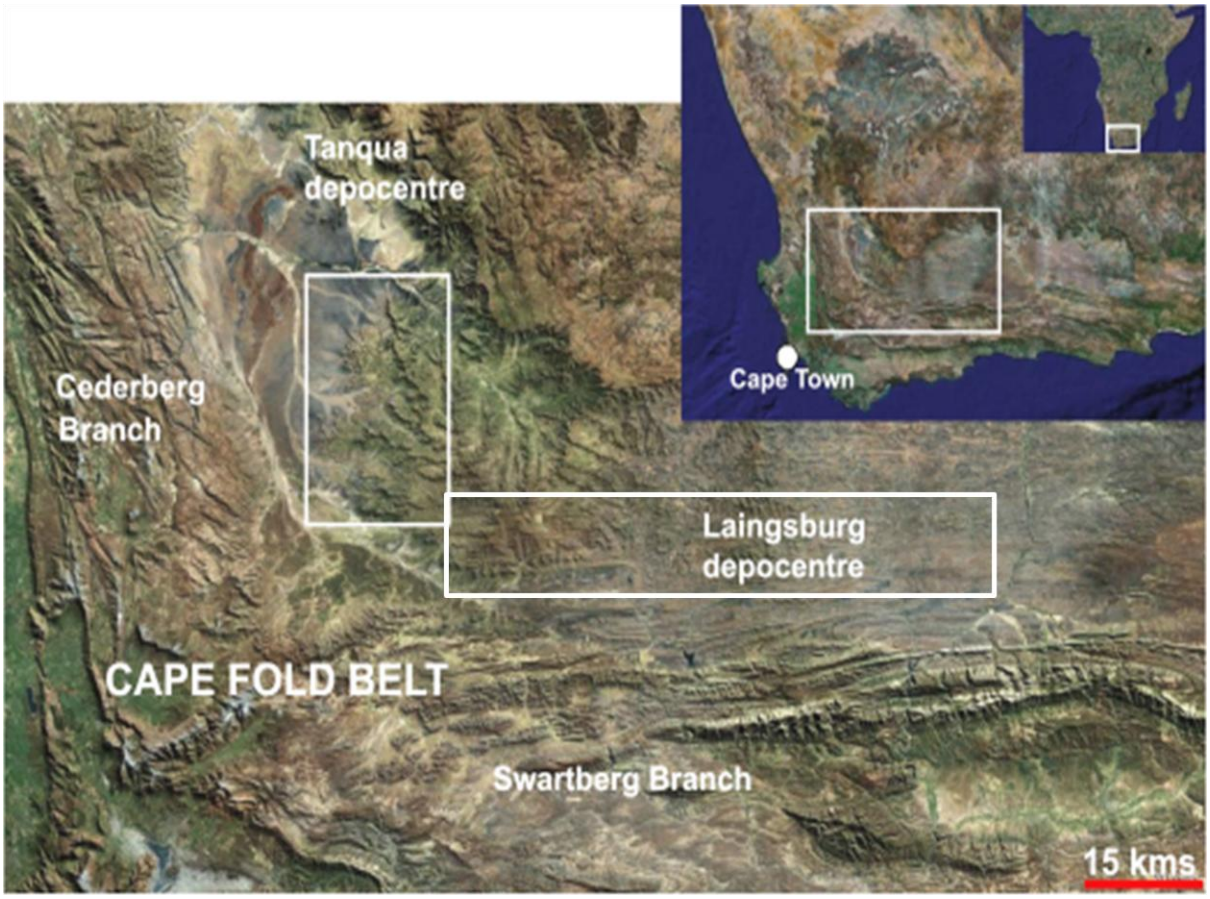

Figure 1.5. Location maps of the study area showing the outline of the Tanqua and Laingsburg depocentres in the SW Karoo basin.

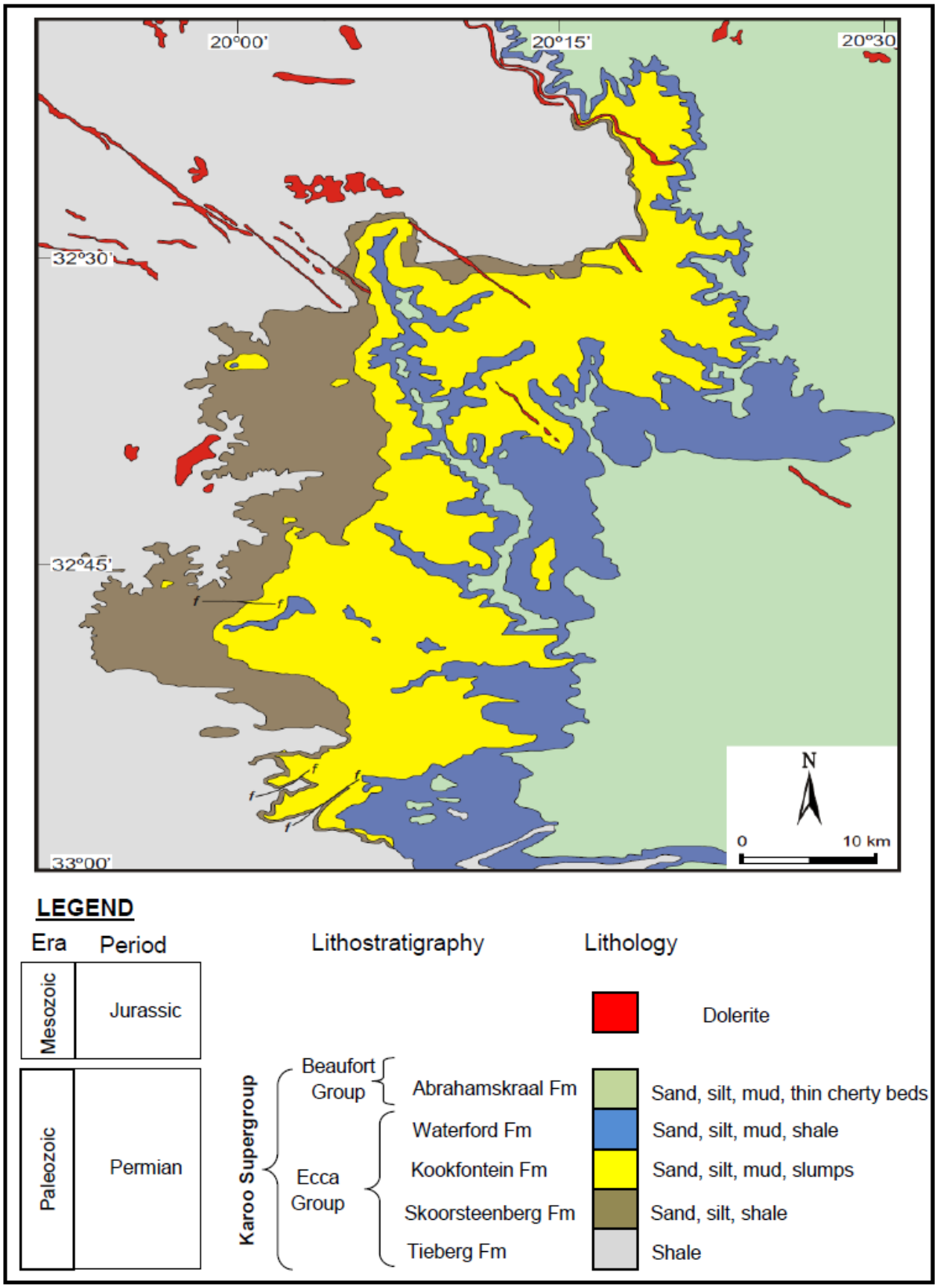

Figure 1.6. Geological map of the Tanqua depocentre showing the stratigraphic properties, distribution and boundaries of the Kookfontein Formation (modified from Van Lente, 2004; based on 1:250 000 Geological series by Geological Survey of South Africa).

sedimentological and stratigraphic evolutionary model proposed by Wild (2005) and Wild et al., (2009) for the Kookfontein deltaic system does not fully constrain the following:

1. The relationship between sediment stacking patterns and the dominant depositional signatures (e.g. sediment supply, tectonic subsidence, eustatic sea-level fluctuations, lobe switching) that create them. This actually requires testing the possibility of each of these signatures from the rock record in order to deduce their dominance.
2. The type of Kookfontein deltaic deposit (i.e. whether Gilbert-type or Mouth-bar-type; whether shallow or deep delta) (Postma, 1990).

Previous petrographic studies by Scott et al. (2000) and Nguema (2005) on the sandstones of the Tanqua submarine fan systems, suggest that Tanqua Karoo sandstones are mainly greywackes to litharenites, fine- to very fine-grained, and moderately sorted. They proposed that these sandstones are texturally and mineralogically immature owing to the abundance of less stable minerals such as feldspars and rock fragments as well as the predominance of angular grains. Van Lente (2004) conducted geochemical and petrographic studies on sandstone samples from the deltaic and submarine fan systems of the Tanqua and Laingsburg depocentres. Van Lente (2004) classified the sandstones geochemically as litharenites and greywackes. According to Van Lente (2004), the sandstones are tightly packed; poorly to moderately sorted; have undergone mechanical and pressure solution; and have no visible porosity and permeability primarily due to narrow range in grain size from very fine- to lower medium-grained and the formation of authigenic quartz cement and secondary chlorite and illite. The work by Sonibare (2009) is the first attempt to carry out a detailed reservoir characterisation of the Kookfontein deltaic succession based on traditional facies analysis on the field-measured sedimentary observations and gamma ray logs. Sonibare (2009) describes three lithofacies associations i.e. mudstone, heterolithic and sandstone facies for the first three sedimentary cycles, which he interprets to belong to two depositional facies i.e. delta front and prodelta. The percentage of shale content evaluated from gamma ray log

for different lithofacies associations is given as: sandstone (0-30%), heterolithic silty/shaly sand and soft-sediment deformation (30-70%) and mudstone facies (60-100%) (Sonibare, 2009).

1.2 Aims of the project

This study is an outcrop analogue study that is established on the previous work by Sonibare (2009) on lithofacies analysis and reservoir characterisation of the Permian siliciclastic Kookfontein deltaic succession. The purpose of Sonibare (2009)'s study was to describe the internal heterogeneity and facies architecture of the lower Kookfontein succession (i.e. cycles 1, 2 and 3) through a detailed lithofacies analysis. Through this work, the need to study the remaining upper Kookfontein succession (i.e. cycles 4 to 13) for better understanding of facies stacking and geometry of the delta system was realised.

The conceptual sedimentological and deterministic approach to this present study is in two parts: a part of this study was devoted on outcrop-based facies analysis that was then used to develop hypothetical 'descriptive' facies model and geometrical geological model for the Kookfontein delta system, while the other part involved empirical prediction of petrophysical properties (i.e. porosity and permeability) through petrographic characterisation and petrophysical calculations. The longer goal of this research is therefore to further our understanding of the Kookfontein delta system as well as to develop a robust workflow for outcrop analogue studies.

1.2.1 Research questions

The questions that instigated the aims of this study are as follows:

1. What type of deltaic architecture is Kookfontein Formation?

2. What type of facies models (i.e. 1D, 2D or 3D) will better predict the geometry and architecture of the Kookfontein deltaic sequence?

3. Can we possibly deduce from the rock record (i.e. texture and sedimentary structures) the dominant depositional controls that are responsible for the Kookfontein sedimentary cycles?

4. Can grain size-based analysis of outcrop data offer reliable prediction of porosity and permeability distribution?

The key objectives of this study are as follows:

1. Describe and analyse various sedimentary facies based on lithological characteristics (i.e. texture and sand to clay ratio) and depositional processes (i.e. sedimentary structures) for depositional environment interpretations.
2. Establish hypothetical 'descriptive' facies model to describe and interpret internal heterogeneity, facies architecture and sediment-body geometry.
3. To explore the relationship between sediment stacking and depositional drivers.
4. Construct idealised reservoir-scale geological 'geometrical' model.
5. To understand the effects of diagenesis and depositional environments on porosity and permeability distribution.
6. Empirical prediction of porosity and permeability distribution from texture, stratigraphic age and burial history data.

CHAPTER TWO

METHODOLOGY

2.1 Methodology

The aforementioned objectives for this study were addressed using a combination of outcrop sedimentary logs, outcrop gamma ray (GR) logs, photopanel analysis and petrographic thin section analysis. The collected and analysed datasets for this study are as follows:

- 4 vertical sections (i.e. VS1, VS2, VS3 and VS4) logged at mm-scale for Kookfontein cycles 1 to 13 representing a total of 1120 m measured profiles. Of these, only VS1 and VS2 were previously logged for cycles 1 to 3 by Sonibare (2009); and these were walked-out again for proper identification of cycle boundaries. Also, the logged 13 cycles that characterise the Kookfontein Formation at the Pienaarsfontein locality correspond to the previously described sedimentary cycles by Wild (2005) and Wild et al. (2009).
- 2 GR profiles logged at a 5 s count rate and 50 cm sample spacing along VS1 and VS2 for cycles 1 to 3.
- 2 ground-based outcrop panels.
- 15 samples for thin section studies out of which 10 samples were selected SEM analysis.

The Kookfontein Formation is well exposed along the slopes of a prominent ridge named Pienaarsfontein se Berge (Figure 2.1) and this locality is the focus of this study. It lies approximately between Longitudes 19° 59’0”E and 20° 07’30”E and Latitudes 32° 44’0”S and 32° 48’30”S. The outcropping part of the Kookfontein deltaic succession selected for this study represents an aerial extent of about 13 km^2 (6.5 x 2.1 km) with a lateral coverage of 6.5 km (Figure 2.1), and ranges in stratigraphic thickness from 250 to 285 m.

The total radioactivity (i.e. total gamma ray count per second-cps) of the rock units was measured with a hand-held scintillometer. Spectral GR logs for each radioactive element in the rock units were not generated for this study. The analysis of the gamma ray logs was used

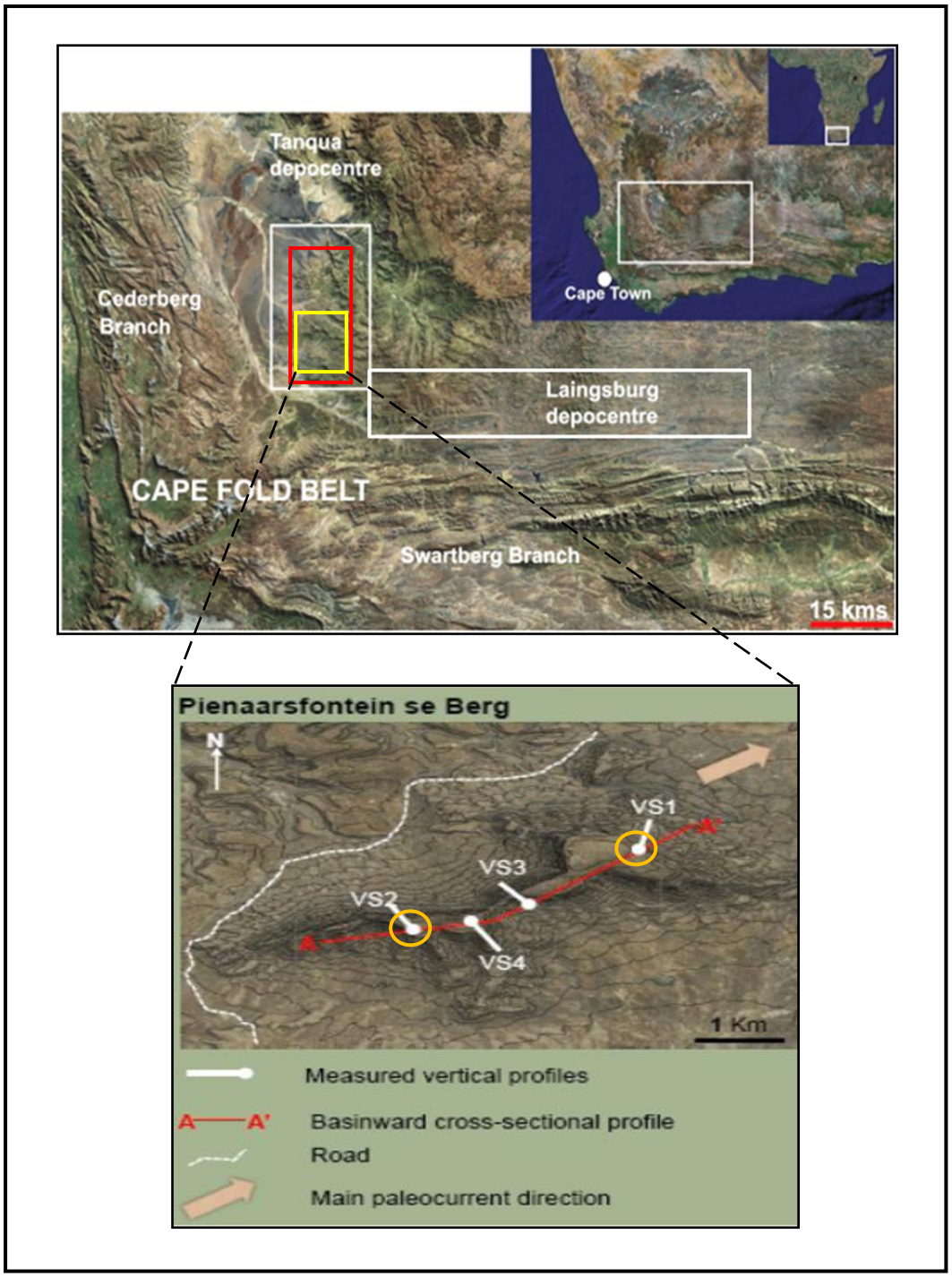

Figure 2.1. Location maps of the study area showing the SW Karoo Basin, outline of its depocentres (i.e. Tanqua and Laingsburg) and Pienaarsfontein se Berg locality. Red box in upper photo shows the outline of Kookfontein formation. Yellow circles in the lower photo show the sampling locations for thin section samples.

for identifying and correlating lithofacies associations and facies successions (i.e. cycles) as well as estimation of shaliness (i.e. clay content) for various lithofacies types. The shaliness of different lithofacies associations was obtained by normalising the gamma ray values using the mathematical expression below:

$$V_{sh} = \frac{Gr_{\log} - Gr_{\min}}{Gr_{\max} - Gr_{\min}} * 100\% \qquad (\textit{Equation 1})$$

Where, Vsh = the shale content expressed as a percentage,

Gr_{log} = gamma ray log,

Gr_{max} = the maximum gamma ray log reading, and

Gr_{min} = the minimum gamma ray log reading.

Textures (i.e. grain size, sorting and roundness) of encountered rock units were initially determined through examination under a handlens in the field followed by petrographic thin section studies. Photo mosaics were derived from ground-based photographs and differential GPS. Lithofacies boundaries were established deterministically through physical "walking-out" on outcrop exposures and photo mosaics. The integration of various datasets enabled a deterministic approach to the spatial and temporal distribution of facies both laterally and vertically, lithological correlation and identification of sandbody architecture, shaliness estimation and interpretation of depositional environments. Schematic description of methodology used in this work is given in Figure 2.2.

2.1.1 Petrographic thin section analysis

The petrographic techniques to determine mineralogy, the relationships between texture (i.e. grain size, sorting, grain roundness and grain sphericity) and diagenetic processes as well as evaluation of the effect of diagenesis and initial depositional environment on porosity and permeability distribution include the following:

1. Thin section slices (about 30 microns thick) of 15 samples (see Table 2.1) were examined under a standard light-transmitted petrological/petrographic microscope to determine the amount of detrital grains, diagenetic components (i.e. authigenic minerals and cement), grain size, sorting and textural maturity (i.e. grain roundness and sphericity).

2. The textural relationships between detrital grains (mainly quartz, feldspars and lithic fragments) and diagenetic components (i.e. quartz overgrowths/cements, calcite cements and authigenic minerals like clays and altered feldspars) were examined under plane-polarised light and crossed polars.

3. Classification of sandstones based on detrital particles and grain size distribution was based on Pettijohn classification (Pettijohn et al., 1987) and Udden-Wentworth grain-size scale (Udden, 1914; Wentworth, 1922) respectively.

4. Petrographic examination of authigenic cements (i.e. quartz overgrowths, authigenic clay minerals and albitic feldspar alterations) was very difficult with an ordinary petrographic microscope, and therefore, some selected samples were examined with a scanning electron microscope (SEM) equipped with a semiquantitative energy dispersive analyser in the backscattered electron imaging modes for some selected samples.

5. Spot mineral identification for minerals that were difficult to determine under normal petrographic microscope was carried out using SmartSEM scanning electron microscope equipped with Oxford INCA mineral analyser.

6. Grain size, sorting parameters and textural maturity were determined based on the methodology of Beard and Weyl (1973) for all the representative samples which covered all the four lithofacies associations.

Table 2.1. Brief description of samples for petrographic analysis and their locations on measured sedimentary logs.

#	Log/Sample name	Depth (m)	Texture			Lithology	SEM dataset	Remarks
			Grain size	Sorting	Roundness			
1	VS1/SGSR3	17	Ml - Mu	MW-S	Sag	Sandstone	X	Dirty with clay clasts
2	VS1/SWA1	22	Slt - Vfl	VP-S		Silty Sandstone		
3	VS1/SGSR5	29	Fu - Ml	W-S	Sag - Sr	Sandstone	X	
4	VS1/SWA6	45	Vfu - Fu	M-S	Ag - Sag	Silty Sandstone	X	
5	VS1/SWA7	45.5	Slt - Vfl			Silty/Clayey Sandstone	X	Very dark grains, probably carbonaceous
6	VS1/SWA8	47	Slt - Vfl	VP-S	Ag - Sag	Silty Clay	X	
7	VS1/SWA13	63	Ml - Mu	W-S	Sag - Sr	Massive Sandstone		
8	VS1/SWA14	68	Ml - Mu	VW-S	Sag - Sr	Massive Sandstone	X	
9	VS2/SWA15.2	20.5	Vfl - Fl	P-S	Ag - Sag	Soft-sediment deformation Sandstone	X	Dirty with mud clasts
10	VS2/SWA15.4	32.5	Ml - Mu	W-S	Sag - Sr	Bedded Sandstone		
11	VS2/SWA16	56	Vfu - Fl	M-S	Sag	Silty Sandstone	X	
12	VS2/SWA17	57	Vfu - Fu	M-S	Sag	Silty Sandstone		
13	VS2/SWA20	69	Ml - Mu	VW-S	Sag - Sr	Bedded Sandstone	X	
14	VS2/SWA21	106	Fl - Ml	W-S	Sag - Sr	Silty Sandstone		
15	VS2/SWA22	113	Ml - Mu	VW-S	Sag - Sr	Sandstone	X	

Slt = Silt; Vfl = Very fine lower; Vfu = Very fine upper; Fl = Fine lower; Fu = Fine upper; Ml = Medium lower; Mu = Medium upper

VW-S = Very well sorted; W-S = Well sorted; MW-S = Moderately well sorted; M-S = Moderately sorted; P-S = Poorly sorted; VP-S = Very poorly sorted

Ag = Angular; Sag = Sub-angular; Sr = Sub-rounded

2.1.2 Grain size-based petrophysical modelling of outcrop data

Sources of permeability measurements for hydrocarbon reservoirs are cores, well-logs, well test analysis, production data and empirical prediction from grain size distribution. At the exploration and development stage of an oilfield, there exists little geological information due to sparse data availability. Hence, the predictive method of estimating permeability especially from grain size distribution observed at outcrops could be a valuable tool. The use of empirical equations (e.g. Kozeny, 1927; Carman, 1937; Berg, 1970) to predict petrophysical properties particularly porosity and permeability distribution of porous media is now a common practice within the oil industry. These empirical models are based on a number of properties of hydrocarbon reservoirs such as porosity, pore connectivity, grain packing, grain size, sorting and rock diagenesis.

In order to assess the reservoir properties of Kookfontein deltaic reservoir facies, well-established empirical equations were used to predict their porosity and permeability distribution. The variables for empirical equations (e.g. Beard and Weyl, 1973; Scherer, 1987; Waples, 2002)) that were used to predict porosity values are: stratigraphic age, burial depth, quartz content and sorting parameters. Likewise for permeability prediction (e.g. Kozeny, 1927; Carman, 1937; Berg; 1970), the variables are: porosity and grain size distribution (i.e. normally distributed median representative grain size). The two permeability predictive models (i.e. Kozeny-Carman model and Berg model) were then correlated so as to determine which textural properties play a major role in porosity and permeability distribution. Textural-related variables (i.e. quartz content, grain size and sorting) were obtained from petrographic thin section analysis. The size-sorting comparator photomicrographs of Beard and Weyl (1973) were used in order to improve accuracy of estimating these variables from thin section. The role of diagenetic processes e.g. compaction and cementation in porosity and permeability reduction were assessed by calculating depositional and present-day

porosities using the methodology of Beard and Weyl (1973) and Scherer (1987), and afterwards the degree of porosity reduction by either compaction or cementation was evaluated using the methodology of Lundegard (1992).

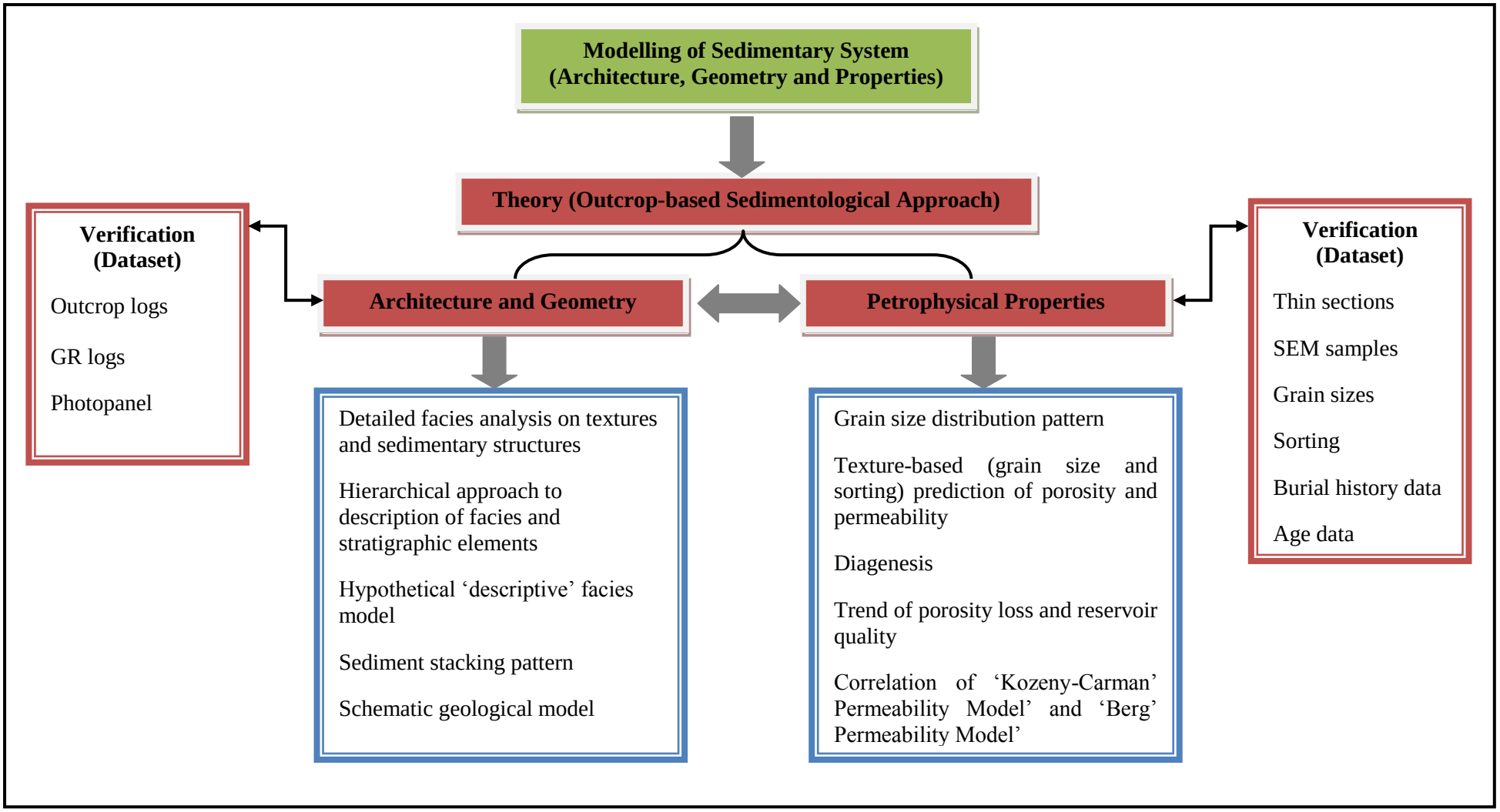

Figure 2.2. Schematic diagram for the methodology of this study.

CHAPTER THREE

REGIONAL GEOLOGY (KAROO BASIN)

3.1 Tecto-stratic evolution of the Karoo Supergroup

The Late Carboniferous to Middle Jurassic cratonic Karoo Basin (Figure 3.1) represents one of the most preserved Gondwanan sequences (i.e. Paraná, Karoo, Huab and Bowen Basins (e.g. Faure and Cole, 1999; Figure 3.2), and forms one of the most complete stratigraphic successions in the world that span this time (Johnson et al., 2006). The Karoo Supergroup covers an area of approximately 700 000 km^2 with the bulk of the sedimentation occurring in the main basin reflecting a maximum thickness of ~5500m above the Namaqua basement block (Tankard et al., 2009), and being laterally extensive during the Permian with two depocentres at the south-western Karoo (i.e. Tanqua and Laingsburg). The Southern margin of the Karoo Basin is underlain by the Cape Supergroup, a lower Paleozoic passive margin clastic wedge up to 8 km thick (Tankard et al., 1982). The coalescence of the two Cape Fold Belt mountain ranges (i.e. the N-S trending Cedarberg Mountains and the E-W trending Swatberg Mountains) at the Hex river mountains in the southwest corner of the Karoo Basin (De Beer, 1990; Van der Werff and Johnson, 2003) resulted in the development of linear NE-trending anticlinal structures which separate the Tanqua depocentre in the west from the Laingsburg depocentre in the east (Figure 3.3).

The Karoo Basin is generally believed by previous authors to have developed as a retro-arc foreland basin behind an inferred magmatic arc and fold-thrust belt with subsidence solely due to loading by the Cape Fold-Thrust Belt, which lies along the southern and south-western margin of the basin (e.g. Lock, 1980; Catuneanu, et al., 2002; Johnson et al., 2006; Figures 3.3, 3.4 and 3.5). Visser and Praekelt (1996) proposed a modification to the retro-arc foreland basin model. They suggested that oblique subduction of the Panthalassan (paleo-Pacific) plate underneath

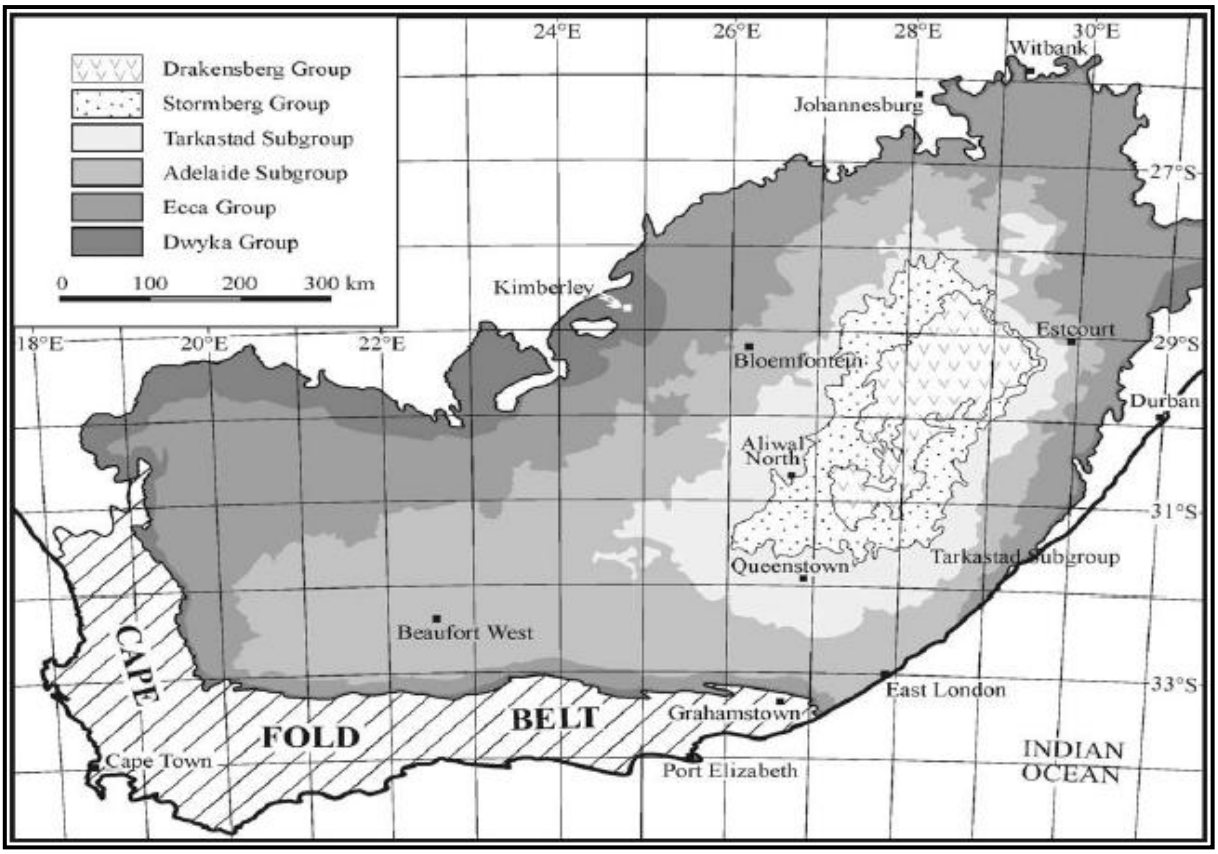

Figure 3.1. Geological map of the preserved Karoo Basin, showing the outcrop distribution of the main lithostratigraphic units of the Karoo Supergroup. The Adelaide and Tarkastad subgroups together form the Beaufort Group (adapted from Catuneanu et al., 2002).

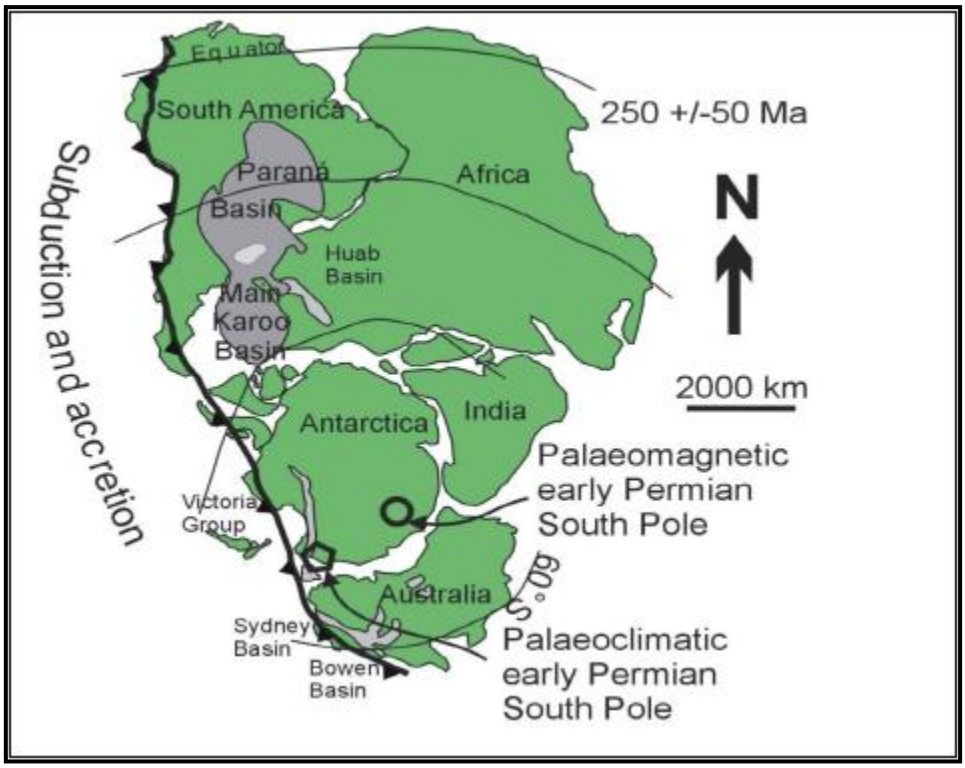

Figure 3.2. Paleogeographic reconstruction of Gondwana during the Permian. Note the position and extent of the Paraná and Karoo basins (from Faure & Cole, 1999).

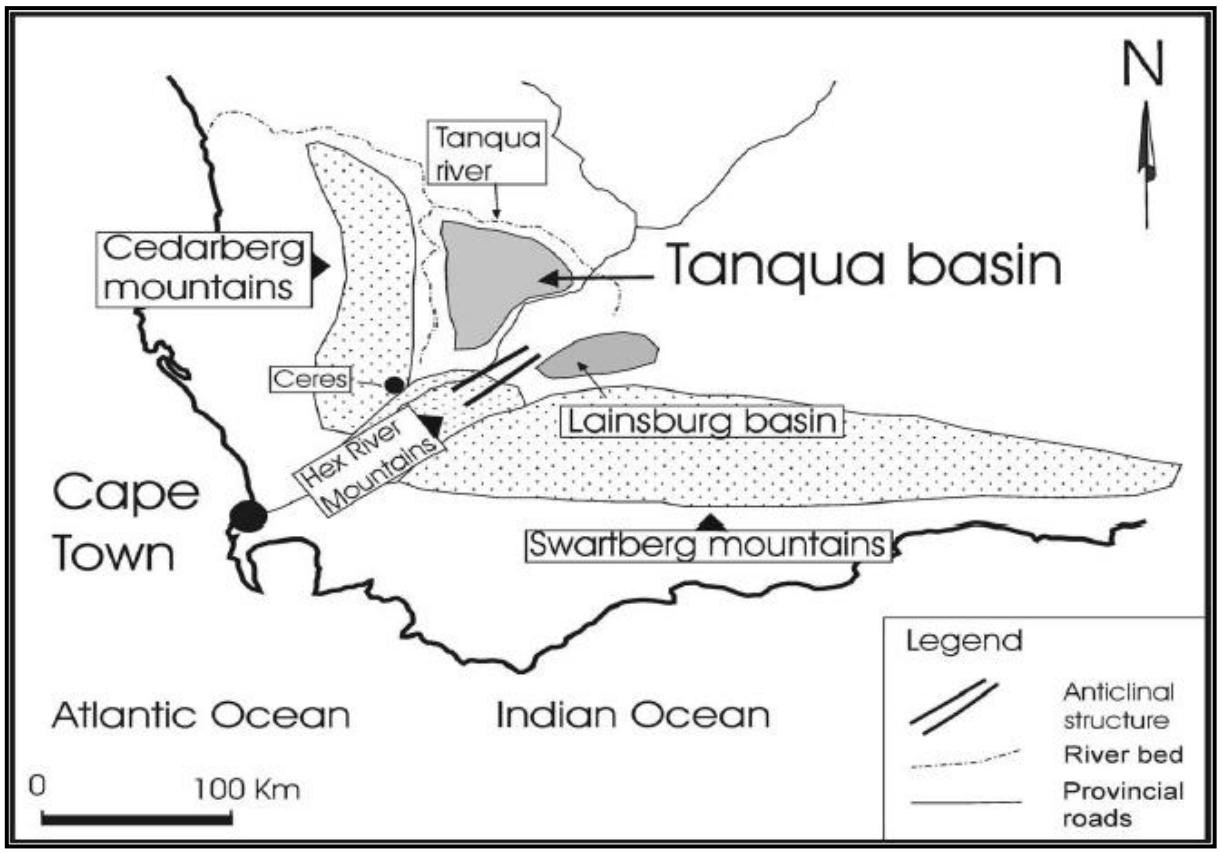

Figure 3.3. Location map showing the Cape Fold Belt (i.e. the N–S trending Cedarberg Mountains, and the E–W trending Witteberg–Swartberg Mountains) and the linear NE- trending anticlinorium which separated the Tanqua depocentre from the Laingsburg depocentre (adapted from Van der Werff and Johnson, 2003).

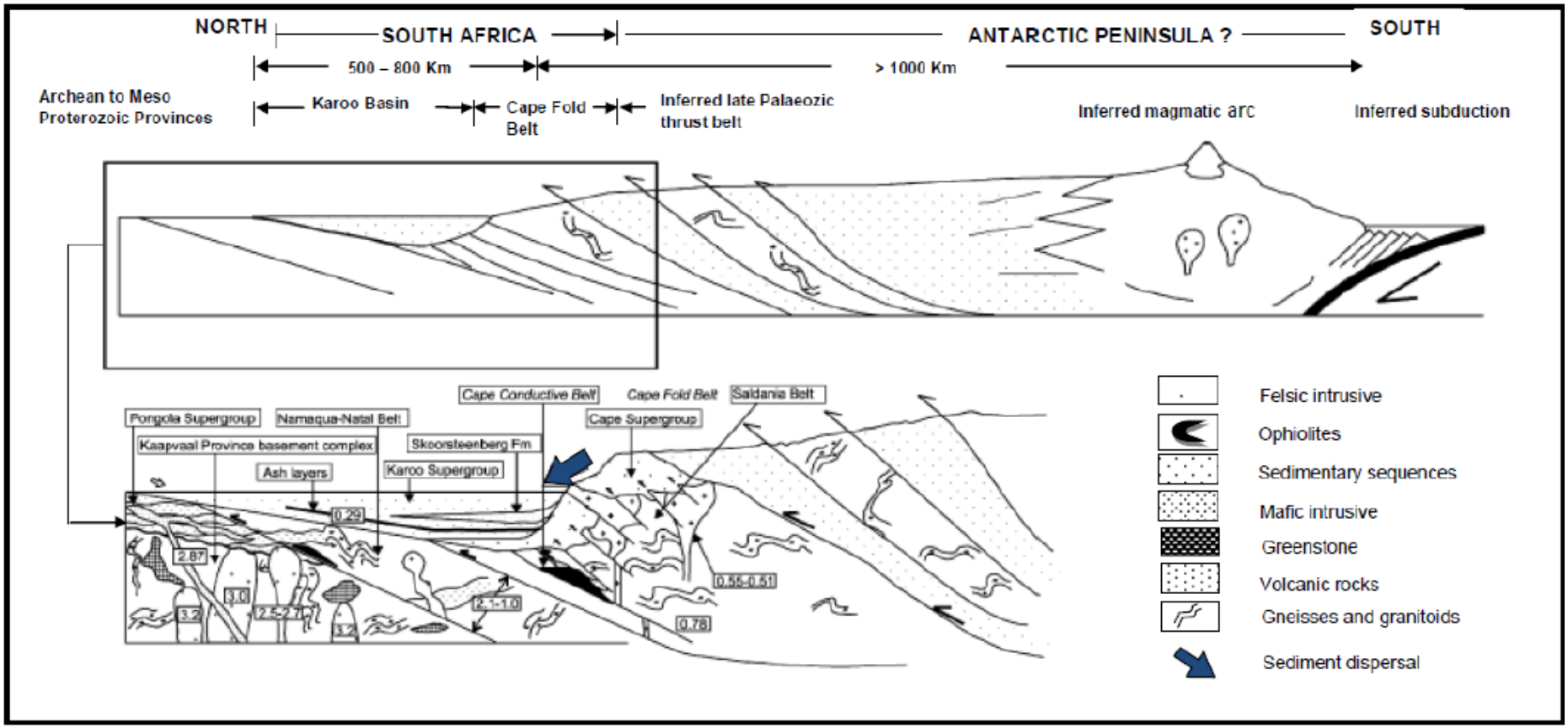

Figure 3.4. Generalised retro-arc foreland basin model for the Karoo Basin during the early Mesozoic, showing the basin in relation to underlying Archean to Proterozoic crustal terranes, the Cape Fold Belt and the inferred position of a possible arc and subduction zone (modified from Andersson et al., 2003).

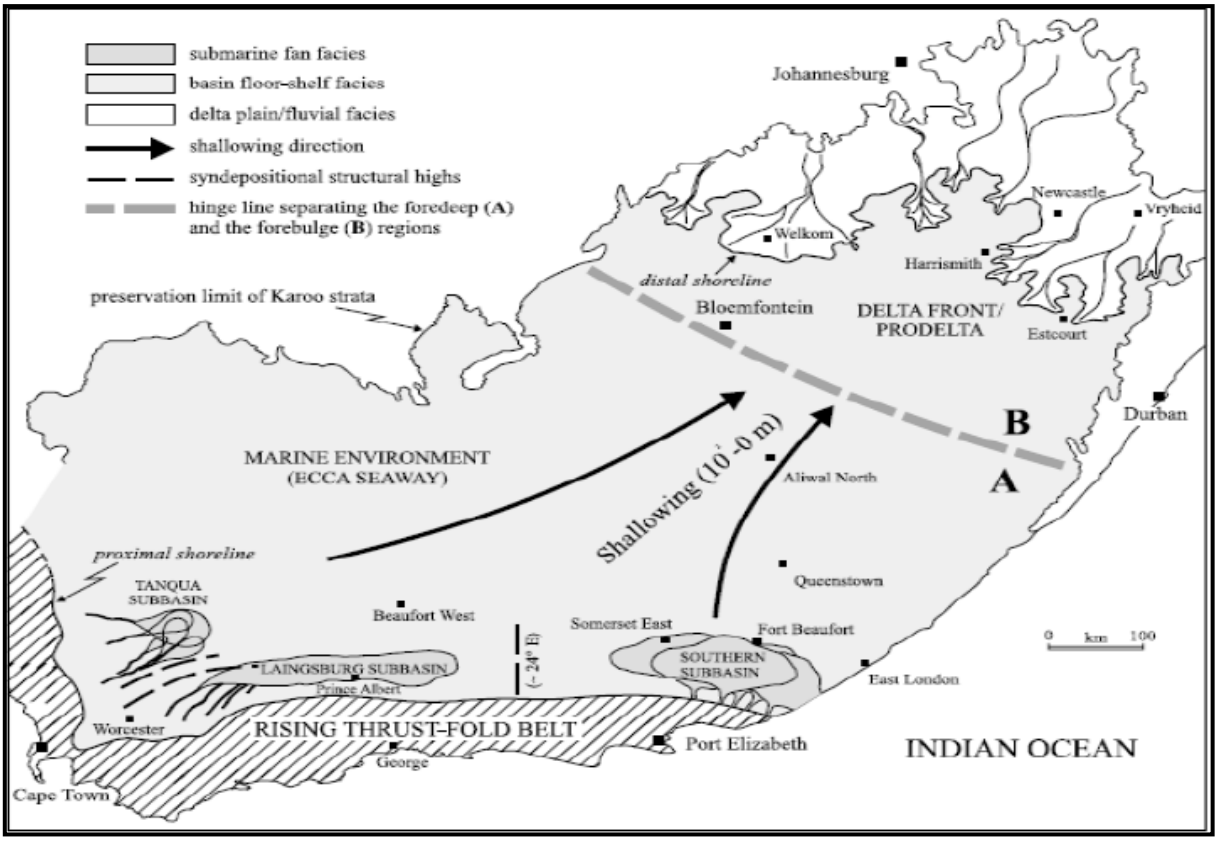

Figure 3.5. Palaeogeographic reconstruction of the environments established in relation to the Ecca interior seaway of the Karoo Basin during the Artinskian showing the flexural provinces of the retro-arc foreland model i.e. foredeep (A) and forebulge (B)(adapted from Catuneanu et al., 2002).

Gondwanaland led to the creation of a large interconnected basin stretching from South America to Antarctica, including the main Karoo Basin. Accommodation space in the main Karoo Basin was created by dextral transpressional strike-slip movements along a major northwest-striking fracture zone named the Atlantic Fracture Zone to the southwest of South Africa and along a major north-striking fracture zone named the Falkland Fracture Zone, between the restored Falkland Islands to the southeast of South Africa and Antarctica. More recently, Tankard et al. (2009) proposed an alternative tectonic model based on the following arguments: (1) that there is no geophysical evidence for the nearby magmatic arc, (2) the Cape Fold Belt is a strike-slip orogen dated to the late Karoo time (Figures 3.6, 3.7 and 3.8) and (3) absence of typical flexural foreland basin onlapping stratigraphic features and the fact that the lithosphere is not laterally uniform (Figure 3.6). Therefore, it can be categorically stated that the tectonic evolution of the Karoo Basin is highly controversial, and also yet to be fully understood.

The stratigraphy of the Karoo Supergroup is divided into three groups namely, the Dwyka Group (Westphalian to early Permian glacial deposits), the Ecca Group (Permian) and the Beaufort Group (Permo-Triassic fluvial sediments) (Figures 3.8 and 3.9). The Permian Ecca Group comprises a total of 16 formations (Johnson et al., 2006) mainly shallow marine, deltaic and fluvial facies, thereby reflecting the lateral facies changes that characterise this group from the south through the east and to the north. In the SW Karoo Basin, there are two depocentres namely: the Tanqua depocentre and the Laingsburg depocentre (Figures 3.10 and 3.11). In these two depocentres, the 1700 m-thick Ecca Group comprises the basal Prince Albert Formation (shale and cherty shale beds; 288 +/- 3 Ma, Bangert et al., 1999), the Whitehill Formation (black, carbonaceous shales with pelagic organisms, Visser, 1992) and the Collingham Formation (fine-grained sheet turbidites and intercalated ashes; 270 +/- 1 Ma, Turner, 1999) (see Figure 3.10), all deposited during a long-term post-glacial sea level rise resulting from melting ice which established an extensive shallow sea (Visser, 1992 and 1993). Overlying the Collingham

Formation in the two depocentres are the ~1500 m-thick deepwater deposits i.e. Tierberg, Skoorsteenberg and Kookfontein Formations in the Tanqua depocentre; and Vischkuil, Laingsburg and Fortbrown Formations in the Laingsburg depocentre (Figure 3.11).

According to Scott (1997) and King (2005), Laingsburg depocentre has more tectonic impressions than the Tanqua depocentre. Also, stratigraphic reconstruction studies by Flint et al. (2004) suggest that sand-prone submarine sedimentation is thicker in the Laingsburg depocentre than the Tanqua depocentre. Most previous workers (e.g. Wickens, 1994; Scott et al., 2000) have proposed a lacustrine setting for the Skoorsteenberg and Kookfontein Formations. However, marine trace fossils that were recently identified (Johnson et al., 2001) coupled with tidal influenced sandstones (Wild, 2005) suggest a marine setting. Visser (1992) suggests that the lack of marine faunas may signify a partially enclosed basin and that restricted oceanic circulation within a morphologically complex basin created anoxia within the water column. Therefore, it is proposed that the basin was not a fully open marine system (Wild, 2005). Though the Tanqua and Laingsburg submarine fan complexes are deposited respectively in an active cratonic basin flanked by an orogenic belt, several previous investigators (e.g. Wickens, 1994; Wickens and Buoma, 2000; Johnson et al., 2001; Van der Werff and Johnson, 2003; Wild, 2005; Hodgson et al., 2006; Wild et al., 2009; IHS Energy, 2009) believe it has depositional characteristics typical of submarine fan complexes deposited in passive margin settings i.e. shelf-slope-basin profile. A radiometric date of 270 +/- 1 Ma from ashes in the Collingham Formation (Turner, 1999) and a 255 Ma date from early reptile fossils in the basal Beaufort Group (Rubidge et al., 2000) bracket the whole deepwater, shelf and basal fluvial deposits (i.e. Tierberg, Skoorsteenberg, Kookfontein and Waterford Formations in the Tanqua depocentre and the Vischkuil, Laingsburg and Fortbrown Formations in the Laingsburg depocentre) to a 15 My period (Figure 3.10).

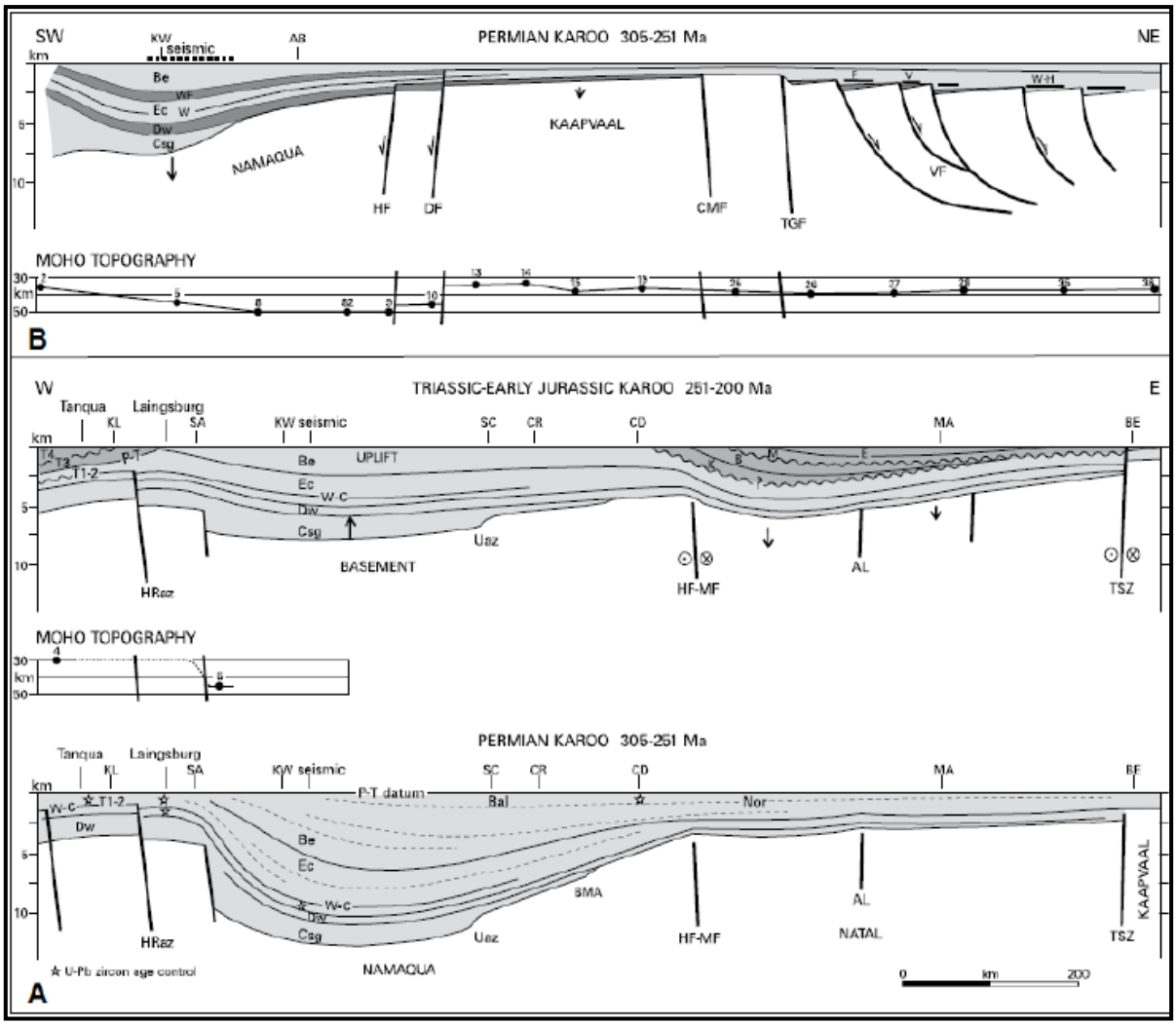

Figure 3.6. Structural controls of Karoo subsidence and Moho topography showing evidence for non-lateral uniformity of the lithosphere during the early Permian Karoo Basin. Stratigraphy: B, Burgersdorp; Bal, Balfour; Be, Beaufort; CD, Commando Drift; Csg, Cape Supergroup; Dw, Dwyka; Ec, Ecca; E, Elliot; F, Free State coalfield; K, Katberg; M, Molteno; Nor, Normandien; W, Whitehill; W–C, Whitehill–Collingham; Wf, Waterford; W–H, Witbank (N) and Highveld (S) coalfields; V, Vereeniging coalfield. Structure: AL, Amanzimtotistructure; BMA, Beattie anomaly; CMF, Colesberg fault; DF, Doringberg fault; HF, Hartbees fault; HRaz, Hex River accommodation zone; MF, Mbotyi fault; TGF, Trompsburg fault; TSZ,Tugela shear zone; Uaz, Uniondale accommodation zone; VF, Virginia fault (adapted from Tankard et al., 2009).

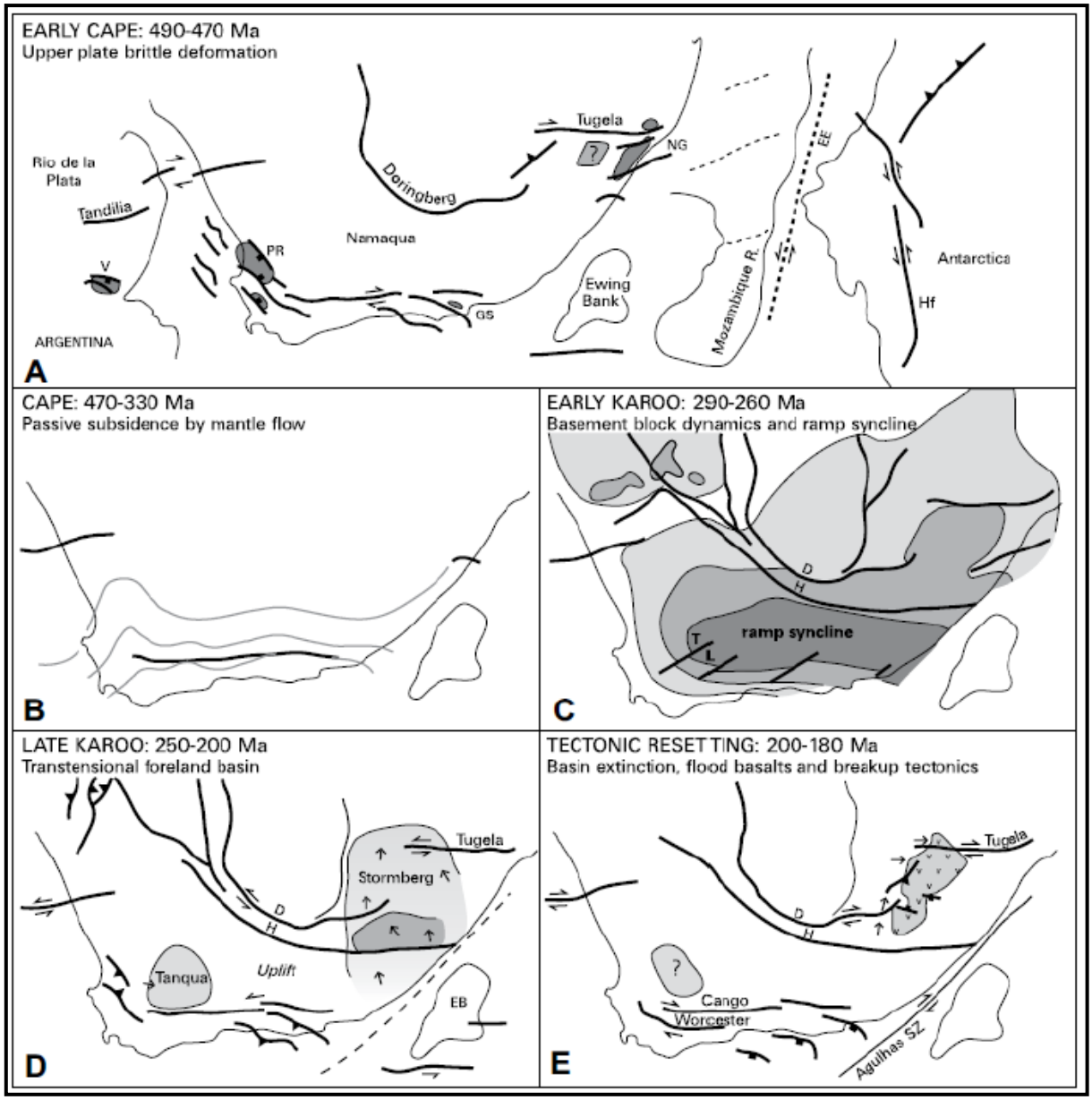

Figure 3.7. Tectonic reconstruction and comparative basin analysis of the Cape and Karoo Basins. **(**A) Strike-slip stepover structures of the Early Paleozoic depocenters. Piekeniers rifts formed in the Rio de la Plata – Namaqua releasing stepover. Antarctic transcurrent shear zones after Jacobs and Thomas (2004). (B) Episutural Cape basin subsidence unaccompanied by brittle failure. (C) Early Karoo subsidence involved decoupled basement blocks and an extensional ramp syncline. (D) Late Karoo tectonism characterized by Namaqua uplift, contemporaneous transtensional subsidence of Natal block, and transpressional uplift of Falkland Plateau–Ewing Bank provenance. (E) Early Jurassic tectonic resetting expressed in Karoo magmatism and breakup rift basins. Arrows show paleocurrents. D, Doringberg fault; EB, Ewing Bank; EE, Explora Escarpment; GS, Gamtoos-Sardinia Bay; H, Hartbees fault; Hf, Heimefront transpressional zone; L, Laingsburg fan; NG, Natal Group; PR, Piekeniers rifts; T, Tanqua fan; V, Ventania (adapted from Tankard et al., 2009).

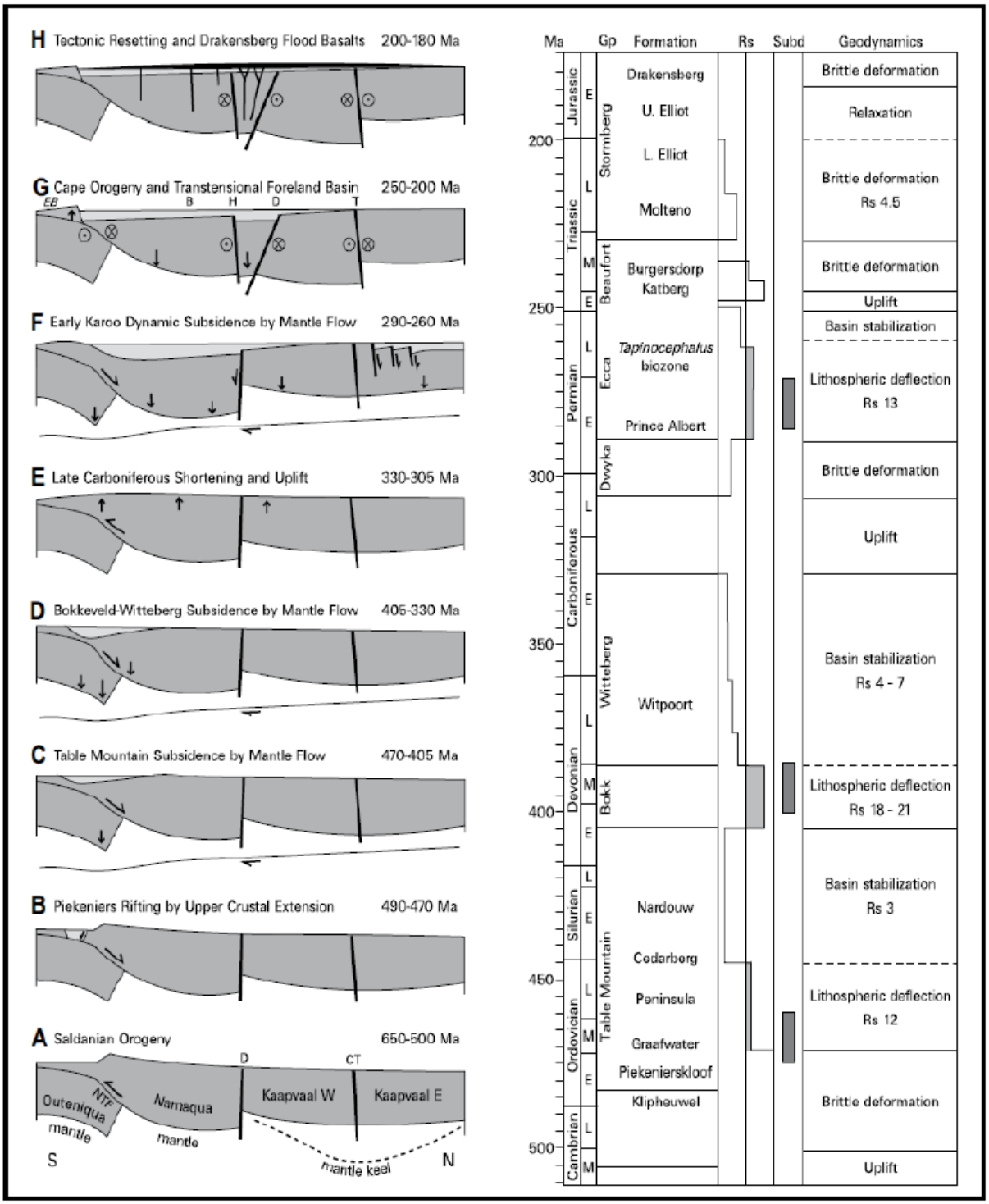

Figure 3.8. Tectonic model evolution, geodynamic history and lithostratigraphy of the Cape and Karoo Basins. The principal episodes of basin formation were (A-D) Saldanian orogeny and Cape basin, (E-F) regional uplift and early Karoo basin (Dwyka-Ecca-lower Beaufort), and (G-H) Cape strike-slip orogeny and late Karoo basin (upper Beaufort-Stormberg) (modified from Tankard et al., 2009).

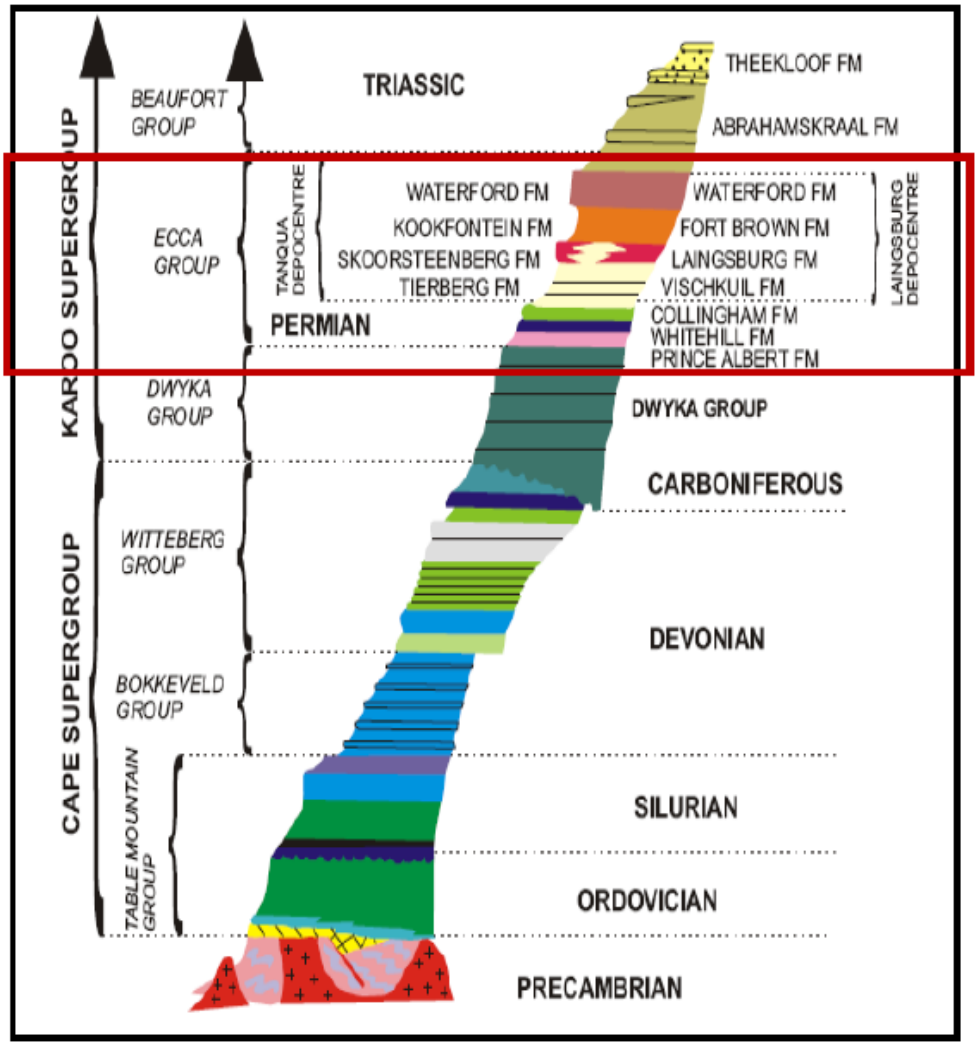

Figure 3.9. Schematic representation of the Cape and Karoo Supergroups stratigraphy in the SW Karoo Basin showing the Tanqua and Laingsburg depocenters (modified after Wickens, 1994). Boxed in red is the Permian Ecca Group.

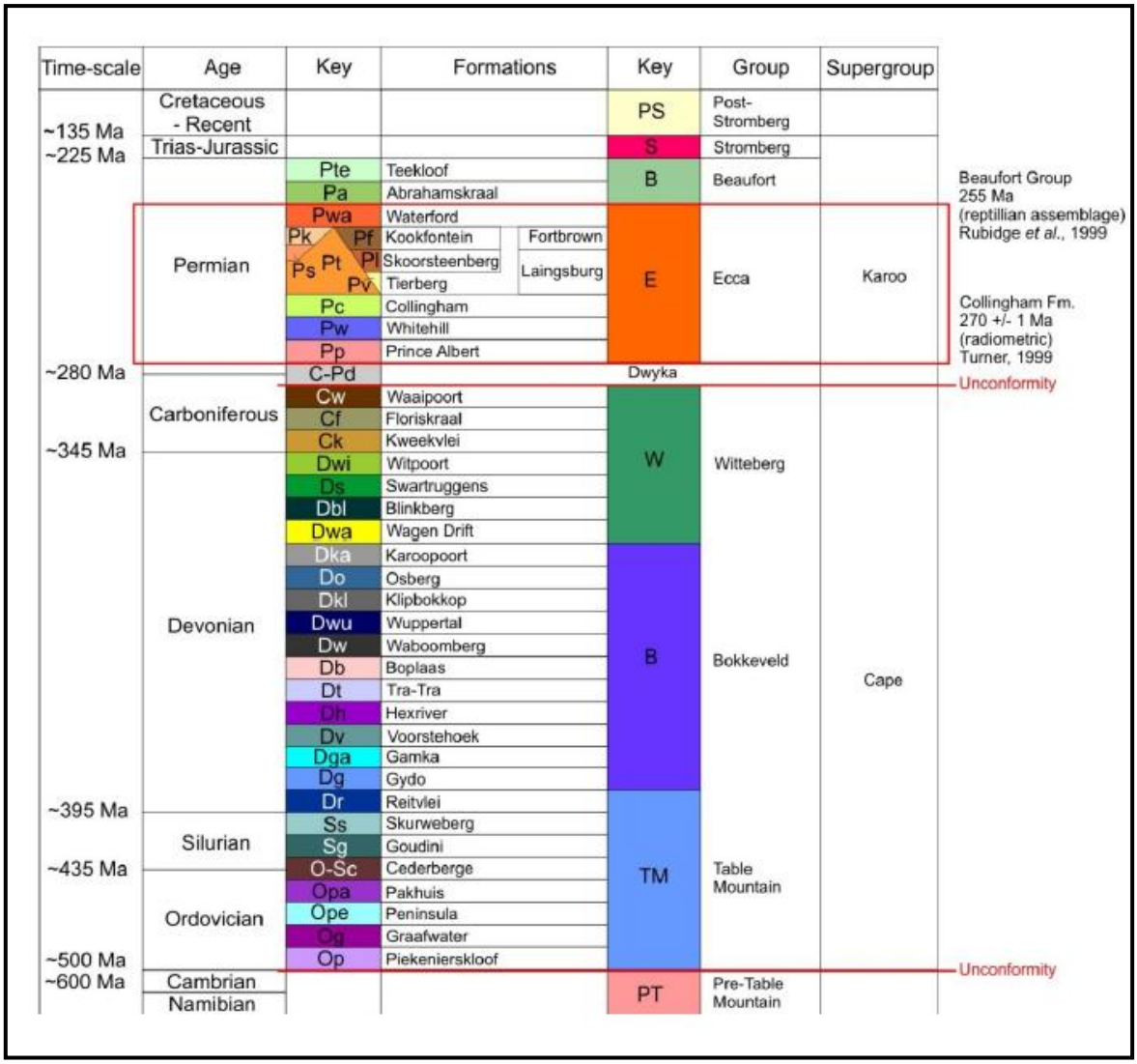

Figure 3.10. Lithostratigraphic column for the Cape Fold Belt (CFB) and SW Karoo basin. Boxed in red is the Permian Ecca Group (modified from King, 2005).

3.2 Stratigraphic succession of the SW Karoo Basin

3.2.1 Tanqua depocentre

In the Tanqua depocentre, the Collingham Formation is overlain by several hundred metres of dark basinal shales (Tierberg Formation) and then the 450 m- thick sand-prone deepwater Skoorsteenberg Formation (Figure 3.11). The overlying deltaic sequence (Kookfontein Formation), shoreface/deltaic (Waterford Formation) and fluvial (Abrahamskraal Formation, Beaufort Group) successions mark the overall progradation of the sedimentary system to the north and east during the mid to late Permian. Six sand-rich turbiditic submarine fan systems (i.e. "Fans" 1-6) have been recognised by the previous workers in the Skoorsteenberg Formation (e.g. Wickens, 1994; Wickens and Bouma 2000; Johnson et al., 2001) with more emphasis on Fans 1-5 (e.g. Johnson et al., 2001; Catuneanu et al., 2002; Van der Werff and Johnson, 2003; Andersson et al., 2004). A recent integrated outcrop and subsurface study clarified this stratigraphy and has shown that "Fans" 5 & 6 are a simple, 100 m-thick lower slope wedge, now termed Unit 5 (Hodgson et al., 2006) (Figure 3.11). The lithostratigraphic unit previously referred to as Fan 5 (Wickens, 1994; Johnson et al., 2001) is now regarded as the sandstone-prone interval of Unit 5, while Fan 6 or the "Hangklip Fan" (Wickens, 1994; Wach et al., 2000) is now recognized to consist the most proximal exposed part of Unit 5 (Hodgson et al., 2006). Wach et al., (2000) suggests that Fan 6 is a slope fan and channel complex that shallows up into deltaic deposits, coincident with decreasing accommodation. The unique combination of large-scale stratigraphy and internal facies architecture (i.e. pinch-out nature of facies which shows lateral variation in thickness) of these fan complexes offer it a good analogue to fine-grained submarine fans (Wickens and Bouma, 2000; Johnson et al., 2001; van der Werff and Johnson, 2003). The base and top of Unit 5 have sharp contacts with the Tierberg and Kookfontein Formations respectively (Figure 3.11).

The Kookfontein Formation is an extremely well-exposed ~250 m- thick deposit with pronounced sedimentary cyclicity of overall thickening upward succession, which represent a continuation of pro-delta sedimentation subsequent to cessation of Skoorsteenberg gravity flow events (IHS Energy, 2009), and changes upward into delta front deposition. The repetition of upward coarsening cycles (Wild, 2005; Wild et al., 2009; IHS Energy, 2009) with anteceded massive and homogenous slump layers reflect rapid progradation with subsequent development of unstable conditions. The abundance of wave ripple marks and bioturbation indicates the overall shallowing of the depositional environment during delta progradation (IHS Energy, 2009).

3.2.2 Laingsburg depocentre

In the Laingsburg depocentre, the Collingham Formation is overlain conformably with a sharp contact by the 200 – 400 m thick Vischkuil Formation i.e. a background mud-rich hemipelagic deposit interrupted by mud-rich and sand-prone turbidites (Wickens, 1994). Overlying Vischkuil Formation is a sand-prone submarine fan complex with a maximum thickness of about 750m i.e. Laingsburg Formation. The Laingsburg Formation is made up of six submarine fan systems usually termed Fans A – F; with each fan being separated by a significantly thick (i.e. about 10 – 90 m) hemipelagic and turbiditic mudstone (Sixsmith et al., 2003) (Figure 3.11). According to Grecula et al. (2003), the term ‘Fan’ is used to distinguish informally a sandstone-dominated unit of deepwater origin, without implication for its geometry. The Fortbrown Formation overlies the Vischkuil Formation with a basal gradational contact at the top of Fan F. It attains a thickness of about 205 m in the Laingsburg area and is interpreted by previous workers (e.g. Wickens, 1994; Sixsmith et al., 2003) as consisting of thickening upward cycles of 2 – 10 m- thick typical of a prograding delta front. This equivalent formation to the Tanqua Kookfontein Formation has not been previously studied in detail. Overlying the Fortbrown Formation are the shoreface/deltaic (Waterford Formation) and the fluvial (Abrahamskraal Formation).

3.2.3 Regional stratigraphic correlation of the SW Karoo Basin

The regional correlation between the Laingsburg depocentre and the Tanqua depocentres has been the focus of many previous structural and stratigraphic workers within the early Permian Karoo Basin. Also, different analytical methods have been employed for examples, lithostratigraphic analysis based on field observations (Wickens, 1994; Flint et al., 2004; King, 2005) and chemostratigraphic analysis (e.g. Scott, 1997; Scott et al. 2000; Andersson et al., 2004). Most of these correlation works are based on the so-called and well-studied sand-prone deepwater submarine fan complexes of the Laingsburg and Tanqua sub-basins and their underlying formations i.e. Collingham, Tierberg (in the Tanqua area) and Vischkuil (in the Laingsburg area) Formations. Correlation based on field observations by Wickens (1994) and Wickens and Bouma (2000) and chemostratigraphy by Scott et al. (2000) suggested that deposition in the two depocentres took place simultaneously. The difference in tectonic impression and basin physiography for the two depocentres has resulted in revision of this earlier interpretation. Most recent correlation by Flint et al. (2004) and King (2005) suggested that sand-prone deepwater depositions in the Laingsburg sub-basin are earlier and thicker than the Tanqua sub-basin (Figures 3.11 and 3.12). Their regional correlations are based on the following arguments:

1. The 10 m-thick regional marker bed i.e. Matjiesfontein chert above the base of the Collingham Formation has a vertical stratigraphic thickness of 270 m to the base of the Laingsburg Formation (i.e. base of Fan A) in the Laingsburg sub-basin whereas it has a vertical thickness of 800 m to the base of Skoorsteenberg Formation's Fan 1 in the Tanqua area.

2. The 12 m-thick claystone correlation marker bed above the Unit 5 of the Skoorsteenberg Formation in the Tanqua is correlated to an equivalent but thicker i.e. 80 m condensed claystone above the Fan 6 of the Laingsburg Formation.

3. Tanqua Fan 1 i.e. the base of Skoorsteenberg Formation is also tentatively and empirically correlated to the top of Laingsburg Fan 6 based on estimated and measured shale thicknesses.

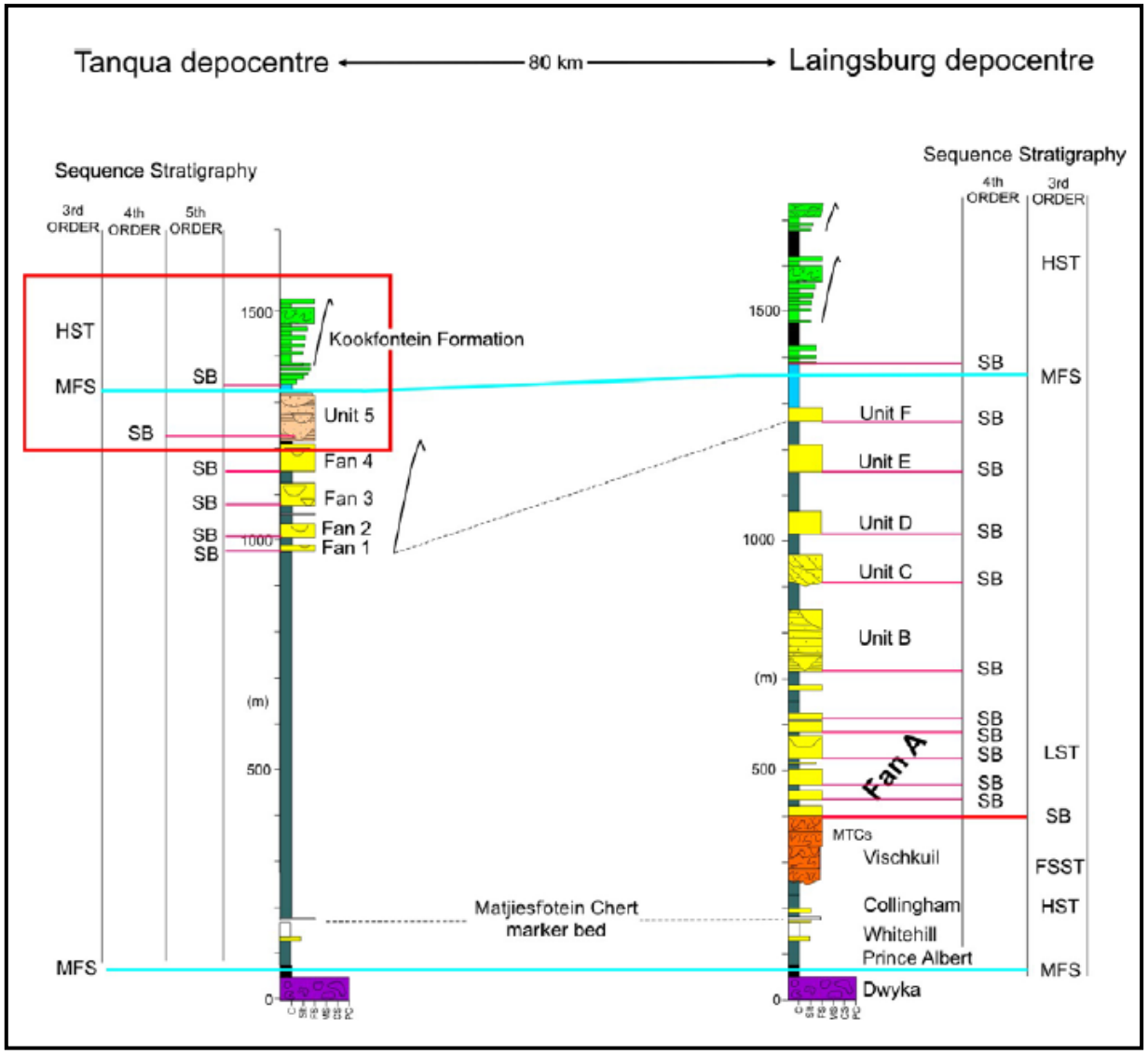

Figure 3.11. Correlation of the Laingsburg and Tanqua successions. Note that deposition of the bulk of the Laingsburg formation deepwater succession is time-equivalent to condensed shale of the deepwater Tierberg Formation in the Tanqua depocentre (from Wild, 2005; after Flint et al., 2004).

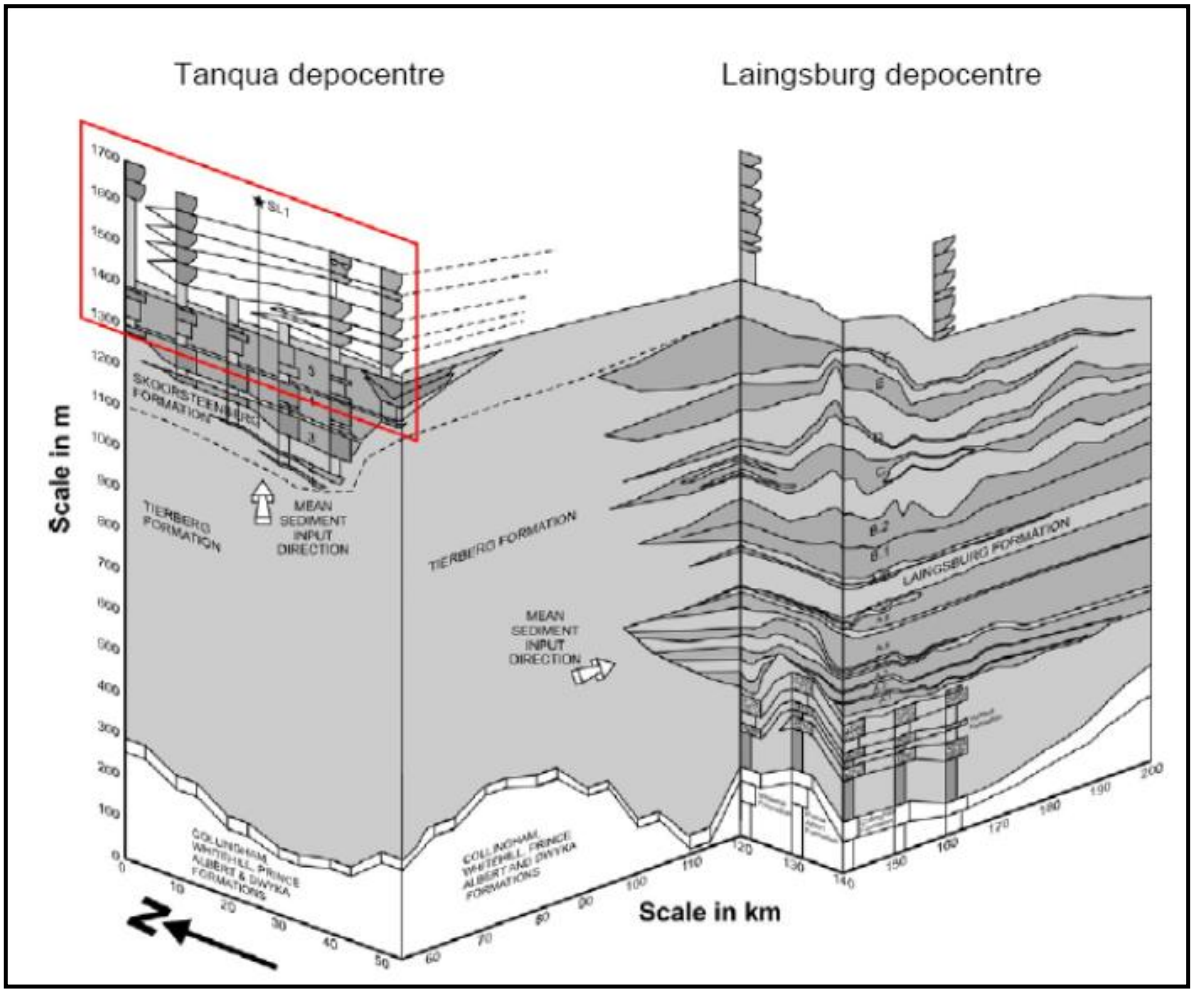

Figure 3.12. Fence diagram showing the revised correlation of the Karoo deepwater stratigraphy between the Laingsburg and Tanqua depocenters (Flint et al., 2004; King, 2005). Boxed in red are Unit 5 and Kookfontein Formation.

The above line of argument suggests that the bulk of deepwater sedimentation in the Laingsburg sub-basin is older than the equivalent deepwater deposit in the Tanqua sub-basin (Flint et al., 2004; King, 2005). According to the fence diagram by these authors, the deltaic successions on top of the submarine fan systems in the two depocentres have not been correlated. A better constraint on the dominant depositional controls that are responsible for the stratigraphic evolution of these two depocentres is to a large extent dependent on the accurate and detailed regional correlation.

3.3 Provenance

The Karoo Basin of South Africa has been the focus of many provenance studies involving very detailed field and laboratory data; and yet it appears that there is still no consensus on the source and sediment routing system of the sedimentary sequence that filled the basin. However, most of these studies have contributed immensely to our present understanding of the Karoo Basin provenance. The conventional objective of any provenance studies is to reconstruct and interpret the history of sediment supply from source to basin; right from initial erosion of a parent rock to the burial of its detritus and so to eventually deduce the characteristics and location of the source area (Andersson et al., 2004; Nichols, 2009). Therefore, understanding the evolutionary trend of sedimentary succession through time will allow a better constraint on factors such as nature of source area, drainage pathway and transport route, relief, climate and tectonic setting which govern the temporal and spatial distribution of facies in a sedimentary setting. It will also allow delineation between depositional parameters and post-depositional diagenetic processes in deducing the evolution and distribution of petrophysical properties in a sedimentary succession.

Most of the early workers on the provenance studies of the Karoo Basin (e.g. Elliot and Watts, 1974; Lock, 1980; Cole, 1992; Veever et al., 1994) believed that both the Ecca and Beaufort Groups of the basin were sourced from the Cape Fold Belt (CFB) except Johnson (1991) who held a contrary opinion. Johnson (1991) studied the sandstone petrography of the Ecca

Group and the lower Beaufort Group (i.e. Adelaide Subgroup) in the southern part of the Karoo Basin and proposed that these successions were sourced from a southern magmatic arc south of the Cape Fold Belt (see Figure 3.4). Later thereafter, Adelmann and Fielder (1998) proposed a revised interpretation based on petrographic studies and suggested that the upper Ecca and lower Beaufort Groups are sourced from the CFB together with an active magmatic arc to the south of the CFB. Electron microprobe studies of the detrital heavy minerals such as garnet, tourmaline and biotite in sandstones from the Skoorsteenberg Formation in the Tanqua area, Vischkuil (equivalent to the Tierberg Formation in the Tanqua area) and Laingsburg Formations in the Laingsburg area by Scott (1997) and Scott et al. (2000) indicate a mixed high-grade metamorphic and granitic provenance with a long transport route from the south of the present CFB. He proposed that this source was located between the magmatic arc on top of the subduction zone and the rising but still submerged fold-thrust belt (CFB). Sm-Nd isotopic analysis based on six sandstone samples from the Skoorsteenberg Formation by Andersson et al. (2003) suggest that the probable source terrain for the sandstones of the Tanqua submarine fan complexes is a late Palaeozoic thrust-belt and a magmatic arc to the south (Figure 3.4).

Petrographic and geochemical studies of the SW Karoo sandstones from Tanqua and Laingsburg depocentres by Van Lente (2004) and tectonic model/structural reconstruction of the CFB by King (2005) suggest that the Cape Fold Belt was not substantially emergent at the time of deepwater deposition (Figure 3.13). Van Lente (2004) proposed that geochemically the sediments of the Tanqua and Laingsburg sub-basins were derived from the same granitic source and deposited in an active continental margin setting, and identified the North Patagonian Massif in South America (presumably south of the present CFB) (Figures 3.4 and 3.13) as the most suitable source area for the sandstones of the SW Karoo sub-basins. Sediment supply was routed first to the Laingsburg depocentre but a tectonic uplift of the De Doorns synclinorium caused a switch in sediment transport to the Tanqua depocentre (King, 2005) (Figure 3.13). King (2005)

proposed a long sediment transport route by a pre-Atlantic Ocean of about 600km from the source area to the Karoo Basin.

However, the most recent chemostratigraphy and provenance study of the sandstones of the Tanqua and Laingsburg submarine fan systems by Nguema (2005) suggest a wide range of igneous provenance. Nguema (2005) proposed a volcano-plutonic source based on the abundance of fine to very angular grains and albitic feldspar of volcanic origin as well as the predominance of volcanic zircons; and therefore identified the late Carboniferous-Permian to Triassic Choiyol volcanic-transitional magmatic arc of northern Patagonian (Figure 3.13) as the main source of the detritus that filled the Tanqua and Laingsburg sub-basins, while the plutonic North Patagonian Massif rock suites (Van Lente, 2004; King, 2005) are part of the possible secondary sources. Nguema (2005) also argued that the abundance of fine to very fine angular grains is indicative of textural immaturity and hence, short sediment transport route as opposed to the long transport route proposed by King (2005).

Although the tectonic evolution reconstruction model of the Cape and Karoo Basins of South Africa proposed by Tankard et al. (2009) corroborates previous provenance studies (e.g. Johnson, 1991; Scott, 1997; Scott et al., 2000; Andersson et al., 2003; Van Lente, 2004; King, 2005; Nguema, 2005) which suggest that the sedimentation of the Permian early Karoo Basin (i.e. Dwyka, Ecca and lower Beaufort Groups) predates the CFB; the tectonic model on which these previous provenance studies are based (i.e. retro-arc foreland system) differs from the tectonic model proposed by Tankard et al. (2009). According to this revised tectonic model by Tankard et al. (2009), the timing of the CFB occurs during the late Karoo Basin (i.e. Triassic-early Jurassic), and therefore CFB could only have been part of the source of the upper Beaufort and Stormberg Groups.

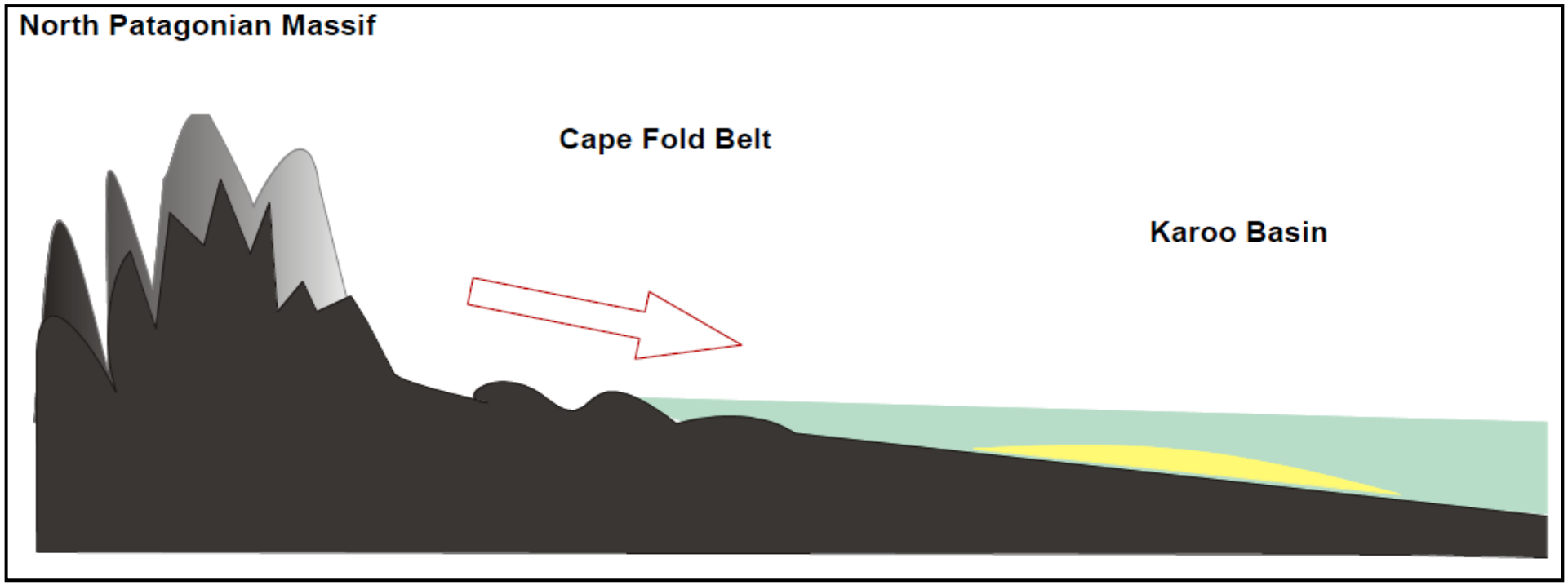

Figure 3.13. Transportation from the source (North Patagonian Massif presumably south of the present Cape Fold Belt) in part through actively deforming but not exposed Cape Fold Belt to the depository (first Laingsburg depocentre then Tanqua depocentre) of the southwestern Karoo Basin (modified from King, 2005).

CHAPTER FOUR

FACIES ANALYSIS

4.1 Stratigraphic elements and depositional sequence hierarchy

The stratigraphic elements which defined the Kookfontein deltaic succession at the Pienaarsfontein type-locality reflect a depositional hierarchy that ranges from cycle (stratigraphic-scale/facies succession, 35 - 49 m), bedsets (lithofacies-scale 0.2 – 30 m), beds (depofacies 0.01 – 1.2 m) to laminae (<0.01 m) in decreasing order over a total stratigraphic thickness of 250 to 285 m (see Table 4.1). The largest stratigraphic elements (i.e. cycles) were grouped into two stratigraphic members namely: Lower member (i.e. cycles 1-5) and Upper member (i.e. C6-13) based on differences in depositional style (Figure 4.1). The depositional features employed for this grouping are: stratigraphic thickness (i.e. variation in cycle thicknesses) and sediment stacking pattern. The lower member has a mean thickness of 37 m with an overall progradational stacking trend; while the upper member has a mean thickness of about 11 m with an overall progradational to aggradational stacking pattern. The vertical succession of these elements and their internal sedimentary structures both in time and space initially depicts all scales of heterogeneity with pronounced sedimentary cyclicity. The word ‘cyclicity’ is used to indicate a rather regular repetition of sedimentary features. The term ‘depofacies’ denotes a body of rock with internally uniform sedimentary features and forms the basic element for facies analysis and modelling, i.e. reconstruction of an ancient depo-system.

4.2 Facies distribution from measured outcrop logs

Twelve sedimentary depofacies based on texture and sedimentary structures were recognised and described in detail. These are then broadly grouped into four main facies associations

Table 4.1. Variation in the major stratigraphic element thicknesses (i.e. cycle and bedset) along basinwards cross-sectional profile (i.e. VS2-VS3-VS4-VS1).

	VS2		**VS4**		**VS3**		**VS1**	
	Cycle (m)	Depofacies (Bedset) (m)	Cycle (m)	Depofacies (Bedset) (m)	Cycle (m)	Depofacies (Bedset) (m)	Cycle (m)	Depofacies (Bedset) (m)
C1	41.4	0.9 - 20.75	28.4	1.35 -14.1	41.4	1 - 26.9	32.15	1 - 21.2
C2	29.6	0.2 - 19.85	25.3	5.4 - 11.25	32.4	1.4 - 24.1	39.06	0.5 - 25.2
C3	45.6	5.5 - 40.15	35.4	2.3 - 26.25	41.9	1.9 - 28.45	35.6	4.9 - 30.7
C4	35.2	5.45 - 23.05	24.2	2.3 - 17.9	46.7	1.8 - 32.45	49.3	3.85 - 30.4
C5	36.7	2.3 - 24.9	35.9	9 - 13.6	36.2	8.6 - 15.75	38.25	8.5 - 20.7
C6	18.9	2.2 - 9.6	10.05	0.3 - 5	7.15	1.45 - 2.95	13.35	2.45 - 7.8
C7	14.15	1.3 - 8.05	11	3.55 - 7.45	11.7	2.2 - 5.8	5.5	1.2 - 3
C8	5.9	0.6 - 2.85	14.5	1.35 - 7.2	10.6	1.2 - 5.7	10.3	3.1 - 3.9
C9	10.35	4.35 - 6	9.6	3 - 6.6	14.6	0.85 - 10.9	2.8	0.5 - 2.3
C10	10.6	2 - 8.6	13.2	1 - 9.2	12.15	4.85 - 7.3	3.7	0.55 - 3.15
C11	5.2	3.6 - 5.2	10.2	2.8 - 7.4	9.4	3.8 - 5.6	10.2	1.2 - 7.7
C12	13.1	4.85 - 8.25	17.6	1.3 - 10.6	11.2	2.4 - 8.8	14.5	3.55 - 6.8
C13			16.9	3.7 - 13.2	12.5	5.4 - 7.1	7.65	0.8 - 4.95

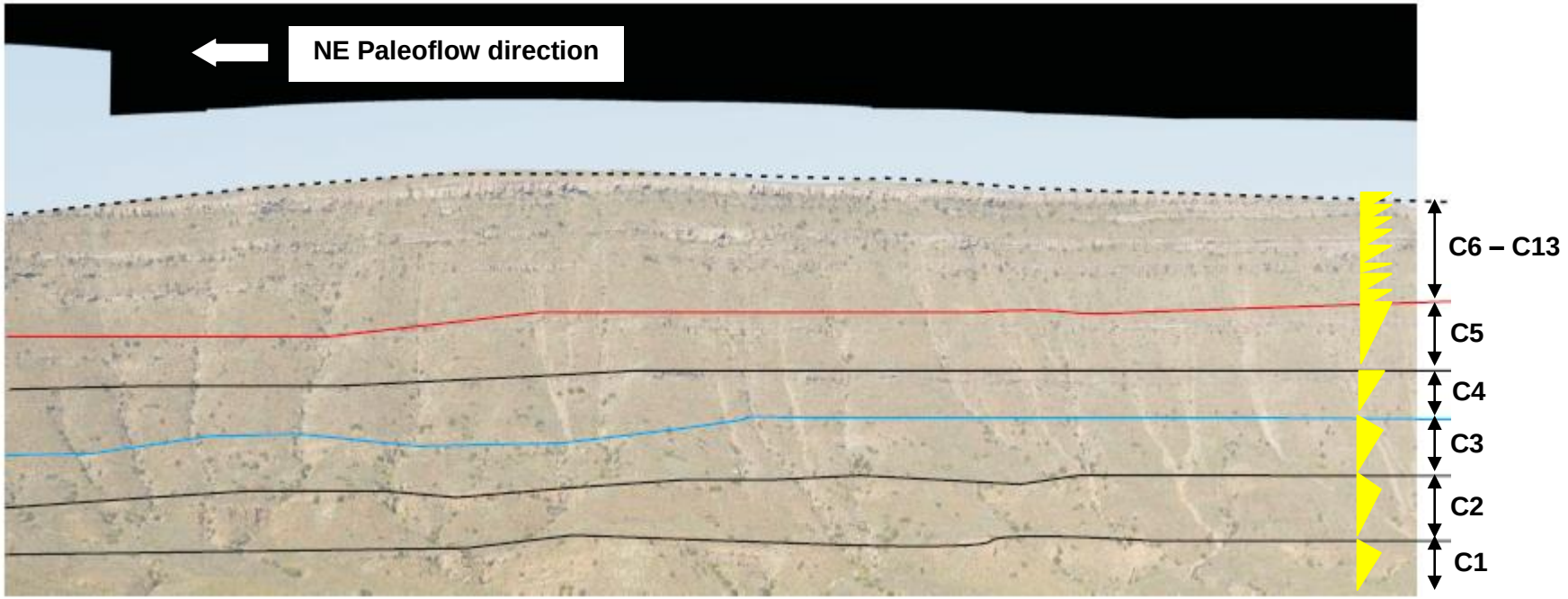

Figure 4.1. Outcrop photomosaic showing Kookfontein cycles i.e. Lower member: cycles 1 to 5 and Upper member: cycles 6 to 13 at the Pienaarsfontein locality.

based on lithological characteristics (i.e. texture and sand to clay ratio) and depositional processes (sedimentary structures). These associations are: (1) sandstone facies (depofacies 10, 11 and 12); (2) heterolithic facies (i.e. alternations of siltstone and sandstone: depofacies 2, 3, 4, 5, 6, 7 and 8); (3) soft-sediment deformation facies (depofacies 9A and 9B); and (4) mudstone facies (depofacies 1) (Table 4.2). Sandstone facies, heterolithic facies, soft-sediment deformation and mudstone facies represent 39%, 37%, 23% and 1% respectively, of the described facies in the studied stratigraphic succession (Figures 4.2a and 4.2b). Figures 4.3 and 4.4 show the variations in the proportion of each of the twelve depofacies for the lower and upper Kookfontein stratigraphic members along basinwards cross-sectional profile. Complete description and interpretation of all facies are given in Table 4.2.

4.3 Sedimentology and depositional environments

4.3.1 Facies model

The combination of detailed facies analysis (i.e. based on texture and sedimentary structures; Figure 4.5) and existing facies models for universal classification of delta systems (Postma, 1990; Bhattacharya, 2006) form the basis for establishing a hypothetical ‘descriptive’ facies model that depicts the distribution of facies, their geometry and architecture in three dimensions (Figure 4.6). This model is based on the generally accepted criteria for classifying deltas i.e. (1) feeder system, (2) depth ratio, (3) river-mouth processes, particularly effluent or jet-types, and (4) basin dynamics (i.e. reworking processes by waves, tides and gravity). Each facies succession (i.e. cycle) in the studied stratigraphic interval represents a clinothem bounded above and below by a flooding surface marked by mudstones and thinly laminated siltstones. The internal architecture and geometry of each clinothem is reconstructed by detailed lateral correlation of facies from west to east (Figure 4.5) along the dominant NE

Table 4.2. Sedimentary facies described and interpreted depositional characteristics.

Depofacies	Lithology	Sedimentary structures	Facies thickness	Lithofacies association	Bioturbation	Sand:Silt ratio	Notes
1	Mudstone	Structureless	0.2m to 1m	Mudstone			Prodeltaic hemipelagic deposition probably by long period of suspension settling
2	Interbedded very fine-grained sandstones and siltstones	Parallel lamination with occasional current ripple lamination; Bedding (very thin to thin)	5.2m at Western section	Heterolithic		55% : 45%	Proximal prodeltaic sedimentation by alternating suspension settling and probably gravity-driven hyperpycnal flow/low-density turbidity current
3	Interbedded very fine-grained sandstones and siltstones	Horizontal lamination to unidirectional current ripples; Bedding (very thin to thin)	2.4m to 3.9m	Heterolithic	Weak	Same as above	This deposition occurred below storm wave base and dominated by inertia/buoyancy and is interpreted as the transitional between proximal prodelta and distal undeformed delta front
4	Interbedded very fine to fine-grained sandstones and siltstones	Unidirectional current ripples with occasional parallel lamination; Bedding (very thin to thin)	4.5m to 8.8m	Heterolithic	Moderate	60% : 40%	Same as above; but with more reworking by current ripples and organic activities
5	Interbedded very fine to fine-grained sandstones and siltstones	Current to wave ripple lamination with small-scale swaley cross-stratification; Bedding (very thin to thin)	2.6m to 14.25m	Heterolithic	Moderate	Same as above	Distal delta front sedimentation with variable reworking by current and wave ripples as well as organic activities; sand deposition is by gravity-driven hyperpycnal flow/inertia and buoyancy
6	Fine-grained sandstones with siltstones	Current to wave ripple lamination with low-angle planar lamination and small-scale swaley cross-stratification (SCS); Bedding (very thin to thin)	2.7m to 5.95m	Heterolithic	Moderate	70% : 30%	Mid-delta front sedimentation below fair weather wave base and above storm wave base. Variation in wave amplitude and sinuosity on different bed surfaces is indicative of fluctuation in wave energies
7	Fine-grained sandstones with siltstones	Planar cross-stratification with wave to current ripples and occasional parallel lamination and SCS; Bedding (thin to thin)	0.8m to 30.7m	Heterolithic		65% : 35%	Same as above
8	Fine to medium-grained sandstones with siltstones	Low-angle planar lamination with wave ripples Bedding (thin to medium)	1.5m to 5m	Heterolithic	Moderate to Intense	80% : 20%	Same as above

Table 4.2. (Continued)

Depofacies	Lithology	Sedimentary structures	Facies thickness	Lithofacies Association	Bioturbation	Sand:Silt ratio	Notes
9A	Soft-sediment deformed sandstones and siltstones (Slump)	Homogenous fine sand/silt with slump fold	4m to 6.5m	Soft-sediment deformation		60% : 40%	This represents product of intense soft-sediment deformation involving horizontal gliding of sediments due to delta front instability and mass transport of sediments under gravity over the shelf break
9B	Soft-sediment deformed sandstones and siltstones (Loading/Dewatering structures)	Homogenous sand and silt with load casts (i.e. fine to medium sand bulbous structures) and flame structures (i.e. very fine sand to silt injectites)	3.35m to 18.2m	Soft-sediment deformation		Same as above	Intense and localised soft-sediment deformation with no horizontal movement, resulting from rapid loading of coarser sediments over finer sediments under gravity effect
10	Fine to medium-grained bedded sandstones	Low-angle planar cross-stratification with wave bedforms; Bedding (medium to thick)	0.51m to 1.55m	Sandstone		90-100% sand	Delta front sandstones deposited by friction i.e. bedload features at or just below fair weather wave base.
11	Medium-grained amalgamated bedded sandstones	Massive to planar cross-bedding with wave bedforms and very rare horizontal lamination	3m to 6.2m	Sandstone		Same as above	Proximal river-dominated delta front sandstones probably deposited as bedload to gravity-driven hyperpycnal flow in subaqueous setting; also sediments are being reworked by wave ripples
12	Medium-grained amalgamated sandstones interbedded with sand/silt interbeds	Massive to planar cross-bedding with wave bedforms and very rare horizontal lamination	5m (northeastern section)	Sandstone	Moderate	90% : 10%	Same as above

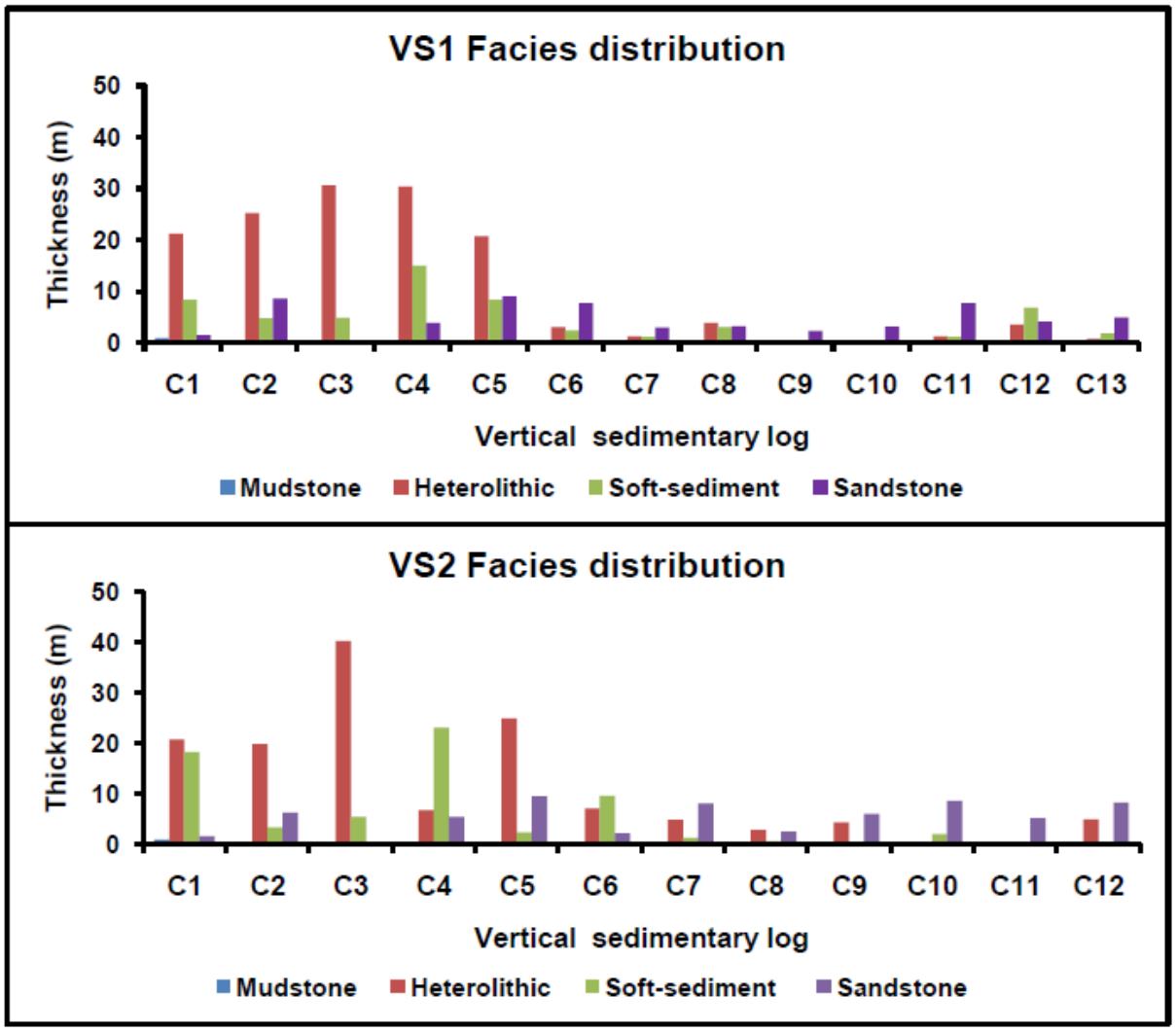

Figure 4.2a. Variation in the proportion (thickness) of facies associations for each cycle along measured vertical sedimentary logs (VS1 and VS2).

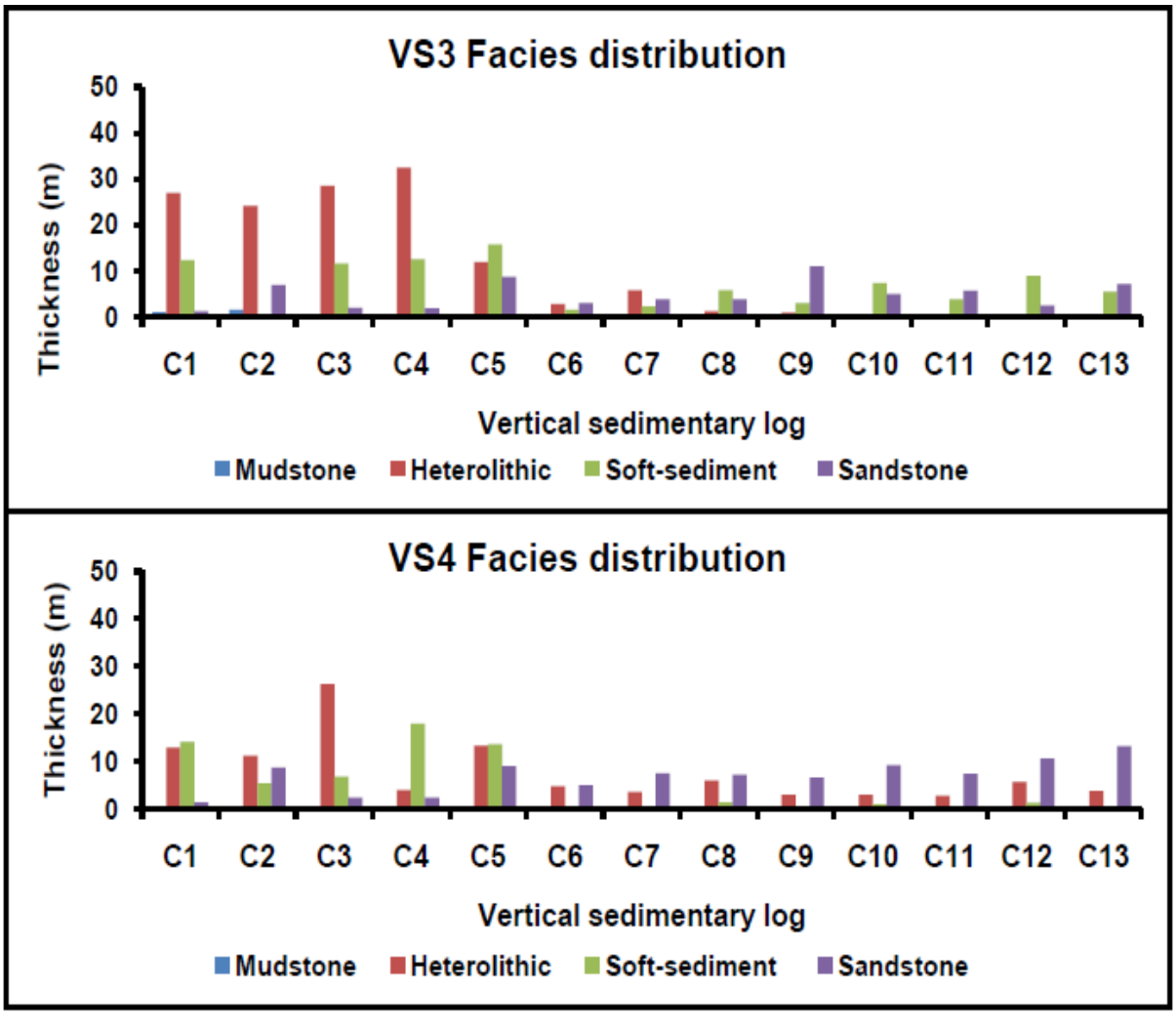

Figure 4.2b. Variation in the proportion (thickness) of facies associations for each cycle along measured vertical sedimentary logs (VS3 and VS4).

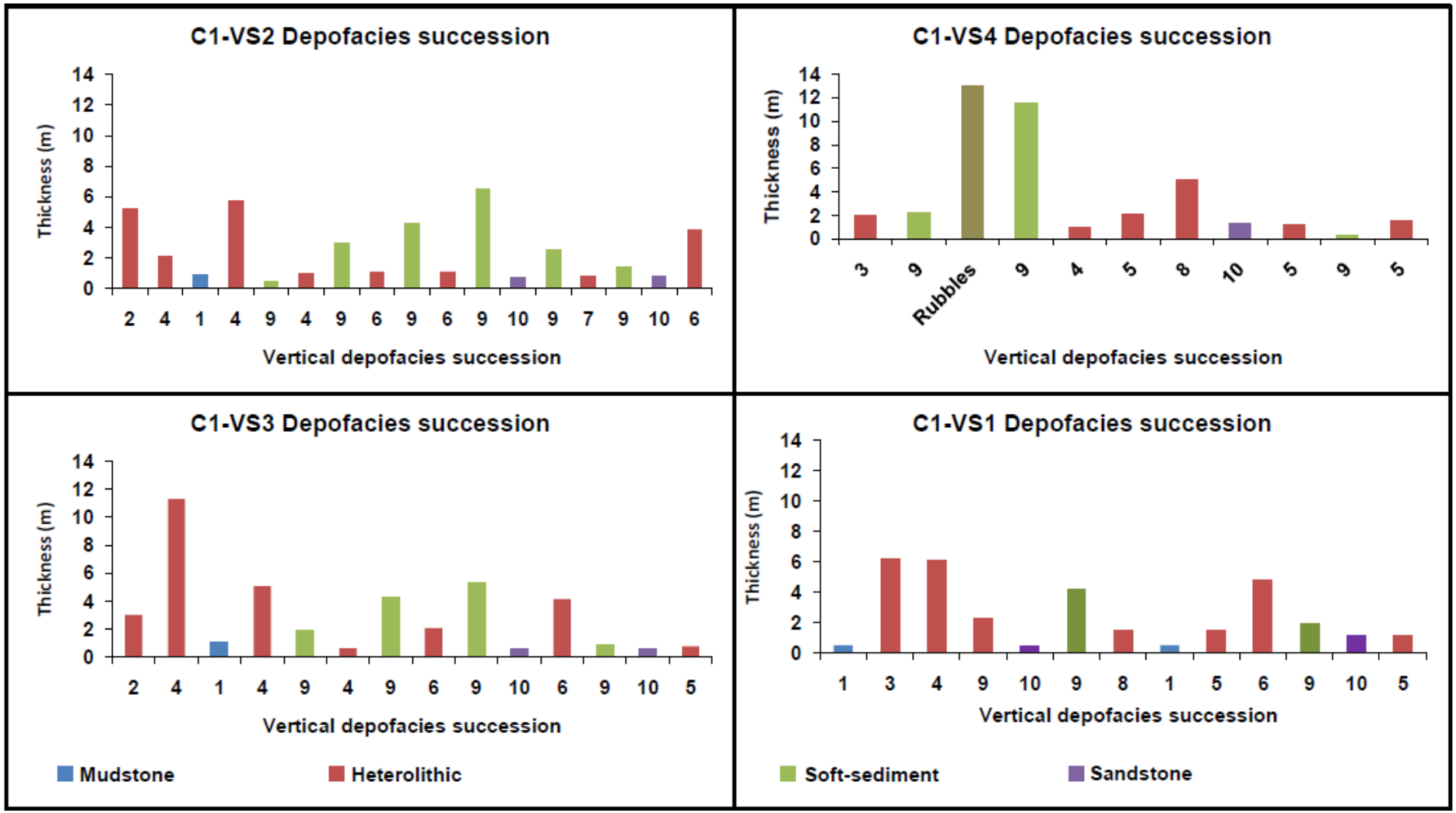

Figure 4.3. Example of basinwards (i.e. VS2-VS4-VS3-VS1) variation in the vertical succession of depofacies within each sedimentary cycle for the lower Kookfontein stratigraphic Member (i.e. cycles 1 – 5). Note the high proportion of soft-sediment deformation (i.e. slope instability processes e.g. gravity and sediment loading) within the lower Kookfontein stratigraphic member and its decrease basinwards.

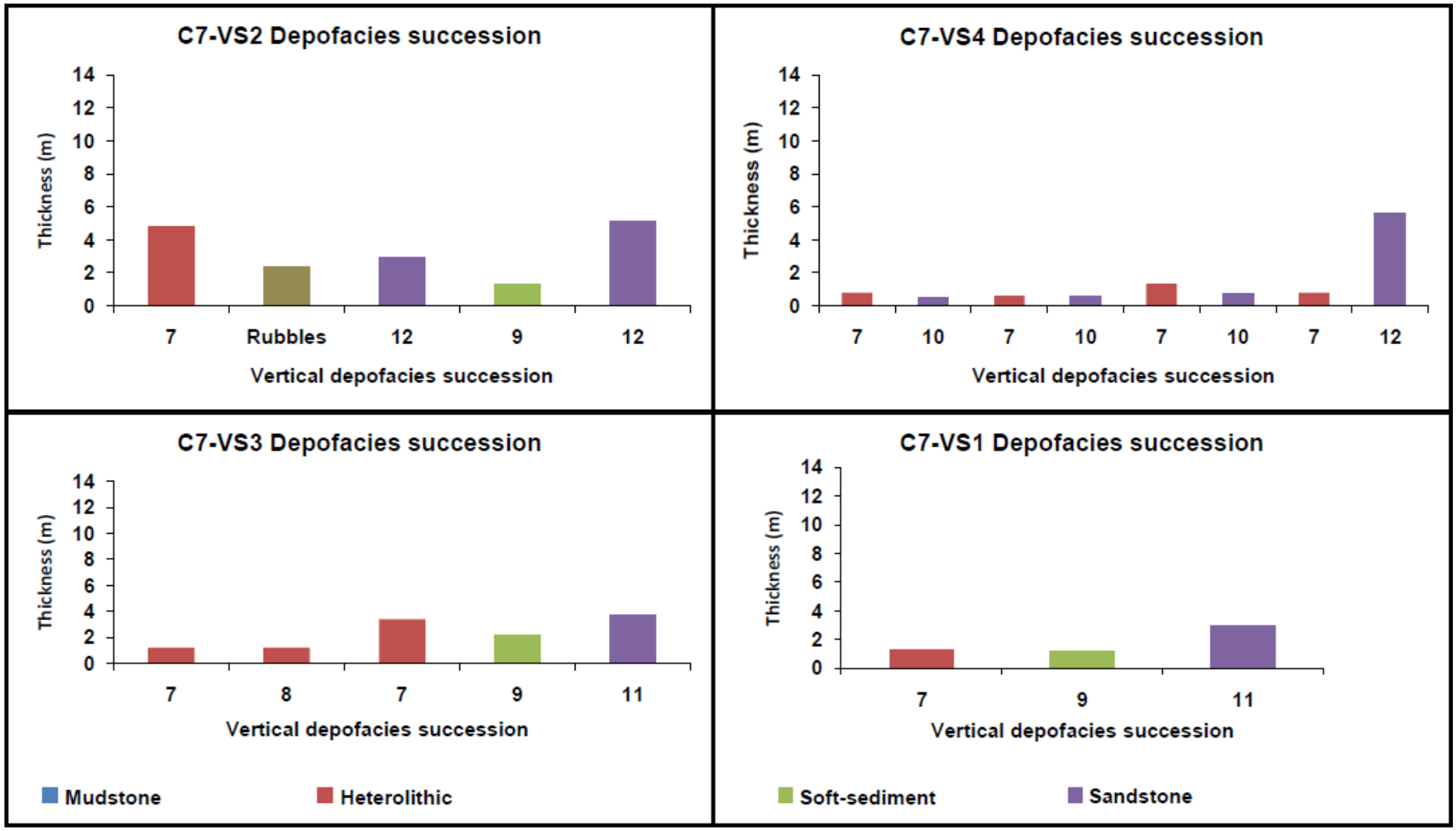

Figure 4.4. Example of basinwards (i.e. VS2-VS4-VS3-VS1) variation in the vertical succession of depofacies within each sedimentary cycle for the upper Kookfontein stratigraphic Member (i.e. cycles 6 – 13). Note the low proportion of soft-sediment deformation (i.e. slope instability processes e.g. gravity and sediment loading) within the upper Kookfontein stratigraphic member and its decrease basinwards indicative of more shelfal depositional environment above or relatively close to the Kookfontein shelf-edge.

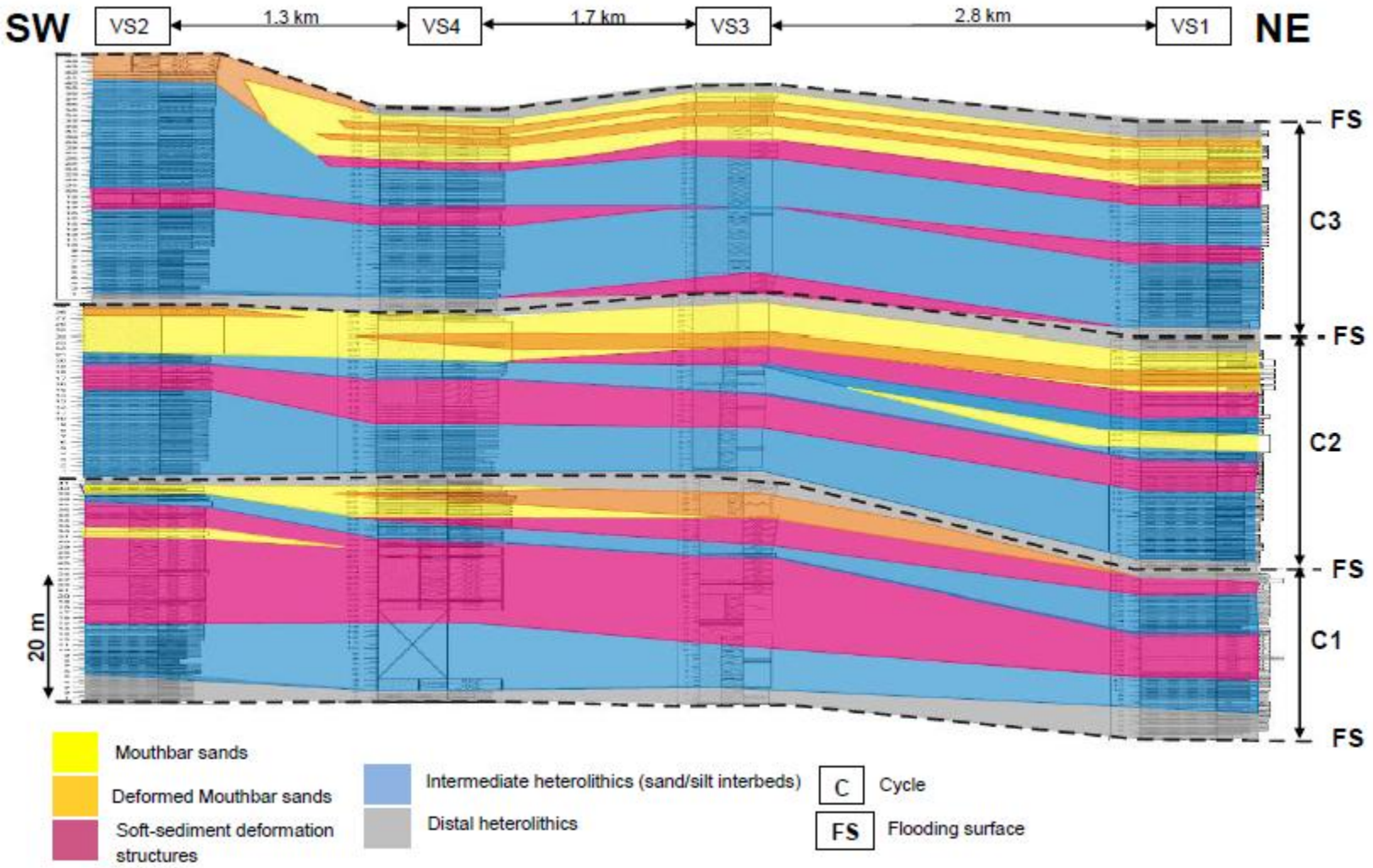

Figure 4.5. Interpreted correlation panel of the lower sedimentary cycles of the Kookfontein deltaic succession (i.e. cycles 1 to 3) observed at the Pienaarsfontein locality oriented parallel to the main paleocurrent direction (i.e. NE). This correlation is based on the four facies associations observed within each facies succession (i.e. cycle).

paleoflow direction measured from unidirectional current ripples. If the vertical facies variations across subsequent cycles reflect lateral facies equivalents within a cycle then the upward change in features – decrease in gravitational effects, increase in wave reworking, and decrease in slope gradient of subsequent cycles – reflects a natural delta progradation (see Figures 4.6 and 4.7). The overall decrease in Kookfontein cycle thicknesses at the Pienaarsfontein locality would then indicate that the vertical sequence covers only the top part of the Kookfontein clinoforms, i.e. from mid-slope to shelf-margin (Figures 4.7, 4.8a and 4.8b). This hypothesis is further supported by vertical facies successions through cycle 1 - 13 (Figures 4.9, 4.10, 4.11 4.12 and 4.13) which reflect a lateral succession from distal (i.e. deeper facies starting at mid-slope) to proximal (i.e. shallower facies ending at top-slope/shelf-margin to outer shelf). The outer shelf to shelf-margin/top-slope is then dominated by: coarser grains, frictional forces, *in situ* soft-sediment deformation structures (with virtually no horizontal movement (Oliviera et al., 2010), i.e. loadcasts, flames and dewatering structures); alternation of rounded- and sharp- crested wave reworked bedforms; current ripples; and moderate to intense bioturbation (Figure 4.7). The mid-slope comprises: finer grains, inertia/buoyancy, slumping (i.e. resulting from some horizontal downslope movement of sediments), *in situ* soft-deformation structures; less wave rippled bed-tops; hummocky; horizontal/current ripple laminations; and weak to moderate bioturbation (Figure 4.7).

This organisation of facies suggests that deposition of these clinothems results from: (1) primary sedimentation of prograding mouthbars governed by stream flow dynamics, and (2) secondary remobilisation of sediments immediately basinwards of river outlets due to rapid loading of sediments under gravity (Figure 4.). The prograding mouthbars for each clinothem coalesce to form a seemingly uniform delta front (i.e. both the topset and foreset strata) which constitutes of the primary deposition by means of traction. The prodelta is governed by

secondary deposition by means of suspension beyond the influence of gravitational and wave reworking processes. The ensuing Kookfontein clinoforms would then consist of a topset (i.e. massive to planar cross-bedded coarse mouthbar sandstones interlayered with localised loadcasts, flames and dewatering structures), basinwards and eastwards dipping foreset (i.e. fine-grained sandstone and siltstone interbeds with interlayered slumps, loadcasts, flames and dewatering structures) and parallel laminated bottomset (i.e. mudstones and thinly laminated siltstones and possibly low-density turbidites). Although, this clinoformal geometry corresponds to the basin-margin (i.e. 'outer shelf-shelf edge-slope') successions previously described by Wild (2005), its usage in this work does not relate to tectonic plate margin setting.

According to the estimated water-depth for the Permian Tanqua-Karoo and the observed sedimentary structures and textures in the field, Postma (1990)'s gravitationally modified deepwater Gilbert-type delta is the closest norm to the Kookfontein delta system. The delta front is therefore a prograding Gilbert-type mouthbar which builds out over the shelf break, and consists of confined channelized flow deposits (i.e. bedload features governed by frictional forces) at the river outlet and channelized to unconfined sheet flow deposits downstream (i.e. bedload and suspended-load features governed by inertial and buoyant effluent dynamics) (Figure 4.7). A low-gradient (i.e. fine sand and silt- dominated) feeder system D of Postma (1990) is observed in this formation. The estimated basin-margin clinoform profile with relatively low slope angle of $0.5\text{-}1^{0}$, water depth of 150-200 m (Wild et al., 2009) and slope length of approximately 17-20 km corroborates this hypothesis. Although all general delta classifications for ancient delta systems (i.e. the ternary "river-, wave- and tide-dominated" diagram by Galloway (1975) or its version extended with grain size proportion by Orton and Reading (1993) and Postma's (1990) prototype deltas- based on feeder system, water depth and gravitational reworking) offer a useful guide for field

observations and interpretations, our ‘descriptive’ model (Figures 4.6 and 4.7) presents a refinement of the existing models for our specific delta. The studied stratigraphic succession is bottomed at the centre (i.e. thickest) part of the Kookfontein clinoforms (Figure 4.7).

Since there is no evidence for sub-aerial exposure in the studied stratigraphic interval, two sub-aqueous lateral profiles are constructed with each representing the major flooding event that deposits the lower and upper Kookfontein members respectively. The first hypothetical model (i.e. the lower Kookfontein member’s flooding event) (Figure 4.8a) consists of lateral succession of structures basinwards from cross bedding to low-angle stratification, sharp- to broad- crested wave ripples, soft-sediment deformation, unidirectional current ripples, swaley cross-stratification and horizontal lamination when the water level is just above the Kookfontein shelf–edge location. The second hypothetical model (for the upper Kookfontein member) (Figure 4.8b) consists of similar sedimentary structures but now with differences in terms of depth of location, position relative to shelf edge, slope gradient, gravity processes and water depth. In the second model, the water level is now above the shelf edge and outer shelf, and there is a reduction in slope gradient and gravity processes.

In the two scenarios, the clean, well-sorted sands transported in distributary channels accumulate at the delta front and form a mouth-bar that passes basinwards laterally into heterolithic facies (i.e. sand and silt interbeds) and prodeltaic mudstone facies. Landwards, as the system gets flooded the mouth-bar sands would be onlapped by basinwards prograding mudstones from the delta top. These standard facies models therefore enable the characterisation and prediction of the relationship between different stratigraphic elements in

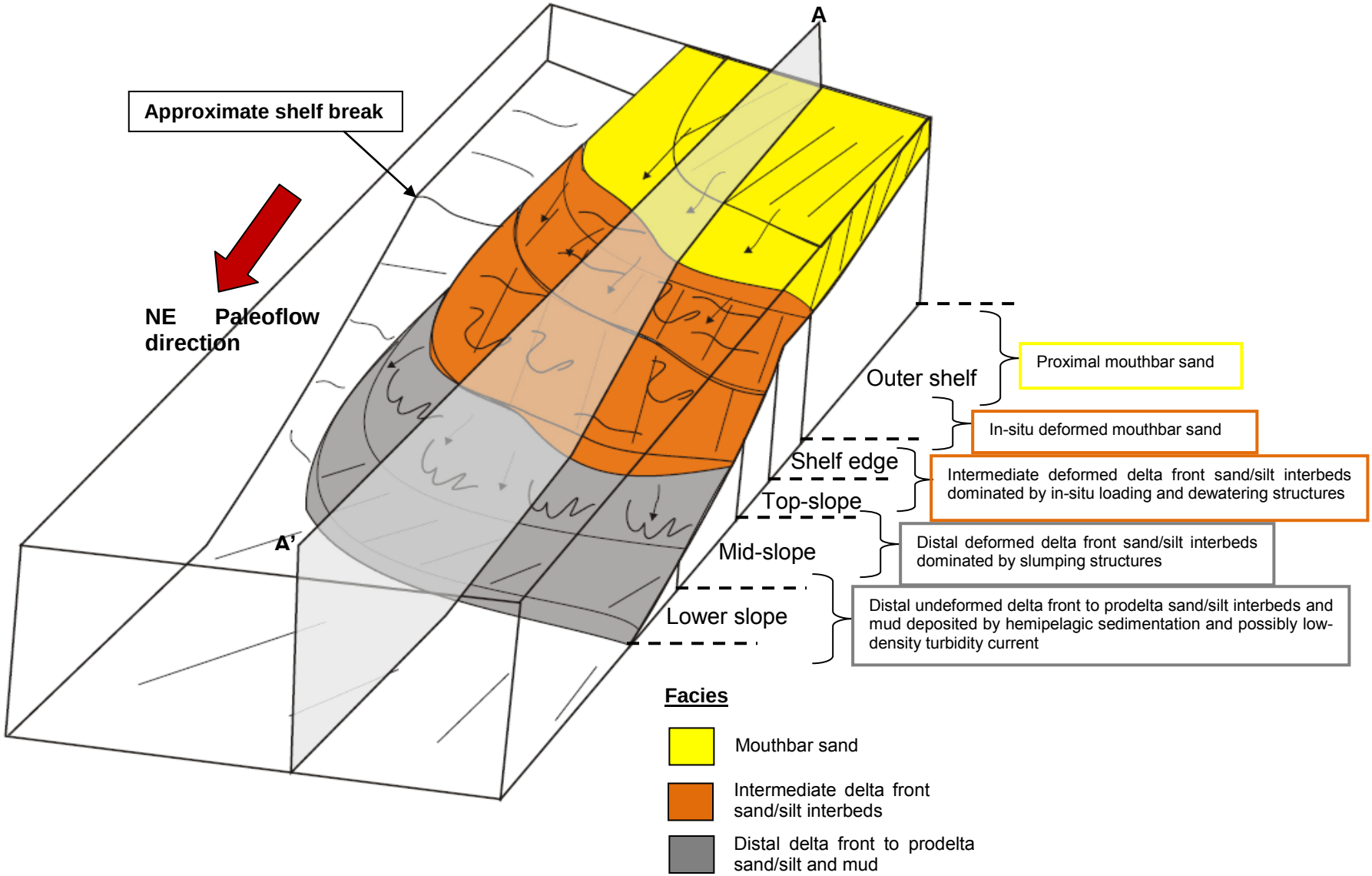

Figure 4.6. Hypothetical 'descriptive' facies model for Kookfontein river-dominated, gravitationally modified and wave-influenced shelf edge Gilbert-type delta. This model forms the basis for describing and interpreting internal heterogeneity and facies architecture of the studied Kookfontein succession (i.e. cycles 1 to 13). Detailed description of longitudinal section A-A' is given in Figure 12.

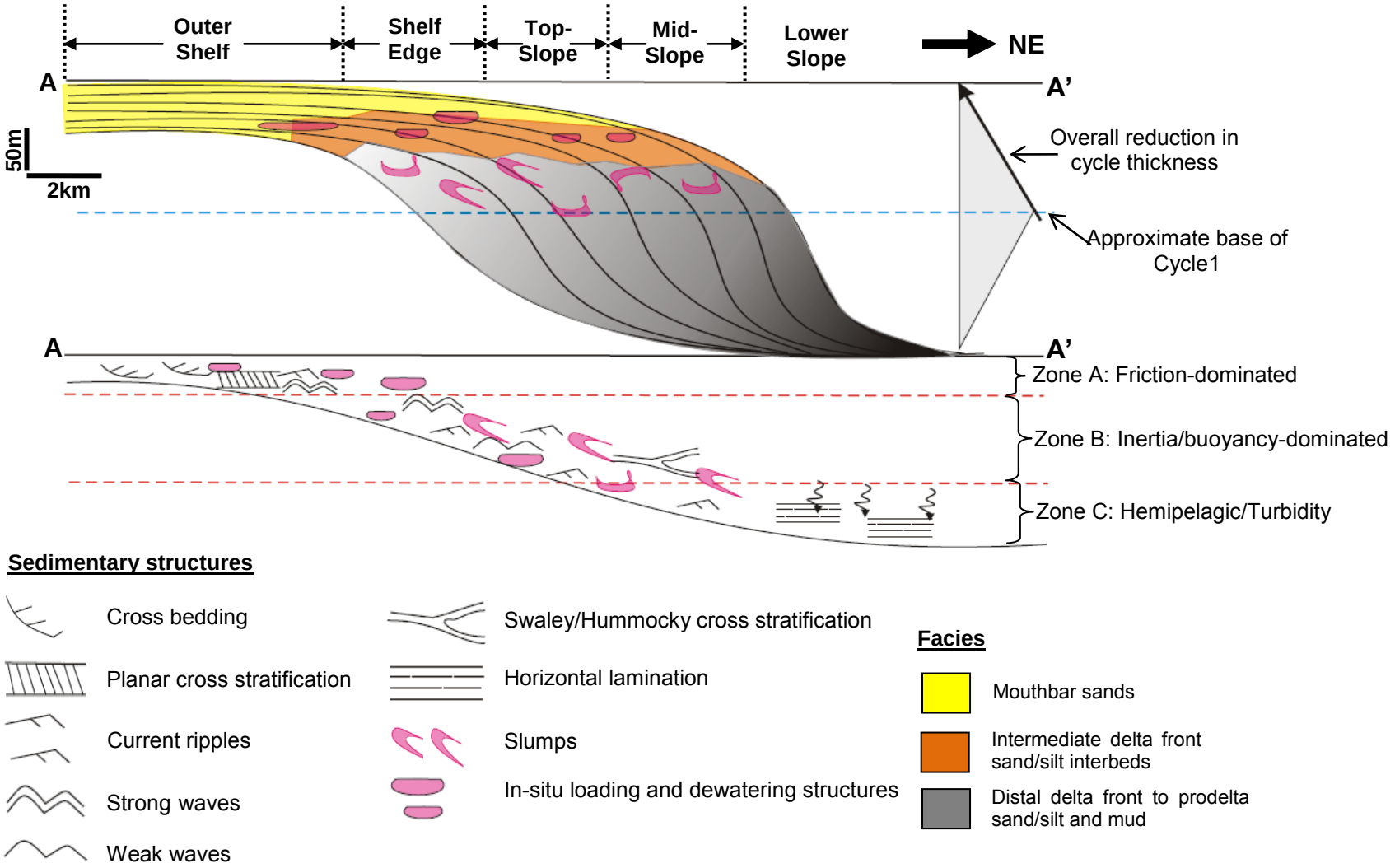

Figure 4.7. Detailed description of a longitudinal section A-A' through hypothetical facies model for Kookfontein river-dominated, gravitationally modified and wave-influenced shelf edge Gilbert-type delta showing Kookfontein clinoformal geometry, its facies stacking and its hydrodynamic zonation. Hydrodynamic Zone A belongs to primary mouthbar deposition governed by stream flow dynamics while hydrodynamic Zone B and Zone C are governed by secondary remobilisation of sediments under gravity.

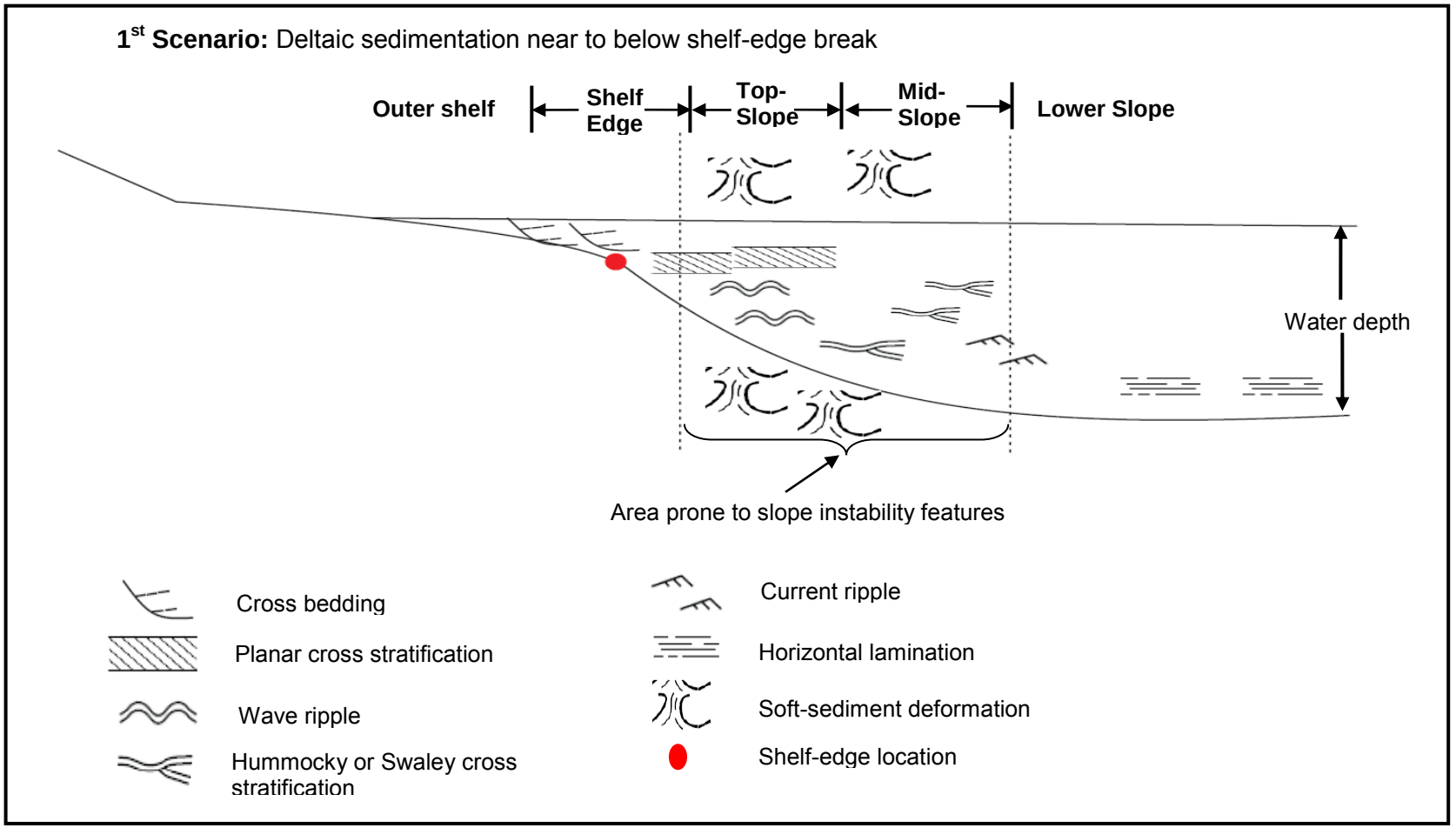

Figure 4.8a. Hypothetical depositional facies model for the lower Kookfontein member (cycles 1-5) showing lateral profile of sedimentary structures in an inferably basinwards direction. Note the associated slope instability features (i.e. soft-sediment deformation structures) due to steep slope gradient.

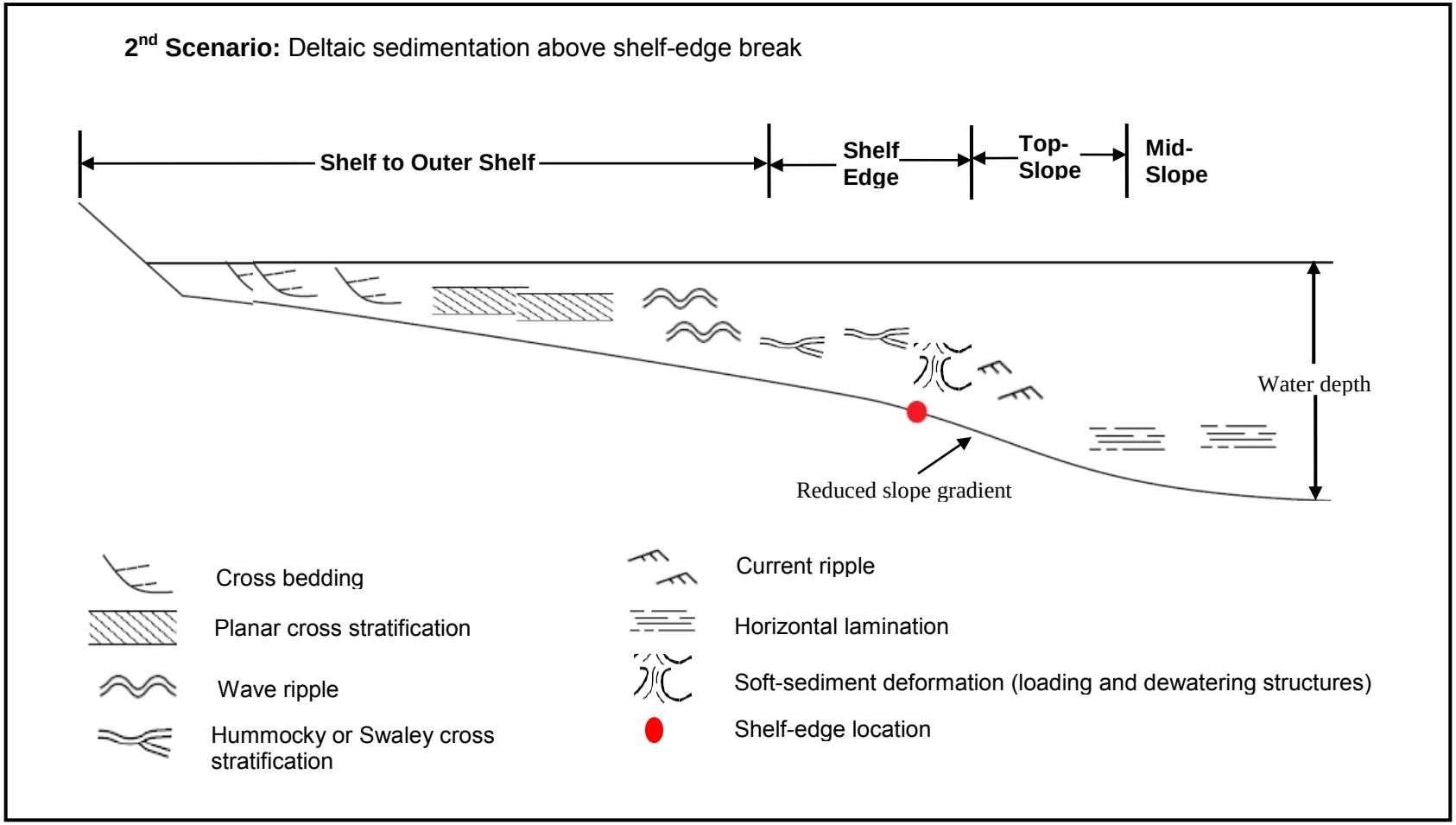

Figure 4.8b. Hypothetical depositional facies model for the upper Kookfontein member (cycles 6-13) showing lateral profile of sedimentary structures basinwards. Note the decrease in slope instability features due to upward decrease in slope gradients.

terms of both depositional processes and spatial distributions. In the following section we will describe the three cycles that we studied in detail from lowest (cycle 1) to highest (cycle 3).

4.3.2 Cycle 1

This sedimentary cycle consists mainly of heterolithic facies and soft-sediment deformation facies with a mean vertical thickness of about 36 m (Tables 4.1 and 4.2; Figures 4.2a, 4.2b, and 4.9). The cycle is underlain by a claystone on top of Unit 5 of the Skoorsteenberg Formation. This claystone has been previously described by Wild (2005) as a 12 m regional claystone marker within the Tanqua depocentre. The cycle is underlain by a claystone on top of Unit 5 of the Skoorsteenberg Formation (Figure 4.9). This claystone has been previously described by Wild (2005) as a 12 m regional claystone marker within the Tanqua depocentre. Along a typical vertical profile, the lithofacies association passes from mudstones, thinly laminated siltstones and undeformed heterolithics (i.e. horizontally to current ripple-laminated sandstones interbedded with siltstones) with no wave reworking processes, (i.e. depofacies 1, 2 and 3; Table 4.2) into heterolithic and sandstone facies that are dominated by soft-sediment deformation structures and symmetrical rippled bed-tops. The sandstone beds of heterolithic facies become thicker and coarser upward with prevalence of unidirectional climbing ripples, swaley-cross stratification, slumps and in-situ soft-sediment deformation structures (i.e. load casts, flames and dewatering structures) (Figures 4.14 and 4.15). Slump structures are commonly homogenised layers and their proportion is generally less than load-casts and dewatering structures. Large scale slump folds within massively deformed unit are encountered towards the middle of this cycle at VS2 (Figure 4.14). The cycle has the highest proportion of slump structures of all the thirteen cycles studied). Heterolithics with no wave reworking processes (i.e. depofacies 2, 3 and 4) graded upward into heterolithics with wave reworked bed-tops (i.e. depofacies 5, 6, 7 and 8; Figures 4.16 and 4.17) and the proportion of the former are relatively higher than the latter. Loadcasts of in-situ soft-sediment deformation

facies exhibit preservation of swaley cross stratification. Amalgamated massive to planar cross-laminated sandstones with wave reworked bed-tops and weak to moderate bioturbation (i.e. 30 – 85 cm thick) close to the top of this cycle contains more deformed layers at the most distal profile (VS1) than at the most proximal profile (VS2) within the studied interval. The stacking pattern of sediments gives an overall character of progradation, thickening and coarsening upward (Figure 4.9). However, the vertical thickening- and thinning-upward trends of bedsets (i.e. lithofacies associations) are somewhat irregular (Figure 4.18); the top of this cycle is characterised by a 3.5 m thick unit of thinning- and fining-upward, unidirectional, current ripple-laminated sandstones with wave reworked bed forms interbedded with siltstones (Figure 5). Typical sand/silt ratios from bottom to top within the succession vary from 55:45%, 60:40%, 65:35% to 70:30%.

Interpretation: This cycle is interpreted as having been deposited on the mid-slope margin of the basin with sub-depositional facies ranging from (i.e. proximal to distal) distal deformed mouthbar sands, intermediate to distal and gravitationally reworked delta front and distal undeformed delta front (Elliot, 1989; Postma, 1990; Figures 4.6 and 4.7). These sediments reflect sands deposited as bedload by mouthbars that prograded beyond the shelf break (Postma 1990; Olariu and Bhattacharya, 2006) and were subsequently reactivated by gravitational processes and transported as slumps (Figure 4.6). This cycle therefore probably corresponds to the steepest part of the delta slope (Figures 4.7 and 4.8a). The 1 m- thick mudstones at the base of this succession and the previously described underlain Unit 5 claystone marker by Wild (2005) would then be the prodeltaic facies which are probably deposited by secondary deposition through hemipelagic suspension.

4.3.3 Cycle 2

The average thickness of this sedimentary succession is 31.5 m, and it consists of prograded packages of heterolithic, i.e. unidirectional ripple, low-angle cross-laminated and moderately bioturbated very fine to fine sandstone with siltstone interbeds (depofacies 2, 3, 4, 5, 6, 7 and 8; Table 4.2; Figures 4.2a, 4.2b and 4.10) in a sheet-like geometry. Towards the upper part of the cycle, these depofacies are overlain by packages of bedded and amalgamated massive coarser sandstones (depofacies 10, 11 and 12; Table 4.2; Figures 4.2a, 4.2b and 4.10). The lateral tracing of a 21 cm- thick silt to very fine carbonaceous sandy-siltstone bed (see Figure 6) on outcrop windows for approximately 50 - 100 m and its presence at about 13 m (for both VS1 and VS2) from the base of cycle 2 is a good tool for resolving and describing the facies successions of this cycle. The proportion of soft-sediment deformation layers (i.e. slumps, loadcasts, flames and dewatering structures; Figures 4.14 and 4.15) is approximately the same for VS1, VS2 and VS4 (Figures 4.2a and 4.2b). Slump folds oriented in SE-NW direction are encountered towards the base of deformed heterolithic units. Lithofacies associations vary vertically from heterolithic facies (i.e. alternation of fine to very fine grained current ripple laminated sandstones interbedded with siltstones influenced by wave processes) to bedded and amalgamated massive to planar cross-laminated sandstone facies with wave reworked bed forms (Figure 4.10). The bed contacts are usually sharp between lithofacies associations, whereas they are mainly gradational within depofacies. The proportion of undeformed heterolithics with no wave rework processes (i.e. depofacies 2, 3 and 4) is less than the overlain heterolithics with wave reworked bed-tops. The wave ripples exhibit symmetrical profiles with alternation of broad (i.e. rounded) and sharp crested wavelengths and are trending mainly NW-SE, E-W and NE-SW (Figure 4.17). Typical wave crest to crest distance ranges from 8 – 10 cm. Paleocurrent data measured from unidirectional current ripples range from NNE, NE to ENE. Bedded and amalgamated massive sandstone

lithofacies are thicker, cleaner and better sorted upward in this cycle than in the cycles below and above it (Figure 4.2a and 4.2b). Amalgamated massive sandstones are thicker and relatively undeformed at the most proximal profile (VS2) whereas they are deformed with mottled appearance and interbedded with sand/silt interbeds (Figure 4.16) at the most distal profile (VS1). This cycle gives an overall thickening- and coarsening- upward sequence which is overlain by a 2.5-3 m thick, thinning- and fining-upward unit of unidirectional current ripple laminated and moderately bioturbated sandstones with wave reworked bed-tops interbedded with siltstones at the top (Figure 6). Variation in sand/silt ratios for the cycle from bottom to top of vertical profiles ranges from 55:45%, 60:40%, 75:25% to 80:20%.

Interpretation: This cycle is interpreted to represent deposition of upper mid-slope to top-slope, with sub-depositional facies ranging from proximal undeformed to distal deformed mouthbar sands, intermediate deformed delta front and distal undeformed delta front (Elliot 1989; Postma, 1990; Olariu and Bhattacharya, 2006; Figures 4.6, 4.7 and 4.8a). The proximal undeformed mouthbar sands are bedload features (i.e. rolling and saltating sediment transport processes) governed predominantly by frictional forces and deposited at the shelf-margin above the shelf break (Wright, 1977; Orton and Reading, 1993; Nemec, 1995; Figure 4.7). The sheet-like and rhythmic delta front heterolithics are dominated by bedload and suspensionload features, and are interpreted as being deposited by periodic (and probably some sporadic) mouthbar events followed by little or no river input and subsequent reworking by wave activities. Secondary remobilisation of sediments due to gradient break at the shelf edge resulted in gravity-driven inertia/buoyancy-dominated deposits and *in situ* soft-sediment deformation and slumping structures (Figure 4.7). The widespread and sheet-like geometry of these rhythmites are indicative of a stable progradation of the delta front. The prevalence of wave activities and reduction in slumping events are indicative of this cycle being shallower than the underlain cycle 1. The alternation of sharp-crested and rounded-

crested wave ripples on bed-tops (Figure 4.17) of delta front heterolithics suggests fluctuations in wave energies (Nichols, 2009). The sharp crested ripples are rolling grain ripples that form at low energies when the wave-generated oscillatory motion within the water column sweeps grains away from the troughs to the edges where sharp (or peaked) ripple crests build up. Whereas, the rounded crested ripples are vortex ripples that form at higher wave energies due to suspension fall-out of grains onto the crests (Nichols, 2009).

4.3.4 Cycle 3

The overall thickness of this succession is 40 m, and it exhibits an asymmetrical profile of thickening and thinning upward successions with overall coarsening upward trend (Figures 4.11 and 4.18). The dominant lithofacies associations are heterolithic (depofacies 4, 5, 6, 7 and 8) and soft-sediment deformation facies (depofacies 9B). This cycle has the highest proportion of heterolithic facies of all the cycles that characterise the Kookfontein Formation (Figures 4.2a and 4.2b). The highly rhythmical and sheet-like layering of interbedded unidirectional current ripple laminated sandstones interbedded with siltstones gradually change upward from thicker siltstone and thinner sandstone packages (i.e. very thin to thin beds) to thinner siltstone and thicker sandstone packages (i.e. thin to medium beds) (Figure 4.11). Wave ripples are less encountered in the lower part of this cycle than in the upper part. Observed wave ripples generally exhibit symmetrical profiles with alternating sharp-crested ripples and rounded-crested ripples, and are trending dominantly NE-SW and NW-SE (Figure 4.17). Typical wave crest to crest distance ranges from 10 – 12 cm while their amplitude ranges from 0.5 – 0.7 cm. Also, the heterolithic facies are weakly to moderately bioturbated. The dominant paleocurrent data measured from unidirectional current ripples within the cycle range from E, ENE to NE. All observed soft-sediment deformation facies are loadcasts, flames and dewatering structures (Figures 4.14 and 4.15), and they variably interbedded heterolithic facies in all the measured vertical profiles. Overlain deformed heterolithics

towards the top are 2 - 3 m thick amalgamated massive to planar cross laminated, cleaner well-sorted fine to medium sandstones with wave reworked and moderately bioturbated bed-tops. The top of this cycle is capped by a 1 – 1.5 m thick heterolithic unit with wave reworked and weak bioturbated bed-tops (Figure 4.11). Variation in sand/silt ratios for the cycle ranges from bottom to top of vertical profiles from 60:40%, 70:30% to 80:20%.

Interpretation: These successions represent sediment deposition of top-slope to shelf-margin successions with sub-depositional facies ranging from proximal undeformed mouthbar sands (i.e. amalgamated massive to planar cross laminated sandstones with wave reworked and weakly bioturbated bed-tops) and intermediate deformed delta front facies (i.e. wave reworked and moderately bioturbated heterolithics and *in situ* loading and dewatering structures) (Elliot, 1989; Postma, 1990; Olariu and Bhattacharya, 2006; Figures 4.6, 4.7 and 4.8a). The widespread and well-developed rhythmic heterolithics with intense wave reworking processes (Figures 4.2a and 4.2b) is indicative of stable progradation and progressive shallowing of the Kookfontein Gilbert-type delta front. Also, the presence of only in-situ loading and dewatering structures and undeformed mouthbar sands are suggestive of decrease in slope gradient of this cycle compared to the underlain cycles 2 and 3.

4.3.5 Cycle 4

The average thickness of this sedimentary cycle is 39 m (Table 4.1), and it consists of symmetrical profile of thickening- and thinning- upward units of depofacies (i.e. bedsets) (Figure 4.18). The dominant facies associations for this succession are heterolithic (i.e. depofacies 5, 6, 7 and 8) and soft-sediment deformation facies (i.e. depofacies 9B) (Table 4.2;

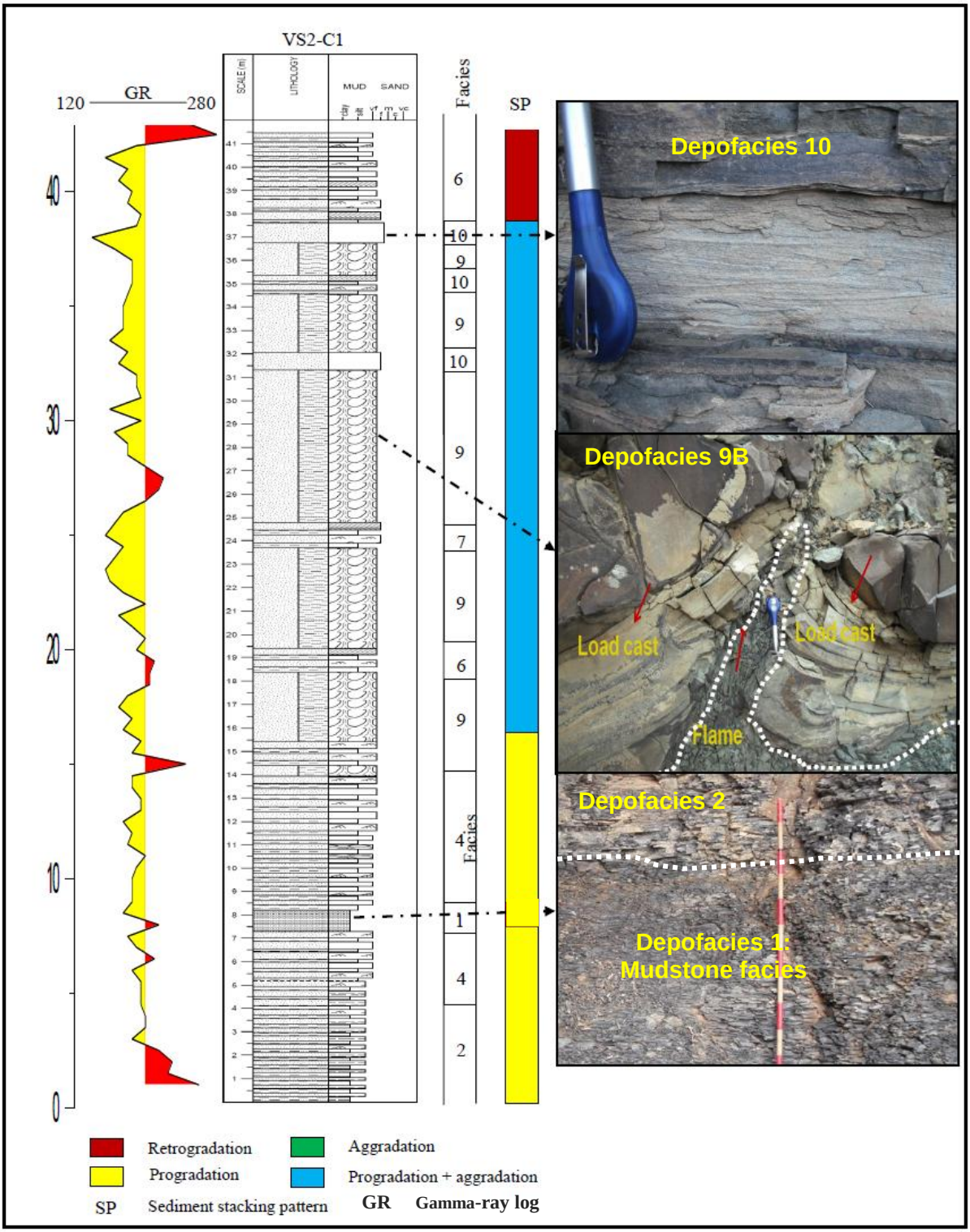

Figure 4.9. Example of a log (VS2-C1) through cycle 1. These vertical facies successions are overlain by abrupt fining and thinning up heterolithic sandstone and siltstone intercalations. Note the overall upward coarsening and low GR values for this succession.

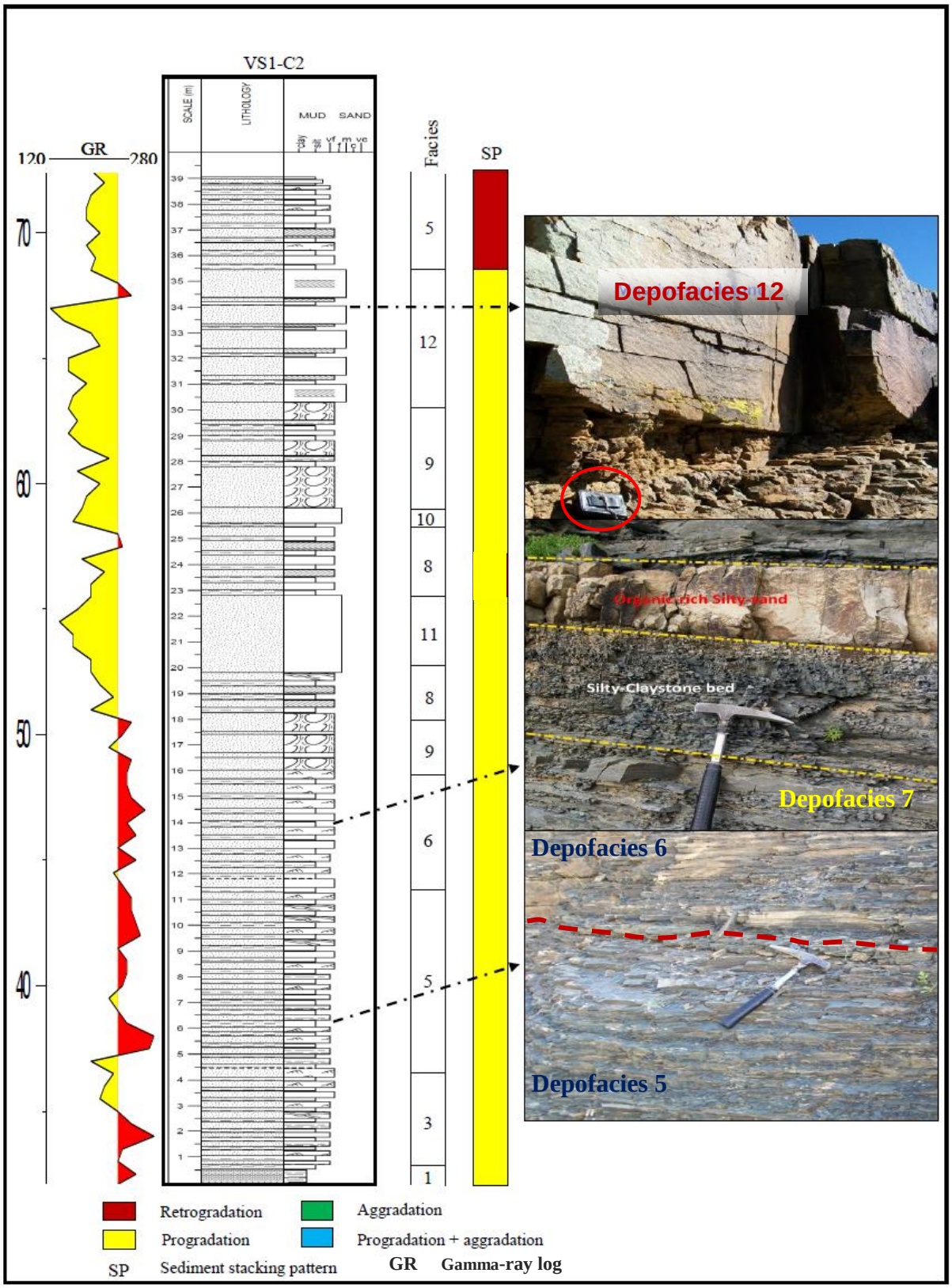

Figure 4.10. Example of a log (VS1-C2) through cycle 2. These vertical facies successions give overall progradational stacking pattern overlain by abrupt fining and thinning up retrogradational stacking trend. Also, note the overall upward decrease in GR values indicating an overall coarsening upward succession.

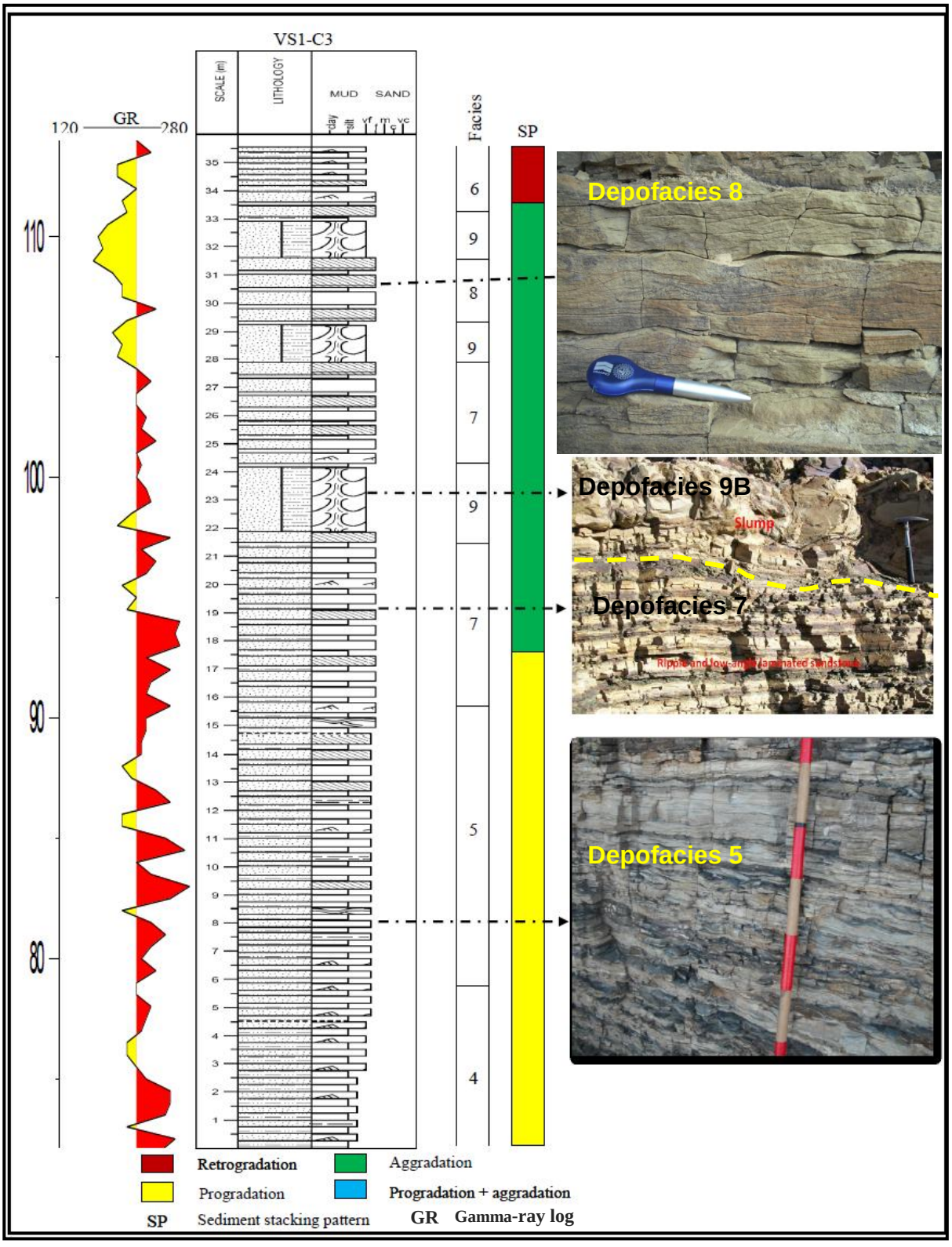

Figure 4.11. Example of a log (VS1-C3) through cycle 3. These vertical successions are predominantly heterolithic facies indicating progradational to aggradational sediment stacking pattern. Note the high GR values for this succession.

Figures 4.2a and 4.2b). The lower to middle parts of the cycle consist of aggraded packages of heterolithic and soft-sediment deformation facies. Upward in a vertical profile, the heterolithic facies vary from interbedded very fine to fine-grained unidirectional current ripple laminated sandstones- (with wave ripples and swaley cross-stratification) and siltstones to fine to medium-grained low-angle planar to wave ripple laminated sandstones interbedded with siltstones The heterolithic facies are bioturbated and the intensity of this bioturbation varies from weak to intense. In a depositional dip-oriented sedimentary log profile (i.e. basinwards cross-sectional profile: VS2-VS4-VS3-VS1; Figure 4.5), the proportion of soft-sediment deformation structures decreases basinwards (Figures 4.2a, 4.2b and 4.20). The dominant soft-sediment deformation structures are loading (i.e. loadcasts, flames and pseudonodules) and dewatering structures (Figures 4.14 and 4.15). Overlying the heterolithic and soft-sediment deformation facies are 2 to 5.5 m- thick massive to planar cross-stratified, medium-grained and well sorted sandstones with wave reworked bed forms and sub-rounded to sub-angular grains (see Appendix A). This sedimentary cycle thickens basinwards along the dominant NE paleoflow direction (i.e. from 35 m at the proximal western part- VS2 to 49 m at the distal eastern part- VS1) (Table 4.1). This succession gives an overall thickening- and coarsening- upward progradational to aggradational sediment stacking pattern. Variation in sand/silt ratios for the cycle ranges from bottom to top of vertical profiles from 60:40%, 70:30% to 80:20%.

Interpretation: The systematic succession of depofacies from heterolithic and soft-sediment deformation to sandstone facies with overall progradational to aggradational stacking trend represents deposition of top-slope to shelf margin successions. The interpreted depositional facies for this cycle are: proximal undeformed to deformed mouthbar sands (i.e. depofacies 12) and intermediate deformed delta front facies (Postma, 1990; Olariu and Bhattacharya, 2006). The occurrence of unidirectional current ripples, gravity-driven processes (i.e. slope

instability features such as load casts and flames) and storm-generated wave activities is suggestive of river-dominated mouth-bar deposition below shelf edge location. Also, the decrease in the proportion of soft-sediment deformation in a depositional dip-oriented profile is interpreted as an upward decrease in slope gradient along the profile and an increase in delta front stability as the mouth-bar aggrades above the shelf edge location.

4.3.6 Cycle 5

This sedimentary cycle has a somewhat uniform thickness across the measured vertical sections. Its thickness in a depositional dip-oriented profile (i.e. VS2-VS4-VS3-VS1) ranges between 36 and 38 m while its average thickness its 37 m (Table 4.1). The main lithofacies associations that characterise this succession are heterolithic, soft-sediment-deformation and sandstone facies (see Appendix A). The rhythmical and sheet-like layering of alternated and bioturbated heterolithic sandstone and siltstone beds (i.e. depofacies 4, 5, 7 and 8; Table 4.2; Figures 4.2a and 4.2b) gradually change upward from thicker siltstone and thinner sandstone packages to thinner siltstone and thicker sandstone packages (see Appendix A). Bioturbation of this facies association varies from moderate to intense. The soft-sediment deformation structures (i.e. predominantly load casts, flames and pseudonodules) initially increase basinwards along the margin of the Tanqua sub-basin from 2.3 to 15 % and later decrease to 8.5 %. Sandstone facies (i.e. depofacies 11 and 12; Table 4.2) has a uniform thickness of about 9 m across the measured vertical sedimentary sections. The sand facies of this cycle is the thickest of the entire lower Kookfontein member (i.e. cycles 1 to 5) (Figures 4.2a and 4.2b). The bed tops of heterolithic and sandstone facies of this succession exhibit preservation of dominantly symmetrical and sharp crested wave ripples with occasional bifurcated crest lines. The wave ripples are trending dominantly NE-SW and NW-SE (see Figure 4.17). The depofacies (i.e. bedsets) thickness dominantly exhibits a somewhat symmetrical thickening- and thinning- upward trend. The successions give an overall

thickening- and coarsening- upward progradational sediment stacking trend (Figure 4.18). Variation in sand/silt ratios for the cycle ranges from bottom to top of vertical profiles from 65:35% to 70:30%.

Interpretation: The successions are interpreted as mainly high-energy delta front deposits (Postma, 1990; Labourdette, 2008) representing deposition of top-slope to shelf-margin successions. The interpreted sub-depositional facies for this succession are: proximal deformed mouthbar sands and intermediate deformed delta front facies (Postma, 1990; Bhattacharya, 2006). The predominance of heterolithic alternations and sandstones with sharp crested and bifurcated wave ripples indicates shallowing of this cycle as the most proximal part of the lower Kookfontein shelf edge delta (i.e. cycles 1 to 5), and probably represents the overall progradational sediment stacking pattern of the lower Kookfontein member.

4.3.7 Upper Kookfontein member (Cycles 6 to 13)

The upper Kookfontein member (i.e. cycles 6 to 13) has average thicknesses that range between 9 and 14 m as obtained from the four measured vertical sections (i.e. VS1-VS4) at Pienaarsfontein locality (Table 4.1). The overall mean cycle thickness for these successions is approximately 11 m. The thinnest and thickest sedimentary cycles for the upper Kookfontein member are cycle 11 (i.e. 8.75 m) and cycles 6 & 13 (i.e. 12.35 m) respectively. Each cycle within this member exhibits a regular pattern of thickening- and coarsening- upward profile unlike the lower Kookfontein member (Figures 4.12, 4.13 and 4.19). The main lithofacies associations that characterise this stratigraphic member are heterolithic facies (i.e. depofacies 7 and 8), soft-sediment deformation facies (i.e. depofacies 9B) and sandstone facies (i.e. depofacies 10, 11 and 12) (Table 4.2; Figures 4.2a and 4.2b). The typical facies succession for each cycle from almost all the measured vertical sedimentary logs around Pienaarsfontein vary from heterolithic and soft-sediment deformation facies at the base to sandstone facies at the top. Of all the three observed facies, the sandstone facies constitute the most dominant

facies in each cycle (Figures 4.2a and 4.2b). The heterolithic packages for each cycle consist of siltstone and very fine-grained sandstone interbeds that coarsen- and thicken- upward into interbedded siltstones and current- to wave- ripple laminated, moderately bioturbated, fine- to medium- grained sandstones. The sandstone beds of these heterolithic facies typically consist of mm- thick mud drapes with some internal flasers while their tops exhibit symmetrical-rippled profiles. The heterolithic units vary in thickness from 0.5 to 5 m thick. Overlying the heterolithic facies are medium- to thick- bedded, low- angle to planar laminated, fine- to medium- grained with sub-rounded to sub-angular grains, well sorted sandstones. The individual sandstone beds range from 0.4 to 10 m thick which are more massive and amalgamated upward (Figures 4.12 and 4.13). Individual bed bases are commonly sharp to erosive. The tops of sandstone beds exhibit symmetrical sharp to rounded wave ripples and are commonly weakly bioturbated. In some instances, the massive and amalgamated sandstones are interlayered by current ripple laminated sand and silt interbeds (Figure 4.16; see also Appendix A). Soft-sediment deformation structures i.e. load casts, flames pseudonodules and dewatering fabrics are less encountered within each cycle in the upper Kookfontein member (i.e. cycles 6-13) than the lower Kookfontein member (i.e. cycles 1-5) (Figures 4.2a and 4.2b). Individual soft-sediment deformation units range in thickness from 0.4 to 8 m thick.

Interpretation: The heterolithic facies at the base of each cycle (i.e. current ripple laminated sandstone and siltstone interbeds) indicate a predominance of unidirectional current processes and are interpreted as distal undeformed to intermediate delta front deposits. The symmetrical ripples and low angle to planar cross stratification of the overlying sandstones are interpreted to be due to the effect of waves and tidal influences (Elliot, 1989; Labourdette, 2008) during progressive shallowing of the depositional system. The sandstones which generally become thicker and more massive upward indicate the overall aggradational stacking pattern of the

upper Kookfontein above the shelf edge location. The occurrence of less sediment-deformation structures suggests an upward reduction in slope gradient (i.e. more stabilised delta front system) as the mouthbar progradation is now more confined above the shelf edge position. The massive to cross-bedded sandstones with erosive bed bases and lenticular geometries in the uppermost cycle 13 are interpreted as evidence of distributary channel deposits. These successions (i.e. the upper cycles 6 to 13) are interpreted as high energy proximal delta front representing deposition of shelf-margin to outer shelf successions. Each upper Kookfontein cycle gives an overall thickening- and coarsening- upward profile with less soft-sediment deformation than the lower five cycles. Each cycle (i.e. facies succession) exhibits internal progradation that is similar to classic shelf parasequences bounded above and below by flooding surfaces (Van Wagoner et al. 1990; see Figure 4.19 and Appendix A). The interpreted sub-depositional facies for this stratigraphic succession (i.e. lower Kookfontein member) are: proximal undeformed to deformed mouthbar sands and intermediate to distal delta front facies (Elliot, 1989; Postma, 1990; Bhattacharya, 2006).

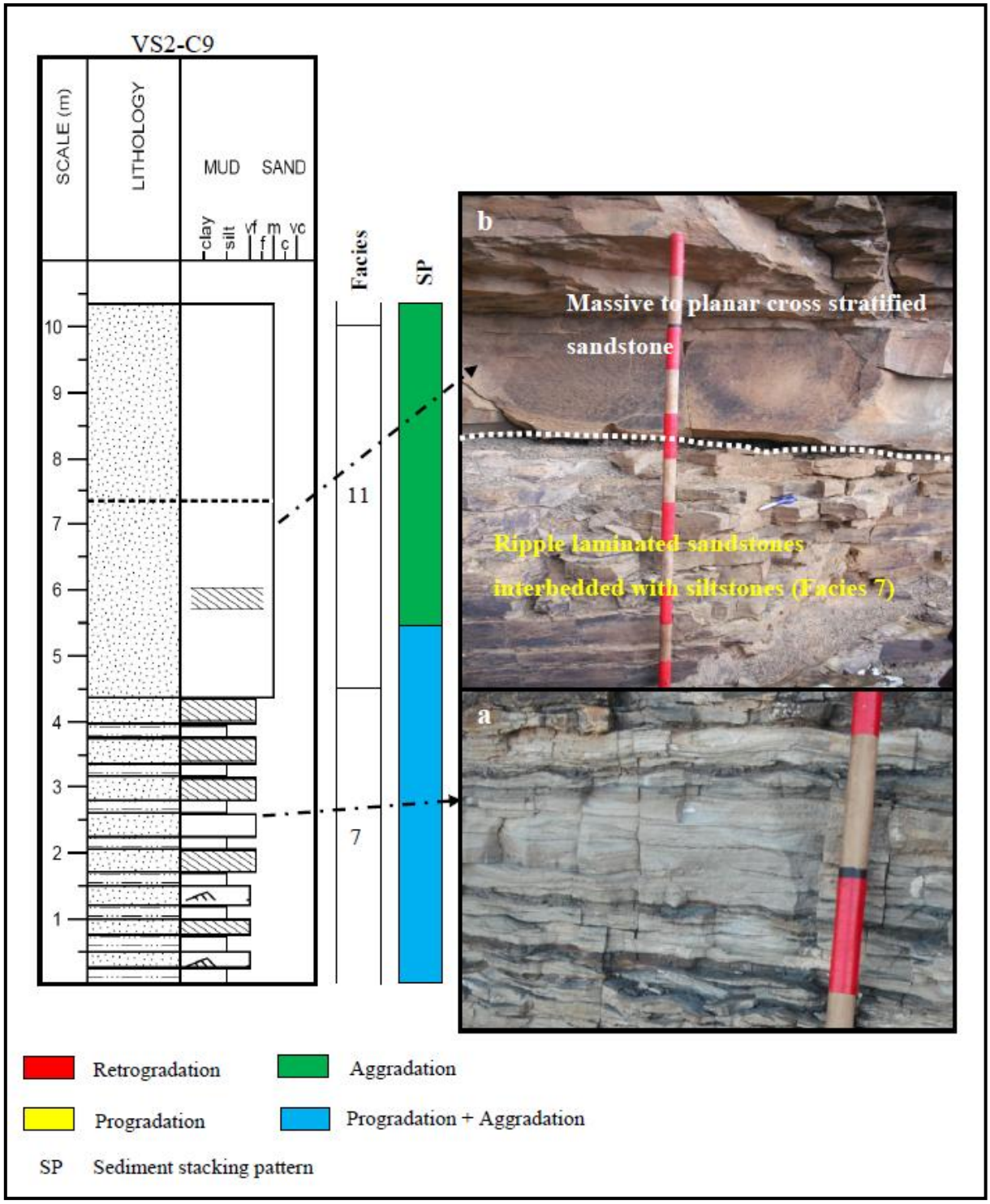

Figure 4.12. Example of a log (VS2-C9) through the upper Kookfontein cycle 9. These vertical successions are more sand prone than the lower Kookfontein cycles, and give an overall coarsening-and thickening- upward aggradational sediment stacking pattern typical of more shelfal deltaic deposits probably above the shelf edge location. The log also shows no evidence of instability within the cycle.

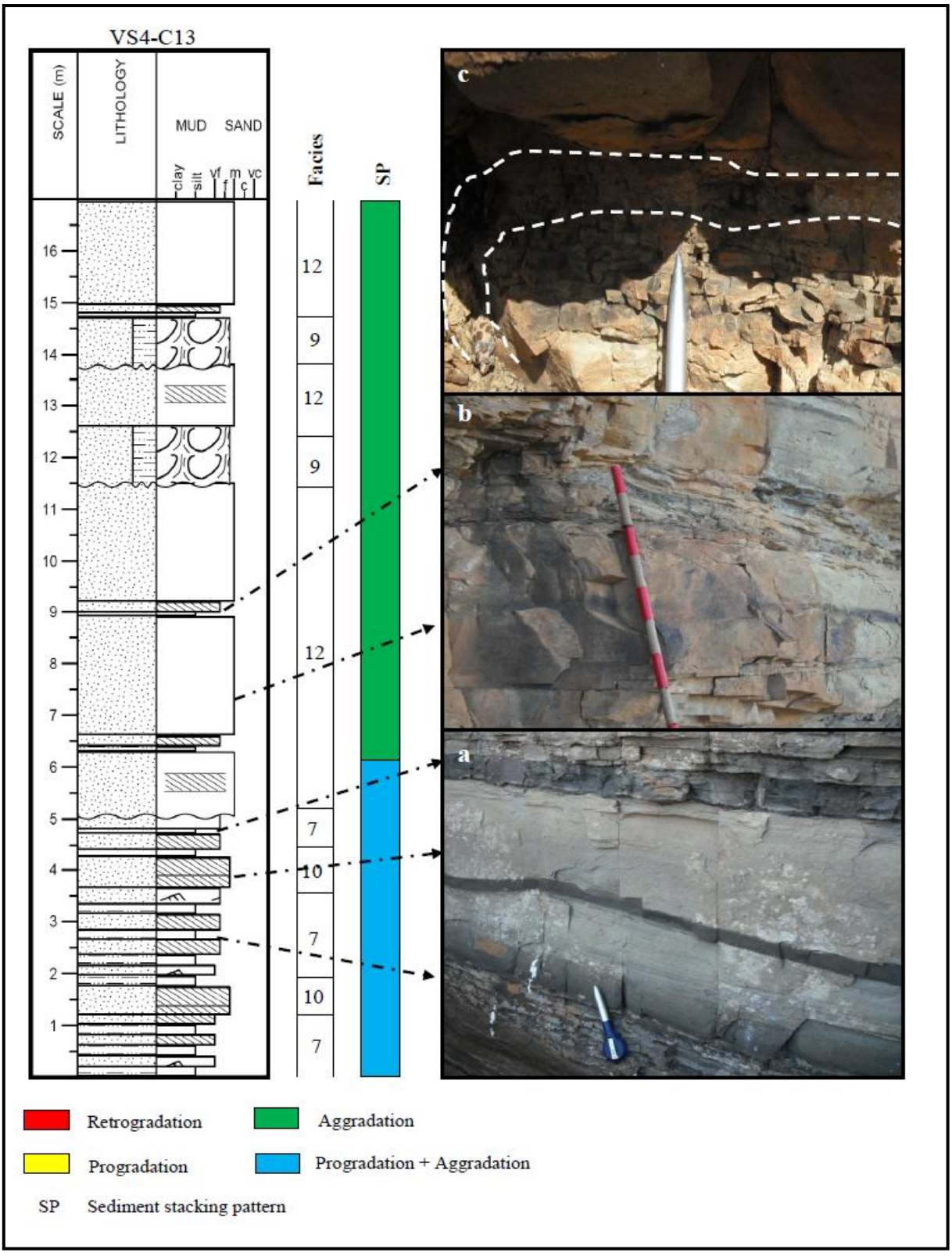

Figure 4.13. Example of a log (VS4-C13) through the upper Kookfontein cycle 13. Photograph (a) shows medium to thick bedded sandstones bounded above and below by heterolithic facies; Photograph (b) showing massive to planar cross stratified amalgamated sandstones with minor mottled appearance and intercalated by sand and silt interbeds; Photograph (c) shows about 5-7 cm thick matrix-supported, sub-angular to well-rounded clasts of siltstone and sandstone. This indicates probable evidence for fluvial distributary channels cutting into cycle 13 at Pienaarsfontein type locality.

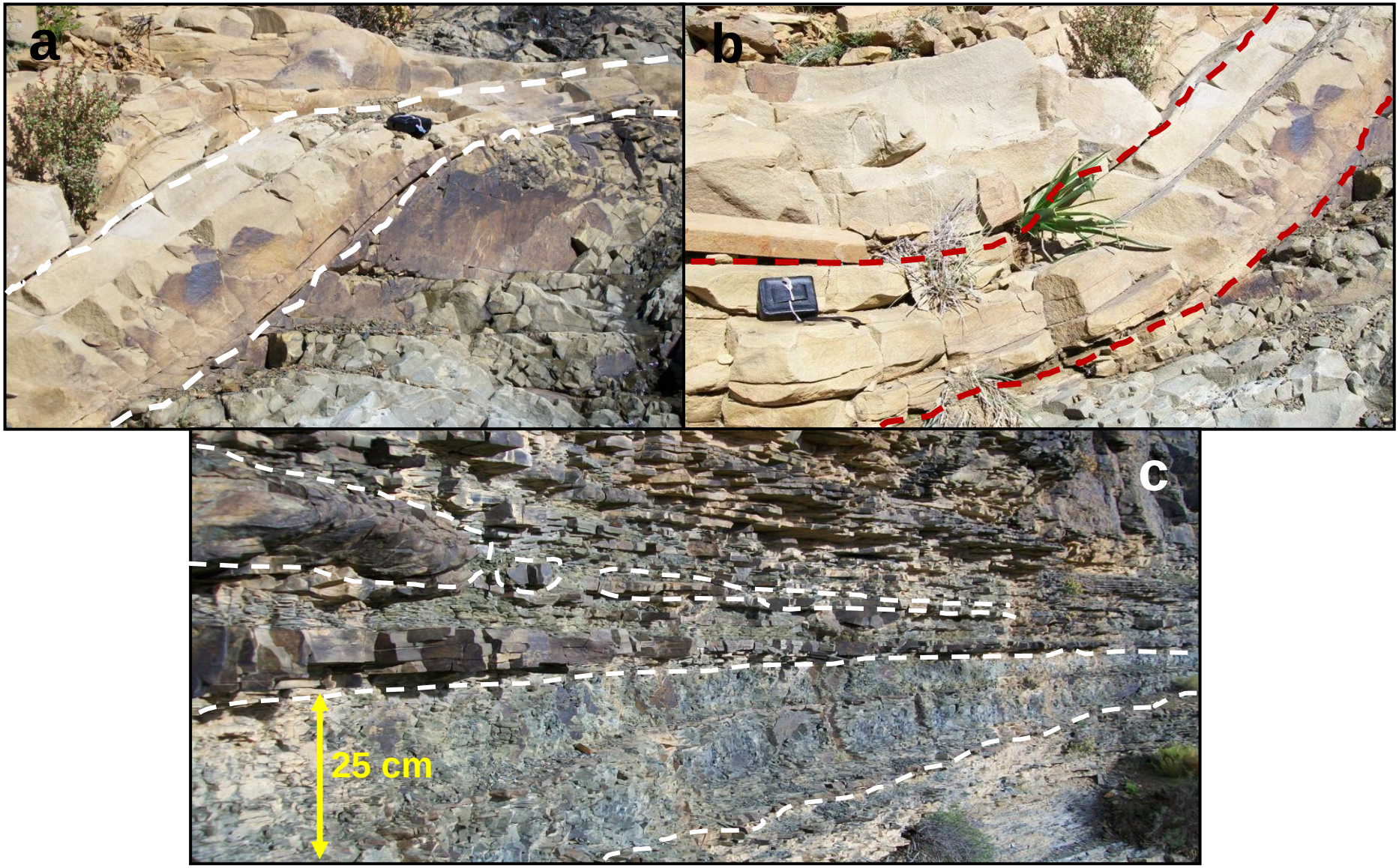

Figure 4.14. Schematic outcrop view of soft-sediment deformation structures at Pienaarsfontein locality. (a) and (b) show large-scale slump folds observed within highly deformed unit of cycle 1 at Pienaarsfontein vertical section VS2; (c) Dewatering of sandstone layer within relatively undeformed thinly bedded sandstones interbedded with siltstones.

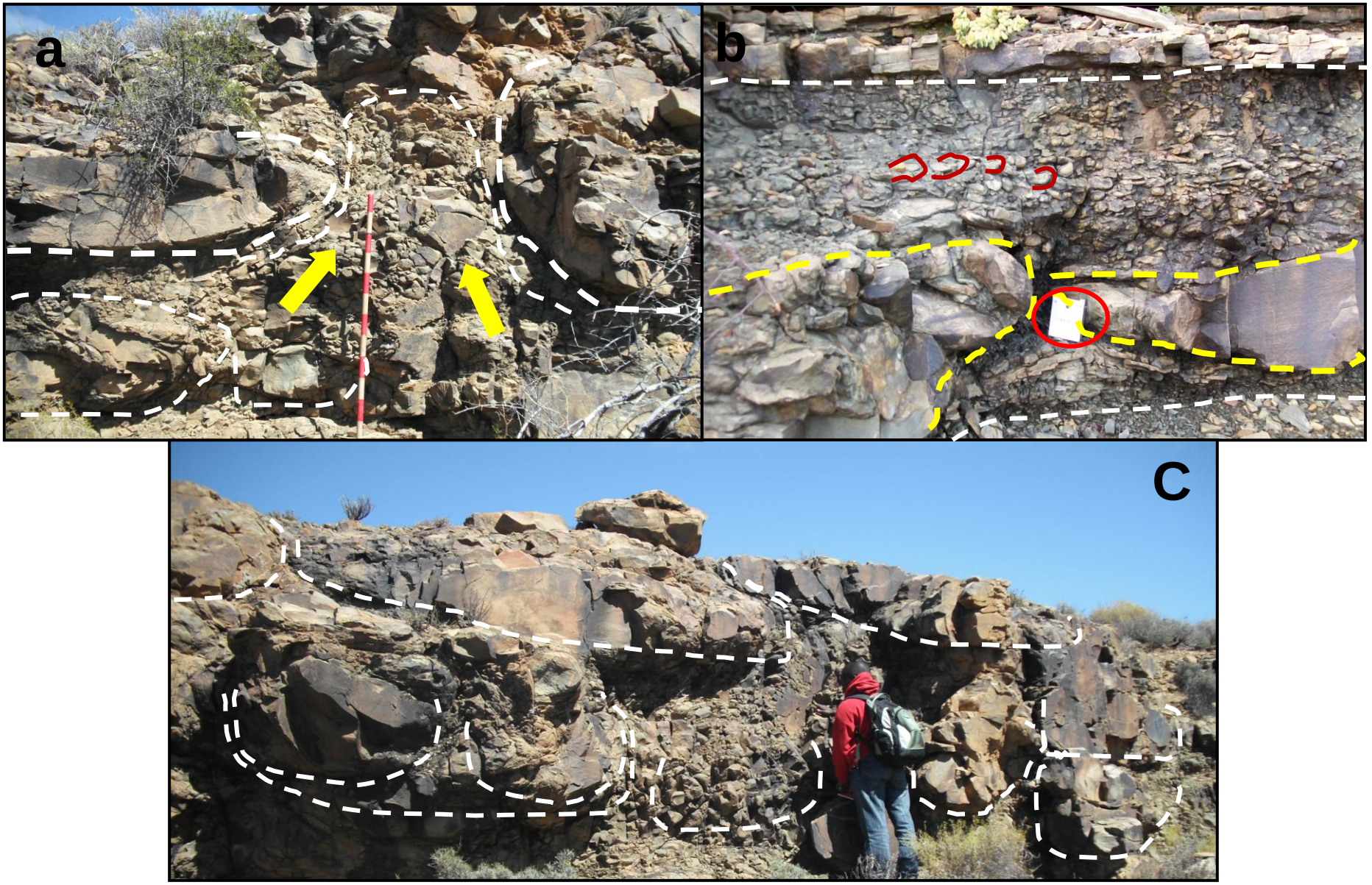

Figure 4.15. Detailed view of loading structures within cycle 2 observed at Pienaarsfontein vertical section VS4. (a) Large-scale loadcasts, flames and pseudonodules; yellow arrows show fine grained sand/silt flames in between elongated coarser sandstones (i.e. loadcasts); (b) Loadcasts and flame overlain by deformed layer with extensive pseudonodules; (c) White dotted lines show large-scale elongation of coarser sandstones (i.e. loadcasts) separated by flame structures.

Figure 4.16. (a) Thinly bedded, unidirectional current ripple laminated, fine grained sandstones with wave reworked bed-tops interbedded with siltstones interpreted as intermediate delta front facies; (b) Amalgamated massive to planar cross laminated sandstones interlayered by sand and silt interbeds (i.e. white dotted lines) interpreted as proximal mouthbar sands.

Figure 4.17. View of wave ripples on bed-tops of thinly bedded sandstones. (a) Different orientations and crest-types (i.e. rounded and sharp) of wave ripples within same unit of heterolithic (i.e. sand and silt interbeds) facies. Red and Yellow arrows show orientation i.e. NW-SE and NE-SW respectively; (b) Sharp crested wave ripples.

4.3.8 Gamma ray log characteristics

The outcrop gamma-ray logs for this study (Figures 4.9, 4.10 and 4.11) were generated by measurement at a 5 s count rate and 50 cm sample spacing along each vertical sedimentary log. 200 cps is used as the midpoint between the maximum (shaded red is 200 cps to maximum) and the minimum (shaded yellow is 200 cps to minimum) gamma radiations. The first point to note is that there is an upward decrease in GR readings within each cycle and overall upward decrease in GR from cycle 1 to cycle 2. Although the cycle 3 GR values are higher than those of cycle 1 and cycle 2, both trends show an upward decrease in GR values punctuated by peaks which correlate usually to changes in lithology, grain-size and possibly mineralogy (Myers and Bristow, 1989; Evans et al., 2007). The GR profiles were then plotted against the respective measured sections as adjacent vertical profiles, and depicted a broadly similar trend between lithofacies associations, grain size and GR logs (Figures 4.9, 4.10 and 4.11). The GR peaks mostly coincide with boundaries between facies associations (i.e. sandstone, heterolithic, mudstone and soft-sediment deformation facies). However, it should be noted that it is very difficult to determine the boundaries between heterolithic facies and soft-sediment deformation facies from the GR logs alone without referring to detailed outcrop logs as these two facies give more or less similar GR readings. Also, comparing the GR profiles with detailed outcrop logs depicts the boundaries between mouthbar sandstones and delta front heterolithics facies (Figures 4.9 and 4.10). As an expected rule, the gamma radiation increases with decreasing grain size. This GR trend normally conforms to the depositional sequence (i.e. overall coarsening-upward succession) that are observed on the outcrop logs. However, there are few exceptions where the gamma-ray measurements do not relate to changes in grain size. For example, a 0.21 m-thick bed of silt to very fine organic-rich silty-sand with a sharp base and top contacts (Figure 6) gives low gamma radiation similar to some sandstone facies. This inverse occurrence could probably be due to low

concentration of radioactive minerals in the silty-sand bed and possibly better sorting of fine-grained sands (Evans et al., 2007). The approximately higher GR values for cycle 3 than cycles 1 and 2 (Figures 5, 6 and 7) could probably be due to high concentration of heavy minerals e.g. radioactive, thorium-bearing monazite mineral (Myers and Bristow, 1989).

Potentiality of different facies associations for reservoir properties was roughly assessed through shaliness evaluation (i.e. Equation 1). The results obtained from this evaluation give the following approximate range of clay content (Vsh) for the main lithologies: clay/silty-clay (60-100%), silty/shaly sand (30-70%) and sand (0-30%). Variations in shaliness distribution pattern with depth for different lithofacies are shown in Figure 4.21. The overlap between heterolithic and mudstone (Figure 4.21) is suggestive for the effect of background sedimentation or initial depositional environment on reservoir quality. The background sedimentation tends to favour fine-grained deposition as the system naturally transits laterally from that dominated by bedload/suspendedload features into that dominated by hemipelagic suspension settling downslope. Generally, proximal mouthbar cleaner and coarser sandstones are characterised by low GR values while delta front heterolithics and prodelta mudstones are characterised by high GR values. This assessment therefore serves as a rather crude estimation for sand to clay ratio, and therefore observations therein require detailed petrographic characterisation for confirmation. It is also worth mentioning that the GR log offers a useful tool for correlating stratigraphic and lithofacies boundaries as well as identifying sandbody architecture in the studied stratigraphic succession.

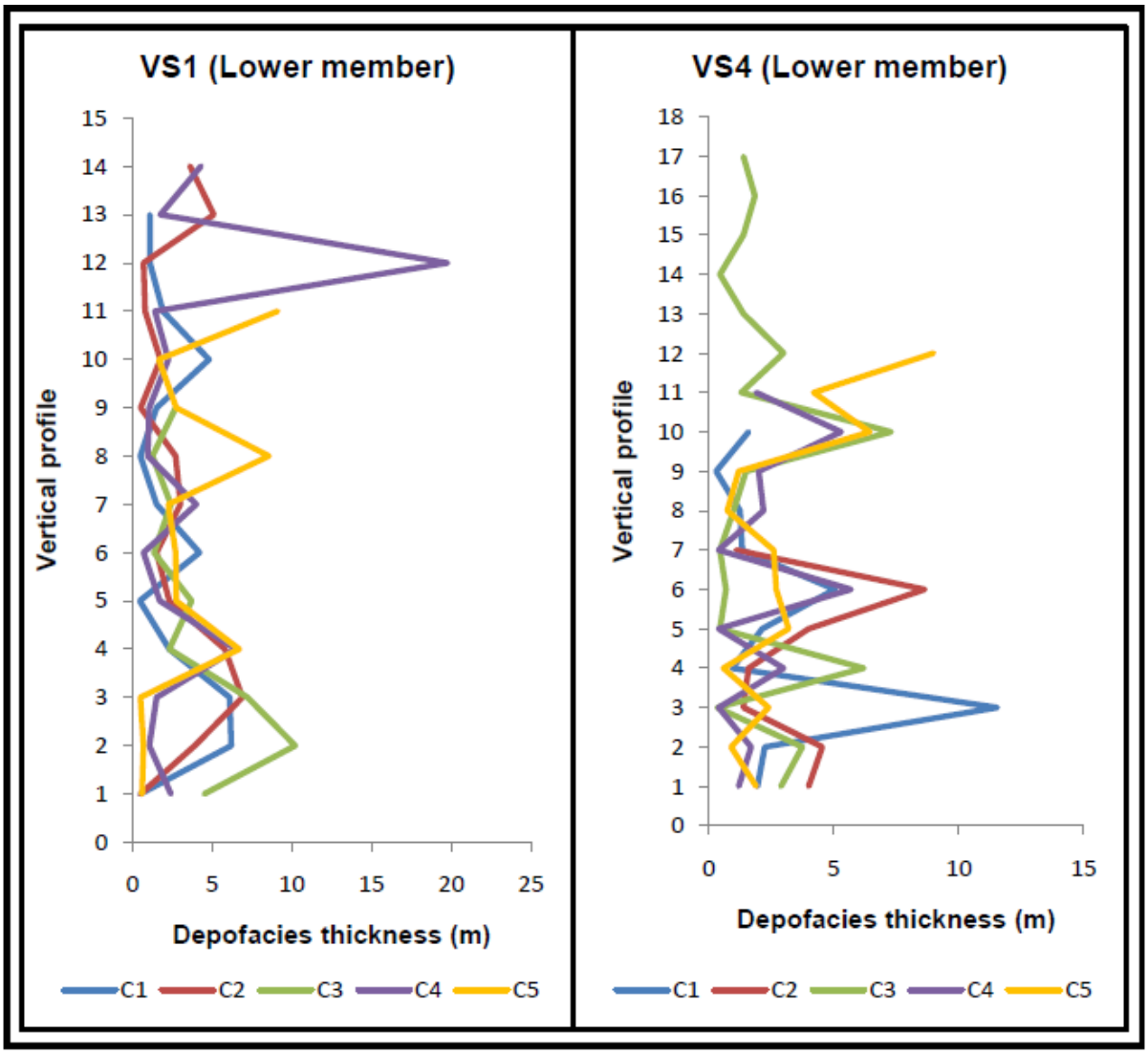

Figure 4.18. Variation in vertical superposition of bedset (i.e. lithofacies scale) thicknesses along the measured sections for cycles 1-5. Note the somewhat asymmetrical/irregular thickening and thinning upward depositional sequence.

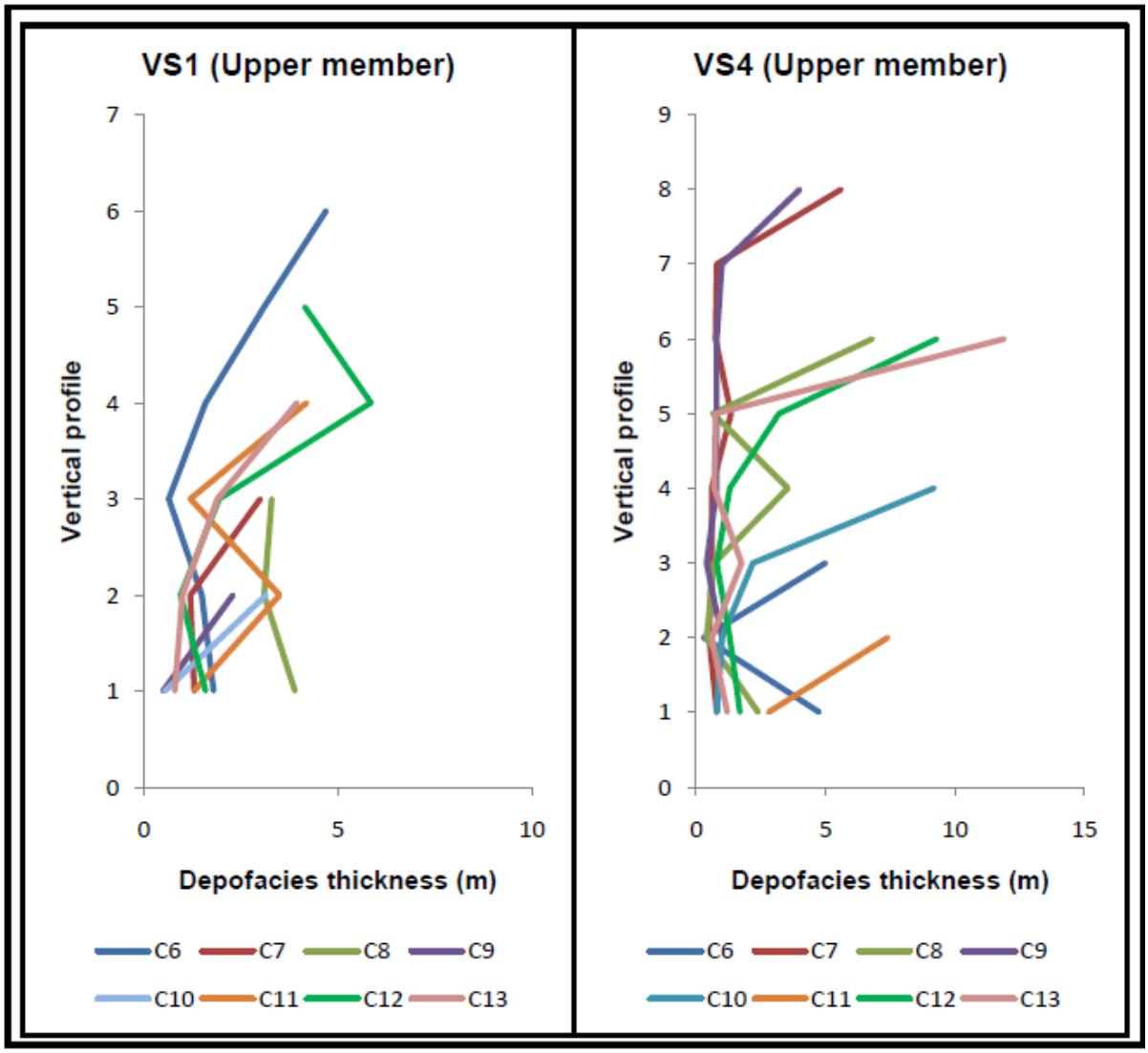

Figure 4.19. Variation in vertical superposition of bedset (i.e. lithofacies scale) thicknesses along the measured sections for cycles 6-13. Note the overall thickening up depositional sequence of the lower Kookfontein member.

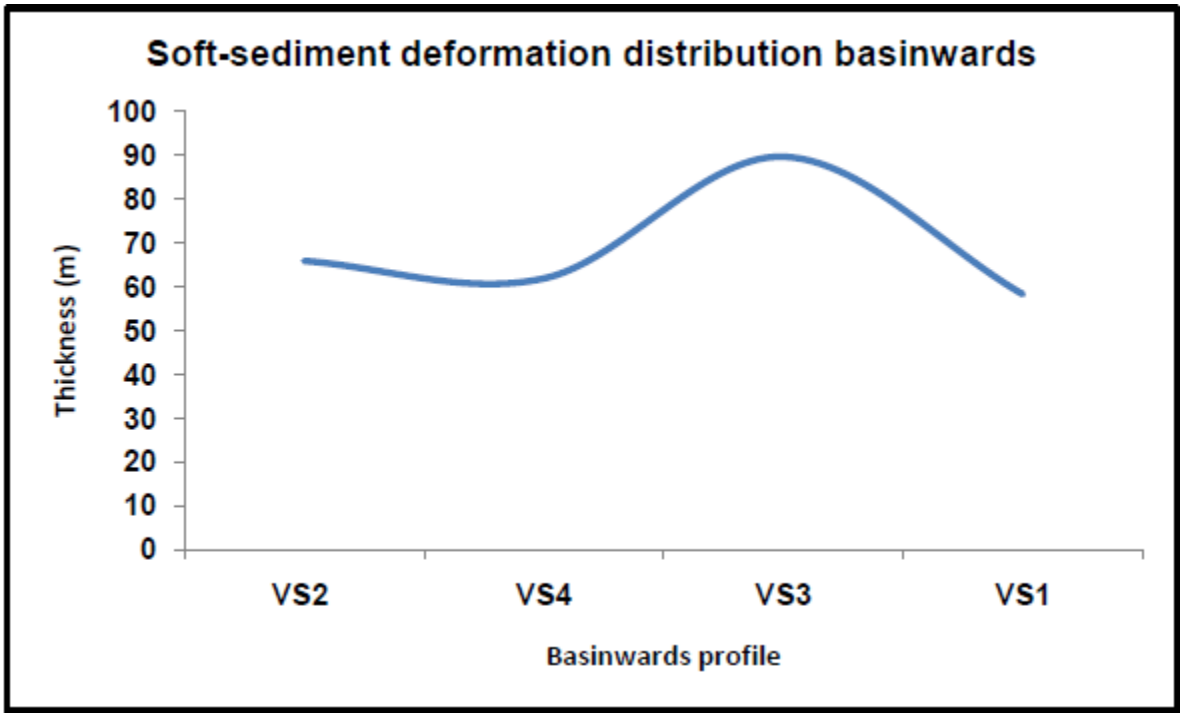

Figure 4.20. Distribution of soft-sediment deformation along basinwards cross-sectional profile. Note the overall decrease in style of soft-sediment deformation basinwards.

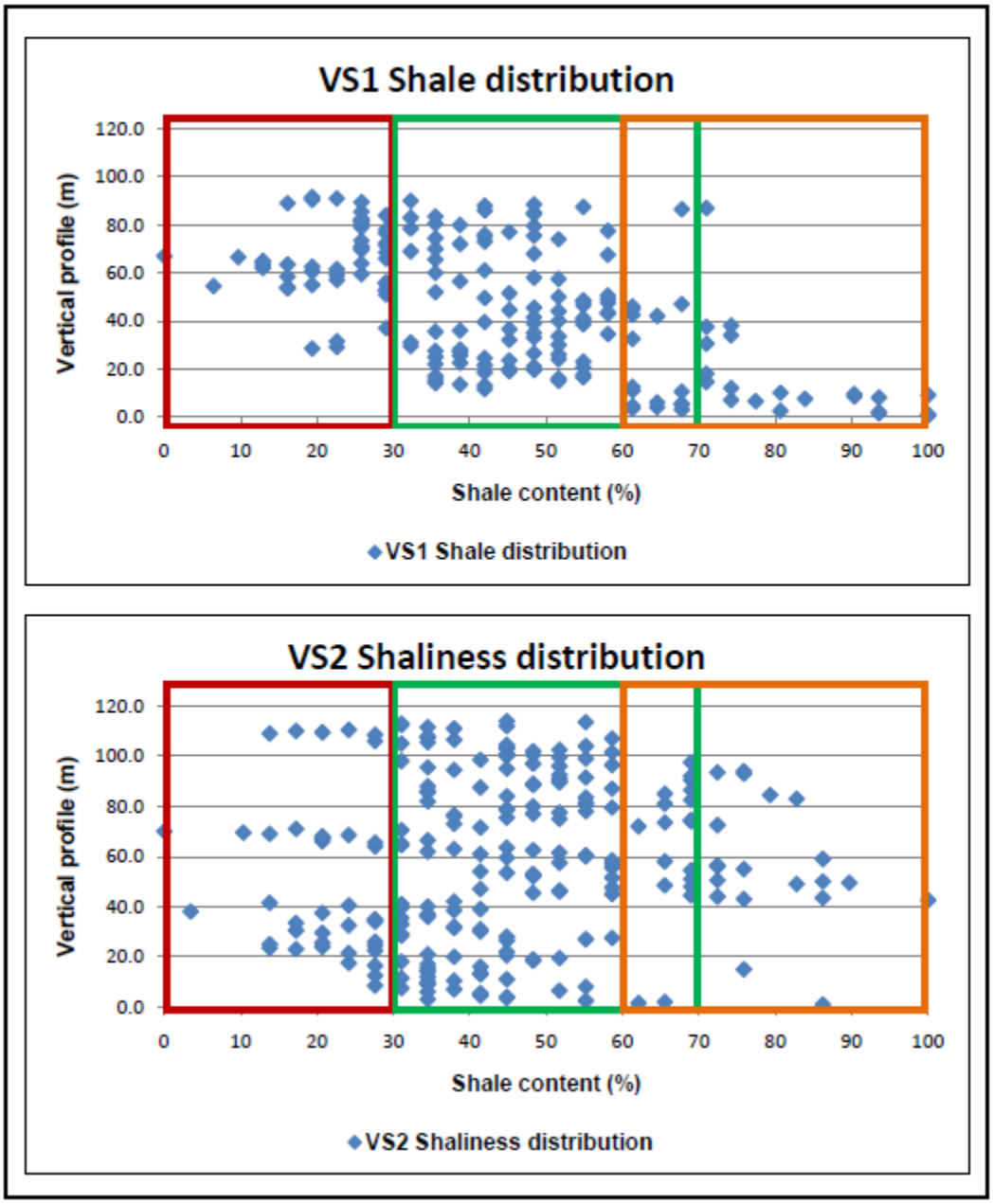

Figure 4.21. Vertical shaliness distribution for the studied stratigraphic interval (i.e. cycle 1 to cycle 3) depicting the overall coarsening up trend of each cycle. Red box = sandstone facies % (0-30%), Green box = heterolithic % (30-70%) and mudstone facies % (60-100%); note the ~10% overlap between heterolithic and mudstone facies.

CHAPTER FIVE

FACIES ARCHITECTURE AND GEOMETRY

5.1 Stratigraphic framework and facies architecture

Establishment of a quantitative hierarchy of stratigraphic framework for describing the Kookfontein deltaic architecture is difficult in the SW Karoo Basin due to a lack of precise chronostratigraphic data. In this study, the stratigraphic elements that characterise the Kookfontein deltaic architecture and geometry are ranked in terms of depositional hierarchy that ranges from cycle-scale/facies succession (35 - 49 m), bedsets (i.e. lithofacies-scale 0.2 – 30 m), beds/depofacies (0.01 – 1.2 m) to laminae (<0.01 m) in decreasing order over a total thickness of 250 to 285 m. These stratigraphic elements form the basic building blocks for describing the internal heterogeneity, facies architecture and geometry of the Kookfontein depo-system. Using thickness patterns, sediment stacking trend, spatial and temporal facies distribution and upward changes in features of the correlated cycles (Figures 4.5, 5.1, 5.2, 5.3 and 5.4) the Kookfontein deltaic successions are grouped into two stratigraphic members namely: Lower Kookfontein member (i.e. lower Kookfontein cycles 1-5) and Upper Kookfontein member (i.e. upper Kookfontein cycles 6-13). The lower member has a mean thickness of 37 m with an overall progradational stacking trend representing deposition of mid-slope to top-slope/shelf-margin; while the upper member has a mean thickness of about 11 m with an overall progradational to aggradational stacking pattern representing deposition of top-slope/shelf-margin to outer shelf.

5.2 Kookfontein deltaic architecture and geometry

The hypothetical “descriptive” facies model for our specific delta (Figures 4.6, 4.7, 4.8a and 4.8b), detailed vertical sedimentary logs and basinwards cross-sectional profiles form the basis for characterising internal architecture and geometry of the studied succession. The

observed architectural elements seem to be typical of a river-dominated, gravitationally reworked Gilbert-type delta deposited in a deepwater setting (i.e. a prograding Gilbert-type mouthbar over the shelf break) (Postma, 1990; Olariu and Bhattacharya, 2006).

The trend of facies successions for each cycle, which grades vertically from distal facies (i.e. prodelta and distal undeformed delta front) to proximal facies (i.e. distal to intermediate deformed delta front, distal deformed mouthbar sands and proximal undeformed mouthbar sands), depicts a naturally prograding delta. Assuming vertical facies variations across subsequent cycles to be equivalent to lateral facies variations within a cycle, then observed upward changes in features, i.e. decrease in gravity effects, increase in waves, decrease in slope gradient would indicate that each facies succession (i.e. cycle) is a deltaic clinothem (Figure 4.7). Though long term 3D diffusion of mouthbar sediments might pose a constraint to this assumption. This study has not been able to follow a complete clinothem laterally as it is difficult to do so alone from the studied outcrops; however, its recognition is reconstructed through upward change in depositional features, overall decrease in cycle thicknesses and basinwards correlation of cycle thicknesses (e.g. Figures 4.5 and 5.4). The studied successions (Kookfontein cycles 1 to 13) are believed to be bottomed within the thickest part of the foreset of Kookfontein clinoforms covering only the upper sequence, i.e. from mid-slope to shelf-margin/outer shelf (Figures 4.6 and 4.7). Juxtaposing observed sedimentary features suggest that each clinothem is deposited by: (1) primary mouthbar deposition governed by stream flow dynamics, and (2) secondary remobilisation of sediments governed by gravity processes. The prograding mouthbars then combine to form a seemingly uniform Gilbert-type delta front that builds out over a shelf break (Postma, 1990) (Figure 4.6). The prevalence of mouthbar sands, heterolithics and soft-sediment deformation facies in the studied interval suggests that Kookfontein Formation are deposited within the active depositional area i.e. delta front of the Tanqua-Karoo delta system.

The highest proportion of highly rhythmical and sheet-like heterolithic facies (i.e. sands and silts) (Figure 4.2a and 4.2b) suggests a stable progradation of delta front facies. On the whole, the ratio of bedload/total-load decreases from proximal to distal mouthbar sands, intermediate delta front facies to distal delta front facies thereby reflecting the overall shallowing and progradation of the Gilbert-type delta front. Supporting evidence for overall shallowing of the delta system are the occurrence of more beadload features (i.e. mouthbar sands) and wave reworked processes at top-slope to shelf-margin/outer shelf successions (i.e. upper Kookfontein cycles 6 to 13) than at mid-slope to top-slope successions (i.e. lower Kookfontein cycles 1 to 5) (Figures 5.2, 5.3 and 5.4). Wave ripples usually exhibit alternation of sharp-crested and rounded-crested waves indicative of fluctuating wave energies. Detailed studies on these wave ripples may yield more information on hydrodynamic conditions. Lateral facies variations within each cycle are probably related to break in depositional events due to either no input of sediments through river processes or switching of distributary mouthbars. Distribution of soft-sediment deformation structures throughout this succession (i.e. cycles 1 to 13) suggests extensive gravitational reworking processes through progradation of distributary mouthbars over the shelf break. Large scale soft-sediment deformations structures have also been recorded on the clinoform gradients of shelf edge deltas in the Gulf of Mexico (average 4 - 8^0; Suter and Berryhill, 1985) and Rhone delta (average ~1^0; Bhattacharya, 2006). Without further study, it is very difficult to determine the influence of close association of observed soft-sediment deformation structures (i.e. slumps, loading and dewatering structures) on one another. However, their spatial distribution suggests that they are empirically related to slope gradient. Slumping structures (e.g. slump folds; Figure 4.14) are encountered within the lower unit (i.e. cycles 1 and 2) of the studied succession representing the deepest soft-sediment deformation structures at maximum slope gradient. Upward reduction in slope gradient of subsequent cycles coincides with a change in

style of soft-sediment deformation from slumps into loading and dewatering structures (Figures 4.6 and 4.7) as well as abrupt reduction in cycle thickness above cycle 5 (Figure 5.1). According to mechanism of soft-sediment deformation development, slumps are governed by gravitational gliding of sediments involving horizontal movement (e.g. Martinsen, 1989; Plink-Björklund et al., 2001) while loading and dewatering structures are due to rapid deposition of sand on mud which may induce density instabilities and subsequent rapid escape of pore-water, i.e. collapse of coarser sediments and vertical sediment motion of finer sediments (Lowe, 1975). As such, loading and dewatering structures tend to be more localised involving no horizontal movement (e.g. Martinsen, 1989; Bhattacharya, 2006; Oliviera et al., 2010). Rapid loading of sediments and increase in grain size due to stable progradation of delta front and upward reduction in slope gradient of subsequent cycles may have been responsible for higher proportion of *in-situ* loading and dewatering structures than slumping structures in the studied succession. A proposition of low-slope gradient (i.e. 0.5 - 1^0) by previous workers, i.e. Wild et al. (2009) and Oliviera et al. (2010) for Kookfontein shelf edge delta system may contribute largely to this phenomenon (Figures 4.14 and 4.15). Bhattacharya (2006) also noted that typical much lower slope gradient in the Alberta shelf edge examples are responsible for mostly restricting soft-sediment deformation features to loading structures rather than large-scale slumps, slides or growth faults.

Each facies succession (i.e. cycle) of the lower Kookfontein member exhibits a somewhat irregular (i.e. asymmetrical) thickening pattern of bedsets (i.e. lithofacies) (Figure 4.18) but on the whole depicts overall thickening- and coarsening-upward succession with

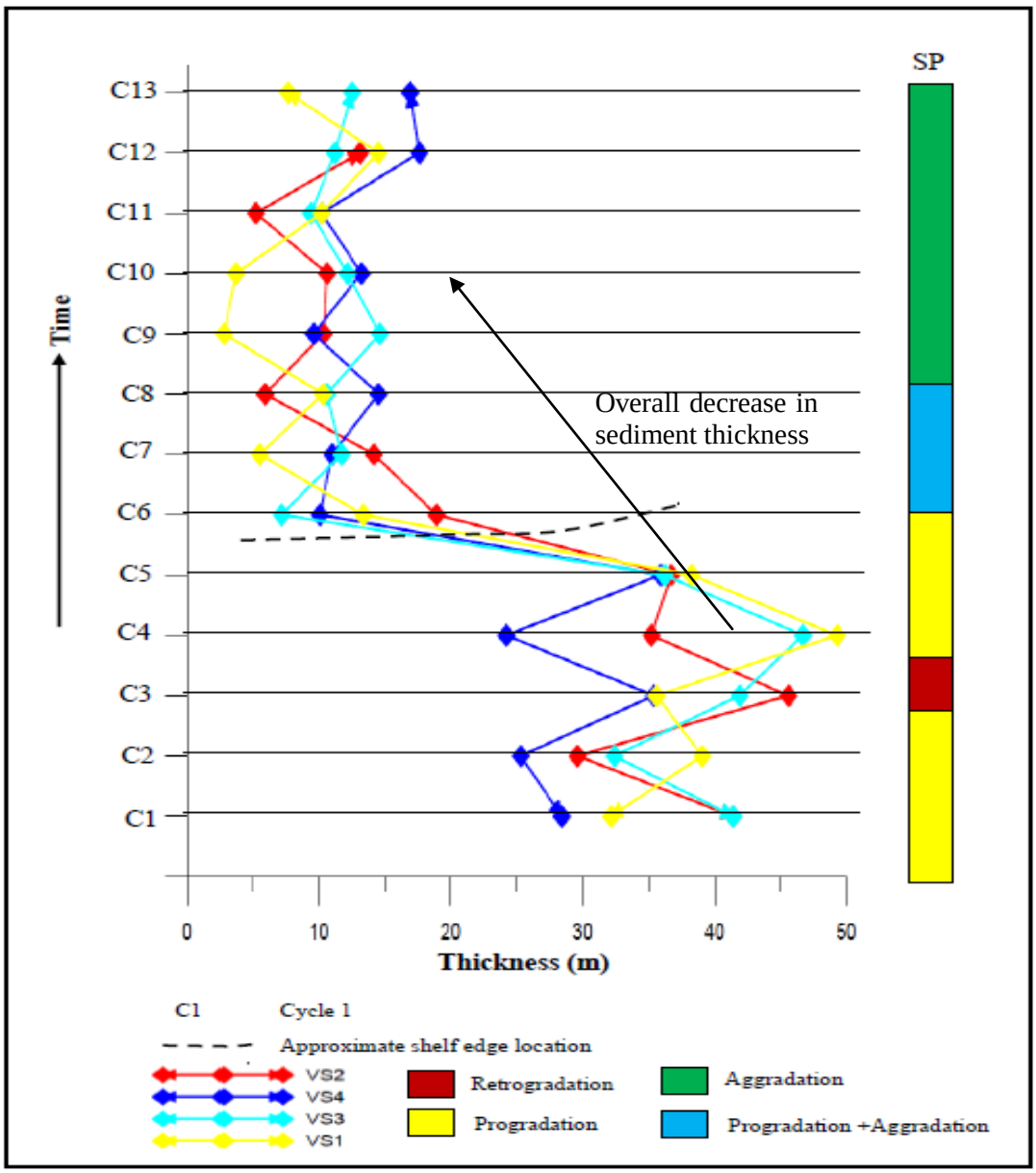

Figure 5.1. Wheeler diagram showing vertical variation in cycle thicknesses and sediment stacking pattern for the Kookfontein deltaic succession. Note the change from thicker sedimentary cycles and progradational stacking trend (i.e. Cycles 1 to 5) to abrupt thinner sedimentary cycles and aggradational stacking pattern (i.e. Cycles 6 to 13). The black arrow indicates overall upward decrease in cycle thickness.

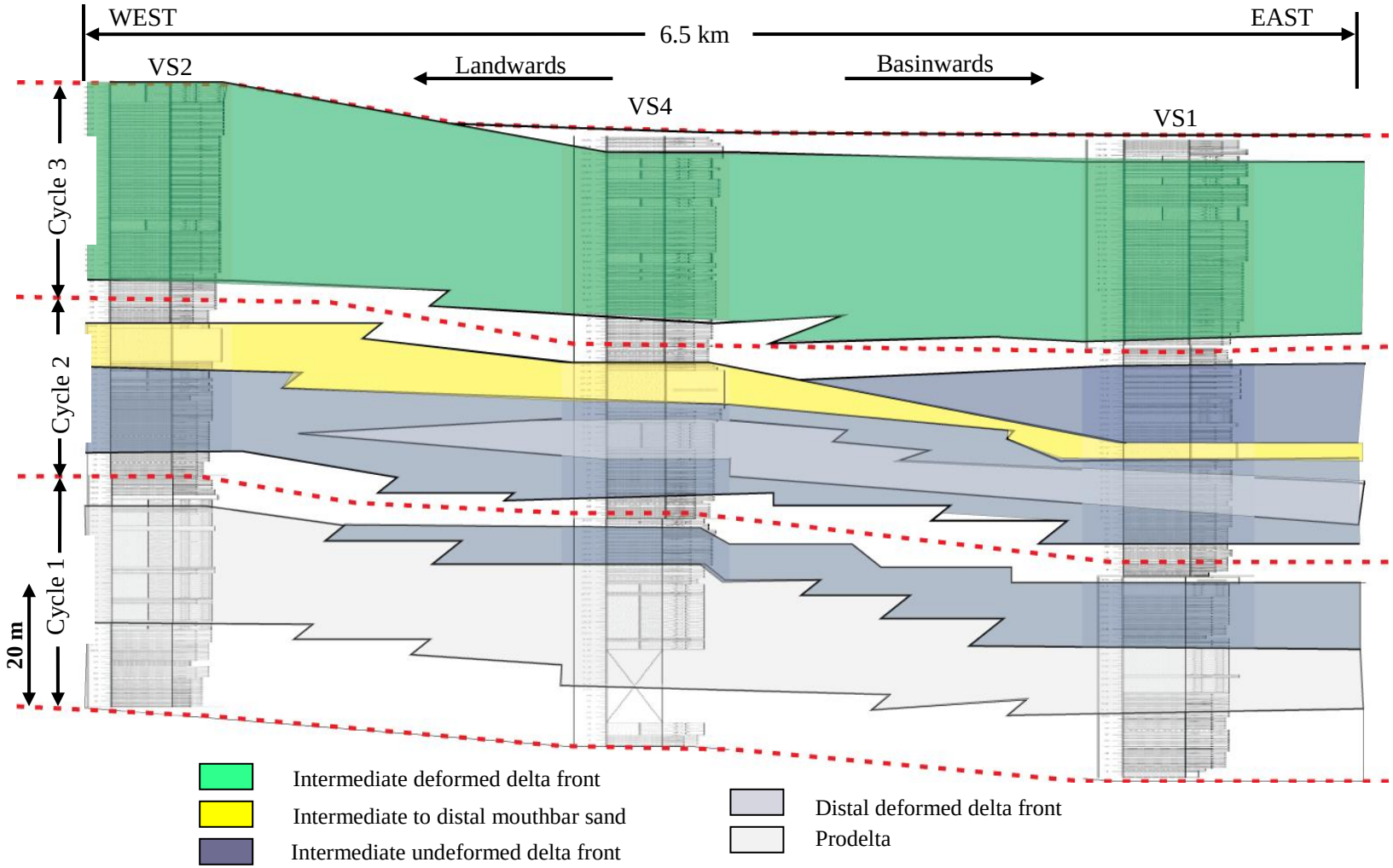

Figure 5.2. Interpreted correlation panel of the lower Kookfontein succession (i.e. cycles 1 to 3) observed at the Pienaarsfontein locality and oriented parallel to the main paleocurrent direction (i.e. NE) showing facies architecture and depositional facies that characterise this succession.

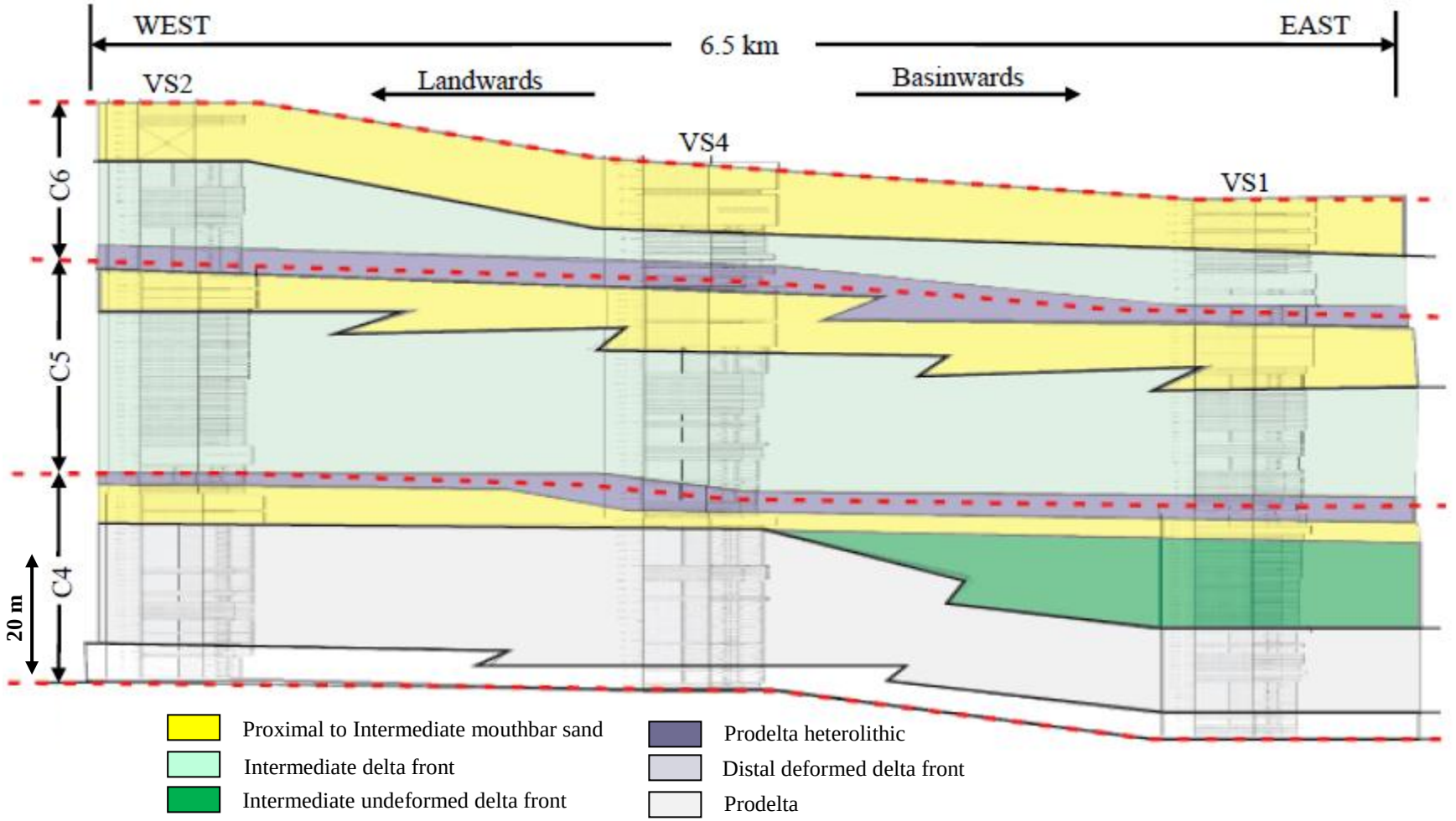

Figure 5.3. Interpreted correlation panel of the upper succession of the lower Kookfontein succession (i.e. cycles 4 to 5) and lowermost cycle of the upper Kookfontein succession (i.e. cycle 6) observed at the Pienaarsfontein locality and oriented parallel to the main paleocurrent direction (i.e. NE) showing facies architecture and depositional facies that characterise these successions. Note the upward prominence of delta front heterolithic facies and proximal mouthbar sands within these successions.

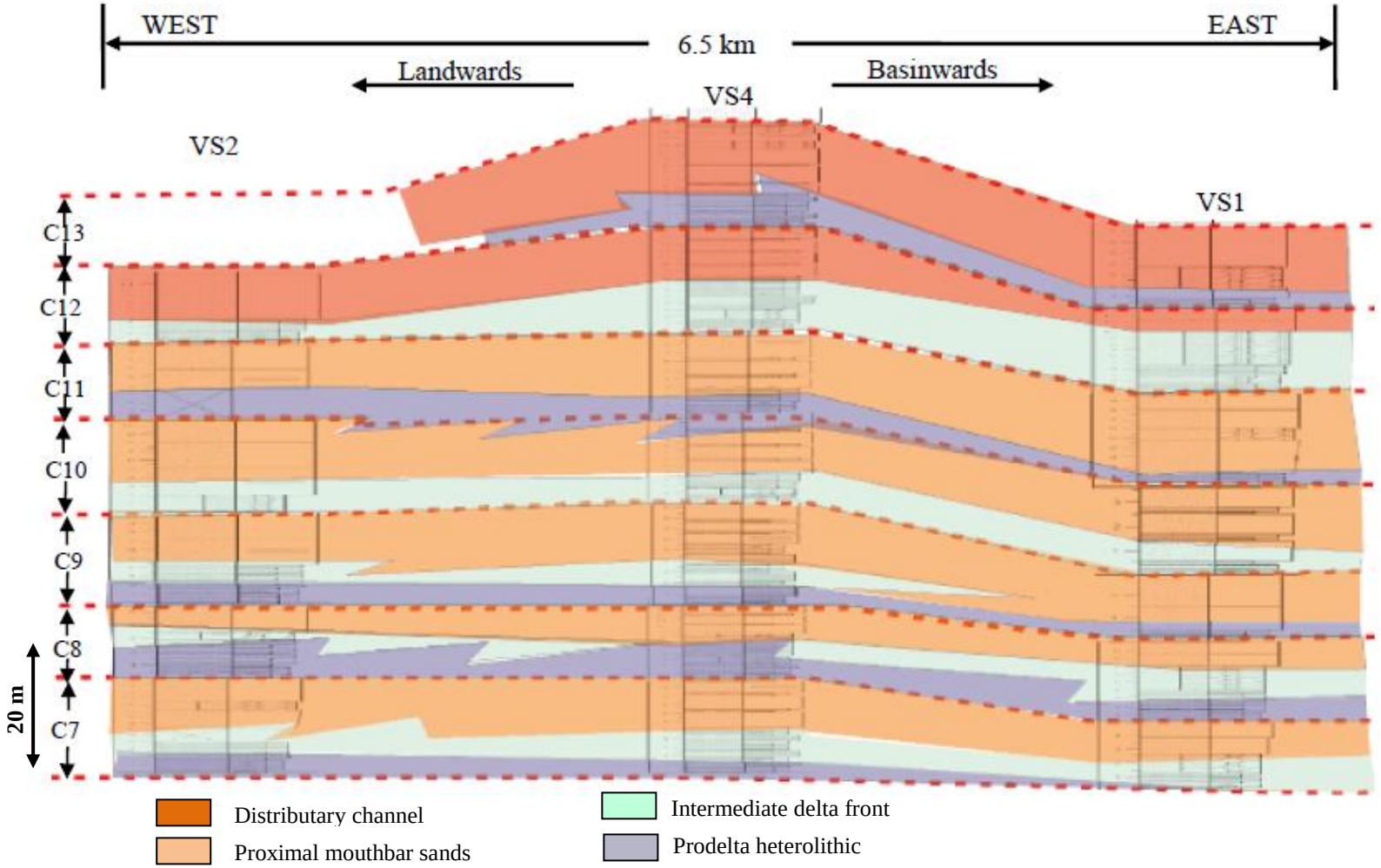

Figure 5.4. Interpreted correlation panel of the upper Kookfontein succession (i.e. cycles 7 to 13) observed at the Pienaarsfontein locality and oriented parallel to the main paleocurrent direction (i.e. NE) showing facies architecture and depositional facies that characterise this succession. Note the prominence of proximal mouthbar sands within this succession which coincides with abrupt reduction in cycle thickness and a change to progradational to aggradational stacking pattern representing deposition of shelf-margin to outer shelf successions above the shelf break.

progradational sediment stacking trend. Whereas, the upper Kookfontein cycles (i.e. cycles 6 to 13) exhibits a somewhat regular thickening pattern of bedsets with overall progradational to aggradational sediment stacking trend. The facies stacking and geometry of the lower and upper Kookfontein depicts an overall progradational pattern indicative of normal regressive shelf edge trajectory path (Muto and Steel, 2002; Catuneanu et al; 2009) through time (Figure 5.5). Thus, each cycle is a flooding surface-bounded parasequence which architecture and geometry are governed by the interplay between internal (i.e. local depositional processes) and external (i.e. regional control on sediment supply, accommodation and base-level changes, e.g. Muto and Steel (2002); Labourdette et al. (2008)) forces. The observed cyclicity (i.e. regular repetition of sedimentary features) within each cycle suggests that this repetitiveness is governed primarily by internal forcing, e.g. switching of prograding distributary mouthbars. Then these cycles would be akin to Van Wagoner et al.'s (1990) definition of classic shelf parasequences that are internally prograding with no external forcing. At sequence scale, regular repetition of flooding surfaces is more influenced by external depositional controls, i.e. climate, tectonics and eustatic fluctuation. The series of flooding events (i.e. transgressive and regressive events) that characterise the architecture and geometry of the Kookfontein delta sequence are discussed in the sub-sections that follow.

5.2.1 Lower Kookfontein parasequences (i.e. Cycles 1-5)

In all the studied vertical profiles, lower Kookfontein member (i.e. cycles 1-5) gives somewhat irregular thickening- and thinning- upward trend with an overall upward-shallowing trend (i.e. upward-thickening and coarsening) and a progradational stacking pattern as prodelta mudstones pass up into delta front heterolithics and then proximal mouth-bar sands (Figures 5.2 and 5.3). The upper parts of cycles 1 to 3 fine and thin upward indicating a gradual landwards shift of facies whereas cycles 4 and 5 exhibit sharp tops

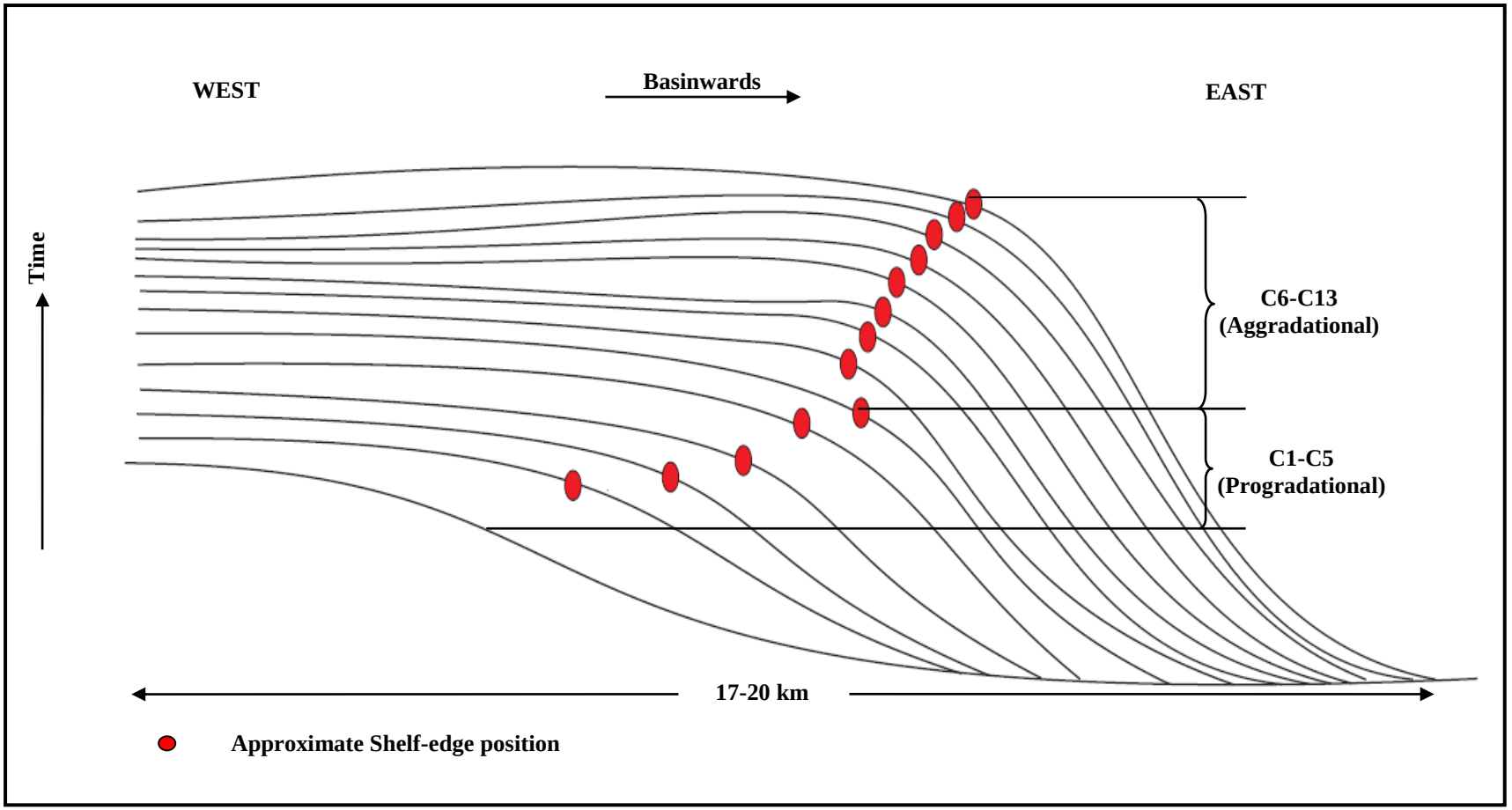

Figure 5.5. Schematic geometrical model of the Kookfontein clinoforms at the Pienaarsfontein locality showing the overall progradational to aggradational sediment stacking pattern of the delta system representing deposition of mid-slope to outer shelf succession. Note the upward change in sediment stacking pattern above cycle 5 which coincides with abrupt reduction in cycle thickness.

indicative of a rapid landwards shift of facies. Each cycle (i.e. facies succession) of the lower Kookfontein member is therefore characterised by the presence of three stratigraphic surfaces i.e. progradational, emergence and flooding surfaces resulting from series of mouthbar flooding events (Allen and Mercier, 1988; Figures 5.6 and 5.7) which can be correlated across all the measured vertical profiles.

The lowermost discontinuity in a deltaic cycle at the base of the first Kookfontein flooding surface-bounded parasequence (i.e. base of cycle 1 or the top of Skoorsteenberg Unit 5; Figures 4.5, 4.9 and 5.2), forms a surface over which the delta progrades (Figures 5.6 and 5.7). This depositional surface coincides with the base of an upward-coarsening succession (i.e. cycle 1). As the delta progrades, shallowing upward deposits are deposited and may reach sea-level depending on the balance between sediment supply and sea-level. This depositional surface that marks the end of a progradational episode is termed an "emergence surface" (Allen and Mercier, 1988). An "emergence surface" in this case is not marked by subaerial or intertidal facies as there is no evidence for subaerial exposure in the studied stratigraphic interval. Therefore, emergence surface within the lower Kookfontein cycles is defined as the most proximal facies (i.e. the most basinwards shift in facies) in each deltaic parasequence (i.e. flooding surface-bounded cycle), and is interpreted as the surface of maximum progradation (Postma, 1990; Labourdette et al., 2008). The next flooding event which are governed by the interplay between sediment supply and base-level changes (i.e. accommodation space) will create a flooding surface over which the mouthbar of the Gilbert-type delta front progrades.

The presence of these three stratigraphic surfaces (i.e. progradational, emergence and flooding surfaces) within the lower Kookfontein cycles resulted in a series of vertically stacked regressive and transgressive delta sequences (Figures 5.7 and 5.8). The upper parts of

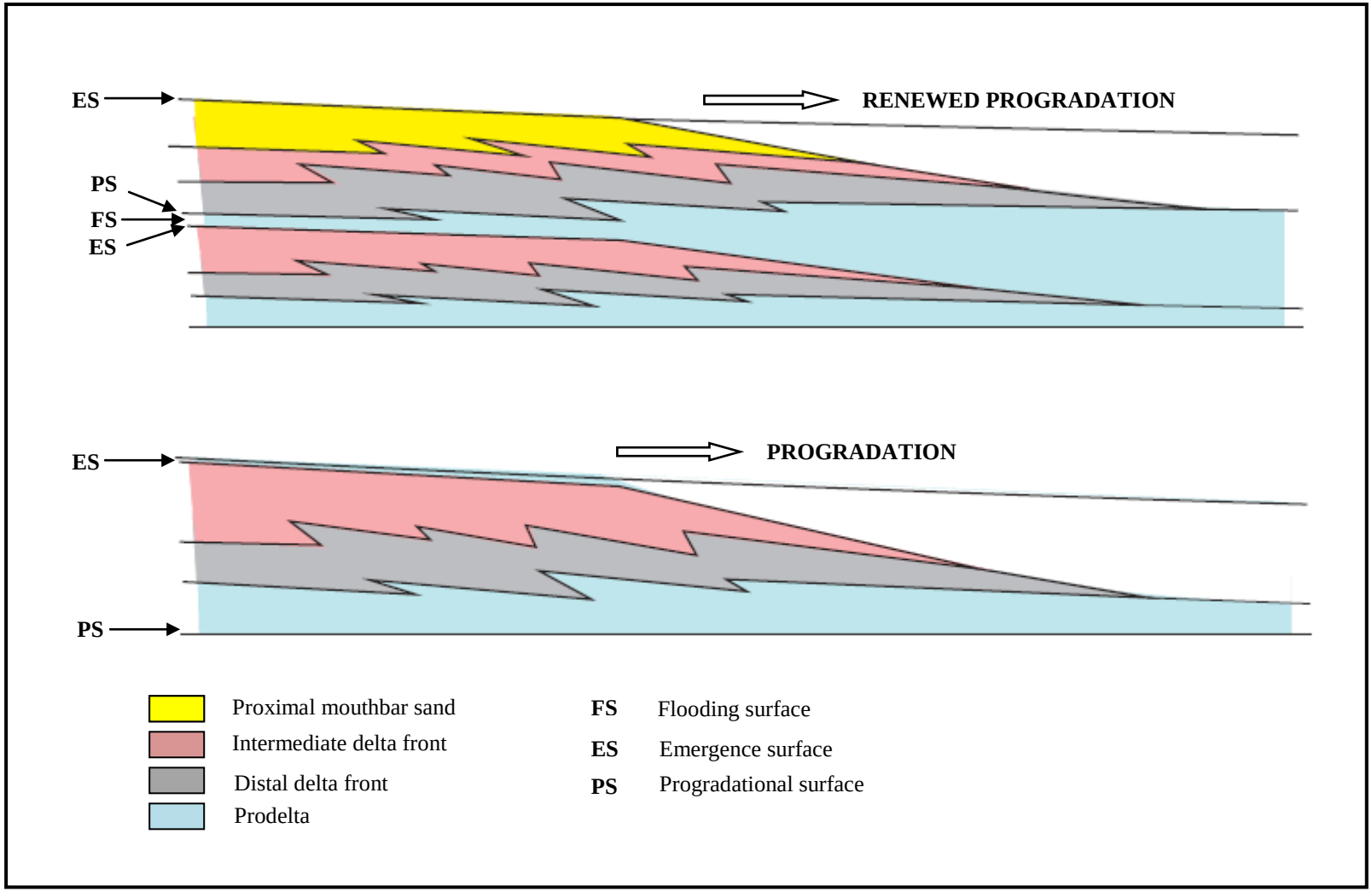

Figure 5.6. Sequences of flooding events in a cycle of delta system with overall normal regressive progradational sediment stacking trend. These series of flooding events result in stacked delta parasequences bounded above and below by flooding surfaces (modified after Labourdette et al., 2008).

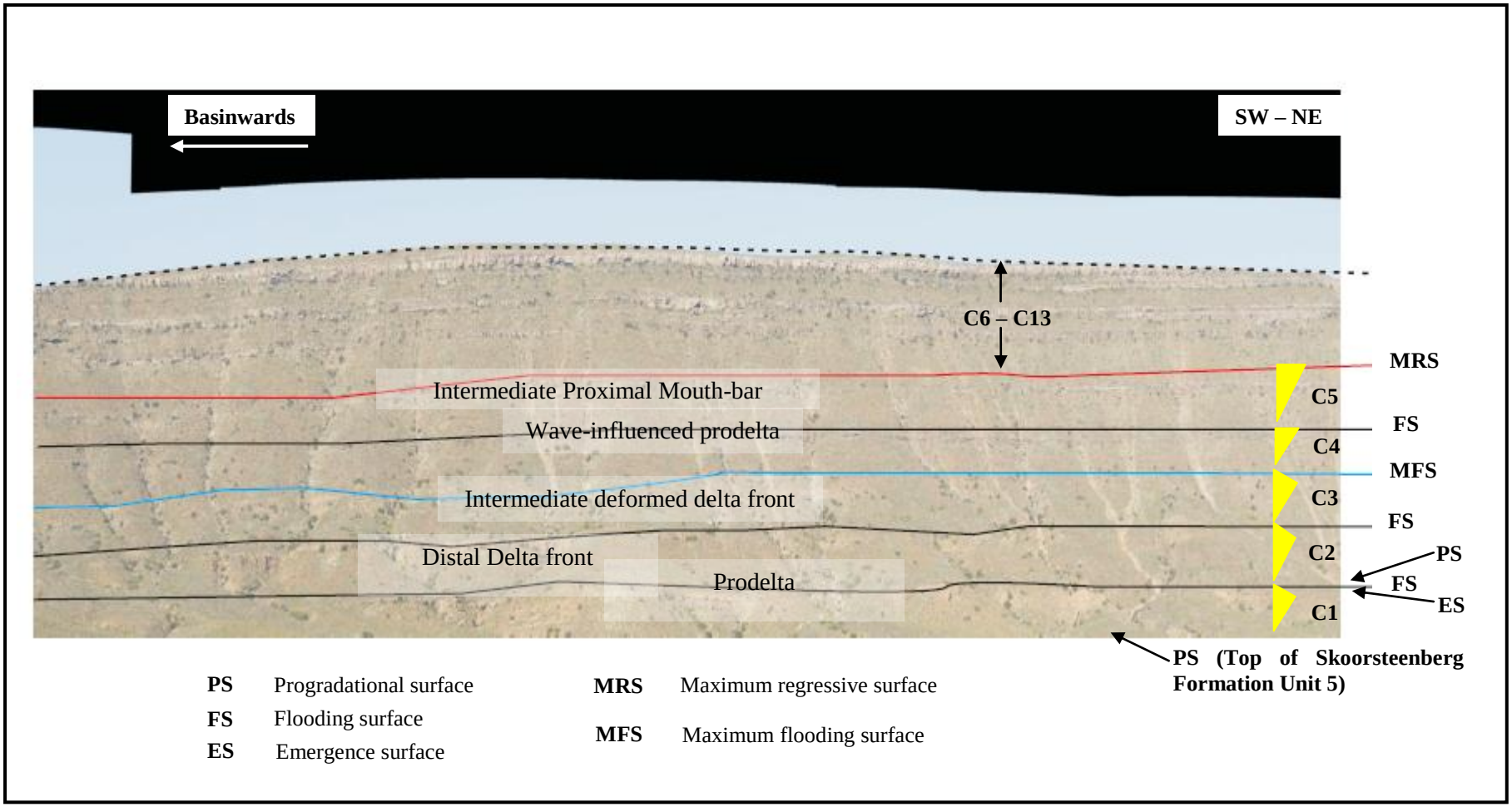

Figure 5.7. Interpreted outcrop photomosaic orientated parallel to the main paleocurrent direction (i.e. NE) showing facies successions and depositional facies, and various depositional surfaces (i.e. boundaries) that characterise the lower Kookfontein member (i.e. cycles 1 to 5). The view of outcrop face is to the south.

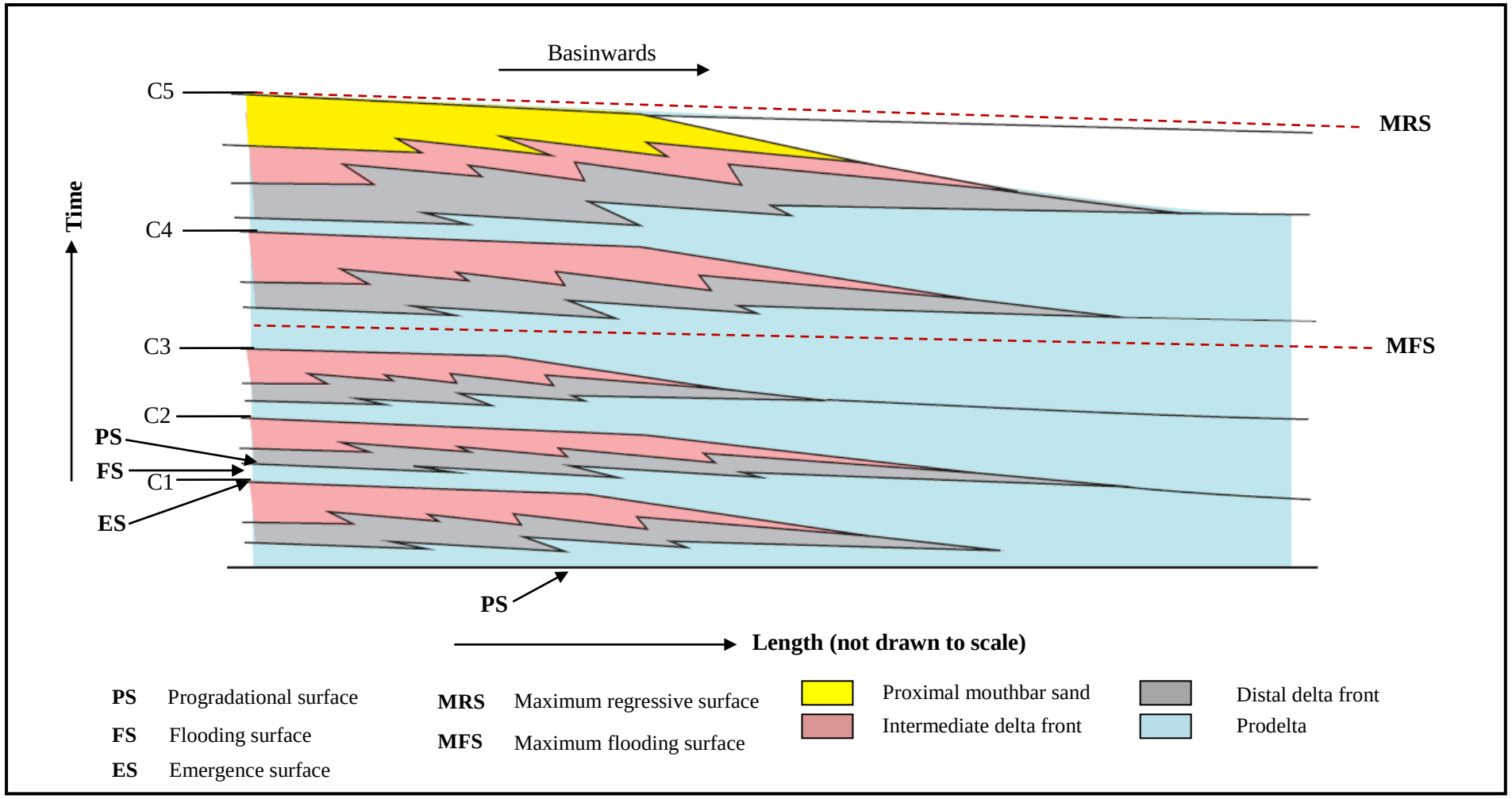

Figure 5.8. Schematic conceptual geometrical model of the lower Kookfontein member (i.e. cycles 1 to 5) showing facies successions, depositional facies as well as depositional surfaces that characterise the succession. Vertically stacked delta flooding surface-bounded parasequences are resulted from series of mouthbar flooding events.

cycles 1 to 3 represent the 3 major transgressive facies (i.e. fining- and thinning- upward, current ripple to plane-parallel laminated, very fine- to fine- grained sandstones with moderate bioturbation interbedded with siltstone and mudstone) within the lower Kookfontein cycles. These flooding surfaces are different from that of cycles 4 and 5, as they represent gradual landwards shift in lithofacies, and therefore interpreted as possible condensed sections (Van Wagoner, 1990) within the lower Kookfontein cycles. The flooding surface above cycle 3 possibly records the most landwards shift in facies, and therefore this flooding surface is interpreted as a maximum flooding surface within the Kookfontein delta sequence (Figures 5.7 and 5.8). Moreover, cycles 4 and 5 represent the most basinwards shift in facies within the lower Kookfontein deltaic succession. As such, the progradation surface (i.e. mouthbar sands) of cycle 5 below the overlain flooding surface is considered a maximum regressive surface (Figures 5.7 and 5.8).

Also, cycles 1-3 represent the deeper and steeper profile of the interpreted mid-slope to top-slope/shelf-margin depositional model for the lower Kookfontein cycles 1-5 due to their higher scale/intensity of soft-sediment deformation than the overlying cycles 4 and 5. Cycles 1-3 are therefore interpreted to be dominated by mouthbar deposition below the shelf break. The interpreted depositional facies that characterise these successions are proximal to distal mouthbar sands, intermediate to distal delta front heterolithics and distal undeformed prodelta heterolithics and mudstones (Figures 5.2, 5.3 and 5.7).

5.2.2 Upper Kookfontein parasequences (i.e. Cycles 6-13)

The upper Kookfontein member (i.e. Cycles 6-13) exhibits an overall upward-shallowing trend with progradational to aggradational sediment stacking pattern, which coincides with their abrupt reduction in cycle thickness above cycle 5 (Figures 5.1, 5.3, 5.4 and 5.5). These sedimentary cycles are very similar in thickness (i.e. ~10-12 m thick), and are made up of upward-thickening and coarsening successions bounded above and below by flooding

surfaces (Figures 5.9 and 5.10). The somewhat regular thickening- and coarsening upward trend of these cycles (Figure 4.19) therefore make them analogous to the classic shelf parasequences of Van Wagoner et al.'s (1990) that are internally prograding. However, there is no evidence of subaerial exposure within this stratigraphic interval. Similar to the lower Kookfontein cycles 1-5, the deltaic architecture and geometry of these cycles are characterised by three stratigraphic surfaces i.e. progradational, emergence and flooding surfaces (Figure 5.6). The upper part of these cycles exhibits sharp tops indicative of a rapid landwards shift of facies. This landwards shift of facies constitutes the deposits of ripple to planar cross-laminated, very fine- to fine- grained sandstones interbedded with siltstones on top of the underlying upward-coarsening succession (i.e. lower Kookfontein cycles 6 to 13). These depositional surfaces are a result of series of Kookfontein delta flooding events governed by the interplay between sediment supply and base-level changes. These series of events during progradation of the upper Kookfontein parasequences resulted in vertically stacked and aggraded regressive and transgressive delta sequences (Figures 5.9 and 5.10).

Moreover, the change from progradational (i.e. lower Kookfontein cycles 1 to 5) to aggradational (i.e. upper Kookfontein cycles 6 to 13) stacking coincides with the abrupt reduction in cycle thickness and soft-sediment deformation as well as increase in sand content above cycle 5. This occurrence is interpreted to represent a repeated episodes of deltaic shallowing trend occasioned probably by decreasing accommodation space and/or decreasing sediment supply. The interpreted depositional facies for these successions are proximal mouthbar sands, intermediate to distal delta front heterolithics and prodelta heterolithics (Figures 5.3, 5.4, 5.9). These interpretations conform to the upper Kookfontein cycles being the final phase of Kookfontein Gilbert-type delta progradation and a change from a mid-slope to top-slope/shelf-margin succession to a more stabilised shelf deposits (i.e. top-slope/shelf-margin to outer shelf).

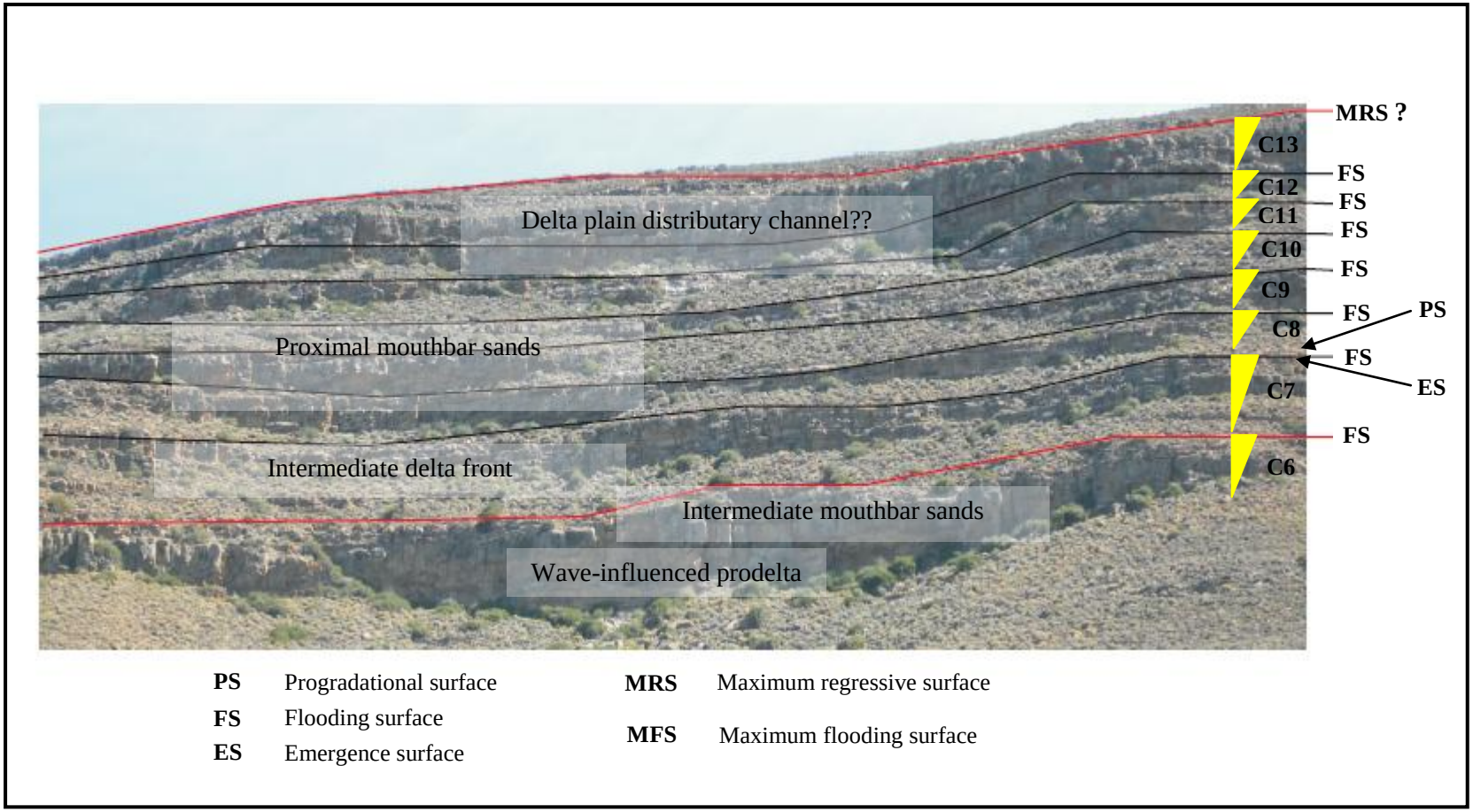

Figure 5.9. Interpreted outcrop photomosaic showing facies successions, depositional facies, and various depositional surfaces (i.e. boundaries) that characterise the upper Kookfontein member (i.e. cycles 6 to 13). The view of outcrop face is to the north.

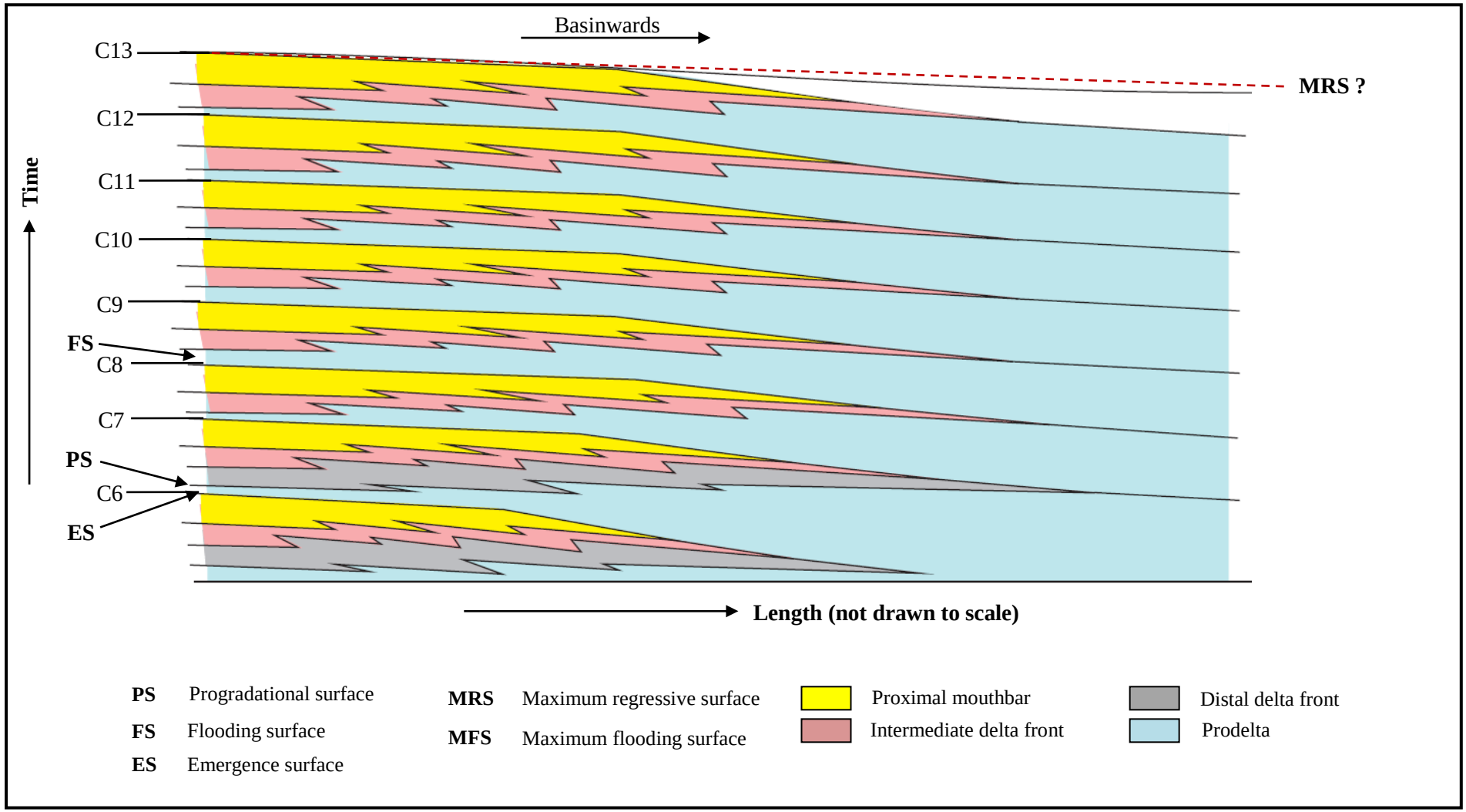

Figure 5.10. Schematic conceptual geometrical model of the upper Kookfontein member (i.e. cycles 6 to 13) showing facies successions, depositional facies as well as depositional surfaces that characterise this succession. Vertically stacked delta flooding surface-bounded parasequences are resulted from series of mouthbar flooding events. Note the overall shallowing of the depo-system typical of a normal regressive prograding delta.

5.2.3 Summary of Kookfontein parasequences

The stratigraphic subdivisions (i.e. sequences) employed in this study are based on the series of mouthbar flooding events and resultant facies stacking through time. These sequences of events (i.e. transgression and regression) give rise to the major stratigraphic surfaces that characterise the Kookfontein (Formation) deltaic architecture and geometry. At cycle- scale (i.e. facie succession), the stratigraphic surfaces that define the relationship between encountered lithofacies as well as the series of flooding events that deposit them are: progradation, emergence and flooding surfaces (see Figure 5.6). A simplified conceptual two-dimensional model to show the distribution of these surfaces and the resultant facies variations during overall progradation of the Kookfontein shelf edge Gilbert-type delta depo-system is given in Figures 5.11 and 5.12. Each cycle boundary is a flooding surface (i.e. base-level change) over which another episode of deltaic progradation develops. Sequences of renewed progradation through time would result in vertically stacked transgressive and regressive delta sequences. Hierarchically, the two megasequences (i.e. parasequence sets) that characterise the Kookfontein deltaic succession are: transgressive sequence set (TSS) and regressive sequence set (RSS). The boundaries between these two parasequence sets are better constraint through the identification of a maximum flooding surface above cycle 3 in the field (Figure 5.11). Cycles 1 to 3 consist of upward- thickening and coarsening successions with each capped by a thinning- and fining- upward succession. Consequently, cycles 1 to 3 constitute the transgressive sequence set while cycles 4 to 13 represent the regressive sequence set (Figures 5.11 and 5.12). A maximum regressive surface is also recognised above cycle 5 of the lower Kookfontein member (i.e. cycles 1 to 5). Thus, the lower Kookfontein member is characterised by a maximum flooding surface above cycle 3 and a maximum regressive surface above cycle 5, and bounded above and below by maximum regressive and flooding (or maximum flooding) surfaces respectively. The overall

progradational sediment stacking pattern of these cycles enables the establishment of maximum regressive surface above cycle 5. The upper Kookfontein member is probably bounded above and below by maximum regressive surfaces.

5.3 Kookfontein delta geometry: indicators for possible depositional controls

Two possible scenarios of deltaic geometry are hypothetically constructed based on the overall sediment stacking patterns and cycle thickness trend for repeated episodes of Kookfontein coarsening- and thickening- upward succession in a mixed influence of shoreline/delta system. These scenarios are summarised below and illustrated schematically in Figure 5.8:

First scenario-(Retrogradational sediment stacking; Figure 5.13): this sediment stacking and thickening patterns are possible in a cycle of deltaic progradation and abandonment. The resultant stacked regressive and transgressive delta sequences are capped by abandonment facies (i.e. transgressive marine shale) deposited during gradual landwards shift in facies (Allen and Mercier, 1988). As subsidence or sea-level rise continues with a decreasing influx of fluvial sediments, relative sea-level rise surpasses sediment supply and a transgressive flooding surface is developed across the delta top. The top of this retrogradational sediment stacking will exhibit thin hemipelagic (marine shale) sedimentation. This type of facies association and geometry is driven by accommodation space (i.e. base-level changes or relative sea-level changes due to tectonic subsidence and/or eustatic fluctuation) plus or minus sediment supply, climate and deltaic lobe switching.

Second scenario-(Progradational sediment stacking; Figure 5.13): the resultant facies associations and geometries are characterised by an overall upward-coarsening and thickening trend during progressive shallowing of the delta system. During delta progradation, shallowing upward deposition may reach sea-level depending on the balance between sediment supply and sea-level rise (Labourdette et al., 2008). As subsidence or sea-level rise

decreases with an increasing supply of fluvial sediments, relative sea-level falls or remains constant to create an overall basinwards shift in facies. The top of this progradational sediment is typically capped by a regressive surface with a characteristic thick sand-prone sedimentation. This sediment stacking pattern is driven by accommodation space (i.e. base-level changes or relative sea- level changes due to tectonic subsidence and/or eustatic fluctuation) plus or minus sediment supply, climate and deltaic lobe switching.

In the studied Kookfontein deltaic succession, the following observations are noted of its geometry (i.e. sediment stacking and cycle thickening patterns):

a) The overall sediment stacking pattern is progradational (i.e. cycles 1-5) to aggradational (i.e. cycles 6-13)

b) The succession represents an overall upward-shallowing profile (i.e. upward-coarsening and thickening succession)

c) Overall basinwards shift in facies also indicates that the succession consists of more regressive facies than transgressive facies.

d) Overall reduction in cycle thickness i.e. gradual upward reduction in cycle thickness of cycles 1-5 and the abrupt reduction in thickness plus increase in sand content of cycles 6-13 above cycle 5.

From the above observations, it can be safely said that the Kookfontein deltaic system is similar to the sediment stacking and geometry proposed for Scenario 2 (particularly observations a, b and c). However, there appears to be non-conformity between the two (i.e. Scenario 2 and Kookfontein deltaic succession) due to overall reduction in cycle thickness of the Kookfontein deltaic succession. This line of evidence is suggestive that the Kookfontein deltaic sequences may not be accommodation space-driven as previously held by previous authors (e.g. Van Lente, 2004; Wild, 2005) but rather they are possibly driven by sediment flux or supply. The implication of this phenomenon is such that the accommodation space

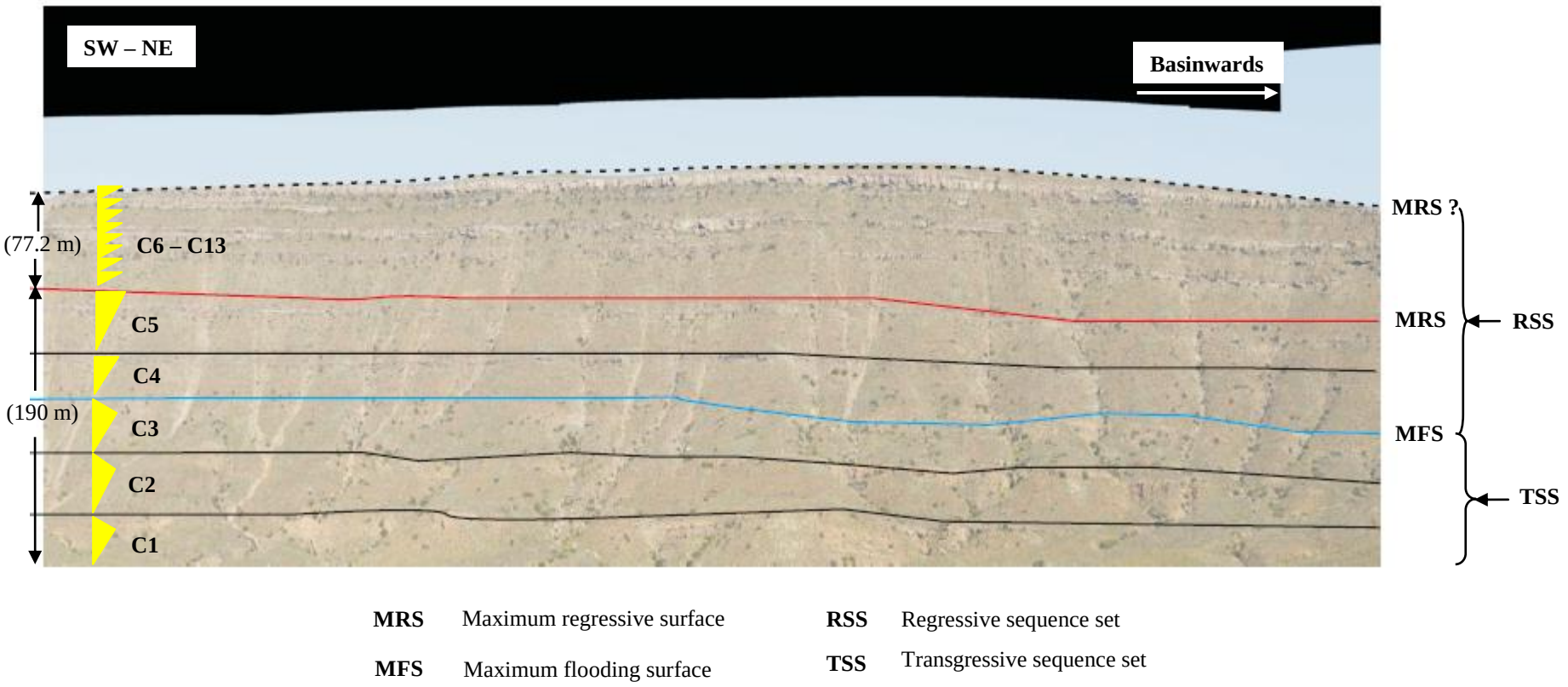

Figure 5.11. Interpreted outcrop photomosaic of the Kookfontein deltaic succession oriented parallel to the main paleocurrent direction (i.e. NE) showing depositional surfaces (i.e. boundaries) as well as the two megasequences (i.e. regressive sequence set and transgressive sequence set) that characterise the succession. Outcrop view is to the south.

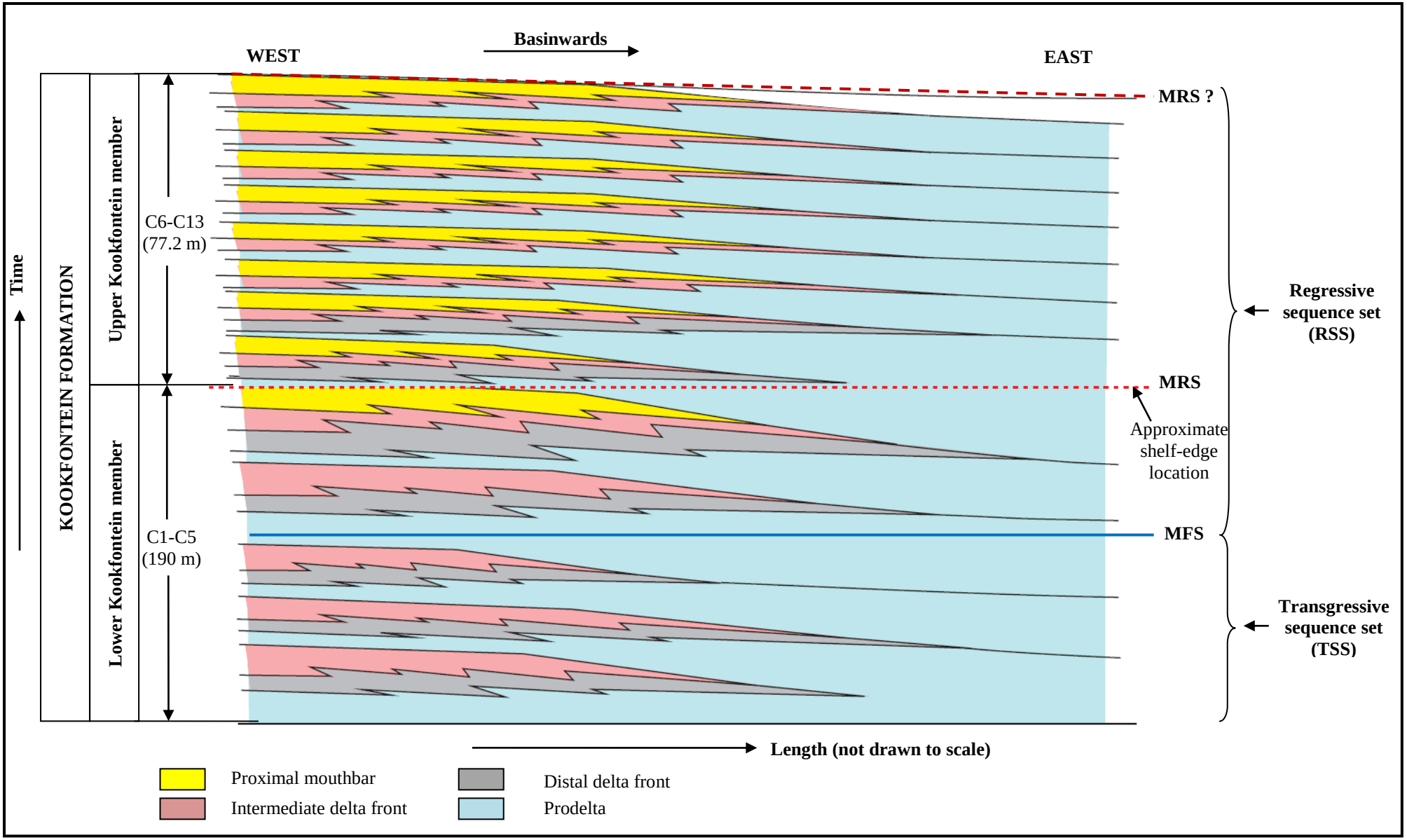

Figure 5.12. Schematic conceptual geometrical model of the Kookfontein deltaic succession (i.e. cycle1 to 13) showing facies successions, depositional facies as well as depositional surfaces that characterise this succession. Vertically stacked flooding surface-bounded parasequences are resulted from series of primary mouthbar flooding events as well as secondary remobilisation of sediments under gravity. Note the overall shallowing of the depo-system typical of a normal regressive prograding delta.

1st scenario: Retrogradational sediment stacking pattern

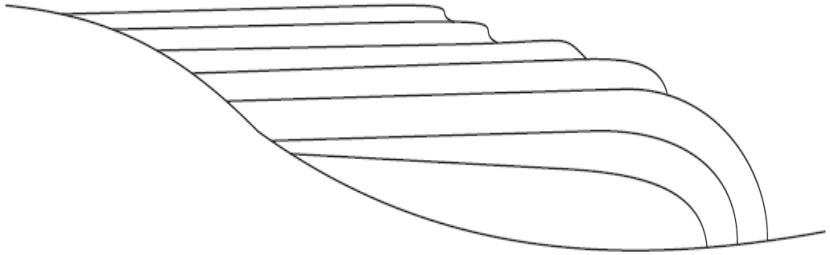

Depositional features:

- Transgression
- Thin sedimentation
- Facies architecture and geometry controlled by accommodation and/or sediment supply rate

2nd scenario: Progradational sediment stacking pattern

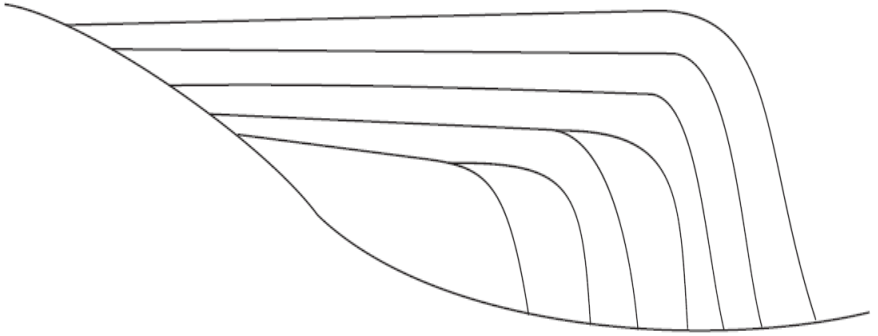

Depositional features:

- Regression
- Thick sedimentation
- Facies architecture and geometry controlled by accommodation and/or sediment supply rate

Figure 5.13. Hypothetical 2D geometrical models constructed for two possible scenarios of sediment stacking patterns (i.e. retrogradational and progradational) for delta depo-system involving series of deltaic retreating and out-building events.

was being created but sediment starvation resulted in abrupt cycle thickness reduction above cycle 5. Sediment flux in a deltaic regime is largely dependent on climate and tectonic setting (Elliot, 1986; Postma, 1990). Therefore, the feasible dominant depositional controls on the Kookfontein deltaic cyclicity could probably be climate and tectonics with minor or no eustatic fluctuations.

5.4 Implications for reservoir modelling

The construction of accurate geological models and upscaling for reservoir simulation has become an important tool within the oil industry for reservoir management and making decisions on drainage strategy (e.g. Lasseter et al., 1986; Mayer and Chapin, 1991; Flint and Bryant, 1993; Qi and Hesketh, 2005; Mikeš and Geel, 2006; Keogh et al., 2007; Labourdette et al., 2008; Cabello et al., 2010). These models, with the objective to incorporate all scales of sedimentary heterogeneities, are built from an integration of subsurface (i.e. seismic, well log, core and borehole image) and analogue (i.e. outcrop and modern) datasets. The success of any reservoir modelling procedure depends on how well facies variability is represented in the geological model. Therefore, detailed facies analysis and sedimentological models from outcrops can provide additional information on facies variability and small scale heterogeneity needed for a robust reservoir model (Flint and Bryant, 1993; Falivene et al., 2006).

The schematic geological model, consisting of facies successions (i.e. cycles or parasequences) as flow units and facies associations/depofacies as flow cells, for the lower Kookfontein cycles 1 to 3 within the studied succession is given in Figure 5.14. The model is populated with facies at different scales (i.e. facies succession, facies association, depofacies and laminae) as the basic building blocks. Thus, it is ready to be transformed into a reservoir model. The most important implications of this work for reservoir modelling of similar subsurface analogues are as follows:

1. A hierarchical description of heterogeneity, i.e. ranging in decreasing order from facies succession (cycle), facies association (bedsets), depofacies (beds) and laminae, offers a simple and straightforward approach to describe internal architecture of facies and particularly sandbodies in the ensuing geological model (Figure 5.14). This approach follows from the previous work by Mikeš and Geel (2006).
2. Each flooding surface-bounded parasequence is a flow unit, and each flow unit (consisting of flow cells, i.e. facies/depofacies) can be divided into rectangular grid cells (Mikeš et al., 2006; Labourdette et al., 2008; Cabello et al., 2010).
3. Two important boundaries that could determine fluid flow are parasequence (i.e. cycle) and depofacies boundaries. Parasequence boundaries being flooding surfaces may be flow barriers, while depofacies boundaries may be flow conductors (particular if they are substantially gradational). Determination of the degree of facies interfingering might also be crucial to predicting facies boundary behaviour to fluid flow.
4. The reworking of sediments by gravity processes, waves and ichnofossils could also have an important effect on porosity and permeability reduction.
5. Recognition of facies variations within facies succession (i.e. cycle) is very difficult from GR log alone without performing “Outcrop log-GR log” tie.
6. The described internal heterogeneity in this work is below the resolution (i.e. mm-scale) of most conventional well-logs, and therefore could supplement well-log data especially where there is no borehole image and core data.

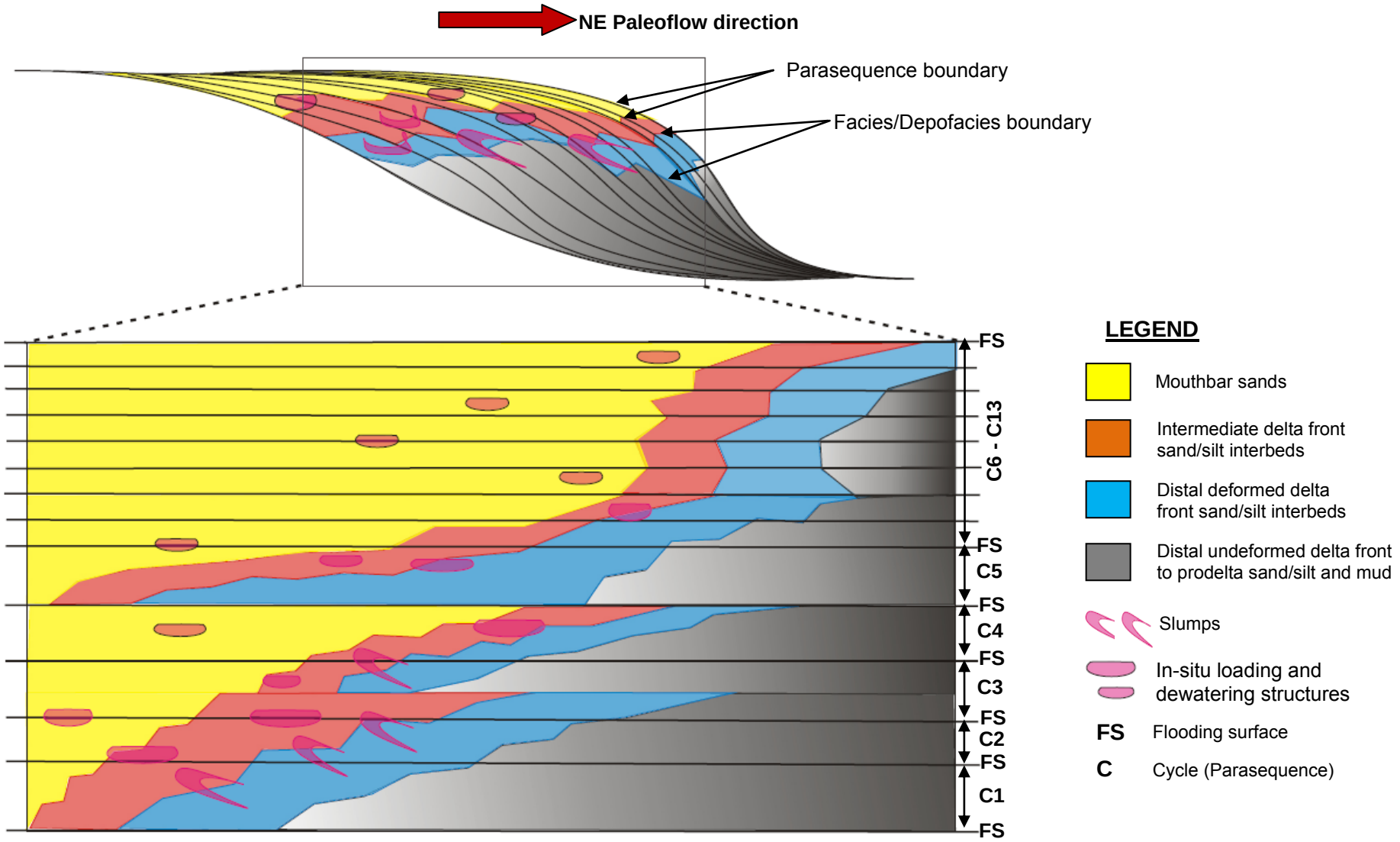

Figure 5.14. Schematic geological model for the Kookfontein shelf edge Gilbert-type delta (i.e. cycles 1to 13) showing facies distribution, stacking and boundaries. At reservoir-scale, I assume flooding surface-bounded parasequence (i.e. facies succession/cycle) to be a flow unit consisting of flow cells (i.e. facies associations/depofacies). Two important boundaries for flow behaviours are: parasequence boundary (i.e. flow barrier) and facies/depofacies boundary (i.e. flow conductor).

CHAPTER SIX

PETROPHYSICAL CHARACTERISATION

6.1 Introduction and analytical techniques

The objective of this chapter is to carry out a grain size-based petrophysical analysis of outcrop data in order to empirically predict porosity and permeability distribution of Kookfontein deltaic reservoir facies. Therefore, the petrologic properties of the studied outcrops at the Pienaarsfontein locality were measured from thin-sections of fifteen sandstone samples. The thin-sections were cut parallel to the bedding in order to obtain directional measurement that incorporate small-scale laminar heterogeneity. These samples were initially observed under a handlens in the field for textural properties, i.e. grain size, sorting and roundness. A polarising microscope and a scanned electron microscope (SEM) were used to determine grain-size distribution, mineralogical and textural maturity (i.e. based on fine-grained content, sorting and roundness of the grains, and the basic detrital and authigenic mineral composition) as well as the morphological relationship between different minerals. The morphology and textural relationships among minerals especially albitic feldspar alterations, cements and authigenic minerals which were not possible with petrographic microscope were examined under a SmartSEM scanning electron microscope (i.e. a Zeiss EVO® MA15 Scanning Electron Microscope) at the Stellenbosch University for some selected samples. Quantitave analysis of phase compositions of the SEM samples and their backscatter images require 15 micrometer thickness (peacock blue colour) of carbon coating, a flat and polished surface. Samples were identified with backscattered electron (BSE) and/or Secondary electron images, and phase compositions were quantified by EDX analysis using an Oxford Instruments® X-Max 20mm^2 detector and Oxford INCA software. Beam conditions during the quantitative analyses were 20 KV, with a working distance of 8.5 mm and approximately beam current of – 20nA. The counting time was 10 seconds live-time.

Internal Astimex Scientific mineral standards were used for standardization and verification of the analyses. Pure Co were used periodically to correct for detector drift.

Sandstone classification scheme was established based on the Udden-Wentworth Scale for grain-size distribution (Udden, 1914; Wentworth, 1922) and Pettijohn et al. (1987) sandstone classification for detrital grain composition and the proportion of muddy matrix (Figure 6.1). For precise estimation of grain size and textural maturity as well as their modal analyses, photomicrographs were taken of representative thin sections under petrographic microscope and; these were analysed using thin section comparators of Beard and Weyl (1973) and later compared with the results obtained by Van Lente (2004). Also, grain size distribution and percentage composition of detrital grains and authigenic minerals were estimated through the SEM analysis. The results obtained are presented in Table 6.1 while photomicrographs are shown in Figures 6.2, 6.3 and 6.4 as well as Appendix C.

6.2 Petrography and mineralogy

The Kookfontein Formation sandstones are predominantly lithofeldspathic to feldspathic sandstones (classification after Folk et al., 1970; Figure 6.5) composed of framework grains of quartz, feldspar, mica, accessory minerals (e.g. zircon, sphene, garnet and apatite) and lithic fragment. Sandstones containing between 15 to 75% muddy matrix are classified as wacke (classification after Pettijohn, 1987; Figure 6.1) and they also range between lithofeldspathic to feldspathic wacke (Table 6.1). The matrix constituents of the wacke were not possible under the petrographic microscope, but their compositions under the SEM include biotite, illite, chlorite and muscovite (Figures 6.4, 6.6 and 6.7). Quartz overgrowths, calcite, kaolinite, chlorite and illite constitute the major pore-filling minerals. There was little petrographic evidence for weathering or alteration of minerals in any of the thin sections. However, possible K-feldspar alterations (i.e. albitisation and clay authigenesis) were observed under the SEM (Figure 6.4).

The petrographic study shows that all the sandstones range in size from lower very fine- to upper medium-grained with the degree of sorting varying from poorly to well sorted. Grains are typically sub-angular to sub-rounded, and this probably implies a short transport distance of sediments from the source location. Mineral composition in sediments varies considerably as a function of particle size. Previous petrographic studies by Van Lente (2004) have indicated that there is no difference in modal grain size distribution for the sandstones from Tanqua and Laingsburg depocenters. However, petrographic estimation for modal grain size distribution of the sandstones from this study (i.e. for Kookfontein Formation) shows that there is difference in modal pattern due to differing depofacies as well as grain sizes (see Table 6.1). Based on estimation under petrographic microscope and the SEM, the quartz content of the studied sandstones varies according to grain size distribution (i.e. different depofacies) from 10 to 45% approximately.

Quartz is the dominant detrital grain constituent (except in some wacke), and the highest quartz content is found in the proximal mouthbar sandstone facies (see Table 6.1). Quartz grains typically present uniform to undulose extinction under stage rotation, and commonly exhibit syntaxial quartz overgrowths at the margins (Figures 6.2 and 6.3). Also, some detrital quartz grains show evidence of grain crushing or fracturing (Figure 6.2). Undulose extinction is a result of strain or grain fracturing which can either be inherited from the sediment source or resulting from mechanical compaction (Taylor, 1950; Basu et al., 1975). Deep burial mechanical compaction involving grain crushing may occur if the rate of grain-contact quartz dissolution and/or quartz overgrowth development cannot compete with the rate of stress increase at grain contacts (Fisher et al., 1999).

Feldspar is the second most abundant detrital grain, present in all the Kookfontein Formation deltaic sandstones. From petrographic examination, the common detrital feldspars

are sodic plagioclase (albite) and potassium feldspar i.e. K-feldspar (principally microcline and orthoclase); and they also probably occur as authigenic feldspars. Feldspathic alterations are very difficult to examine under petrographic microscope. From SEM analyses, the majority of feldspars (particularly K-feldspars) exhibit some degree of alteration ranging from clay authigenesis, albitisation to partial or complete leaching. Possible partial to complete leaching of K-feldspars might have aided alteration to albite and created pore spaces for precipitation of authigenic chlorite and illite (Figures 6.4, 6.6 and 6.7). Detrital feldspar grains also show evidence of grain straining or fracturing, but this is not as widespread as that of detrital quartz grains.

Other major detrital components are lithic fragments of various types- igneous, metamorphic and sedimentary (5-15%) (Figures 6.3 and 6.4). Mica (predominantly biotite) is typically a minor constituent of most fine-grained sandstones; and in some cases exhibits alteration to clay-rich mica or clay minerals such as kaolinite and chlorite (Figure 6.4). Higher mica contents occur in the delta front sandstone facies (see Table 6.1). Traces of accessory or heavy minerals such as zircon, sphene, epidote, garnet and apatite are present in all sandstones from this study. The matrix is dominated by detrital clay and generally ranges from 5 to 20%, and up to 50 to 60% in some wackes. The intermediate delta front facies contain less muddy matrix than the distal delta front and prodelta facies.

The main authigenic constituents are quartz overgrowth cements, authigenic feldspars, calcite, chlorite, illite, and traces of sulphide. There is little or no petrographic evidence of visible intergranular pore spaces probably due to burial diagenesis i.e. mechanical and chemical (pressure solution) compaction and simple pore-filling by authigenic cements. Previous petrographic studies (e.g. Van Lente, 2004) have also indicated no visible porosity or permeability for the sandstones from Tanqua and Laingsburg areas. However, this study

has been able to empirically predict porosity and permeability values for the Kookfontein deltaic sandstones using burial history data and petrologic variables (mainly grain size, sorting and quartz content). Three types of porosity values are obtained relating to different stages of burial diagenesis; these are: depositional porosity (9.78-39.83%), pre-cement or minus cement intergranular porosity (7.51-26.54%) and present intergranular porosity after cementation (0.55-8%, and up to 10-14% in some sandstones) (see Table 6.2). The downward trend of these porosity values initially depicts the effect of burial diagenesis on sandstone pore space evolution. Most sandstone samples from the Kookfontein delta front mouthbar facies typically display a better pore space development.

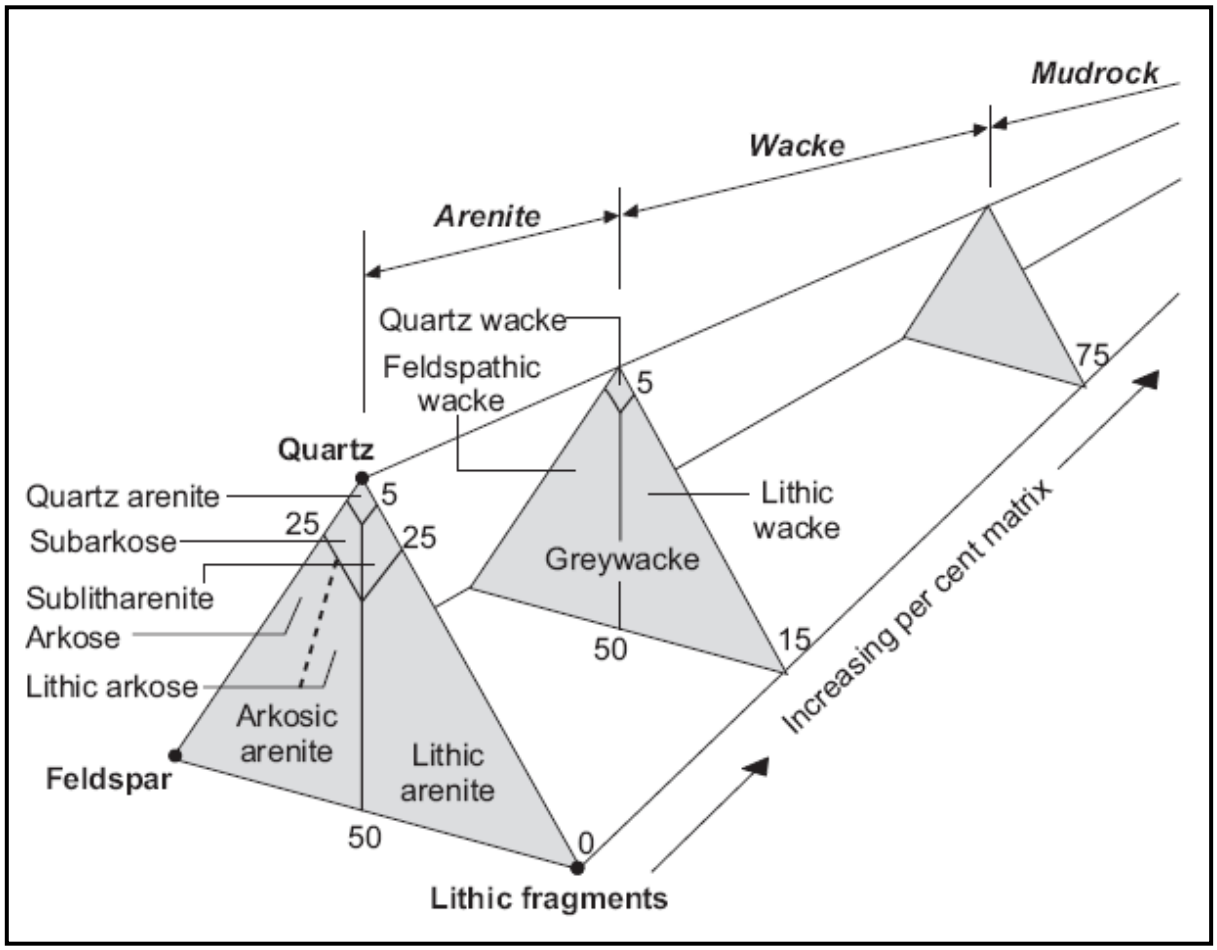

Figure 6.1. Detrital-grain and matrix composition of sandstones (modified after Pettijohn, 1987).

Table 6.1. Statistical summary of the petrologic parameters (i.e. texture and % composition) of the Kookfontein (Formation) deltaic reservoir facies.

#	Log/Sample name	Depth (m)	Facies code	Detrital components						Authigenic minerals				Texture				Rock class
				Q	F	Mc	Rf	Mtx	A/Hm	Qc	Ct	Ch	I	Grain size	Median size (mm)	Sorting	Roundness	
1	V1/SGSR3	17	10	30	20	5	15	12	2	7	2	5	1	Ml - Mu	0.359	MW-S	Sag	Lithofeldspathic sandstone
2	V1/SWA1	22	2	10	15		5	65	5					Slt - Vfl	<0.074	VP-S		Quartzo-Feldspathic wacke
3	V1/SGSR5	29	10	25	20	5	10	15	1	10	3	5	2	Fu - Ml	0.254	W-S	Sag - Sr	Feldspathic sandstone
4	V1/SWA6	45	6	30	20	2	15	10	2	3	5	5		Vfu - Fu	0.149	M-S	Ag - Sag	Lithofeldspathic sandstone
5	V1/SWA7	45.5	2	10	15		10	60	3					Slt - Vfl	<0.074			Feldspathic wacke
6	V1/SWA8	47	3	10	15		10	50	3	2		5	5	Slt - Vfl	0.065	VP-S	Ag - Sag	Lithofeldspathic wacke
7	V1/SWA13	63	11	40	15	5	10	10	1	7	3	5		Ml - Mu	0.359	W-S	Sag - Sr	Lithofeldspathic sandstone
8	V1/SWA14	68	11	45	20		7	5	1	14		5	3	Ml - Mu	0.359	VW-S	Sag - Sr	Subfeldspathic sandstone
9	V2/SWA15.2	20.5	9	25	15	5	10	20	5	7	5	5	2	Vfl - Fl	0.11	P-S	Ag - Sag	Lithofeldspathic wacke
10	V2/SWA15.4	32.5	11	45	20	5	10	5	1	10		3	1	Ml - Mu	0.359	W-S	Sag - Sr	Feldspathic sandstone
11	V2/SWA16	56	5	25	20	7	15	10	2	8		7	3	Vfu - Fl	0.127	M-S	Sag	Lithofeldspathic sandstone
12	V2/SWA17	57	6	30	20	2	15	10	2	8	5	5		Vfu - Fu	0.149	M-S	Sag	Lithofeldspathic sandstone
13	V2/SWA20	69	11	45	15	5	7	5	2	10	3	3	2	Ml - Mu	0.359	VW-S	Sag - Sr	Subfeldspathic sandstone
14	V2/SWA21	106	11	45	20	2	13	10	1	8		2		Fl - Ml	0.149	W-S	Sag - Sr	Lithofeldspathic sandstone
15	V2/SWA22	113	12	45	15		12	7	1	10	2	5	2	Ml - Mu	0.359	VW-S	Sag - Sr	Lithofeldspathic sandstone

Q = Quartz; F= Feldspar; Mc = Mica; Rf = Rock fragment; Mtx = Matrix; A/Hm = Accessory or heavy minerals; Qc = Quartz cement; Ct = Calcite; Ch = Chlorite; I = Illite

Slt = Silt; Vfl = Very fine lower; Vfu = Very fine upper; Fl = Fine lower; Fu = Fine upper; Ml = Medium lower; Mu = Medium upper

VW-S = Very well sorted; W-S = Well sorted; MW-S = Moderately well sorted; M-S = Moderately sorted; P-S = Poorly sorted; VP-S = Very poorly sorted

Ag = Angular; Sag = Sub-angular; Sr = Sub-rounded

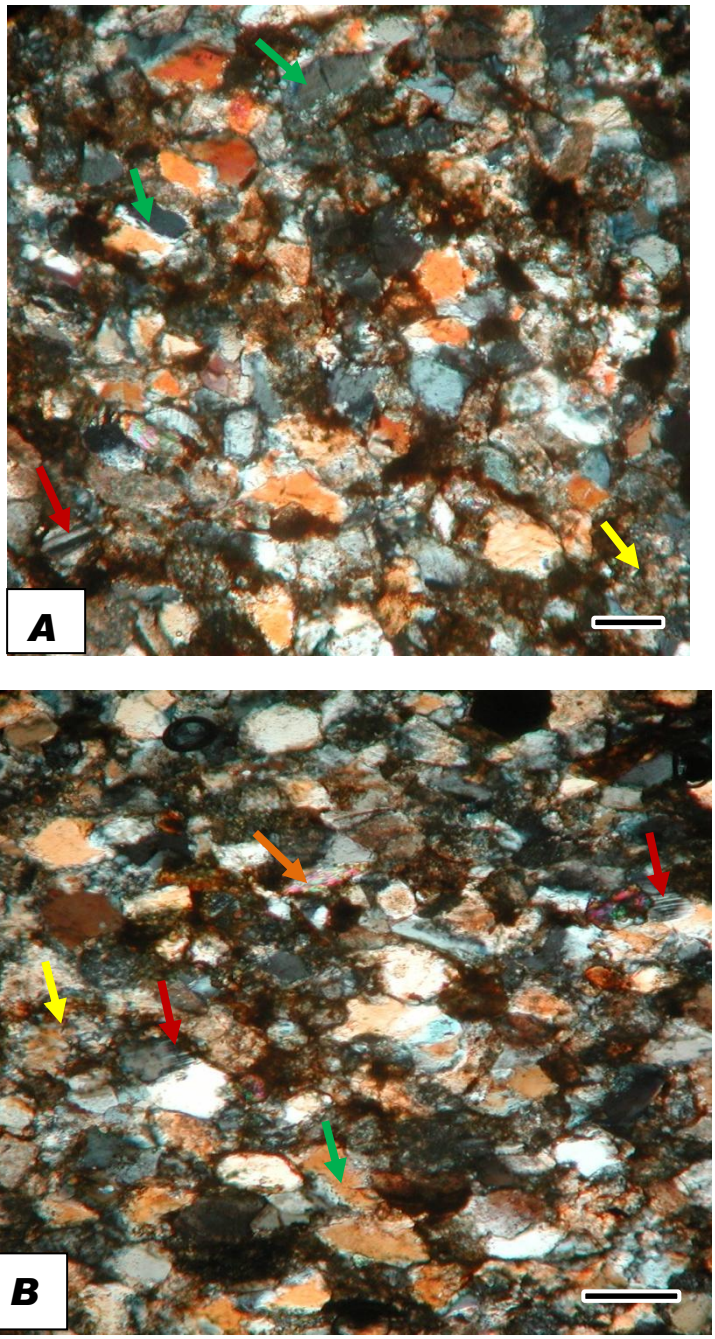

Figure 6.2. Photomicrographs of Kookfontein (Formation) deltaic sandstones. 20X magnification; scale bar is 0.3mm. (A) Indicated by arrows: Green = quartz grains exhibiting undulose extinction, fracturing and overgrowth; Red = plagioclase (albite); Orange = biotite; Yellow = lithic fragment; (B) Indicated by arrows: Green = quartz grains with extensive quartz overgrowth cements; Red = K-feldspar (microcline); Yellow = lithic fragment.

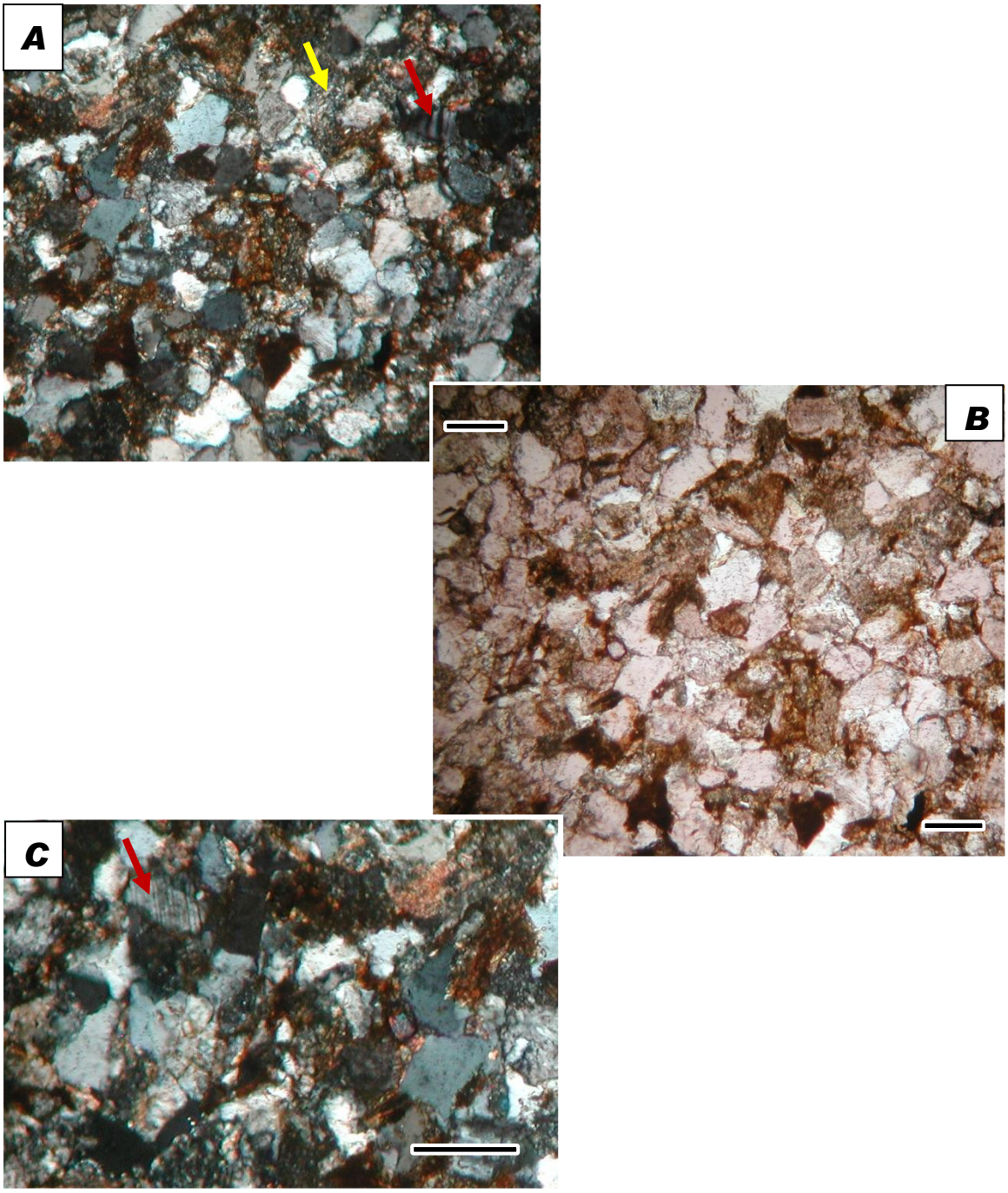

Figure 6.3. Photomicrographs of Kookfontein (Formation) deltaic sandstones. Photographs A and B is 20X magnification; Photograph C is 50X magnification; scale bar is 0.3mm. (A) Indicated by arrows: Red = plagioclase (albite- probably albitised K-feldspar?); Yellow = lithic fragment; (B) Sample viewed under plane-polarised light showing long and concavo-convex grain contacts (with very few to rare sutured contacts) due to mechanical and chemical compaction; (C) Indicated by arrow: Red = K-feldspar (microcline).

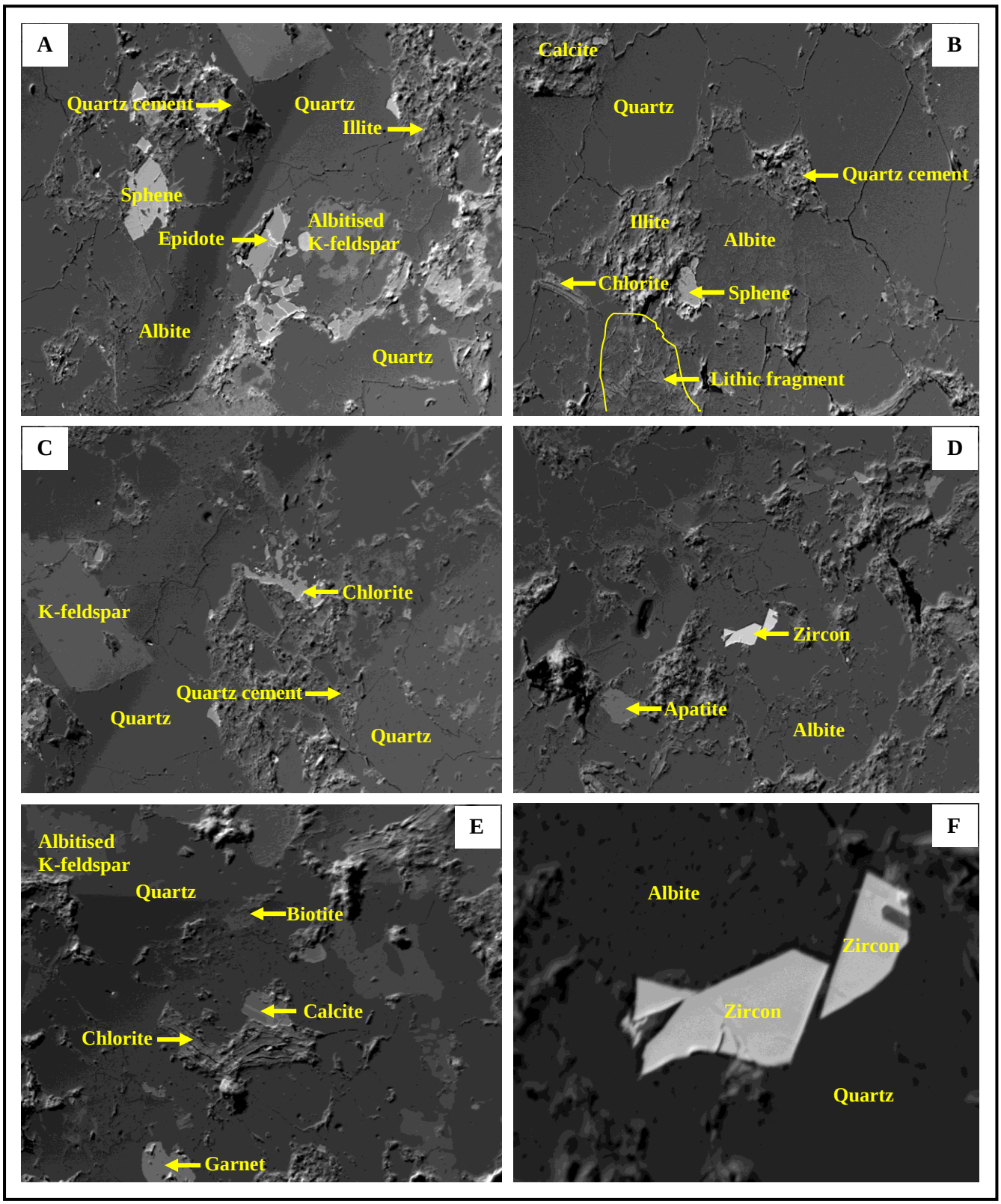

Figure 6.4. SEM backscattered electron images of selected Kookfontein sandstone samples showing textural and morphological relationships among detrital grains and authigenic pore-filling cements. Evidence of feldspars alterations are indicated by albitisation and clay authigenesis shown in photos A, B and E. Note the angularity and inherited fracturing of zircon grains in photos D and F. Zircon grain angularity indicates possible short sediment transport route i.e. close proximity to sediment source.

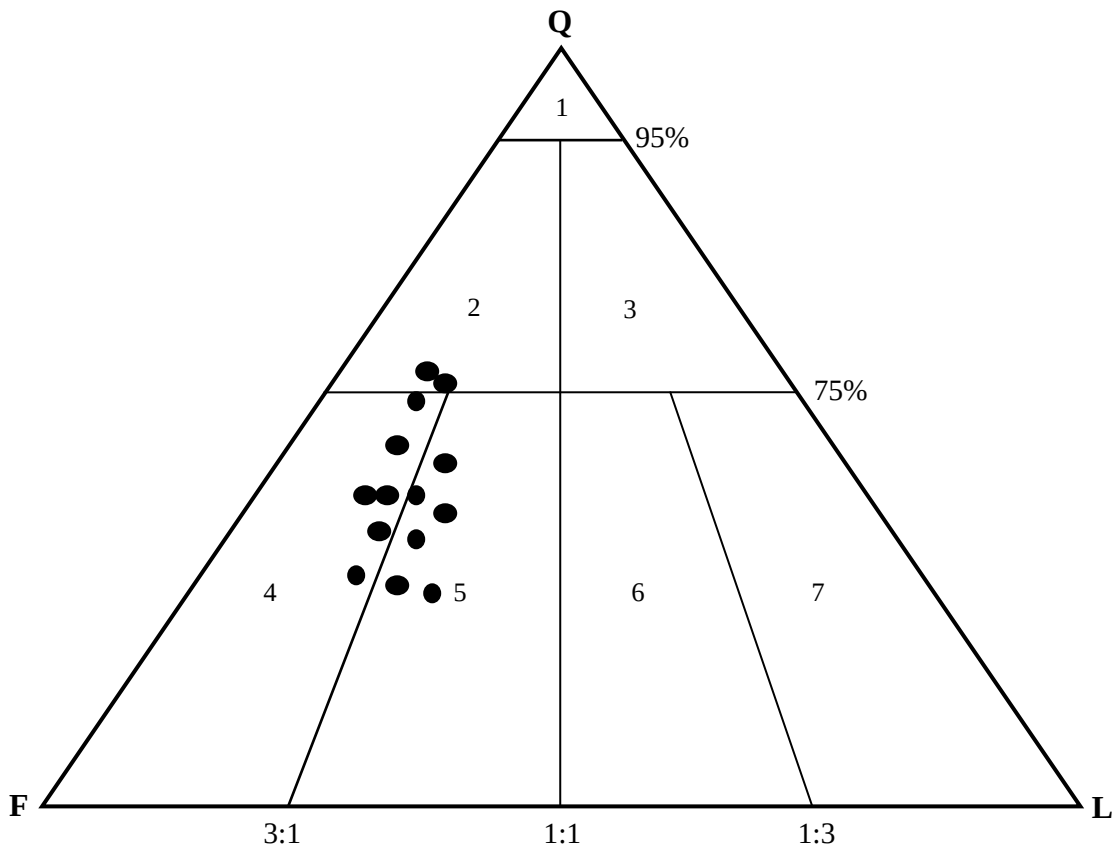

Q = Monocrystalline quartz
F = Feldspar
L = Rock fragments (igneous, metamorphic and sedimentary, including chert), and polycrystalline quartz

1 = Quartzose sandstone (i.e. Quartzarenite)
2 = Subfeldspathic sandstone (i.e. Subfeldspathic arenite, Subarkosic arenite or Subarkose)
3 = Sublithic sandstone (i.e. Sublitharenite)
4 = Feldspathic sandstone (i.e. Feldspathic arenite, Arkosic arenite or Arkose)
5 = Lithofeldspathic sandstone (i.e. Lithofeldspathic arenite or Lithic arkose)
6 = Feldspathic-lithic sandstone (i.e. Feldspathic litharenite or Arkosic-lithic sandstone)
7 = Lithic sandstone (i.e. Litharenite)

Figure 6.5. Detrital-grain composition of the Kookfontein deltaic reservoir facies showing the sandstones are largely lithofeldspathic to feldspathic sandstones (classification after Folk et al., 1970 and Pettijohn, 1987).

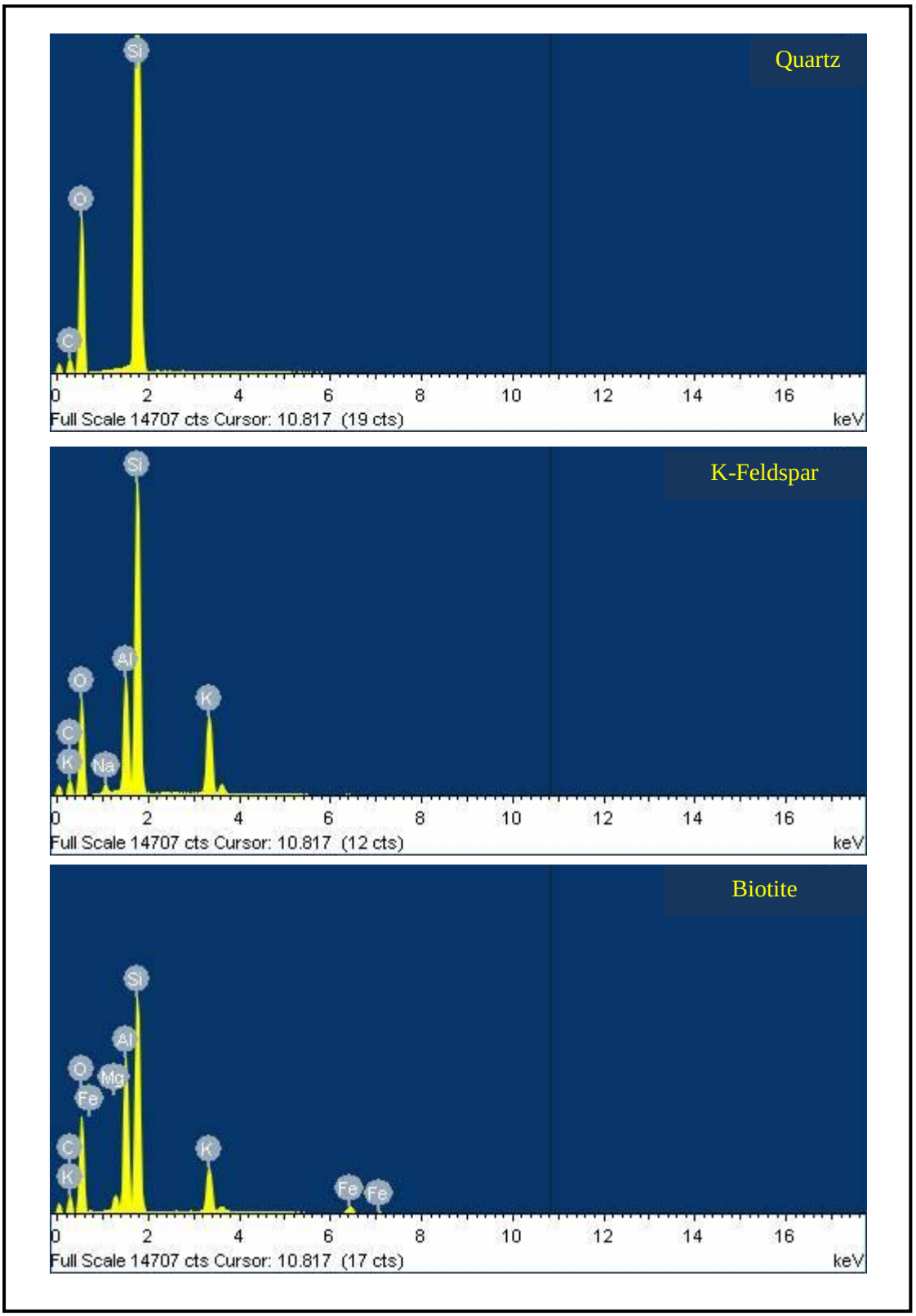

Figure 6.6. SEM spot mineral identification results showing energy-dispersive spectra of phase (elemental) compositions for different mineral constituents of Kookfontein sandstones.

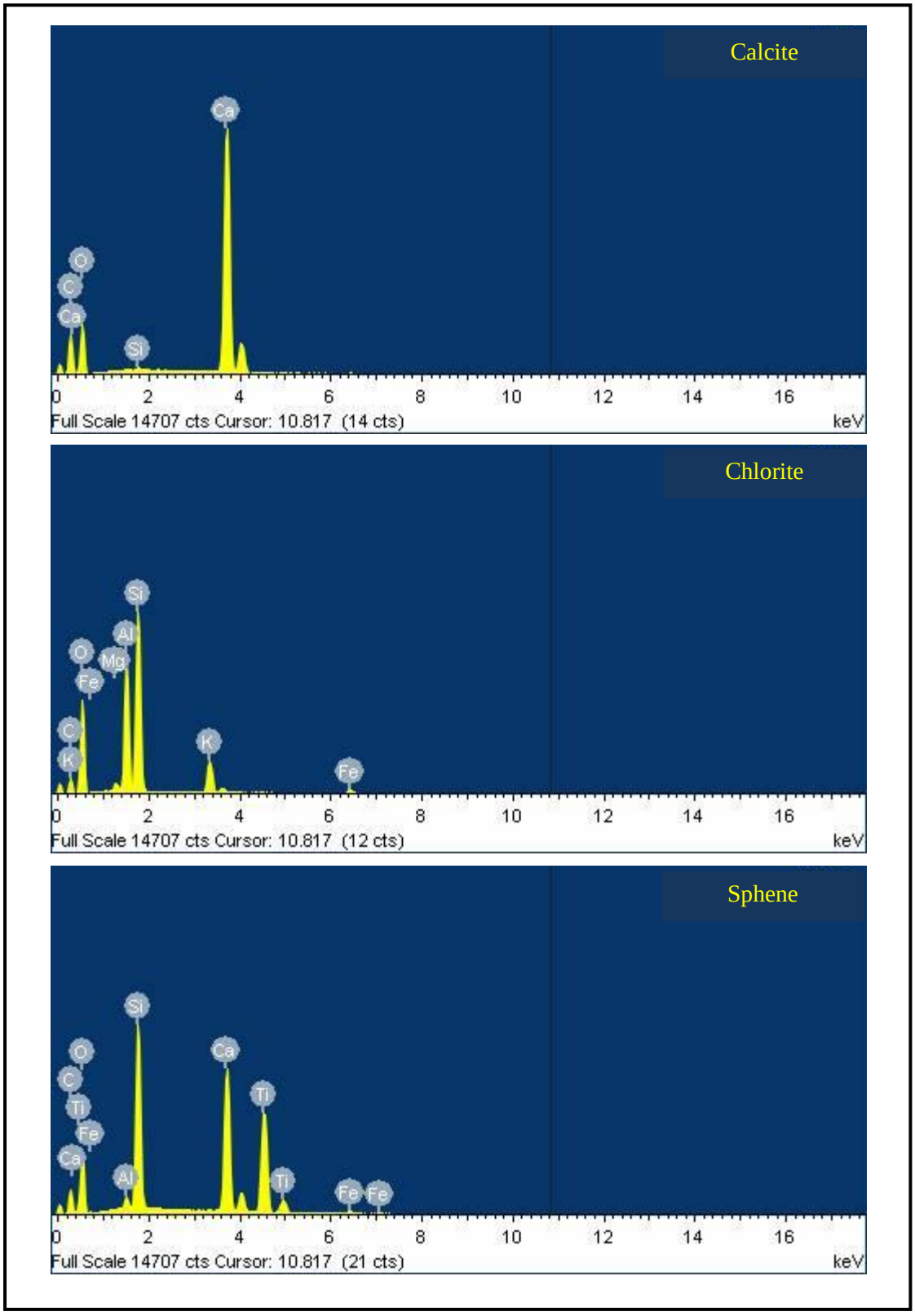

Figure 6.7. SEM spot mineral identification results showing energy-dispersive spectra of phase (elemental) compositions for different mineral constituents of Kookfontein sandstones.

Table 6.2. Calculated porosities (%) at 7 km maximum burial depth for Kookfontein Formation sandstones.

#	Depofacies	Depositional Environment	Quartz content (%)	Cement (%)	Grain size	Median size (mm)	Sorting	Trask Sorting	MBD (Km)	Stratic Age (Ma)	$Ø_0$ (%)	$Ø_{IGV}$ (%)	$Ø_{PIGV}$ (%)	COPL (%)	CEPL (%)
1	10	Intermediate delta front	30	15	Ml - Mu	0.359	MW-S	1.5	7	258.5	29.21	20.41	5.41	14.76	10.62
2	2	Prodelta	10		Slt - Vfl	<0.074	VP-S		7	258.5			0.00	0.00	0.00
3	10	Intermediate delta front	25	20	Fu - Ml	0.254	MW-S	1.5	7	258.5	29.21	19.55	-0.45	15.37	14.16
4	6	Distal delta front	30	13	Vfu - Fu	0.149	M-S	1.8	7	258.5	24.34	18.48	5.48	10.36	9.84
5	2	Prodelta	10		Slt - Vfl	<0.074	VP-S		7	258.5			0.00	0.00	0.00
6	3	Proximal prodelta	10	12	Slt - Vfl	0.065	VP-S	4.48	7	258.5	9.78	7.51	-0.97	9.67	9.76
7	11	Proximal mouthbar	40	15	Ml - Mu	0.359	W-S	1.3	7	258.5	33.70	23.55	8.55	18.08	9.95
8	11	Proximal mouthbar	45	22	Ml - Mu	0.359	VW-S	1.1	7	258.5	39.83	26.54	4.54	23.86	13.24
9	9	Distal delta front	20	19	Vfl - Fl	0.11	P-S	2.35	7	258.5	18.64	14.30	0.55	15.37	13.45
10	11	Proximal mouthbar	45	14	Ml - Mu	0.359	W-S	1.3	7	258.5	33.70	24.11	10.11	17.71	9.28
11	5	Distal delta front	25	18	Vfu - Fl	0.127	M-S	1.8	7	258.5	24.34	17.62	-0.38	11.01	13.62
12	6	Intermediate delta front	30	18	Vfu - Fu	0.149	M-S	1.8	7	258.5	24.34	18.48	0.48	10.36	13.62
13	11	Proximal mouthbar	45	18	Ml - Mu	0.359	VW-S	1.1	7	258.5	39.83	26.54	8.54	23.86	10.83
14	11	Proximal mouthbar	45	10	Fl - Ml	0.149	W-S	1.3	7	258.5	33.70	24.11	14.11	17.71	6.63
15	12	Proximal mouthbar	45	19	Ml - Mu	0.359	VW-S	1.1	7	258.5	39.83	26.54	7.54	23.86	11.43

MBD = Maximum burial depth; $Ø_0$ = Original or depositional porosity; $Ø_{IGV}$ = Intergranular porosity due to mechanical compaction before cementation
$Ø_{PIGV}$ = Present intergranular porosity i.e. $Ø_{IGV}$ minus cement content
Slt = Silt; Vfl = Very fine lower; Vfu = Very fine upper; Fl = Fine lower; Fu = Fine upper; Ml = Medium lower; Mu = Medium upper; VW-S = Very well sorted
W-S = Well sorted; MW-S = Moderately well sorted; M-S = Moderately sorted; P-S = Poorly sorted; VP-S = Very poorly sorted

6.3 Synthesis for petrophysical modelling

6.3.1 Burial history

Tracking the burial history of sediments that filled a basin is a very important step in modelling the petrophysical properties of that sedimentary basin. While sedimentological and stratigraphic analyses predict the temporal and spatial distribution of facies in a sedimentary setting, the analysis of sediment burial history predict the evolution of petrophysical properties (i.e. porosity and permeability) of these facies through time. The interplay between sedimentation and rate of subsidence determines the maximum depth to which sediments will be buried as well as the series of accompanying post-depositional diagenetic changes. Since burial of sediments through time involves two main processes i.e. pressure and temperature changes, geohistory and thermal history analyses have become important tools of establishing the burial history of sedimentary basins.

Geohistory is the quantitative study of subsidence and sedimentation in a basin (Allen and Allen, 2005) while thermal history is the analysis of palaeotemperature changes with depth during sediment burial (Nichols, 2009). Geohistory analysis is performed through decompaction of the sedimentary successions i.e. step-wise backstripping to initial depositional time, using water depth information obtained from facies and paleontological studies. Fission-track analysis and vitrinite reflectance studies are important analytical tools for determining the maximum temperature sedimentary successions have been subjected to, and hence to infer their maximum burial depth. Therefore, the combination of burial history data (i.e. burial rate, temperature and stratigraphic depth) and stratigraphic ages could yield valuable information for predicting sandstone porosity and permeability evolution through time (Scherer, 1987; Waples, 2002; Nichols, 2009).

Based on vitrinite reflectance data, Rowsell and De Swart (1976) suggested that maximum palaeotemperatures in the main Karoo Basin were between 150 and 300^{0}C, and estimated the thickness of the overburden in the Tanqua and Laingsburg depocentre areas to be between 6 and 7 km. Zircon fission-track analysis in the southwestern Karoo Basin indicated maximum palaeotemperatures somewhat greater than 200^{0}C (Brown et al., 1994). These authors interpreted these high temperatures to be the result of magmatically driven hydrothermal circulation within the sedimentary sequence, accompanied by the late Karoo sill/dyke intrusions. Sensitivity models constructed through a 1D basin thermal and maturity modelling program i.e. WinheatXL by Van Lente (2004) indicated that sedimentary successions of the Tanqua depocentre (i.e. Skoorsteenberg, Kookfontein and Waterford Formations) and Laingsburg depocentre (i.e. Collingham, Vischkuil, Laingsburg and Fort Brown Formations) could reach temperatures of 250 ±50^{0}C through burial under overlying strata with a thickness of at least 7000 m. Contrary to Brown et al. (1994), the results of these sensitivity models also suggest that the late Karoo basaltic dykes during the Jurassic do not affect or elevate the temperatures of these sediments to a significant extent (Van Lente, 2004). Moreover, according to vitrinite reflectance profiles obtained for foreland basins, geothermal gradients can be in the range of 26 to >33 ^{0}C/km depending on thermal regimes and structural provinces (Zhang and Davis, 1993). Therefore, under conditions of average basinal heat flow (32.5 ^{0}C/km), hydrostatic conditions, average fluid density of 1.1 g/cm^3 (Ambers, 2001), and a surface temperature of 20^{0}C, a temperature of 250^{0}C would be reached at 7 km burial depth (Van Lente 2004).

The above line of argument and evidence forms the basis for the burial history data (particularly 7 km maximum depth) used for estimating porosity evolution of the Kookfontein sandstones in this study.

6.3.2 Burial diagenesis

The term diagenesis refers to post-depositional changes (i.e. both physical and chemical) that alter initial depositional characteristics of sediments. These diagenetic changes take place at relatively low temperature, typically below ~200^{0}C and at depths up to about 5000 m (Nichols, 2009; Figure 6.8). Diagenetic processes are primarily dependent on burial depth of sediments through time, which influences the temperature and pressure conditions, as well as the composition of interstitial pore fluids of the sedimentary successions. The main diagenetic processes in clastic sediments are mechanical and chemical compaction, cementation of various forms of carbonates, quartz, pyrites and sulphates as well as the formation of authigenic clay minerals (Zhang et al., 2008).

Previous petrographic analyses and diagenetic studies of the sandstones from Tanqua and Laingsburg depocentres by Van Lente (2004) indicated that compaction (due to overburden pressure), quartz cementation (resulting from pressure solution) and the formation of authigenic clay minerals (i.e. illite and chlorite- resulting from alteration of detrital feldspars and kaolinite), are the main diagenetic processes responsible for the porosity and permeability reduction in the studied sandstones. Based on mineralogical composition and textural relationship, Van Lente (2004) suggested that these sandstones could have possibly undergone high grade burial diagenesis to low-grade regional burial metamorphism (i.e. lower greenschist facies: 90 - 250^{0}C; ~2 kbars using the schemes of Winkler (1965) and Press and Siever (1986); also Figures 6.9 and 6.10).

Generally, in the studied sandstones, mechanical and chemical compactions as well as authigenic pore-filling as a result of sandstone diagenesis are superimposed on the depositional grain-size control of reservoir quality. Diagenesis is to some extent controlled by initial depositional environment, grain size distribution and burial depth, as finer-grained

sandstones having a higher clay content being more susceptible to diagenetic alteration (particularly mechanical compaction and mineral authigenesis).

Several elements such as packing of framework grains, strains or fractures and dissolution/mineral overgrowths along intergranular contacts within the Kookfontein deltaic sandstones indicate the presence of mechanical and chemical compaction at different stages of diagenesis. Compaction causes the reduction of the existing pore space in two forms: (1) the change of contacts between the framework grains in grainstones; (2) re-precipitation of dissolved cements involving certain physical and chemical conditions (Zhang et al., 2008). In the studied sandstones, mechanical compaction includes grain or fracturing as well as the nature of grain contacts. The dominant grain contacts are long and concavo-convex, and in some rare cases may involve sutured contacts (see Figures 6.2 and 6.3). Chemical compaction occurred mainly by pressure solution both along intergranular contacts and fractures. The degree of compaction of individual sandstones can be calculated as the difference between pre-cement porosity and initial porosity value (Dutton, 1977). The effect of compaction on porosity reduction was estimated through the methodology of Lundegard (1992) (i.e. Equation (5) in the succeeding section). The calculated compactional porosity loss (i.e. COPL) from Equation (5) ranges from 10.4% to 23.9% for calculated sandstone depositional porosity ranging from 18.64% to 39.83% (see Table 6.2). This implies that, the Kookfontein deltaic sandstones have lost 35.56% to 81.3% (mostly above 50%) of the original porosity by compaction alone.

Quartz overgrowths constitute the most important pore-filling cements in most sandstone samples especially in the coarser-grained sandstones. The potential sources of silicon dioxide for quartz cement are pressure solution, dissolved and replaced feldspars and clay transformation (Rodrigo and Luiz, 2002; Zhang et al., 2008). Based on the quantity of

feldspars, Zhang et al., (2008) suggested that the dissolution of an average of 2 vol% of K-feldspar would produce 4 vol% of quartz. The following clay transformation reactions (i.e. illitisation and chloritisation of smectite into illite and chlorite, and illitisation of kaolinite into illite) release silicon dioxide for quartz cement precipitation (Rodrigo and Luiz, 2002):

$$\text{K-feldspar} + \text{Smectite} \longrightarrow \text{Illite} + \text{Chlorite} + SiO_2\,(\text{quartz})$$

$$\text{K-feldspar} + \text{Kaolinite} \longrightarrow \text{Illite} + SiO_2\,(\text{quartz}) + H_2O$$

Other important porosity-occluding authigenic pore-filling cements in most of the studied Kookfontein deltaic sandstones are feldspar alteration and transformation into clay minerals (mainly chlorite and illite). The relative low content of carbonate cement (mainly calcite) in most sandstone samples from this study indicates carbonate cementation does not contribute to major pore-space reduction (Figures 6.4, 6.6 and 6.7). This implies that calcite cementation at the onset of burial diagenesis at shallow depth was very minimal, thereby leaving enough pore spaces to be reduced by mechanical compaction with increasing burial; and later by chemical compaction (i.e. pressure solution) and authigenesis of quartz, feldspar and clay minerals. The presence of chlorite and illite from petrographic studies (particularly SEM) indicates that detrital K-feldspar and biotite must have undergone weathering and alteration into kaolinite and possibly smectite. This is then followed by the transformation of kaolinite and smectite with increasing burial depth into chlorite and illite (see Figure 6.11). Increasing crystallinilty of illite with increasing burial depth (Turker, 1991) is another possibility for its preservation as pore-filling cement in some of the studied sandstones. The presence of accessory minerals (i.e. zircon, sphene, epidote, garnet and apatite) in all the studied Kookfontein sandstones suggests that diagenetic dissolutions during deep burial

diagenesis are relatively not effective in reducing the suite of accessory minerals to the most stable types e.g. zircon (Carozzi, 1993).

In this study, petrographic thin-section analysis under plane-polarised light and cross-polars as well as SEM analysis reveal the paragenetic sequence of diagenetic processes that exert a strong influence on potential reservoir properties (i.e. porosity and permeability) of the studied sandstone facies. The main diagenetic events which influenced the reservoir quality of the Kookfontein Formation deltaic sandstones in the Tanqua-Karoo sub-basin are listed below and illustrated in Figure 6.11.

1. Calcite cementation immediately after sediment deposition and during early diagenesis at shallow burial depth.
2. Mechanical compaction due to overburden pressure with increasing depth of burial at both shallow and deep burial depth.
3. Chemical compaction (i.e. pressure solution) for quartz overgrowth cements.
4. Authigenesis of quartz, albite and K-feldspars, and clay minerals to produce mainly quartz cement, kaolinite and smectite at shallow burial depth.
5. Development of authigenic illite and chlorite at deep burial depth.

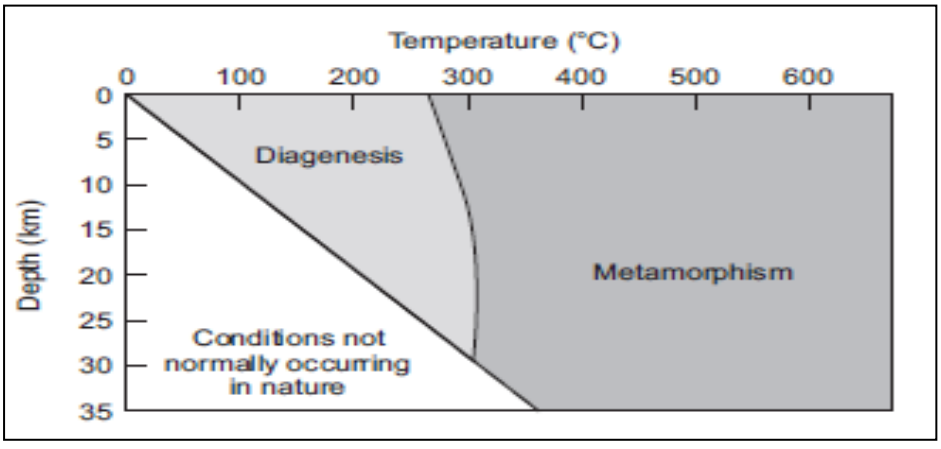

Figure 6.8. Depth and temperature ranges of diagenetic process (Modified from Nichols, 2009).

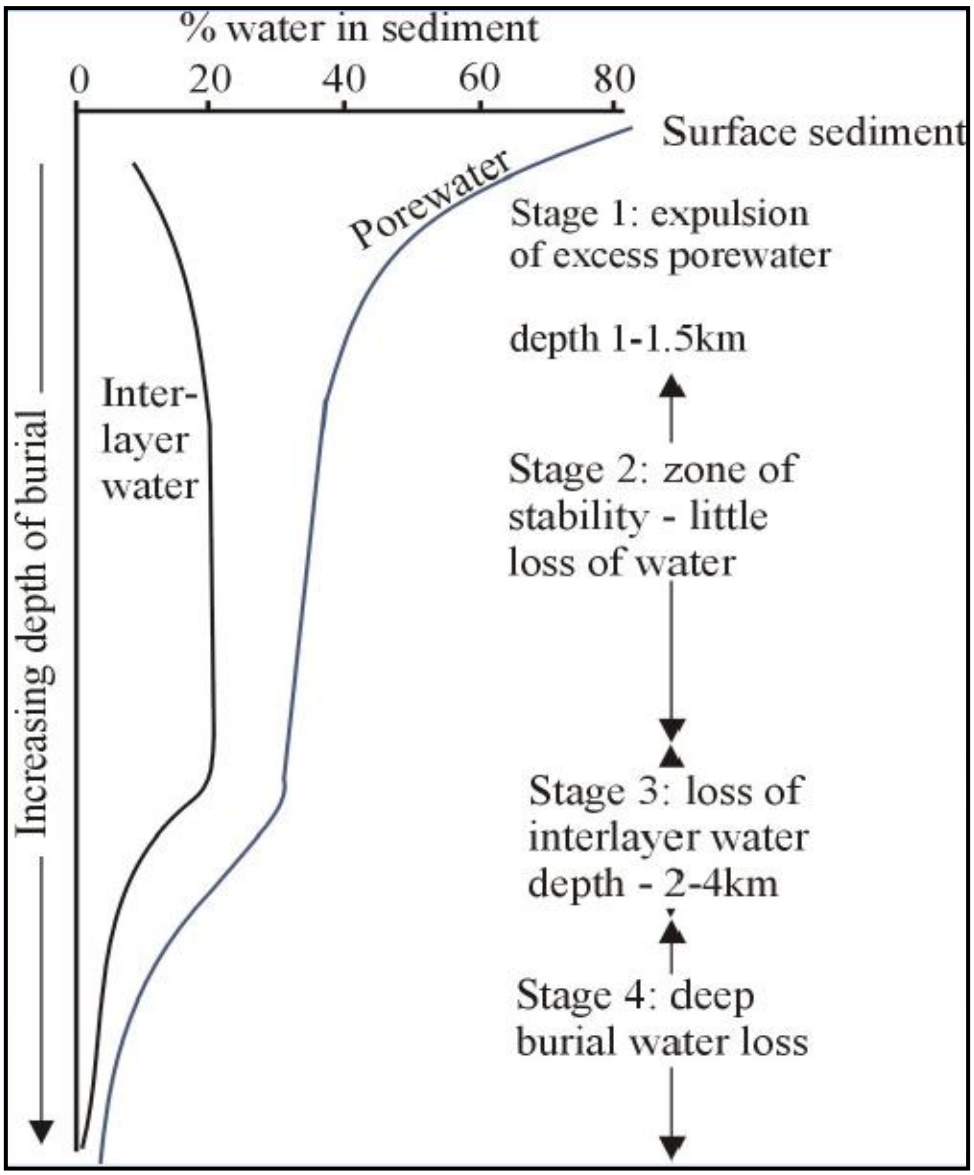

Figure 6.9. Water loss from compacting mudrocks during burial (adapted from Tucker, 1991).

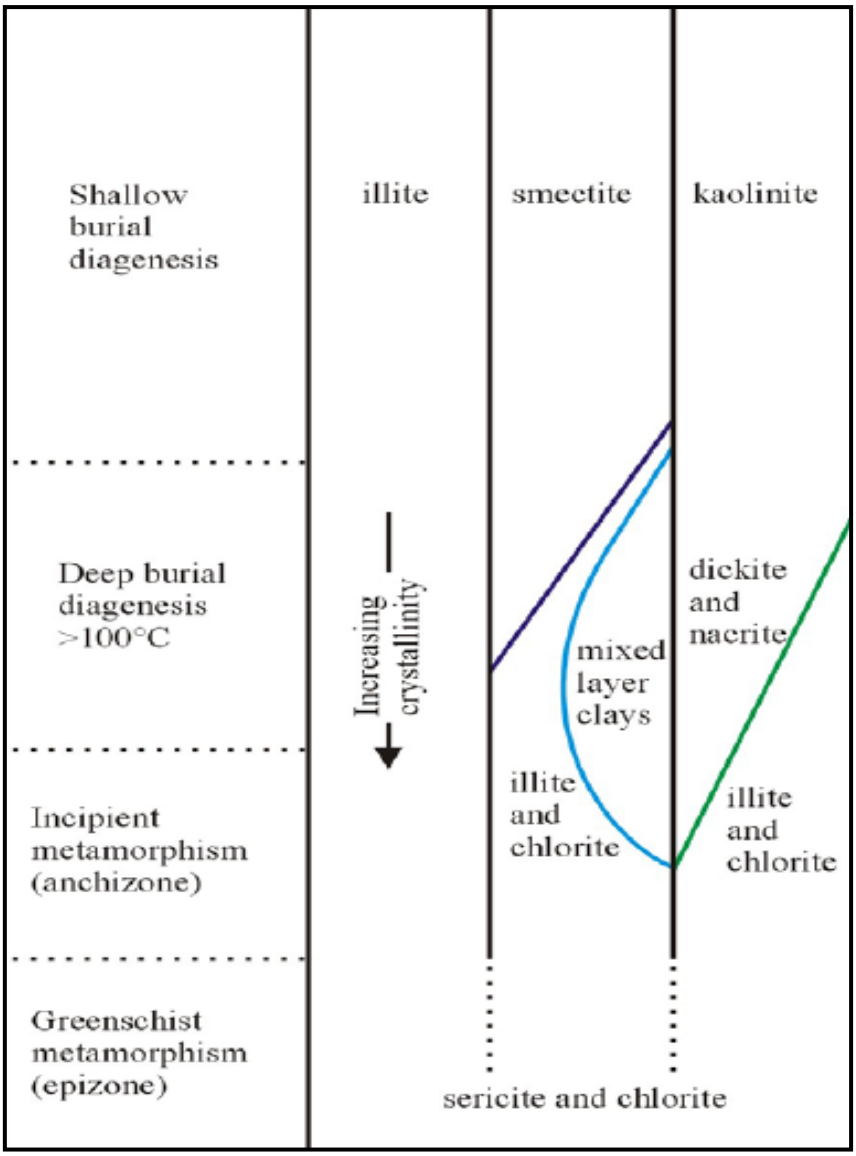

Figure 6.10. Changes of clay minerals with increasing burial depth and into metamorphism (Turker, 1991).

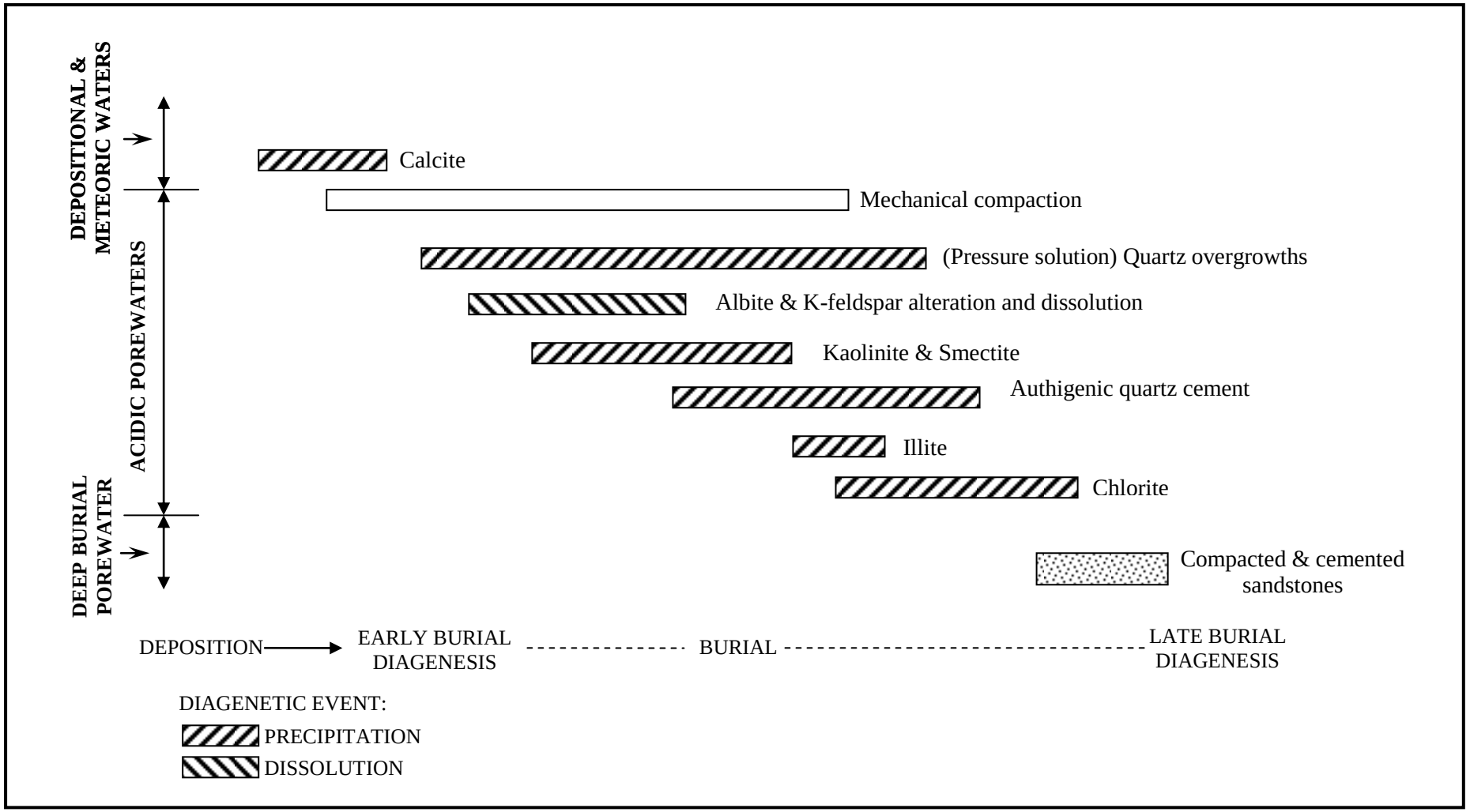

Figure 6.11. Schematic chart summarising sequence of diagenetic events for the Kookfontein (Formation) sandstones.

6.4 Petrophysical modelling strategy

The strategy for modelling the distribution of petrophysical properties i.e. porosity and permeability of the different sandstone facies for this study is a grain size-based empirical approach. Since there is no visible porosity and permeability from petrographic thin-section analysis probably due to high grade diagenesis, this approach lends itself the best way to assess the reservoir properties of the studied Tanqua-Karoo deltaic sequence as an outcrop analogue. A number of established predictive methods which are expressed in the equations listed below were used for the petrophysical modelling:

1. Depositional porosity ($Ø_0$) was calculated using the methodology of Scherer (1987) by generalising the experimental results of Beard and Weyl (1973) i.e.

   $$Ø_0 = 20.91 + 22.9/S_0 \qquad \textit{Equation (2)}$$

   where, S_0 is the Trask sorting coefficient based on sorting parameter (see Table 6.3).

2. Present-day porosity was estimated using the equation of Scherer (1987) for predicting the porosity of normally pressured sandstones. This equation is based on four variables: maximum burial depth, rock age, degree of sorting and quartz content.

   $$Ø = 18.60 + 4.73 \ln (Q) + 17.37/S_0 – 0.0038(Z) – 4.65 \ln (A) \qquad \textit{Equation (3)}$$

   where, Ø is the present-day porosity in percent, Q is the percent of quartz in the mineral fraction, S_0 is the Trask sorting coefficient, Z is the maximum burial depth in meters, and A is the age of the roc in millions of years.

   The “Modified Scherer” Model (MSM) by Waples (2002) predicts porosity evolution through time for sedimentary successions provided that burial rate is known. The MSM equation is as follows:

$$Ø = 18.60 + 4.73 \ln (Q) + 17.37/S_0 – 0.0038(Z) – 4.65 \ln (A\text{-}t) \qquad \textit{Equation (4)}$$

where, A is the stratigraphic age of the sandstone and t is the time (Ma) at each particular step in the calculation sequence. Both Equations (3) and (4) largely depend on mechanical compaction due to increasing depth of burial; they therefore lack direct consideration for major cementation, chemical compaction (i.e. intergranular pressure solution) or leaching. Also, Equation (4) could not be used for predicting porosity evolution through time for the studied sandstones in this study due to the fact that there is no appropriate constraint on burial history data that allows the determination of burial rate for the Karoo sedimentation. As a result, only present-day porosities at maximum burial depth were predicted using Equation (3).

3. The effect of compaction and cementation respectively on porosity loss was estimated using the methodology of Lundegard (1992). For compactional effect, the equation (5) was used:

———————— *Equation (5)*

where, COPL is the compactional porosity loss, OP is the original porosity (i.e. depositional porosity), IGV is the intergranular porosity before cementation but after compaction, its value is the sum of present intergranular porosity plus cement content (Houseknecht, 1987); while for porosity loss due to cementation, the Equation (6) below was employed:

—— *Equation (6)*

where, CEPL is the porosity loss by cementation, CEM is the total cement volume percentages of rock volume.

4. The permeability values were calculated using the Kozeny-Carman (Kozeny, 1927; Carman, 1937; Equation (6) and Berg (Berg, 1970; Equation (7)) models. Carman (1939) suggested that constant, c in Equation (6) gave the best experimental results when it equals 2.

$$K_{KC} = \frac{cd^2\phi^3}{(1-\phi)^2}$$

Equation (7)

where, c = constant, d = median grain size i.e. representative grain size (mm), ϕ = porosity. The Kozeny-Carman model is dependent on rock pore size; and its assumption is that pore spaces are composed of a bundle of identical capillary tubes- this is clearly a simplified description of natural porous media (Wu, 2004). Whereas, Berg (1970) derived his equation for permeability based on sphere packing:

$$K_B = 5.1\times10^{-6}\times d^2\phi^{5.1}e^{-1.385}$$

Equation (8)

where, *d*= median grain size i.e. representative grain size (mm), ϕ = porosity. Therefore, Berg model is an equation linking petrological variables- grain size, shape and sorting to permeability. It is based on uniform sphere packing in several regular ways with porosities in the range 26% to 47.6%. The results for these two models were later correlated.

Variables such as grain sizes, detrital quartz content and cement proportion were estimated from petrographic thin-section analysis; while IGV values were estimated from Equation (3) and petrographic observations. The petrophysical modelling strategy is summarised in the workflow given in Figure 6.12 below. The results obtained for various petrophysical properties (i.e. porosity and permeability values) are presented in Tables 6.2 and 6.4.

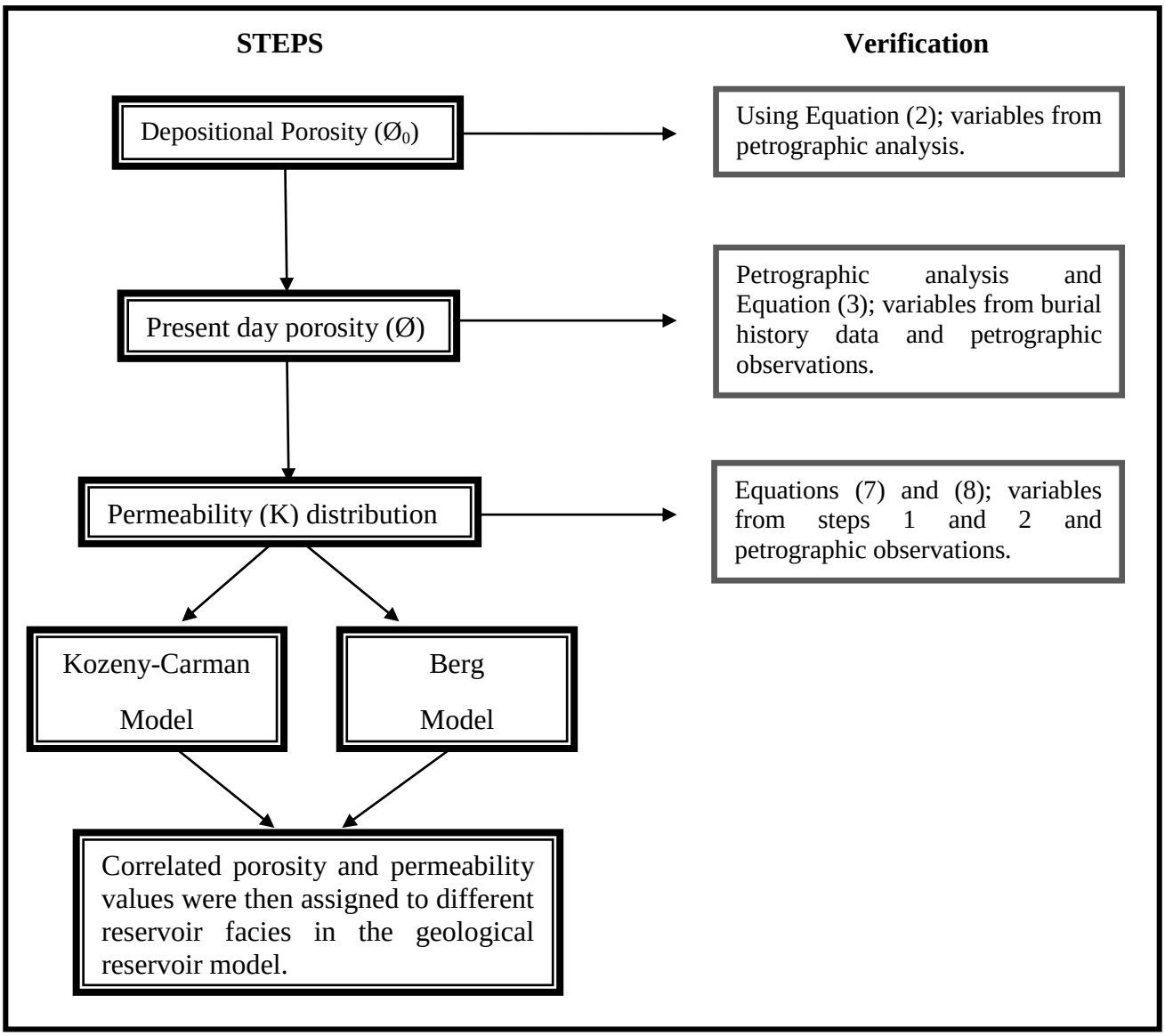

Figure 6.12. Petrophysical modelling workflow for this study.

Table 6.3. Trask Sorting Coefficients (S_0) for six different degree of sorting (Beard and Weyl, 1973).

Description	Trask sorting coefficient, S_0
Very well sorted	1.1
Well sorted	1.3
Moderately well sorted	1.5
Moderately sorted	1.8
Poorly sorted	2.35
Very poorly sorted	4.48

Table 6.4. Calculated permeabilities (in Darcy) for Kookfontein Formation sandstones using Kozeny-Carman and Berg models.

#	Depofacies	Depositional Environment	Grain size	Median size (mm)	Sorting	$Ø_0$ (%)	$Ø_{IGV}$ (%)	$Ø_{PIGV}$ (%)	K_{KC} ($Ø_0$) (D)	K_{KC} ($Ø_{IGV}$) (D)	K_{KC} ($Ø_{PIGV}$) (D)	K_B ($Ø_0$) (D)	K_B ($Ø_{IGV}$) (D)	K_B ($Ø_{PIGV}$) (D)
1	10	Intermediate delta front	Ml - Mu	0.359	MW-S	29.21	20.41	5.41	8.072	5.817	2.099	4.900	0.788	0.001
2	2	Prodelta	Slt - Vfl	<0.074	VP-S			0.00	0.000	0.000	0.000	0.000	0.000	0.000
3	10	Intermediate delta front	Fu - Ml	0.254	MW-S	29.21	19.55	0.45	4.041	2.802	0.006	2.453	0.317	0.000
4	6	Distal delta front	Vfu - Fu	0.149	M-S	24.34	18.48	5.48	1.175	0.917	0.364	0.333	0.082	0.000
5	2	Prodelta	Slt - Vfl	<0.074	VP-S			0.00	0.000	0.000	0.000	0.000	0.000	0.000
6	3	Proximal prodelta	Slt - Vfl	0.065	VP-S	9.78	7.51	0.97	0.176	0.113	-0.002	0.016	0.001	0.000
7	11	Proximal mouthbar	Ml - Mu	0.359	W-S	33.70	23.55	8.55	9.226	6.621	2.827	10.167	1.636	0.009
8	11	Proximal mouthbar	Ml - Mu	0.359	VW-S	39.83	26.54	4.54	10.802	7.387	1.925	23.833	3.007	0.000
9	9	Distal delta front	Vfl - Fl	0.11	P-S	18.64	14.30	0.55	0.758	0.525	0.020	0.460	0.059	0.000
10	11	Proximal mouthbar	Ml - Mu	0.359	W-S	33.70	24.11	10.11	9.226	6.764	3.210	10.167	1.843	0.022
11	5	Distal delta front	Vfu - Fl	0.127	M-S	24.34	17.62	0.38	0.854	0.639	0.001	0.242	0.047	0.000
12	6	Intermediate delta front	Vfu - Fu	0.149	M-S	24.34	18.48	0.48	1.175	0.917	0.018	0.333	0.082	0.000
13	11	Proximal mouthbar	Ml - Mu	0.359	VW-S	39.83	26.54	8.54	10.802	7.387	2.824	23.833	3.007	0.009
14	11	Proximal mouthbar	Fl - Ml	0.149	W-S	33.70	24.11	14.11	1.589	1.165	0.726	1.751	0.317	0.021
15	12	Proximal mouthbar	Ml - Mu	0.359	VW-S	39.83	26.54	7.54	10.802	7.387	2.583	23.833	3.007	0.005

Slt = Silt; Vfl = Very fine lower; Vfu = Very fine upper; Fl = Fine lower; Fu = Fine upper; Ml = Medium lower; Mu = Medium upper;
VW-S = Very well sorted; W-S = Well sorted; MW-S = Moderately well sorted; M-S = Moderately sorted; P-S = Poorly sorted; VP-S = Very poorly sorted.
$Ø_0$ = Original or depositional porosity; $Ø_{IGV}$ = Intergranular porosity due to mechanical compaction before cementation; $Ø_{PIGV}$ = Present intergranular porosity
K_{KC} and K_B are measured Kozeny-Carman and Berg permeabilities in Darcy (D) respectively for the three calculated porosity values.

6.5 Petrophysical parameters and reservoir quality

The distribution of reservoir properties in the Kookfontein Formation deltaic sandstones is strongly influenced both by depositional processes and by diagenetic factors, the latter being more important with increased burial depth. The observed reservoir heterogeneities- ranging from laminae, bedding, sub-facies and facies, of the Kookfontein deltaic succession are typically attributed to the dominant depositional processes governing the sedimentation of the deltaic system. Pore space development in sandstone is largely dependent on grain size, sorting and the amount of clay content. However, Beard and Weyl (1973) noted that it is more of sorting parameter than grain size parameter. Generally, the introduction of clay content and other fines by mechanical means such as burrowing or bioturbation and slope instability features (i.e. soft-sediment deformation), as observed in the studied depositional environment, can affect this relationship.

Based on petrophysical variables (i.e. grain size, sorting and quartz content) and burial history data, three types of porosity values were obtained using empirical Equations (2) and (3) as well as petrographic examination (see Tables 6.1 to 6.4). The three porosities are: depositional or original porosity (9.78-39.83%, averaging 24.81%), pre-cement or minus cement intergranular porosity (7.51-26.54%, averaging 17.03%) and present intergranular porosity (0-14.11%, averaging 7.06%). The effect of initial depositional environment on porosity evolution is evident from the depositional porosity estimation. For instance, the proximal prodelta and distal delta front sandstones present calculated depositional porosity that ranges from 9.78% to 18.64% (averaging 14.21%) as against the delta front to proximal mouthbar sandstones 24.34% to 39.83% (averaging 32.09%). Therefore, at this stage of the porosity development of the studied sandstones, depositional processes (e.g. hydrodynamic condition, basin depth and length, basin margin gradient and its variations, sediment transport

mechanism (Postma, (1990)) constitute the major control on grain size, sorting and clay content.

The next phase of petrophysical development in sandstones is the series of diagenetic events that follows starting from initial to final burial of the sediments. Of the three calculated porosities for the studied sandstones, the pre-cement or minus cement intergranular and present intergranular porosities are as a result of diagenetic factors. The sandstone porosity loss from 24.81% mean depositional porosity to about 7.06% mean present intergranular shows that burial diagenesis are more efficient in pore space reduction than initial depositional processes. Therefore, the main determinant of the reservoir quality of the sandstones from this study is diagenesis. Though, the degree of diagenesis is in most cases related to the initial depositional environment. That is, the finer-grained sandstones undergo higher degree of diagenesis than the coarser-grained sandstones. The major diagenetic factors influencing the reservoir properties of the studied sandstones are mechanical compaction, chemical compaction (pressure solution) and authigenic pore-filling cements (quartz cement, feldspar alteration and replacement, calcite cement, chlorite and illite). The degree of compaction i.e. compactional porosity loss (COPL) estimated from Equation (5) shows that compaction is more responsible for porosity reduction in the studied sandstones than cementation. The calculated COPL for sandstones (with depositional or original porosity ranging from 18.64% to 39.83%) ranges from 10.4% to 23.9%. Whereas, the calculated porosity loss due to cementation (CEPL) (obtained from Equation (6)) gives porosity loss percentage that ranges from 6.63% to 14.2% for the same sandstones. This implies that, the Kookfontein sandstones have lost about 35.56% to 81.3% (mostly above 50%) of the original porosity to compaction alone, while they have lost only about 22.67% to 48.56% (mostly below 35%) of the original porosity to cementation.

Out of all the pore-filling cements, the quartz overgrowth cements are the most prominent in all the studied sandstones especially in the coarser-grained sandstones. Although, there is a very strong relationship between the calculated porosity and permeability values obtained for this study, there are some instances where cementation (especially chlorite and illite) contributes more to permeability reduction than compaction. The calculated permeabilities obtained through Equations (7) and (8) i.e. Kozeny-Carman and Berg models respectively are summarised in Table 6.4. The permeability values were estimated based on the three different porosity evolutionary trends obtained from this study. The different porosity values and their respective permeabilities (i.e. for the two permeability models) are as follows: (1) Kozeny-Carman model: depositional or original porosity (Ø = 9.78-39.83%, averaging 24.81%; K = 0.18-10.81D, averaging 5.5D), pre-cement or minus cement porosity (Ø = 7.51-26.54%, averaging 17.03%; K = 0.11-7.39D, averaging 3.75D) and present intergranular porosity (Ø = 0-14.11%, averaging 7.06%; K = 0-2.58D, averaging 1.3D); and (2) Berg model: depositional or original porosity (Ø = 9.78-39.83%, averaging 24.81%; K = 0.016-23.83D, averaging 11.9D), pre-cement or minus cement porosity (Ø = 7.51-26.54%, averaging 17.03%; K = 0.001-3.01D, averaging 1.51D) and present intergranular porosity (Ø = 0-14.11%, averaging 7.06%; K = 0-0.005D, averaging 0.003D). Generally, the mean permeability values (measured in Darcy) calculated for Kozeny-Carman model are higher than the corresponding permeabilities obtained for Berg model, except for the depositional or original porosity in which Berg model permeability is much higher than the Kozeny-Carman model.

The various porosity and permeability data obtained from the two permeability models were then plotted on a linear log-permeability and porosity cross-plot graph (Figures 6.13, 6.14 and 6.15). In many consolidated sandstones, plots of petrophysical data have shown that the logarithm of permeability is often linearly proportional to porosity (Beard and Weyl, 1973;

Nelson, 1994). The slope, intercept and degree of scatter of these log(k)-Ø trends vary from formation to formation, and these variations are attributed to differences in initial grain size and sorting, as well as diagenetic history (Nelson, 1994). Although, Kozeny-Carman model related rock pore size to permeability while Berg model attributed porosity to permeability based on grain size, shape and sorting, both models are based on the same petrophysical data (i.e. grain size and sorting) which determine porosity and permeability distribution in sandstone reservoirs. The somewhat higher Kozeny-Carman permeability values than the corresponding Berg model permeabilities could probably be attributed to the fact that- the Berg model incorporates more, the effect of finer-grained sandstones and degree of sorting than the Kozeny-Carman model.

The log(k)-Ø trends obtained for the studied sandstones show that there is a linear relationship between porosity and permeability (Figures 6.13, 6.14 and 6.15). This linear relationship is also evident in the results of the statistical regression analyses (i.e. R^2 = 0.71, 0.63 and 0.51 for Kozeny-Carman model; R^2 = 0.74, 0.77 and 0.68 for Berg model) carried out for the two permeability models. As illustrated in poroperm Figures 6.13, 6.14 and 6.15, there is a very strong correlation between Kozeny-Carman and Berg models. This implies that the two models are both dependent on the same depositional processes (i.e. initial grain size and sorting) and diagenetic factors (i.e. mechanical and chemical compaction, and authigenic cementation) that created the Kookfontein deltaic sandstones.

The reservoir quality of the studied Kookfontein Formation sandstones thus decreases upward and in inferably basinwards direction from proximal mouthbar sands, intermediate delta front facies to distal delta front facies. The porosity and permeability values obtained from this study can then be assigned to different facies in the conceptual reservoir-scale geological model for possible down-depositional dip and up-depositional dip flow simulation

models. A better simulation result is envisaged if the simulated geological model could be constructed in 3D.

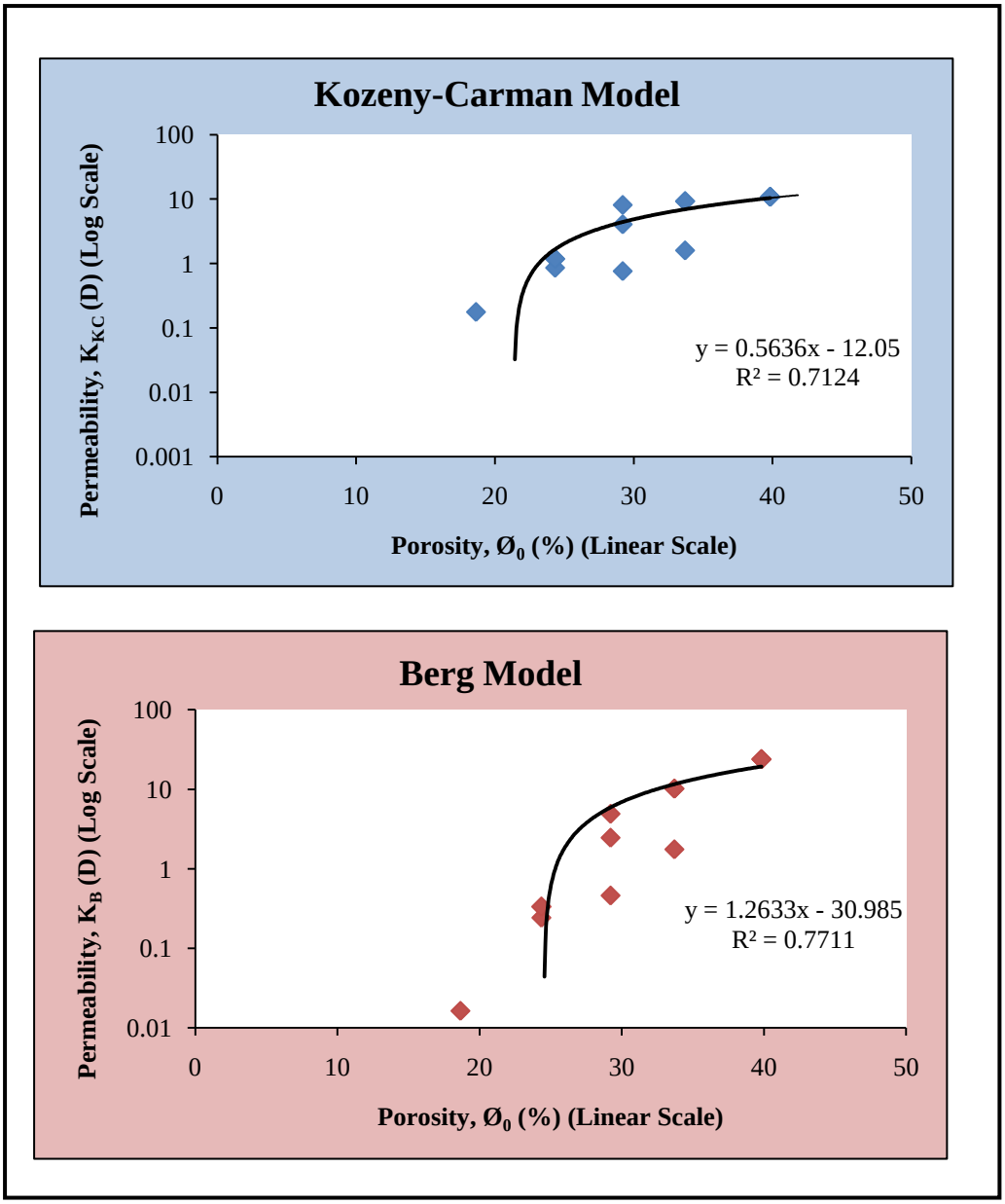

Figure 6.13. Poroperm cross-plot (i.e. log-permeability against porosity) for Kozeny-Carman and Berg models. This poroperm relationship is based on depositional or original porosity ($Ø_0$).

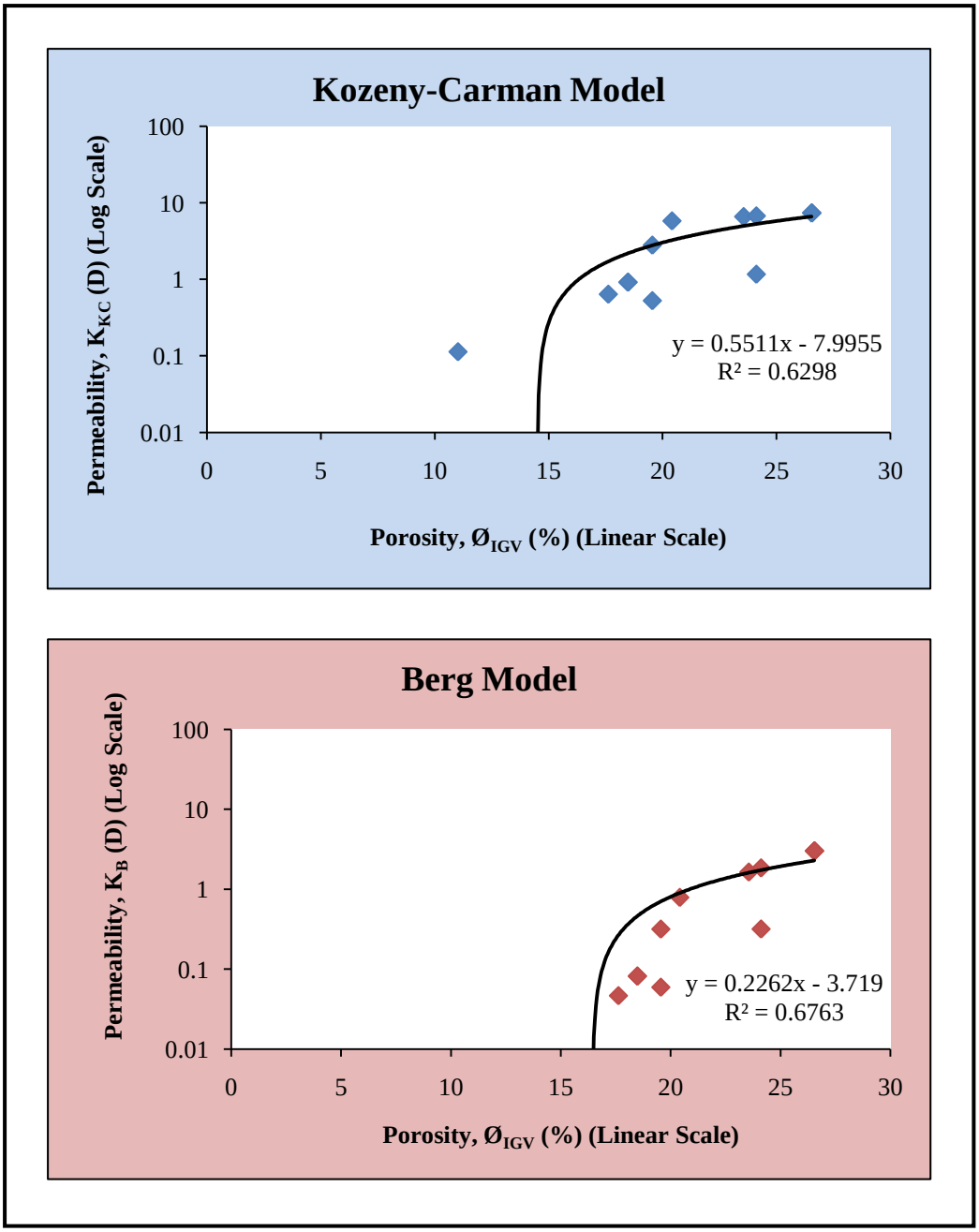

Figure 6.14. Poroperm cross-plot (i.e. log-permeability against porosity) for Kozeny-Carman and Berg models. This poroperm relationship is based on pre-cement or minus cement porosity ($Ø_{IGV}$). Note the decrease in porosity and permeability values with increasing burial depth and compaction.

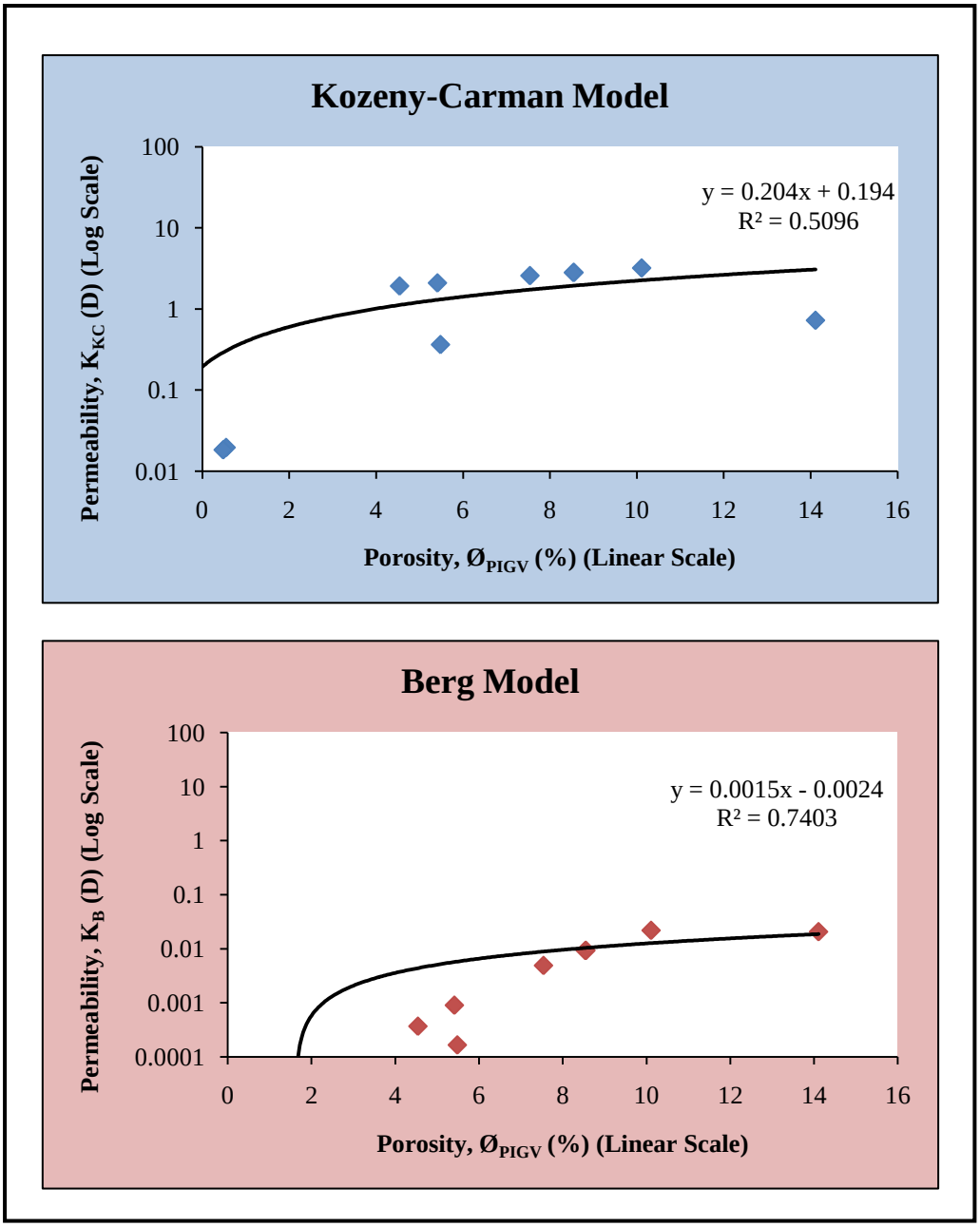

Figure 6.15. Poroperm cross-plot (i.e. log-permeability against porosity) for Kozeny-Carman and Berg models. This poroperm relationship is based on present intergranular porosity ($Ø_{PIGV}$). Note the decrease in porosity and permeability values due to increase in burial depth and the formation of authigenic cements.

CHAPTER SEVEN

CONCLUSIONS AND RECOMMENDATION

7.1 Conclusions

The Permian Kookfontein Formation constitutes an excellent outcrop analogue for basin-margin successions i.e. outer shelf to shelf-margin to mid-slope deltaic reservoirs. The area extent and excellent exposure of the studied outcrops at the Pienaarsfontein locality as well as this study's analytical and modelling techniques enable an accurate description of internal heterogeneity, facies architecture and sediment-body geometries, depofacies characterisation and correlation, and grain size-based empirical prediction of petrophysical properties (i.e. porosity and permeability) of the studied Kookfontein succession. The aforementioned therefore allows the following conclusions:

7.1.1 Facies distribution, architecture and geometry

- A hierarchical approach to facies description depicts all levels of heterogeneity (i.e. facies succession/cycle, facies association/bedsets, depofacies/beds and laminae) which form the basic building blocks for the studied Kookfontein depo-system. This led to the identification of twelve depofacies and which are grouped into four facies associations (i.e. sandstone, heterolithic, soft-sediment deformation facies and mudstone facies).
- The Kookfontein Formation comprises 13 sedimentary cycles which are sub-divided stratigraphically based on cycle thickness trend, sediment stacking pattern and relative position to the shelf break into: the lower Kookfontein member (i.e. cycles 1 to 5) and the upper Kookfontein member (i.e. cycles 6 to 13).
- The lower Kookfontein cycles 1 to 5 exhibit somewhat irregular thickening- and thinning- upward trend with an overall upward-shallowing trend (i.e. upward-

thickening and coarsening succession) and a progradational sediment stacking pattern representing deposition of mid-slope to top-slope/shelf-margin successions; while cycles 6 to 13 exhibits a symmetrical thickening upward profile and overall upward-thickening and coarsening succession with aggradational stacking pattern. Also, the abrupt change from progradational trend to aggradational coincides with reduction in cycle thicknesses from 37 m mean cycle thickness to about 11 m mean cycle thickness.

- Lateral juxtaposition of observed vertical facies variations across each cycle in an inferably basinwards direction exhibits upward change in features, i.e. decrease in gravity effects, increase in waves and decrease in slope gradient of subsequent cycles.
- This upward transition in features represents a deposition of mid-slope (i.e. distal consisting of finer grains, inertia/buoyancy deposits, less waves, horizontal/current ripples, swaley/hummocky, loading/dewatering structures and slumps) to shelf-margin/outer shelf (i.e. proximal consisting of coarser grains, friction/bedloads, more wave reworking processes, current ripples and loading/dewatering structures) succession.
- Deposition of each facies succession (i.e. flooding surface-bounded cycle) is a result of primary deposition by periodic and probably sporadic mouthbar events governed by stream flow dynamics, and secondary remobilisation of sediments under gravity.
- Lateral facies variations within each cycle are due to breaks in depositional events resulting from either no sediment input from river flow processes or switching of distributary mouthbars.
- Therefore, facies distribution within the Kookfontein deltaic sequence is mainly a consequence of the series of mouthbar flooding events.

- The main sedimentary heterogeneities in the Kookfontein Formation are related to: (a) the depositional hierarchy of stratigraphic elements which ranges in decreasing order from facies succession/cycle-scale (35-49 m), bedsets (i.e. facies-scale, 0.2-30 m), beds (i.e. depofacies-scale, 0.01-1.2 m) to laminae (i.e. lamina-scale, <0.01 m); and (b) the sequence stratigraphic subdivisions (i.e. parasequence sets and parasequences) and their characteristic depositional surfaces.
- Two parasequence sets consisting of flooding surface-bounded parasequences (i.e. cycles) are identified: (1) transgressive sequence set i.e. cycles 1 to 3 and (2) regressive sequence set i.e. cycles 4 to 13. The identification of these parasequence sets is aided through the recognition of a maximum flooding surface above cycle 3 in the field. Each parasequence is characterised by 3 stratigraphic surfaces: progradational, emergence and flooding surfaces.
- The basinwards transition of depositional facies ranges from undeformed mouthbar sands into deformed mouthbar sands, intermediate and distal deformed delta front and distal undeformed delta front and prodelta. Based on this transition, the architecture and geometry of the Kookfontein depo-system is interpreted to be river-dominated, gravitationally reworked and wave-influenced shelf edge Gilbert-type delta.
- Facies stacking trend, cycle thickness pattern and 2D hypothetical geometrical models suggest that the sedimentary heterogeneities and cyclicity of the Kookfontein deltaic succession are dominantly sediment supply-driven rather than accommodation space-driven. Therefore, the probable dominant depositional controls on the Kookfontein cyclicity are climate and tectonics with minor influences from eustatic fluctuations and possibly delta lobe switching.

- Widespread distribution of soft-sediments deformation structures, their growth-style and morphology within the studied succession are empirically related to progradation of Gilbert-type mouthbars over the shelf break as well as the slope gradients of the Kookfontein clinoforms. Low-slope gradients may have favoured mostly loading and dewatering structures rather than large-scale slumps.
- 'Outcrop log-GR log' tie offers a useful tool for identifying and correlating trends in facies succession, facies boundaries and particularly sandbody architectures.
- The described internal heterogeneity in this work is below the resolution (i.e. mm-scale) of most conventional well-logs, and therefore could supplement well-log data especially where there is no borehole image and core data.

7.1.2 Petrophysical analysis and characterisation

- The Kookfontein Formation sandstones are predominantly lithofeldspathic to feldspathic, lower very fine to upper medium- grained, poorly to well sorted, sub-angular to sub-rounded sandstones. The angularity of most framework grains implies a short transport distance from sediment provenance.
- The distribution of reservoir properties in the Kookfontein Formation deltaic sandstones is strongly influenced both by depositional processes and by diagenetic factors, the latter being more important with increased burial depth.
- Using well established empirical petrophysical equations and petrographic examination, three types of porosity values were obtained while permeabilities were calculated based on these porosities using Kozeny-Carman and Berg models.
- The porosity-permeability relationship (i.e. log(k)-Ø) trends obtained for the studied sandstones show that there is a linear relationship between porosity and permeability. Also, there is a very strong correlation between the two modelled permeabilities.

- The effect of initial depositional environment on porosity evolution is evident from depositional porosity estimation. For instance, the proximal prodelta and upper slope sandstones present calculated depositional porosity that ranges from 9.78% to 18.64% (averaging 14.21%) as against the delta front to proximal mouth-bar sandstones 24.34% to 39.83% (averaging 32.09%).
- The sandstone porosity loss from 24.81% mean depositional porosity to about 7.06% mean present intergranular porosity shows that burial diagenesis are more efficient in pore space reduction than initial depositional processes.
- The major diagenetic factors influencing the reservoir properties of the studied sandstones are mechanical compaction, chemical compaction (pressure solution) and authigenic pore-filling cements (quartz cement, feldspar alteration and replacement, calcite cement, chlorite and illite).
- The results obtained for compactional porosity loss (COPL) and porosity loss due to cementation (CEPL) shows that compaction especially mechanical compaction is more responsible for porosity reduction in the studied sandstones than cementation.
- The reservoir quality of the studied Kookfontein Formation sandstones decreases upward and inferably in a basinwards direction from proximal mouthbar sands, intermediate delta front to distal delta front facies.
- The workflow employed for this close-to-deterministic, grain size-based petrophysical analysis of outcrop data could serve as a standard workflow for estimating porosity and permeability distribution in outcrop exposures as well as in less-constrained subsurface scenarios.

7.2 Recommendation

- A 3D geological model of the Kookfontein deltaic succession with digital modelling software (e.g. Schlumberger's Petrel and ArcGIS) is recommended in order to test the hypothetical facies model and advance our understanding of the effect of three-dimensionality on the evolution of the Kookfontein clinoformal geometry.
- Possible down-depositional dip and up-depositional dip flow simulation models based on the established 2D schematic geological model and petrophysical parameters are suggested in order to test the effect of sedimentary heterogeneities on fluid flow behaviour.
- Application of the workflow (i.e. for modelling of facies architecture and geometry, and petrophysical characterisation) employed in this study to other similar ancient depo-systems and less-constrained subsurface scenarios is recommended in order to test its workability and for its possible refinement.

REFERENCES

Adelmann, D., Fiedler, K., 1998. Origin and characteristics of Late Permian submarine fan and deltaic sediments in the Laingsburg sub-basin (SW Karoo Basin, Cape Province/South Africa). In: P.O.D. Andersson, A. Johansson and R.A. Kumpulainen (Editors), Sm–Nd isotope evidence for the provenance of the Skoorsteenberg Formation, Karoo Supergroup, South Africa. *Journal of Earth Sciences*, **36**, 173-183.

Ainsworth, R.B. (2005). Sequence stratigraphic-based analysis of reservoir connectivity: influence of depositional architecture – a case study from a marginal marine depositional setting. *Petroleum Geoscience*, **11**, 257–276.

Allen, P.A. and Allen, R.J. (2005). Basin analysis: principles and applications. Blackwell Publishing Ltd., 2nd edition, pp 267-326.

Allen, G.P. and Mercier, F. (1988). Subsurface sedimentology of deltaic systems. In: R. Labourdette, J. Casas and P. Imbert (Editors), 3D Sedimentary modelling of a Miocene Deltaic reservoir unit, Sincor Field, Venezuela: A new approach. *Journal of Petroleum Geology*, **31(2)**, 135-152.

Ambers, C. P. (2001). Evidence of elevated pressure and temperature during burial of the Salem Limestone in south-central Indiana, USA, and its implications for surprisingly deep burial. *Sedimentary Geology* **143**, 245 – 257.

Andersson, P.O.D., Johansson, A. and Kumpulainen, R.A. (2003). Sm–Nd isotope evidence for the provenance of the Skoorsteenberg Formation, Karoo Supergroup, South Africa. *Journal of Earth Sciences*, **36**, 173-183.

Andersson, P.O.D., Worden, R.H., Hodgson, D.M. and Flint, S. (2004). Provenance evolution and chemostratigraphy of a Palaeozoic submarine fan-complex: Tanqua Karoo Basin, South Africa. *Marine and Petroleum Geology*, **21**, 555-577.

Bangert, B., Stollhofen, H., Lorenz, V. and Armstrong, R. (1999). The geochronology and significance of ash-fall tuffs in the glaciogenic Carboniferous-Permian Dwyka Group of Namibia and South Africa. *Journal of African Earth Sciences*, **29**, 33-49.

Basu, A., Young, S.W., Suttner, L.J., James, W.C. and Mack, G.H. (1975). Re-evaluation of the use of undulatory extinction and polycrystallinity of detrital quartz for provenance interpretation. *Journal of Sedimentary Geology*, **45**, 873-882.

Beard, D.C. and Weyl, P.K. (1973). Influence of texture on porosity and permeability of unconsolidated sand. *AAPG* Bulletin, **57**, 349–369.

Berg, R.R. (1970). Method for determining permeability from reservoir rock properties. In: S.R. Ogilvie, S. Cuddy, C. Lindsay and A. Hurst (Editors), Novel methods of permeability prediction from NMR tool data. Submitted to *DIALOG* September, 2002, pp1-14.

Besley, B. and Williams, H. (1989). Quantification of permeability barrier geometries within deltaic sandstone reservoir bodies – a case study of Carboniferous analogues. Conference review abstract, *Marine and Petroleum Geology*, **6**, 379-380.

Bhattacharya, J.P. (2006). Deltas. In: H.W. Posamentier and R.G. Walker (Editors), Facies models revisited. Society for Sedimentary Geology, Special Publication, **84**, 237-292.

Bhattacharya, J.P. and Giosan, L. (2003). Wave-influenced deltas: geomorphological implications for facies reconstruction. *Sedimentology*, **50**, 187–210.

Bouma, A.H. and Wickens, H. de V. (1991). Permian passive margin submarine fan complex, Karoo Basin, South Africa: possible model to Gulf of Mexico. *Transactions of the Gulf Coast Association of Geological Societies*, **41**, 30-42.

Brown, R., Gallagher, K. and Duane, M. (1994). A quantitative assessment of the effects of magmatism on the thermal history of the Karoo sedimentary sequence. In*:* Van Lente, B. (Editor), Chemostratigraphic trends and provenance of the Permian Tanqua and Laingsburg depocentres, Southwestern Karoo Basin, South Africa. Unpublished PhD Thesis, University of Stellenbosch, 339 p.

Cabello, P., O. Falivene, O., Lopez-Blanco, M., Howell, J., Arbues, P. and Ramos, E. (2010). Modelling facies belt distribution in fan deltas coupling sequence stratigraphy and geostatistics: The Eocene Sant Llorenç del Munt example (Ebro foreland basin, NE Spain). *Marine and Petroleum Geology*, **27**, 254-272.

Carman, P.C. (1937). Fluid flow through granular beds. In: F.K. Boadu (Editor), Hydraulic conductivity of soils from grain-size distribution: new models. *Journal of Geotechnical and Geoenvironmental Engineering*, **(8)126**, 739-746.

Carozzi, A.V. (1993). Sedimentary petrography. PTR Prentice-Hall, Inc. New Jersey, 257 p.

Catuneanu, O., Hancox, P.J., Cairncross, B. and Rubidge, B.S. (2002). Foredeep submarine fans and forebulge deltas: orogenic off-loading in the underfilled Karoo Basin. *Journal of African Sciences*, **35**, 489-502.

Catuneanu, O., Abreu, V., Bhattacharya, J.P., Blum, M.D., Dalrymple, R.W., Eriksson, P.G., Fielding, C.R., Fisher, W.L., Galloway, W.E., Gibling, M.R., Giles, K.A., Holbrook, J.M., Jordan, R., St.C. Kendall, C.G., Macurda, B., Martinsen, O.J., Miall, A.D., Neal, J.E., Nummedal, D., Pomar, L., Posamentier, H.W., Pratt, B.R., Sarg, J.F., Shanley, K.W., Steel, R.J., Strasser, A. and Tucker, M.E., Winker, C. (2009). Towards the standardisation of sequence stratigraphy. *Earth-Science Reviews*, **92**, 1-33.

Catuneanu, O., Bhattacharya, J.P., Blum, M.D., Dalrymple, R.W., Eriksson, P.G., Fielding, C.R., Fisher, W.L., Galloway, W.E., Gianolla, P., Gibling, M.R., Giles, K.A., Holbrook, J.M., Jordan, R., St.C. Kendall, C.G., Macurda, B., Martinsen, O.J., Miall, A.D., Nummedal, D., Posamentier, H.W., Pratt, B.R., Shanley, K.W., Steel, R.J., Strasser, A. and Tucker, M.E. (2010). Sequence stratigraphy: common ground after three decades of development. *First break*, **28**, 1-14.

Cole, D. I. (1992). Evolution and development of the Karoo Basin. In: M. J. De Wit and I. G. D. Ransome (Editors), Inversion Tectonics of the Cape Fold Belt, Karoo and Cretaceous Basins of Southern Africa, pp. 87 – 99.

Darman, H., Sidi, F.H., Wiweko, A., Lambert, B. and Seto, B. (1999). Facies type and distribution of modern Mahakam delta, East Kalimantan (Borneo), Indonesia. A web-site version of Indonesia Sedimentologists Forum (FOSI) foldouts series Number 1.

De Beer, C. H. (1990). Simultaneous folding in the western and southern branches of the Cape Fold Belt. *In*: W. Van der Werff and S. Johnson (Editors), High resolution stratigraphic analysis of a turbidite system, Tanqua Karoo Basin, South Africa, *Marine and Petroleum Geology*, **20**, 45-69.

Deutsch, C.V. (1999). Reservoir modelling with publicly available software. *Computers and Geosciences*, **25**, 355-363.

Dubrule, O. and Damsleth, E. (2001). Achievements and challenges in petroleum geostatistics. *Petroleum Geoscience*, **7**, S1–S7.

Dutton, S.P. (1977). Diagenesis and porosity distribution in deltaic sandstones. Strawn Series (Pennsylvanian), *Gulf Coast Association of Geological Societies Transactions*, north-central Texas, **27**, 272-277.

Elliot, D.H., and Watts, D.R., (1974). The nature and origin of volcaniclastic material in some Karoo and Beacon rocks. In: P.O.D. Andersson, A. Johansson and R.A. Kumpulainen (Editors), Sm–Nd isotope evidence for the provenance of the Skoorsteenberg Formation, Karoo Supergroup, South Africa. *Journal of Earth Sciences*, **36**, 173-183.

Elliott, T. (1989). Deltaic systems and their contributions to an understanding of basin-fill successions. In: Whateley, M.K.G. and Pickering, K.T. (Editors), Deltas: Sites and Traps for Fossil Fuels, *Geological Society Special Publication*, **41**, 21-46.

Evans, R., Mory, A.J. and Tait, A.M. (2007). An outcrop gamma ray study of the Tumblagooda Sandstone, Western Australia. *Journal of Petroleum Science and Engineering*, **57**, 37-59.

Falivene, O., Arbues, P., Howell, J., Fernandez, O., Cabello, P., Munoza, J.A. and Cabrera. L. (2006). A FORTRAN program to introduce field-measured sedimentary logs into reservoir modelling packages. *Computers and Geosciences*, **32**, 1519-1522.

Faure, K. and Cole, D. 1999. Geochemical evidence for lacustrine microbial blooms in the vast Permian Main Karoo, Parana, Falkland Islands and Huab basins of southwestern Gondwana. *Palaeogeography, Palaeoclimatology, Palaeoecology*, **152**, 189-213.

Fisher, Q. J., Casey, M., Clennell, M. B. and Knipe, R. J. (1999). Mechanical compaction of deeply buried sandstones of the North Sea. *Marine and Petroleum Geology* **16**, 605 – 618.

Flint, S.S. and Bryant, I.D. (1993). The geological modelling of hydrocarbon reservoirs and outcrop analogues. Special publication number **15** of the *International Association of Sedimentologists, unpaginated.*

Flint, S. S., Hodgson, D. M., King, R. C., Potts, G. J., Van Lente, B. and Wild, R. J. (2004). The Karoo Basin Slope Project: Phase 1. In: R.J. Wild (Editor), Sedimentological and sequence stratigraphic evolution of a Permian Lower Slope to Shelf Succession, Tanqua Depocentre, SW Karoo Basin, South Africa. Unpublished PhD Thesis, University of Liverpool, 350 p.

Galloway, W.E. (1975). Process framework for describing the morphologic and stratigraphic evolution of deltaic depositional systems. In: M.L. Broussard (Editor), Deltas, Models for Exploration. Houston Geological Society, Houston, Texas, 87–98.

Grecula, M., Flint, S. S., Wickens, H. DeV. and Johnson, S. D. (2003). Upward-thickening patterns and lateral continuity of Permian sand-rich turbidite channel fills, Laingsburg Karoo, South Africa. *Sedimentology* **50**, 831 – 853.

Helland-Hansen, W. and Martinsen, O.J. (1996). Shoreline trajectories and sequences: description of variable depositional-dip scenarios. *Journal of Sedimentary Research*, **66**, 670-688.

Helland-Hansen, W. and Hampson, G.J. (2009). Trajectory analysis: concepts and applications. *Basin Research*, **21**, 454-483.

Helland-Hansen, W. (2009). Discussion: Towards the standardisation of sequence stratigraphy. *Earth Science Reviews*, **94**, 95-97.

Hodgson, D.M., Flint, S.S., Hodgetts, D., Drinkwater, N.J., Johannesson, E.J. and Luthi, S.M. (2006). Stratigraphic evolution of fine-grained submarine fan systems, Tanqua depocentre, Karoo Basin, South Africa. *Journal of Sedimentary Research*, **76**, 20-40.

Honarpour, M.M., Cullick, A.S., Saad, N., and Humphreys, N.V. (1995). Effective of rock heterogeneity on relative permeability: Implications for scale-up. SPE paper 29311. In: D. Qi, and T. Hesketh (Editors), An Analysis of Upscaling Techniques for Reservoir Simulation. *Petroleum Science and Technology*, **23**, 827 — 842.

IHS Energy. (2009). Basin monitor Karoo Basin, South Africa and Lesotho. IHS Energy publication. *Unpaginated*.

Johnson, M.R., Van Vuuren, C.J., Visser, J.N.J., Cole, D.I., Wickens, H. de V., Christie, A.D.M., Roberts, D.L. and Brandl, G. (2006). Sedimentary rocks of the Karoo Supergroup. In: M.R. Johnson, C.R. Anhaeusser and Thomas, R.J. (Editors), the Geology of South Africa. *Geological Society of South Africa/Council of Geoscience, South Africa*, 461-499.

Johnson, M.R. (1991). Sandstone petrography, provenance and plate tectonic setting in Gondwana context of the southeastern Cape-Karoo Basin. *South African Journal of Geology*, **94**, 137-154.

Johnson, S.D., Flint, S., Hinds D. and Wickens, H.de V. (2001). Anatomy, geometry and sequence stratigraphy of basin floor to slope turbidite systems, Tanqua Karoo, South Africa. *International Association of Sedimentologists*, **48,** 987-1023.

Kozeny, J. (1927). ‘‘Uber kapillare Leitung des Wassers in Boden,’’- (in German). In: F.K. Boadu (Editor), Hydraulic conductivity of soils from grain-size distribution: new models. *Journal of Geotechnical and Geoenvironmental Engineering*, **(8)126**, 739-746.

Keogh, K.J., Martinius, A.W. and Osland, R. (2007). The development of fluvial stochastic modelling in the Norwegian oil industry: A historical review, subsurface implementation and future directions. *Sedimentary Geology,* **202**, 249-268.

King, R.C. (2005). The Structural Evolution of the Cape Fold Belt and SW Karoo Basin: Implications on sediment storage and routeing to the SW Karoo Basin, South Africa. Unpublished PhD Thesis, University of Liverpool, 330 p.

Kortekaas, Th.F.M. (1985). Water/oil displacement characteristics in crossbedded reservoir zones. In: D. Mikeš, O.H.M. Barzandji, J. Bruining and C.R. Geel (Editors), Upscaling of small- scale heterogeneities to flow units for reservoir modelling. *Marine and Petroleum Geology*, **23**, 931-942.

Kostic, B., Andreas Becht, A. and Aigner, T. (2005). 3-D sedimentary architecture of a Quaternary gravel delta (SW-Germany): Implications for hydrostratigraphy. *Sedimentary Geology*, **181**, 143-171.

Krum, G.L., and Johnson, C.R. (1993). A 3-D modelling approach for providing a complex reservoir description for reservoir simulations. In: S.S. Flint and I.D. Bryant (Editors), The Geological Modelling of Hydrocarbon Reservoirs and Outcrop Analogues. *Special Publication of the International Association of Sedimentologists*, **15**, 253–258.

Labourdette, R., Casas, J. and Imbert, P. (2008). 3D Sedimentary modelling of a Miocene Deltaic reservoir unit, Sincor Field, Venezuela: A new approach. *Journal of Petroleum Geology*, **31(2)**, 135-152.

Lake, L.W. and Carroll, H.B. (1986). Reservoir Characterization. In: K.J. Keogh, A.W. Martinius, and R. Osland (Editors), The development of fluvial stochastic modelling in the Norwegian oil industry: A historical review, subsurface implementation and future directions. *Sedimentary Geology,* **202**, 249-268.

Lasseter, T. J., Waggoner, J. R. and Lake, L. W. (1986). Reservoir heterogeneities and their influence on ultimate recovery. In: Qi, D. and Hesketh, T. (Editors), An Analysis of Upscaling Techniques for Reservoir Simulation. *Petroleum Science and Technology*, **23**, 827-842.

Lock, B.E. (1980). Flat-plate subduction and the Cape Fold Belt of South Africa. *Geology*, **8**, 35-39.

Longhitano, S.G. (2008). Sedimentary facies and sequence stratigraphy of coarse-grained Gilbert-type deltas within the Pliocene thrust-top Potenza Basin (Southern Apennines, Italy). *Sedimentary Geology*, **210**, 87-110.

Lowe, D.R. (1975). Water escape structures in coarse-grained sediments. *Sedimentology*, **22**, 157-204

Lundegard, P.D., 1992. Sandstones porosity loss- a big picture view of the importance of compaction. *Journal of Sedimentary Petroleum*, **62**, 250–260.

MacDonald, A.C., Halland, E.K., 1993. Sedimentology and shale modelling of a sandstone-rich fluvial reservoir; upper Statfjord Formation, Statfjord Field, Northern North Sea. *AAPG Bulletin*, **77 (6)**, 1016–1040.

MacDonald, A.C. (1995). Subsurface reservoir characterisation from outcrop observations. *Marine and Petroleum Geology*, **12**, 110-111.

Martinsen, O.J. (1989). Styles of soft-sediment deformation on a Namurian (Carboniferous) delta slope, Western Irish Namurian Basin, Ireland. In: M.K.G. Whateley and K.T. Pickering (Editors), Deltas: Sites and Traps for Fossil Fuels. Geological Society, London, Special Publication, **41**, 21-46.

Matheron, G., Beucher, H., de Fouquet, H., Galli, A., Gerillot, D. and Ravenne, C. (1987). Conditional simulation of the geometry of fluvio-deltaic reservoirs. *Society of Petroleum Engineers*, Paper Number **16753**, 591–599.

Mayer, D.F. and Chapin, M.A. (1991). A comparison of outcrop and subsurface geologic characteristics and fluid flow properties in the lower Cretaceous muddy J. Sandstone. In: Bill Linville (Editor), Reservoir Characterisation III. PennWell Publishing Company, Oklahoma, 327-352.

Miall, A. D. and Miall, C. E. (2001). Sequence stratigraphy as a scientific enterprise: the evolution and persistence of conflicting paradigms. *Earth-Science Reviews*, **54**, 321-348

Mikeš, D. and Geel, C.R., (2006). Standard facies model to incorporate all heterogeneity levels in a reservoir model. Elsevier Ltd., *Marine and Petroleum Geology*, **23,** 943-959.

Mikeš, D., Barzandji, O.H.M., J. Bruining, J. and Geel, C.R. (2006). Upscaling of small-scale heterogeneities to flow units for reservoir modelling). *Marine and Petroleum Geology*, **23**, 931-942.

Muto, T. and Steel, R.J. (2002). In Defense of Shelf-Edge Delta Development during Falling and Lowstand of Relative Sea Level. *The Journal of Geology*, **110**, 421–436

Myers, K.J., Bristow, C.S., 1989. Detailed sedimentology and gamma ray log characteristics of a Namurian deltaic succession II: Gamma-ray logging. In: M.K.G. Whateley and K.T. Pickering (Editors), Deltas: Sites and Traps for Fossil Fuels. *Geological Society Special Publication*, **41**, 81–88.

Nelson, P.H. (1994). Permeability-porosity relationships in sedimentary rocks. *The Log Analyst*, May-June 1994, 38-61.

Nemec, W. (1995). The dynamics of deltaic suspension plumes, In: M.N. Oti and G. Postma (Editors), Geology of Deltas: Rotterdam, Balkema, pp 31–93.

Nguema Mve, O.P. (2005). Petrology, geochronology and provenance of the Laingsburg and Tanqua Karoo submarine fan systems, Ecca Group, South Africa. Unpublished MSc Thesis Stellenbosch University, 280 p.

Nichols, Gary. (2009). Sedimentology and stratigraphy, 2nd edition. Wiley-Blackwell Publication UK, 411 p.

Oliveira, C.M.M., Hodgson, D.M. and Flint, S.S. (2010). Distribution of soft-sediment deformation structures in clinoform successions of the Permian Ecca Group, Karoo Basin, South Africa. *Sedimentary Geology*, **235**, 314-330.

Orton, G. and Reading, H.G. (1993). Variability of deltaic processes in terms of sediment supply, with particular emphasis on grain size. *Sedimentology*, **40**, 475–512.

Pettijohn, F.J., Potter, P.E. and Siever, R. (1987). Sand and Sandstone, 2nd edition. Springer-Verlag, New York, 571 p.

Phillips, P. and Wen, R. (2007). Improving net-to-gross reservoir estimation with small-scale reservoir modelling. *AAPG search and discovery article #40252 delivered at AAPG annual convention, California, April 2007, unpaginated*.

Plink-Björklund, P., Mellere, D. and Steel, R.J. (2001). Turbidite variability and architecture of sand-prone, deep-water slopes: Eocene clinoforms in the Central Basin, Spitsbergen. *Journal of Sedimentary Research*, **71**, 895–912.

Postma, G. (1990). An analysis of the variation in delta architecture. *Terra Nova*, **2**, 124-130.

Press, F. and Siever, R. (1986). *Earth*. W. H. Freeman and Company, New York, 656 p.

Roberts, H.H. and Sydow, J. (2003). Late quaternary stratigraphy and sedimentology of the offshore Mahakam delta, East Kalimantan, Indonesia. *Society for Sedimentary Geology special publication*, **76**, 125-145.

Rodrigo, D.L. and Luiz, F.D.R. (2002). The role of depositional setting and diagenesis on the reservoir quality of Devonian sandstones from the Solimo~es Basin, Brazilian Amazonia. *Marine and Petroleum Geology*, **19**, 1047–1071.

Rowsell, D.M. and De Swardt, A.M.J. (1976). Diagenesis in Cape and Karoo sediments, South Africa, and its bearing on their hydrocarbon potential. *Transactions of the Geological Society of South Africa* **79 (1)**, 81-145.

Rubidge, B.S., Hancox, P.J. and Catuneanu, O. (2000). Sequence analysis of the Ecca-Beaufort contact in the southern Karoo of South Africa. *South African Journal of Science*, **103**, 81-96.

Samuel, O.J., Jones, D.M. and Cornford, C. (2007). Intra-delta versus sub-delta sourcing of petroleum – a global review. AAPG search and discovery article #40243 extended abstract prepared for AAPG International Conference and Exhibition, Perth Australia, November, 2006, pp 1-7.

Satur, N., Keeling, G., Cronin, B.T., Hurst, A. and Gurbuz, K. (2005). Sedimentary architecture of a canyon-style fairway feeding a deep-water clastic system, the Miocene Cingoz Formation, southern Turkey: significance for reservoir characterisation and modelling. *Sedimentary Geology*, **173**, 91–119.

Scherer, M. (1987). Parameters influencing porosity and in sandstones: A model for sandstone porosity prediction. In: D.W. Waples (Editor), Evolution of sandstone porosity through time: The Modified Scherer Model: A calculation method applicable to 1-D maturity modelling and perhaps reservoir prediction. *Natural Resources Research*, **(4)11**, 257-272.

Scotchman, I.C. and Johnes, L.H. (1990). Wave-dominated deltaic reservoirs of the Brent Group, Northwest Hutton Field, North Sea. In: J.H. Barwis, J.G. McPherson and J.R.J. Studlick (Editors), Sandstone petroleum reservoirs, Springler-Verlag New York, Inc., pp 227-261.

Scott, E.D. (1997). Tectonics and sedimentation: the evolution, tectonic influences, and correlation of the Tanqua and Laingsburg sub-basins, southwest Karoo basin, South Africa. In: O.P. Nguema Mve (Editor). Petrology, geochronology and provenance of the Laingsburg and Tanqua Karoo submarine fan systems, Ecca Group, South Africa. Unpublished MSc Thesis, Stellenbosch University, 280 p.

Scott, E.D., Bouma, A.H. and Wickens, H.deV. (2000). Influence of tectonics on submarine fan deposition, Tanqua and Laingsburg sub-basins, South Africa. In: A.H. Bouma and C.G. Stone, (Editors), Fine-grained turbidite systems, *American Association of Petroleum Geologists Memoir **72**/Society of Economic Palaeontologists and Mineralogists Special Publication*, **68**, 47-56.

Sixsmith, P., Flint, S.S., Wickens, H. de V. and Johnson, S.D. (2003). Anatomy and stratigraphic development of a basin floor turbidite system in the Laingsburg Formation, main Karoo Basin, South Africa. *Journal of Sedimentary Research*, **74**, 239-254.

Sonibare, W.A. (2009). Lithofacies analysis and modelling of the Kookfontein deltaic succession, Tanqua depocentre, SW Karoo Basin, South Africa. Unpublished Honours thesis, Stellenbosch University, 53 p.

Suter, J.H. and Berryhill, H.L. JR. (1985). Late Quaternary shelf-margin deltas, Northwest Gulf of Mexico: *American Association of Petroleum Geologists*, Bulletin, **69**, 77–91.

Syvitski, J.P.M. and Farrow, G.E. (1989). Fjord sedimentation as an analogue for small hydrocarbon-bearing fan deltas. In: Whateley, M.K.G. and Pickering, K.T. (Editors), Deltas: Sites and traps for fossil fuels, *Geological Society Special Publication*, **41**, 21-46.

Tankard, A.J. and Barwis, J.H. (1982). Wave-dominated deltaic sedimentation in the Devonian Bokkeveld basin of South Africa. In: A. Tankard, H. Welsink, P. Aukes, R. Newton and E. Stettler (Editors), Tectonic Evolution of the Cape and Karoo Basins of South Africa. *Marine and Petroleum Geology,* doi:10.1016/j.marpetgeo.2009.01.022, 1-34.

Tankard, A., Welsink, H., Aukes, P., Newton R. and Stettler, E. (2009). Tectonic Evolution of the Cape and Karoo Basins of South Africa. *Marine and Petroleum Geology,* doi:10.1016/j.marpetgeo.2009.01.022, 1-34.

Taylor, J.M. (1950). Pore-space reduction in sandstones. *AAPG* Bulletin, **34(4)**, 701-716.

Tucker, M.E. (1991). Sedimentary Petrology: An introduction to the origin of sedimentary rocks. 2nd edition, Blackwell Scientific Publications, UK, 260 p.

Turner, B.R. (1999). Tectonostratigraphical development of the Upper Karoo foreland basin: orogenic unloading versus thermally-induced Gondwana rifting. *Journal of African Earth Sciences,* **29**, 215–238.

Udden, J.A. (1914). Mechanical composition of clastic sediments. In: G. Nichols (Editor), Sedimentology and stratigraphy, 2nd edition. Wiley-Blackwell Publication UK, 411p (pp 179-196).

Van der Werff, W. and Johnson, S. (2003). High resolution stratigraphic analysis of a turbidite system, Tanqua Karoo Basin, South Africa. *Marine and Petroleum Geology,* **20**, 45-69.

Van der Werff, W. and Johnson, S.D. (2003). Deep-sea fan pinch-out geometries and their relationship to fan architecture, Tanqua Karoo Basin (South Africa). *International Journal of Earth Sciences,* **92**, 728-742.

Van Lente, B. (2004). Chemostratigraphic trends and provenance of the Permian Tanqua and Laingsburg depocentres, Southwestern Karoo Basin, South Africa. Unpublished PhD Thesis, University of Stellenbosch, 339 p.

Veevers, J.J., Cole, D.I. and Cowan, E.J. (1994). Southern Africa: Karoo basin and Cape Fold Belt. In: J.J. Veevers and C.McA. Powell (Editors), Permian-Triassic Pangean Basins and Foldbelts along the Panthalassan Margin of Gondwanaland. *Geological Society of America*, Memoir, **184**, 223-279, Boulder, Colorado.

Visser, J.N.J. (1992). Deposition of the Early to Late Permian Whitehill Formation during a sea-level highstand in a juvenile foreland basin. *South African Journal of Geology*, **95**, 181-193.

Visser, J.N.J. (1993). Sea-level changes in a back-arc foreland transition, the Late Carboniferous – Permian Karoo Basin of South Africa. *Sedimentary Geology*, **83**, 115-131.

Visser, J.N.J. and Praekelt, H.E. (1996). Subduction, mega-shear systems and Late Paleozoic basin development of Gondwana. *Geologische Rundschau*, **86**, 632-646.

Wach, G.D., Lukas, T.C., Goldhammer, R.K., Wickens, H.de V. and Bouma, A.H. (2000). Submarine fan through slope to deltaic transition basin-fill succession, Tanqua Karoo, South Africa. In: Bouma, A.H. and Stone, C.G.(Editors), Fine-grained turbidite systems, American Association of Petroleum Geologists Memoir **72**/Society of Economic Palaeontologists and Mineralogists Special Publication, **68**, 173-180.

Waples, D.W. (2002). Evolution of sandstone porosity through time: The Modified Scherer Model: A calculation method applicable to 1-D maturity modelling and perhaps reservoir prediction. *Natural Resources Research*, **(4)11**, 257-272.

Weber, K.J., Kantorowicz, J.D. and Williams, H. (1991). Geological modelling of hydrocarbon reservoirs: A symposium held at the 13th International Sedimentological Congress, Nottingham, UK, 27-31 August 1990. *Marine and Petroleum Geology*, **8**, 244-246.

Wentworth, C.K. (1922). A scale of grade and class terms for clastic sediments. In: G. Nichols (Editor), Sedimentology and stratigraphy, 2nd edition. Wiley-Blackwell Publication UK, 411p (pp 179-196).

Wickens, H. de V. (1994). Basin floor fan building turbidites of the southwestern Karoo Basin, Permian Ecca Group, South Africa. Unpublished PhD Thesis, University of Port Elizabeth, 223 p.

Wild, R.J. (2005). Sedimentological and sequence stratigraphic evolution of a Permian Lower Slope to Shelf Succession, Tanqua Depocentre, SW Karoo Basin, South Africa. Unpublished PhD Thesis, University of Liverpool, 350 p.

Wild, R.J., Flint, S.S. and Hodgson, D.M. (2009). Stratigraphic evolution of the upper slope and shelf edge in the Karoo Basin, South Africa. Blackwell Publishing Ltd., *European Assoc. of Geoscientists and Engineers and International Assoc. of Sedimentologists*, **10**, 1-26.

Winkler, H. F. (1965). Petrogenesis of metamorphic rocks. *Springer-Verlag*.

Wright, L.D. (1977), Sediment transport and deposition at river mouths: a synthesis: *Geological Society of America*, Bulletin, **88**, 857–868.

Wu, T. (2004). Permeability prediction and drainage capillary pressure simulation in sandstone reservoirs. Unpublished PhD Thesis, Texas A and M University, 167 p.

Yu, X., Li, S., Zhao, S., Chen, J. and Hou, G. (2008). Constraining method of stochastic modelling for fluvial petroleum reservoir controlled by depositional facies using wells and seismic data. *Earth Science Frontiers*, **15(4)**, 33-41.

Zhang, E. and Davis, A. (1993). Coalification patterns of the Pennsylvanian coal measures in the Appalachian foreland basin, western and south-central Pennsylvania. *Geological Society of America Bulletin* **105 (2)**, 162 – 174.

Zhang, J., Qin, L. and Zhang, Z. (2008). Depositional facies, diagenesis and their impact on the reservoir quality of Silurian sandstones from Tazhong area in central Tarim Basin, western China. *Journal of Asian Earth Sciences*, **33**, 42-60.

Appendix A – Vertical sedimentary logs

LOG KEY

Sedimentary structures

	Cross bedding
	Planar cross stratification
	Wave ripples
	Hummocky or Swaley cross stratification
	Current ripple cross-lamination
	Horizontal planar lamination
	Soft-sediment deformation structures (slumps; loading and dewatering structures)

Lithologies

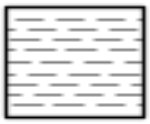 Claystone

 Mudstone

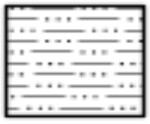 Siltstone

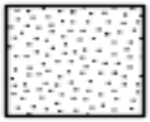 Sandstone

Base boundaries

 Sharp

 Gradational

Middle to Top of Cycle 1

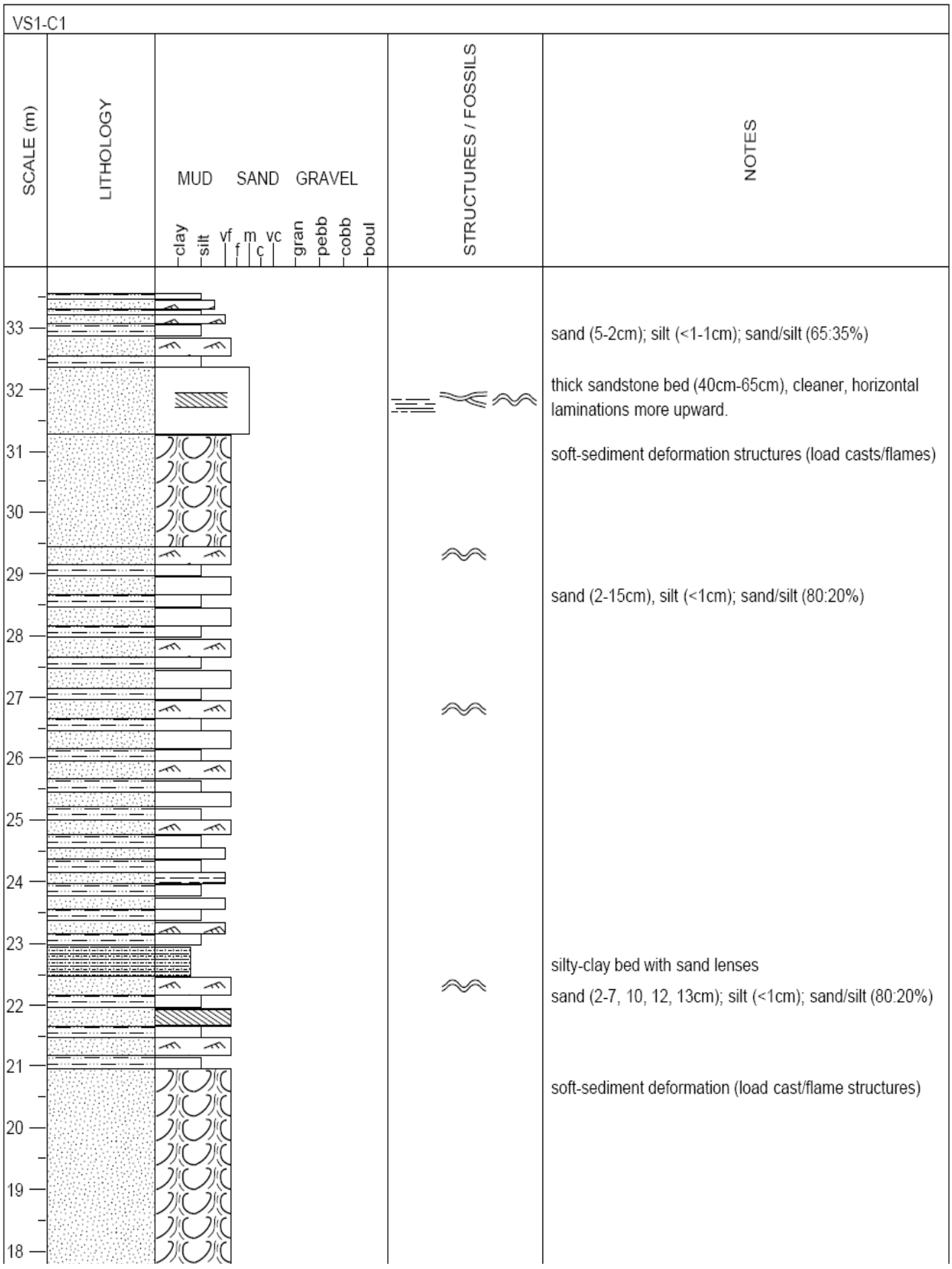

Base to Middle of Cycle 1

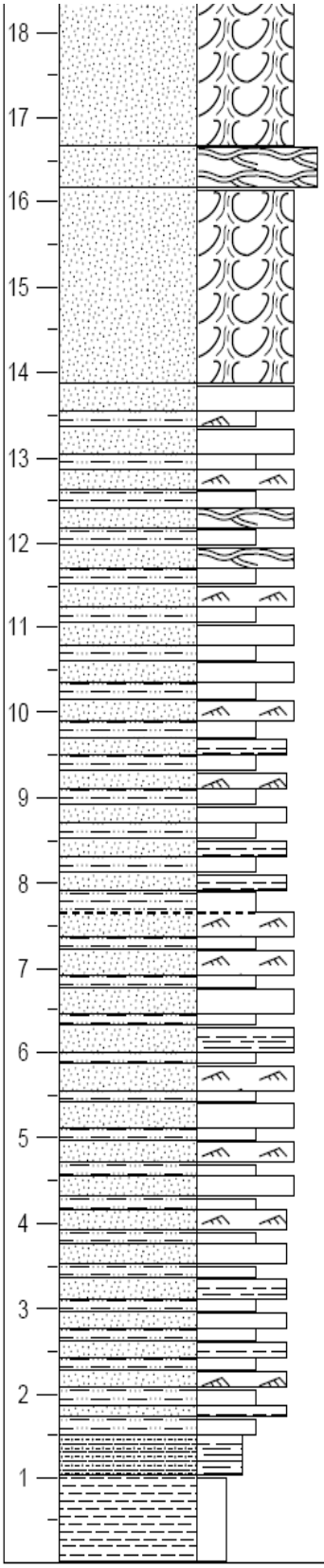

45cm thick sst bed within slump, less deformed?

massive and homogenous slump with blocky weathering, slump orientation E-W

sand (1-8cm); silt (<1-1.5cm); sand/silt (75:25%); bioturbation (2-3)

sand (2-8cm); silt (<1cm); sand/silt (75:25%)

Bioturbation (1-2)

sand (1-3.5cm); silt (<1cm-2cm); sand/silt (60:40%)

Regional claystone marker (1.5m) with scree-like weathering, base of cycle 1

Middle to Top of Cycle 2

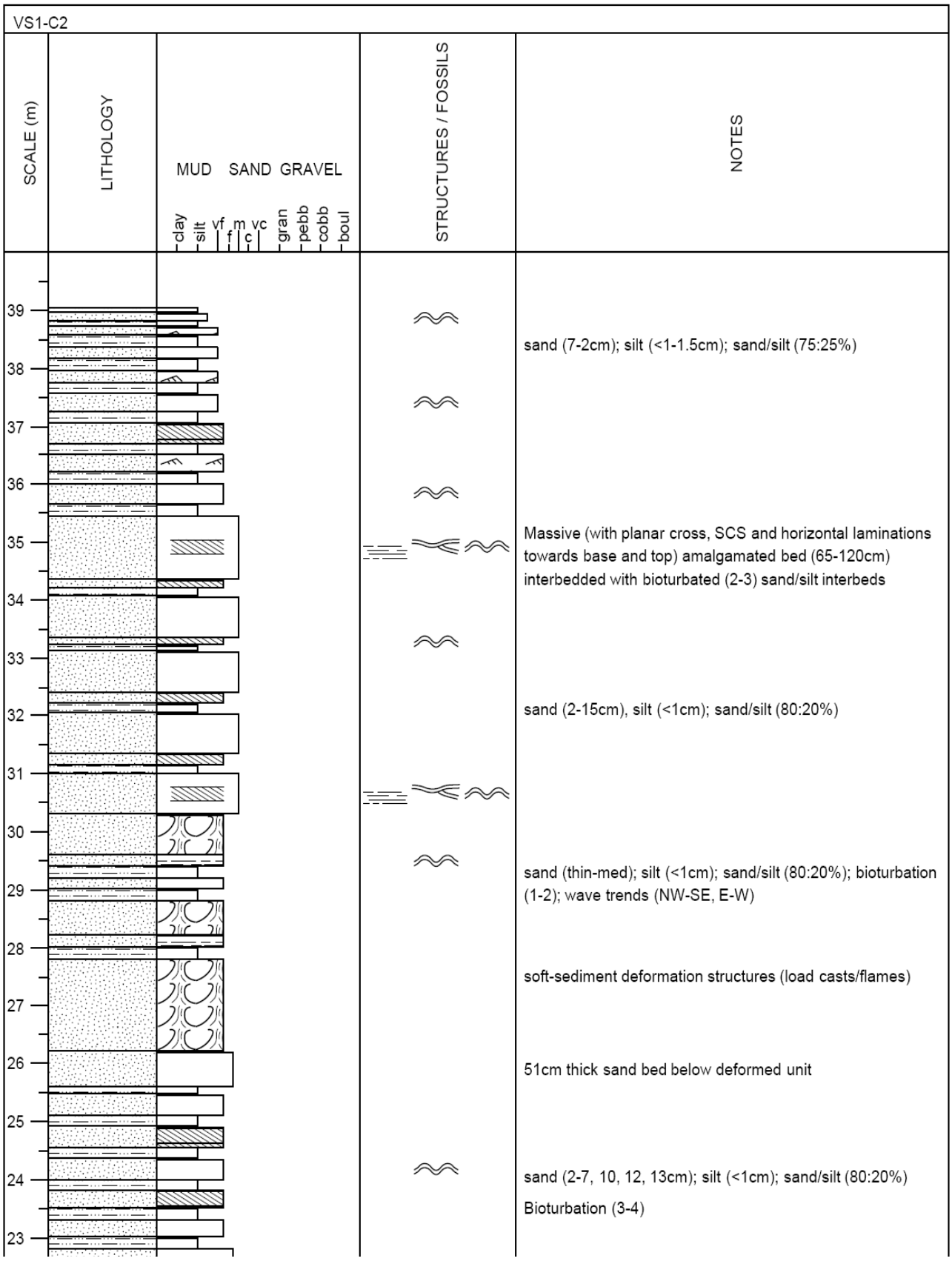

Base to Middle of Cycle 2

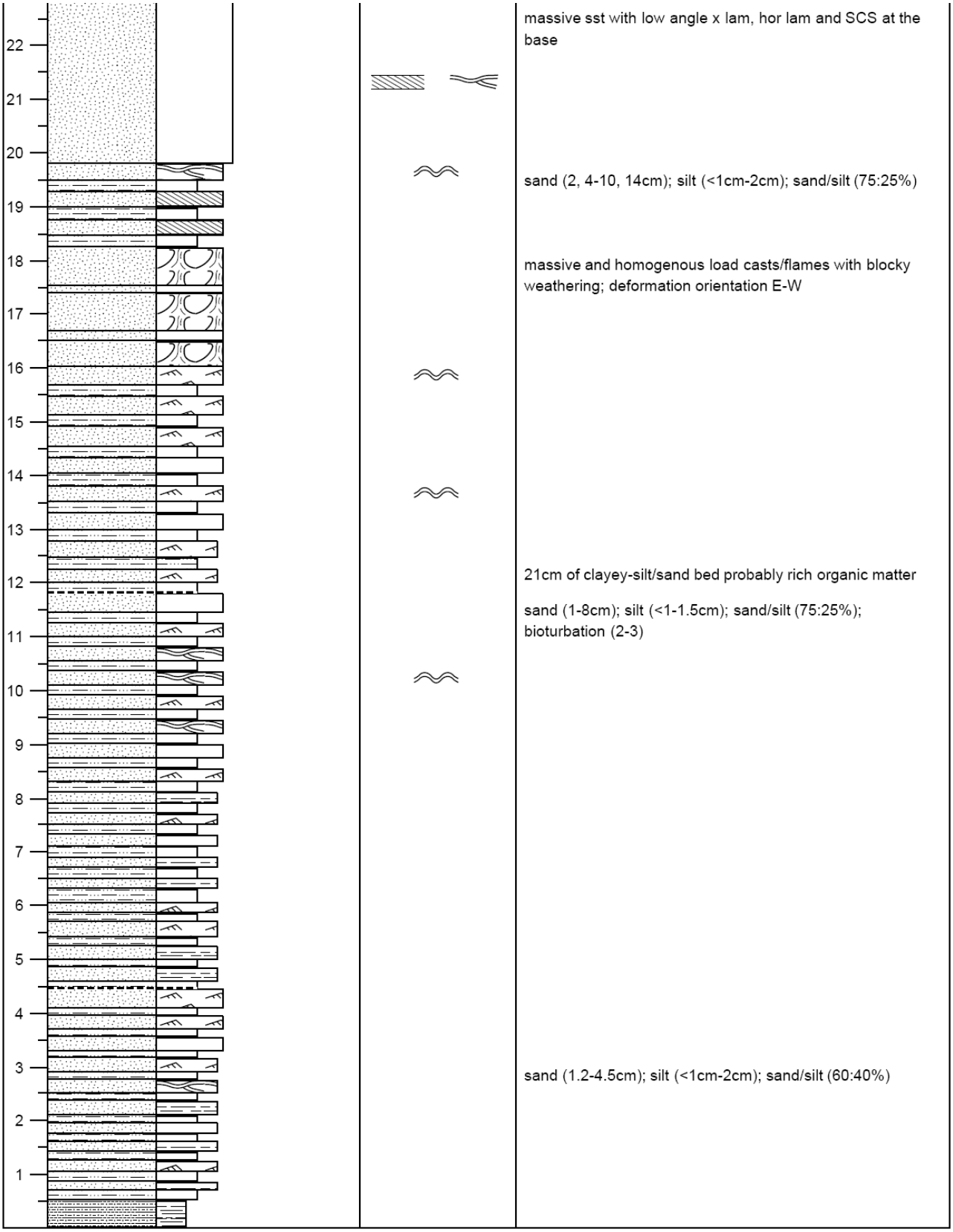

Middle to Top of Cycle 3

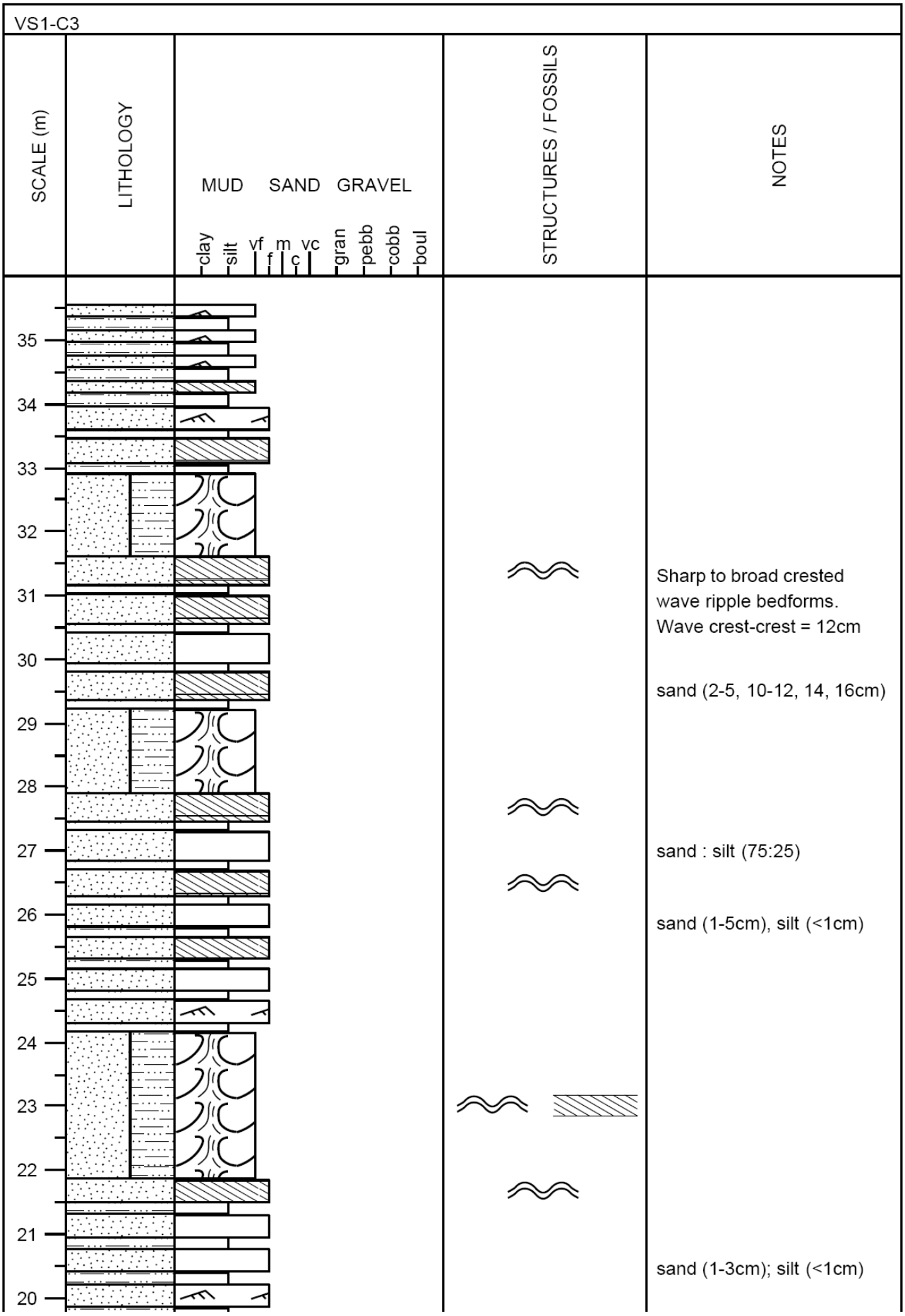

Base to Middle of Cycle 3

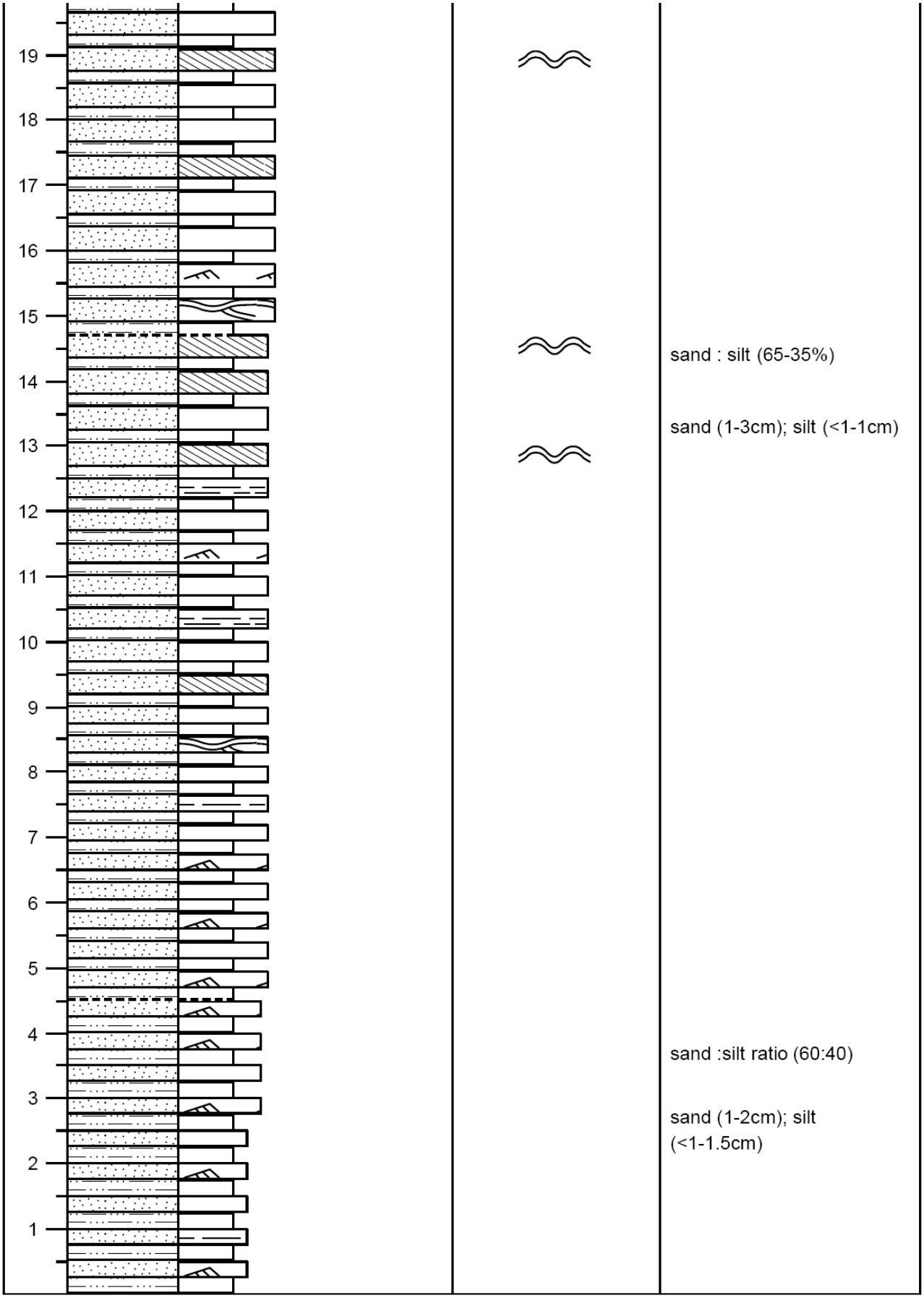

Middle to Top of Cycle 4

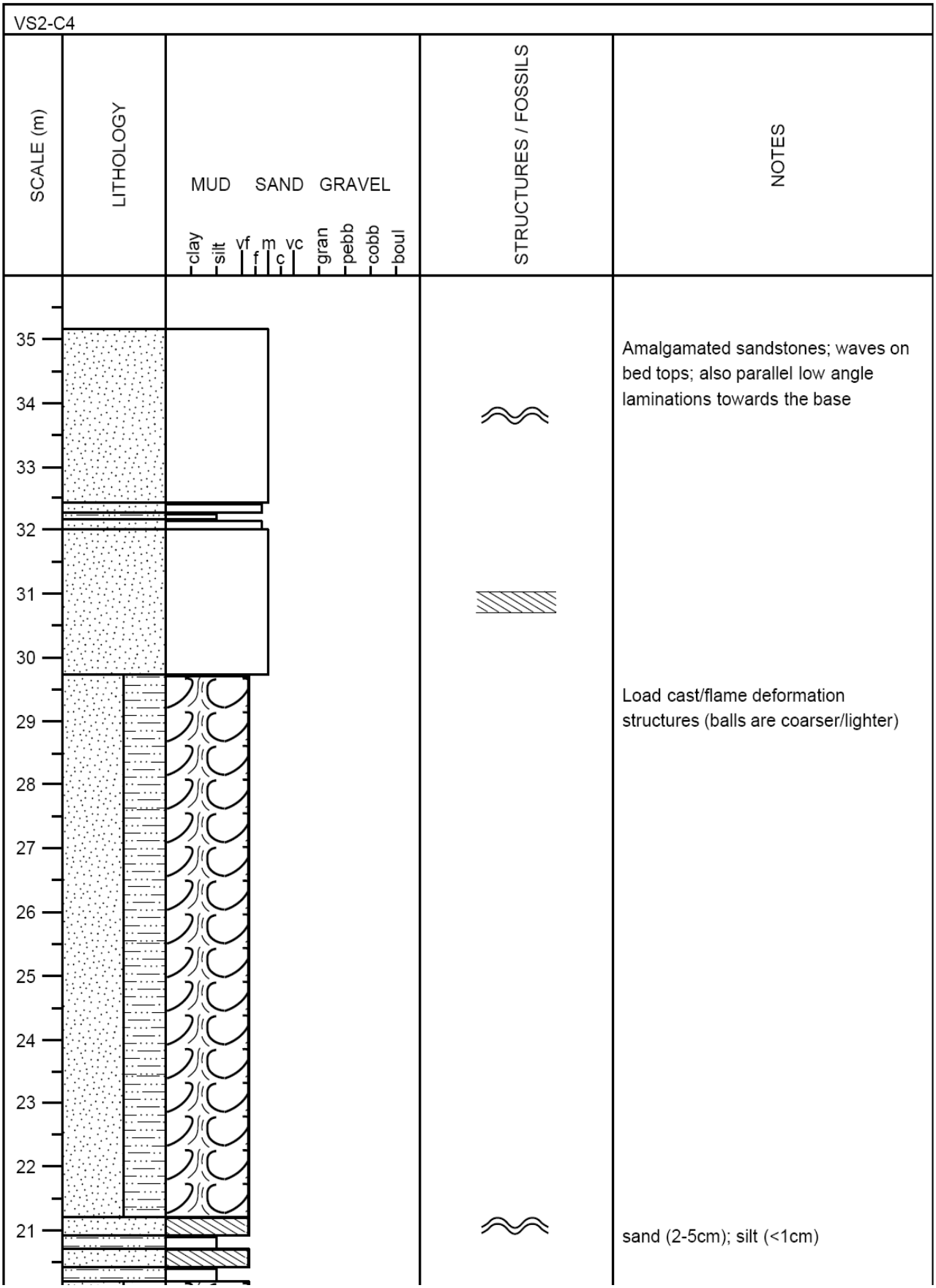

Base to Middle of Cycle 4

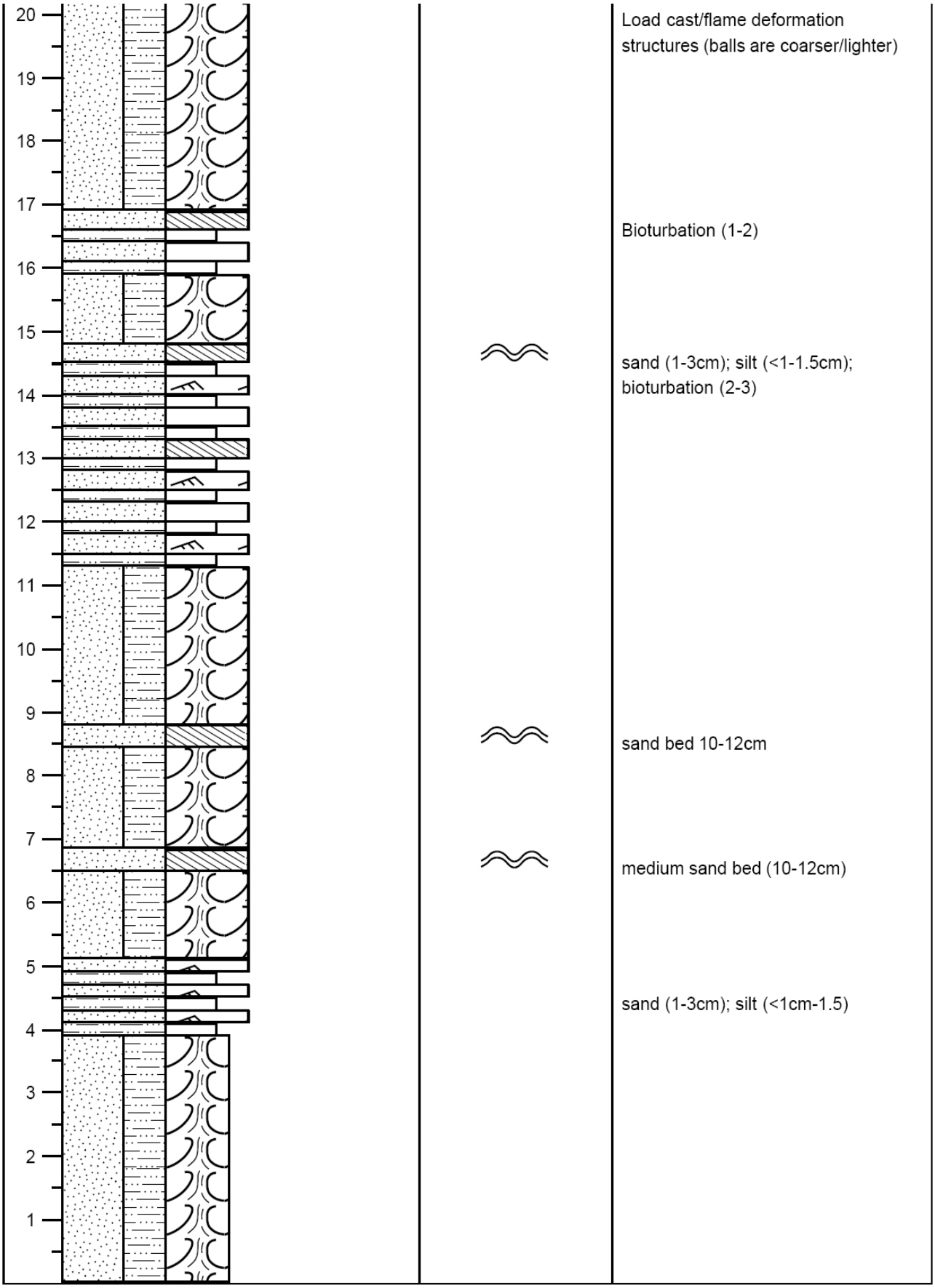

Middle to Top of Cycle 5

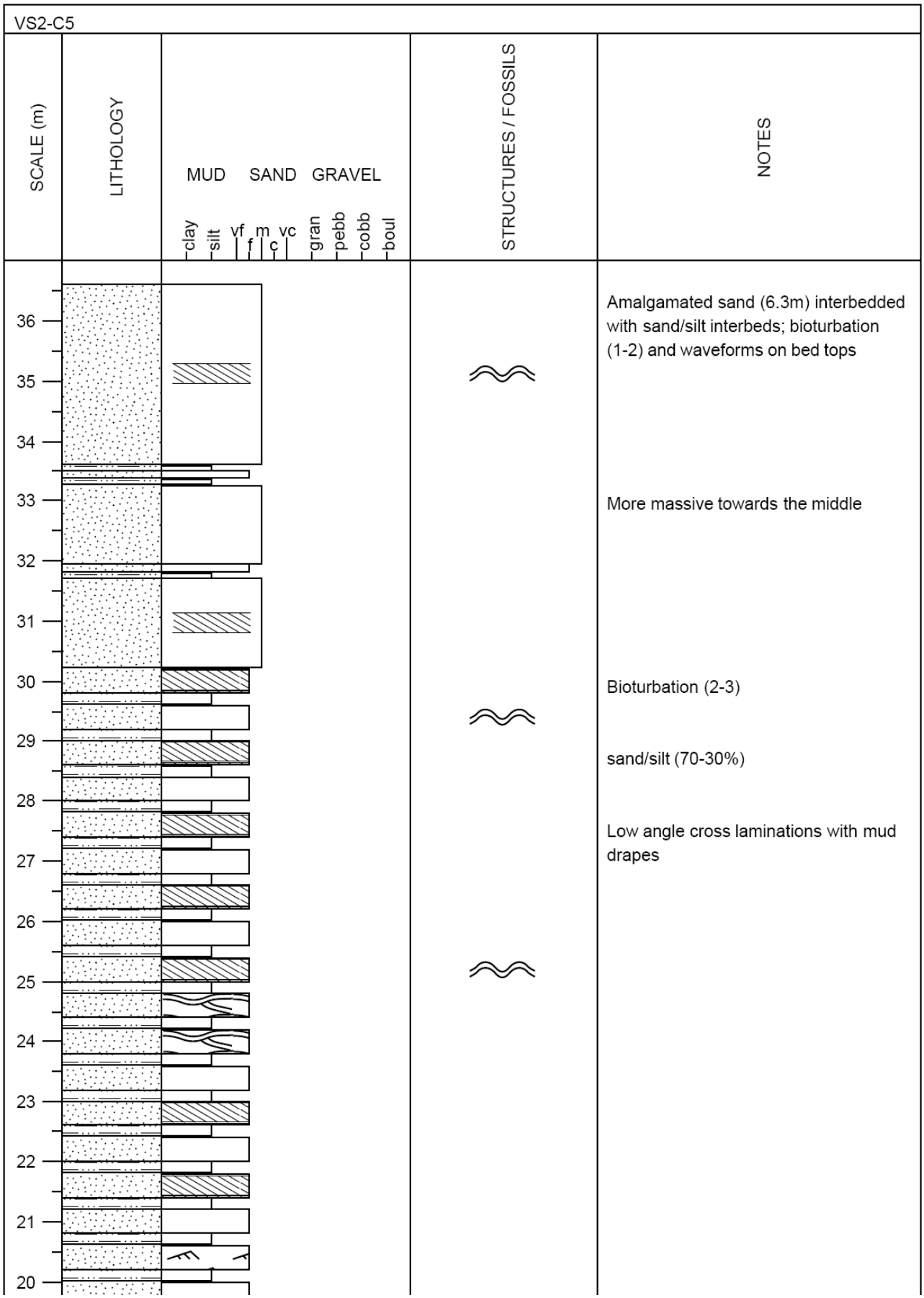

Base to Middle of Cycle 5

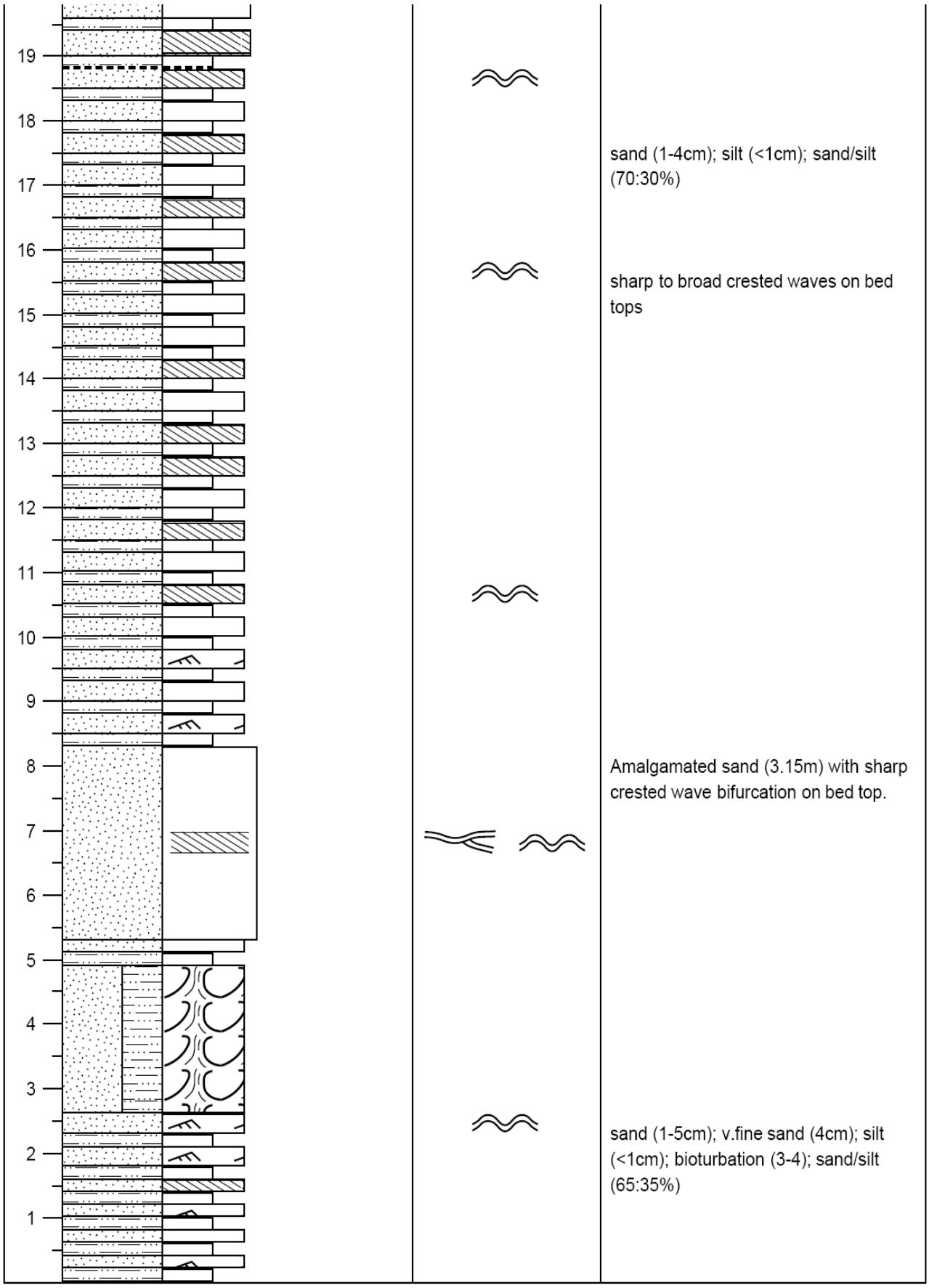

Cycle 6

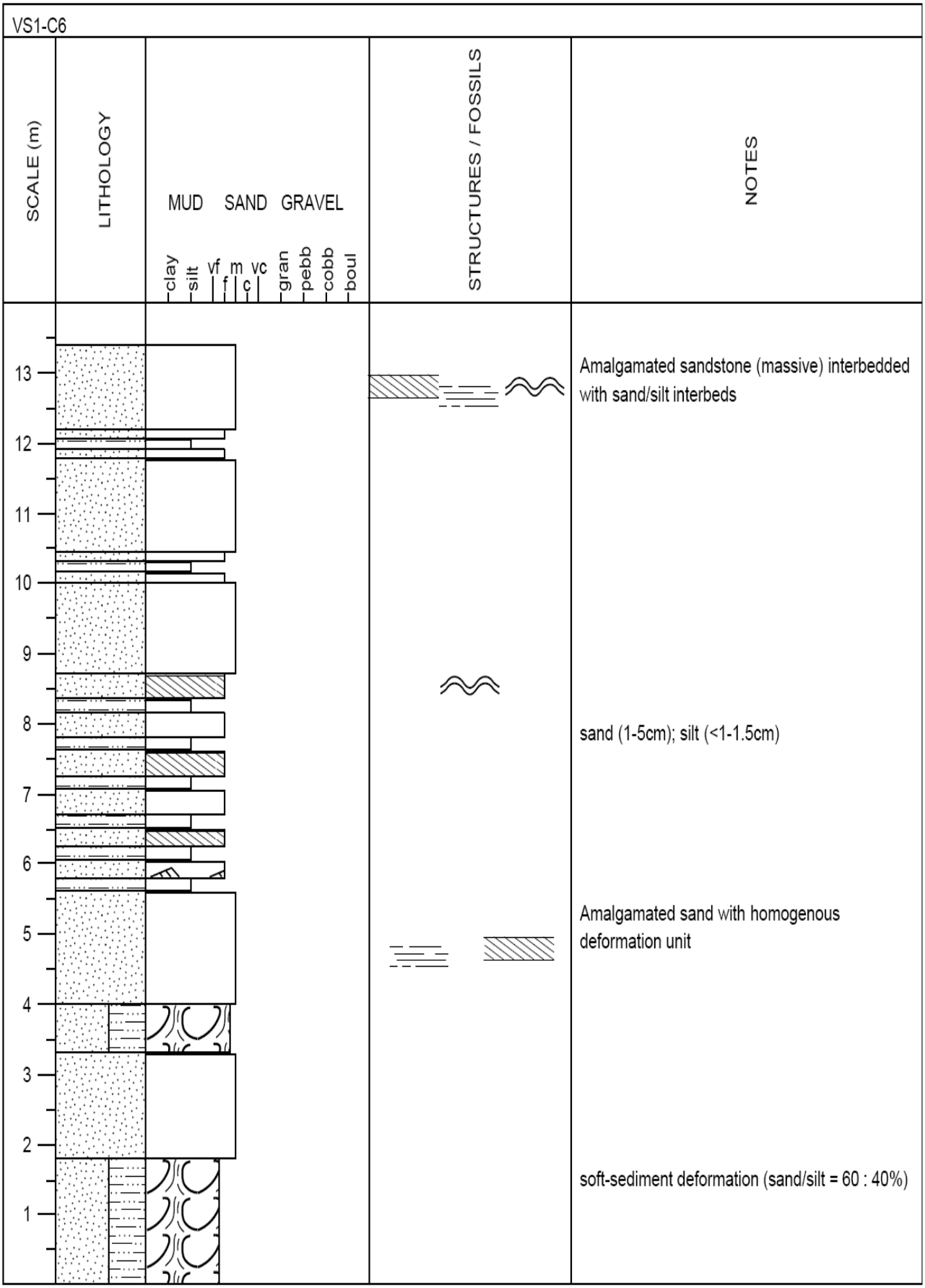

Cycle 7

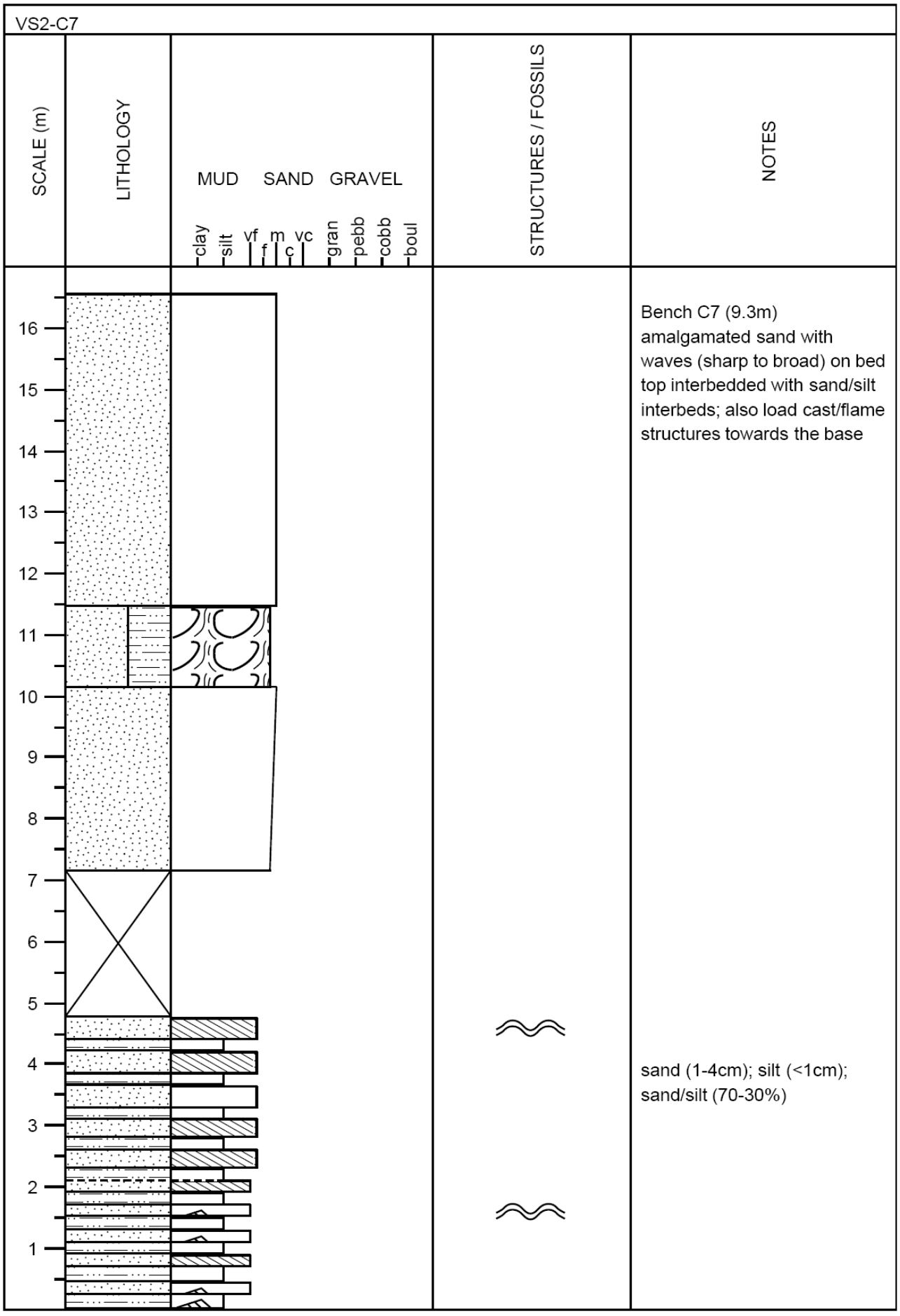

Cycle 8

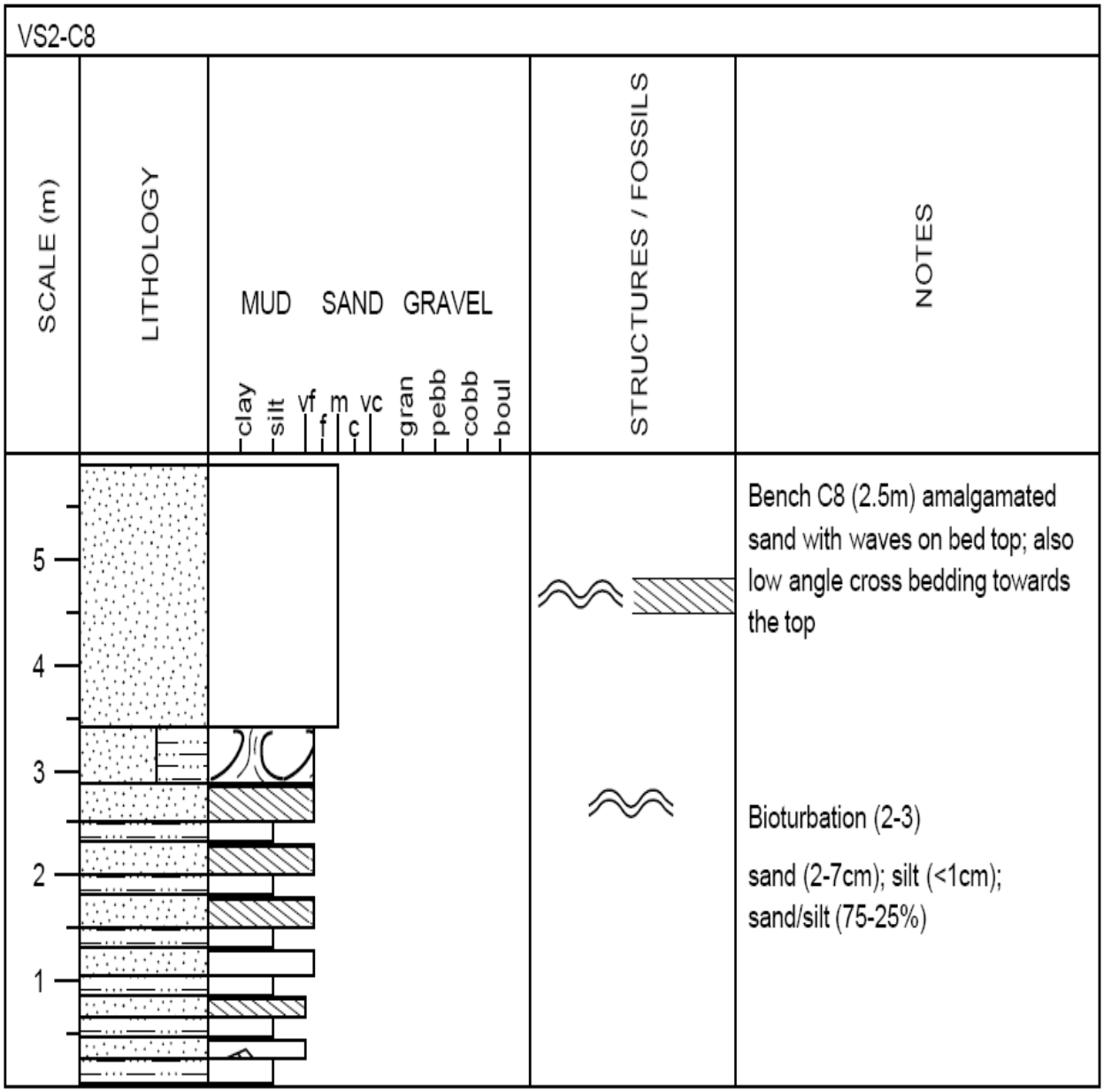

Cycle 9

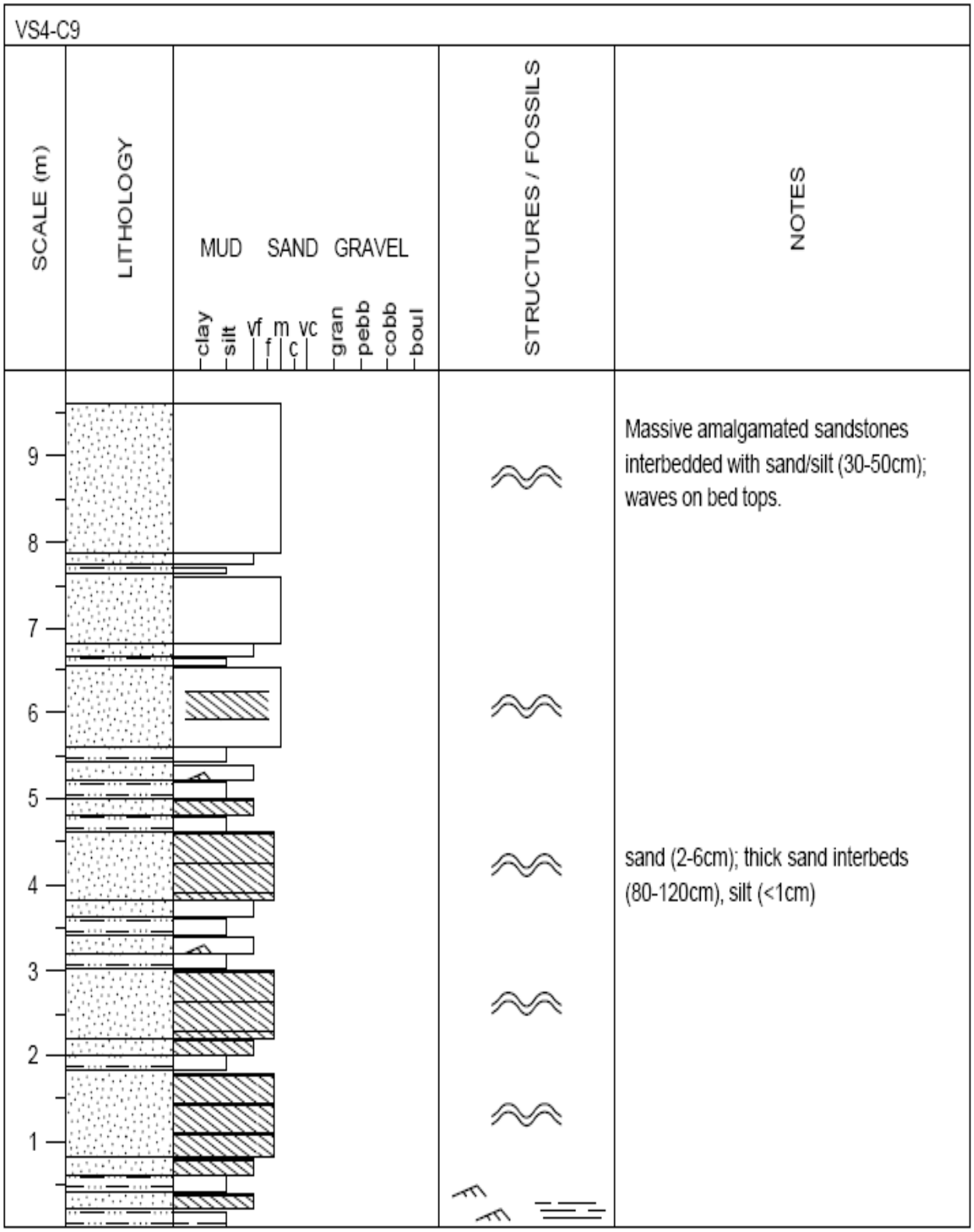

Cycle 10

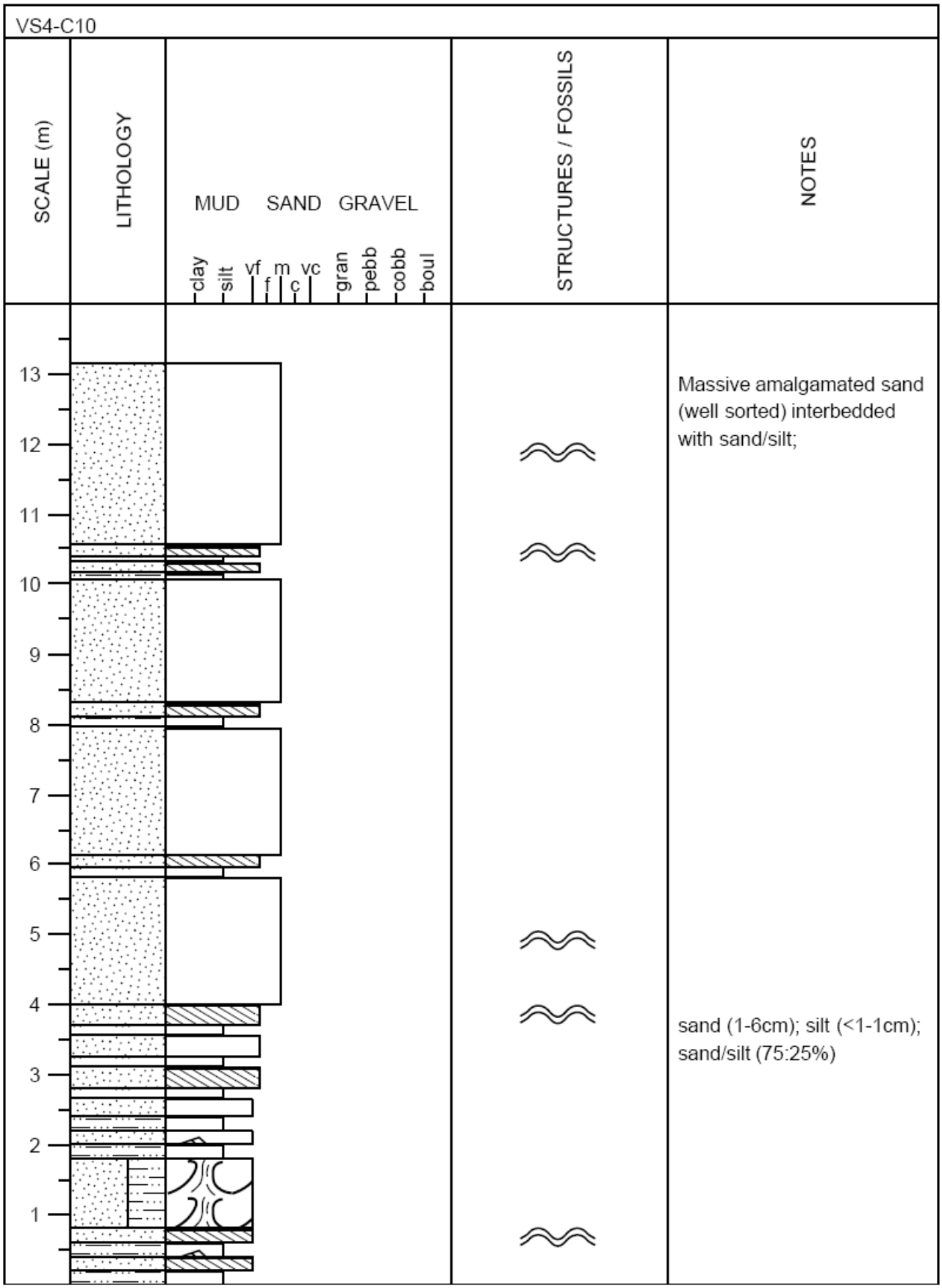

Cycle 11

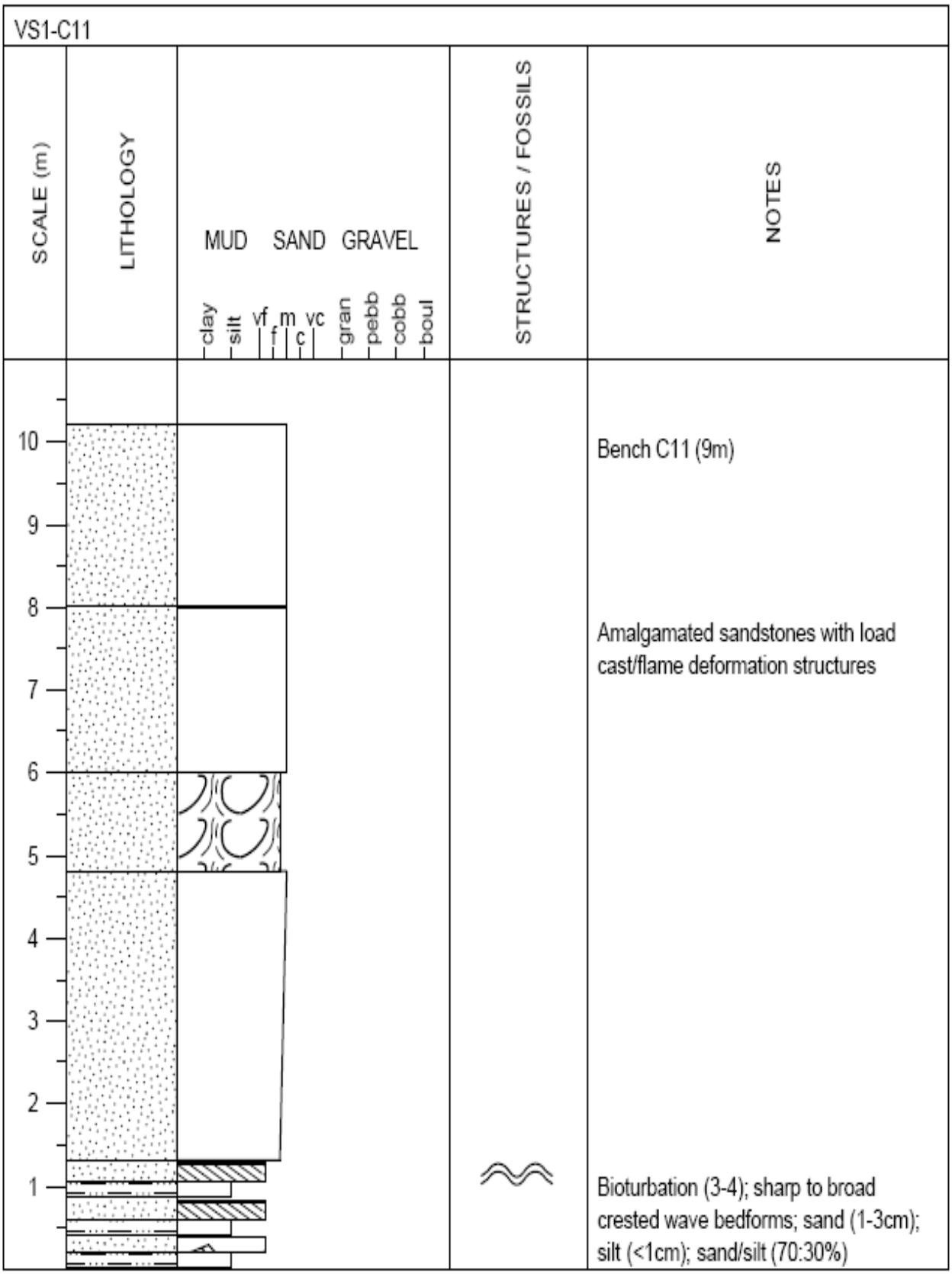

Cycle 12

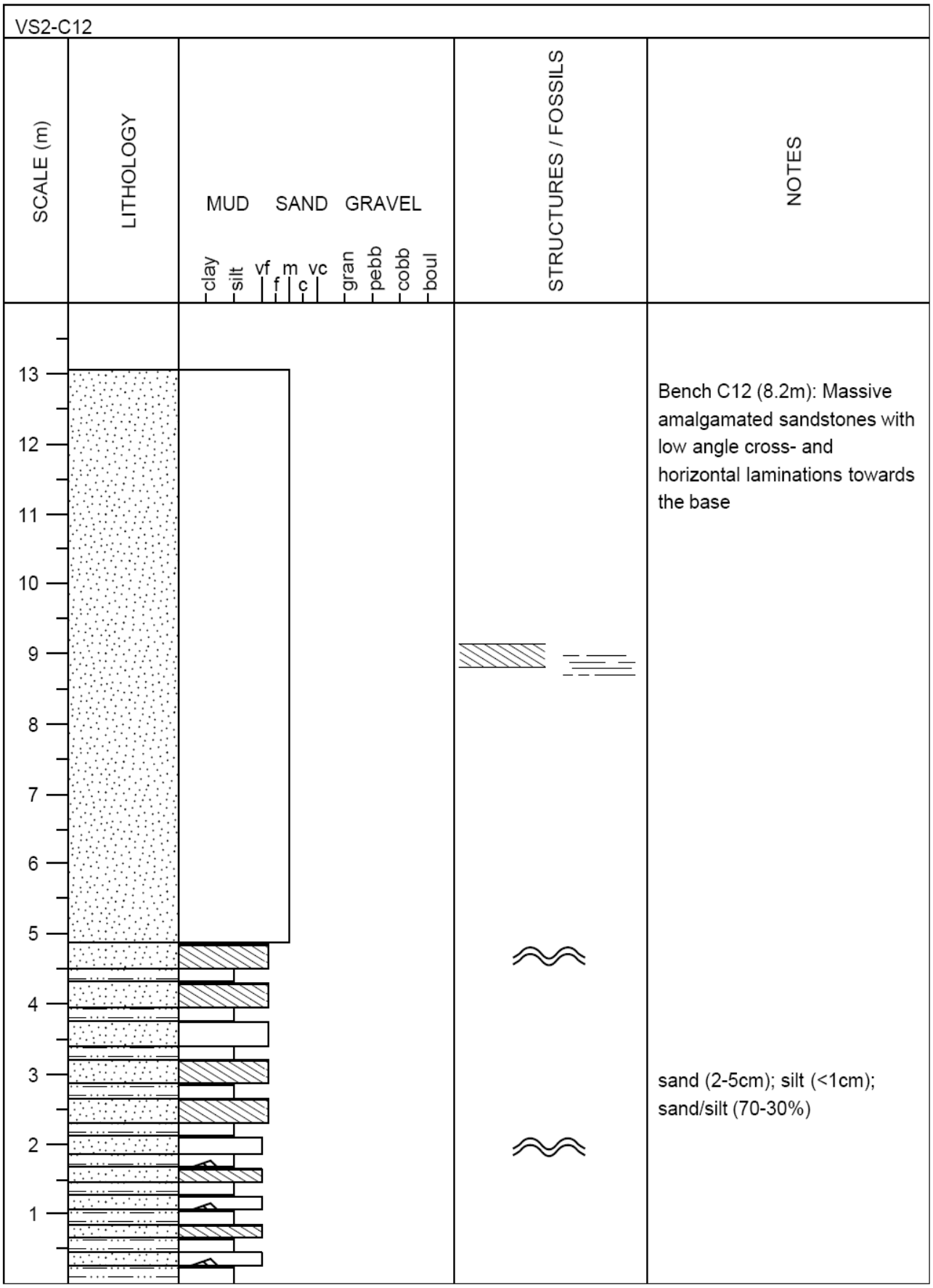

Cycle 13

VS4-C13

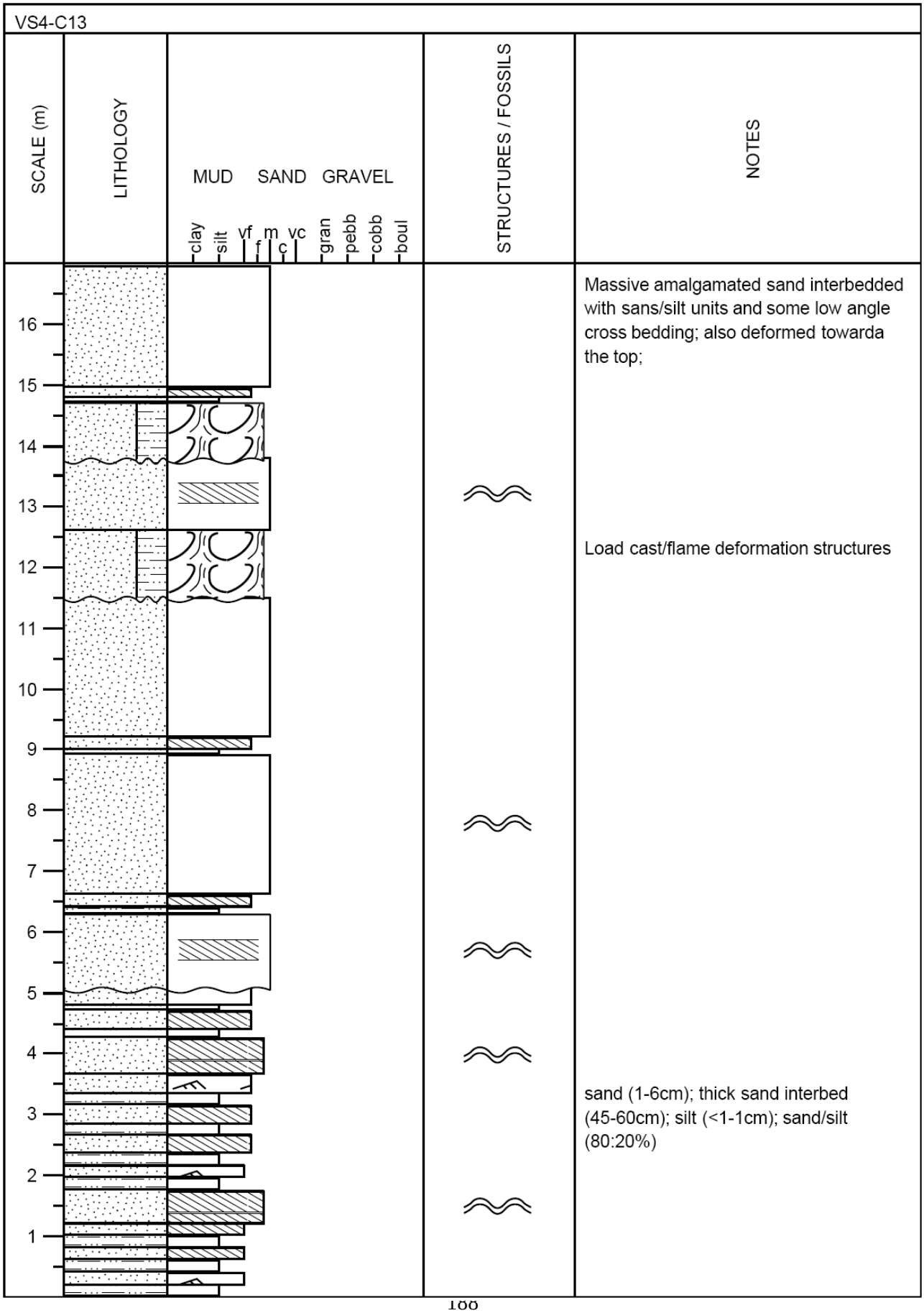

Appendix B – Lithofacies and sedimentary structures

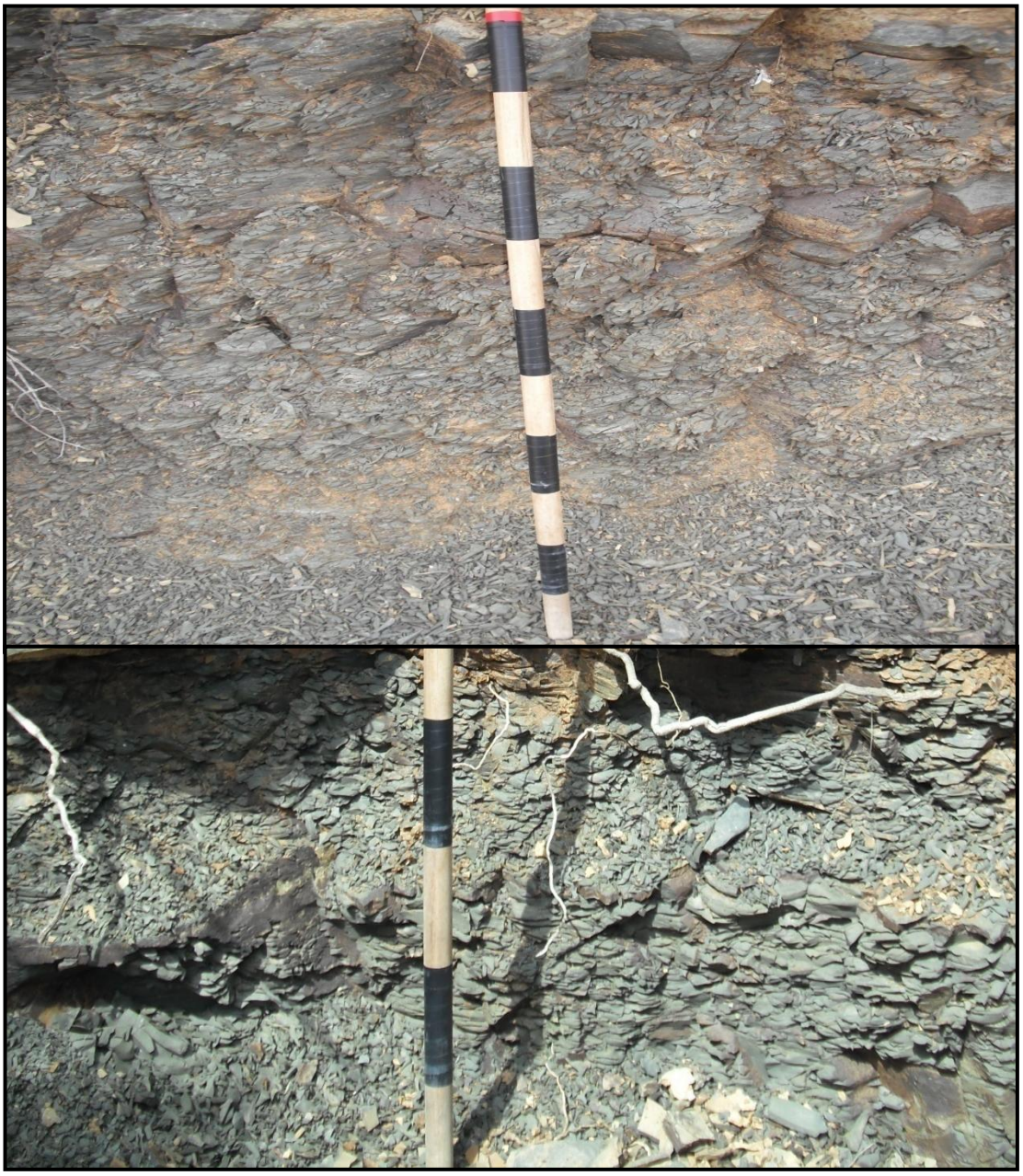

Depofacies 1- Mudstone: Structureless with very rare parallel to wavy laminations. Facies thickness varies from 0.2 m to 1 m. This facies represents prodeltaic hemipelagic sedimentation, deposited probably by long period of suspension settling.

Depofacies 2- Interbedded very fine-grained sandstones and siltstones: Parallel lamination with occasional current ripple lamination. Bed thickness varies very thin to thin. Facies thickness could reach 5.2 m at the western outcrop section. Sand to silt ratio is approximately 55% to 45%. This succession represents proximal prodeltaic sedimentation by alternating suspension settling and probably hyperpycnal flow driven by low-density turbidity current.

Depofacies 3- Interbedded very fine-grained sandstones and siltstones: Horizontal lamination to unidirectional current ripples with weak bioturbation. Bedding varies from very thin to thin. Facies thickness varies from 2.4 m to 3.9 m. Sand to silt ratio is approximately 55% to 45%. Processes are same as for depofacies 2; this deposition occurred below wave base towards the toe of the delta slope and is interpreted as the transitional between proximal prodelta and distal delta front.

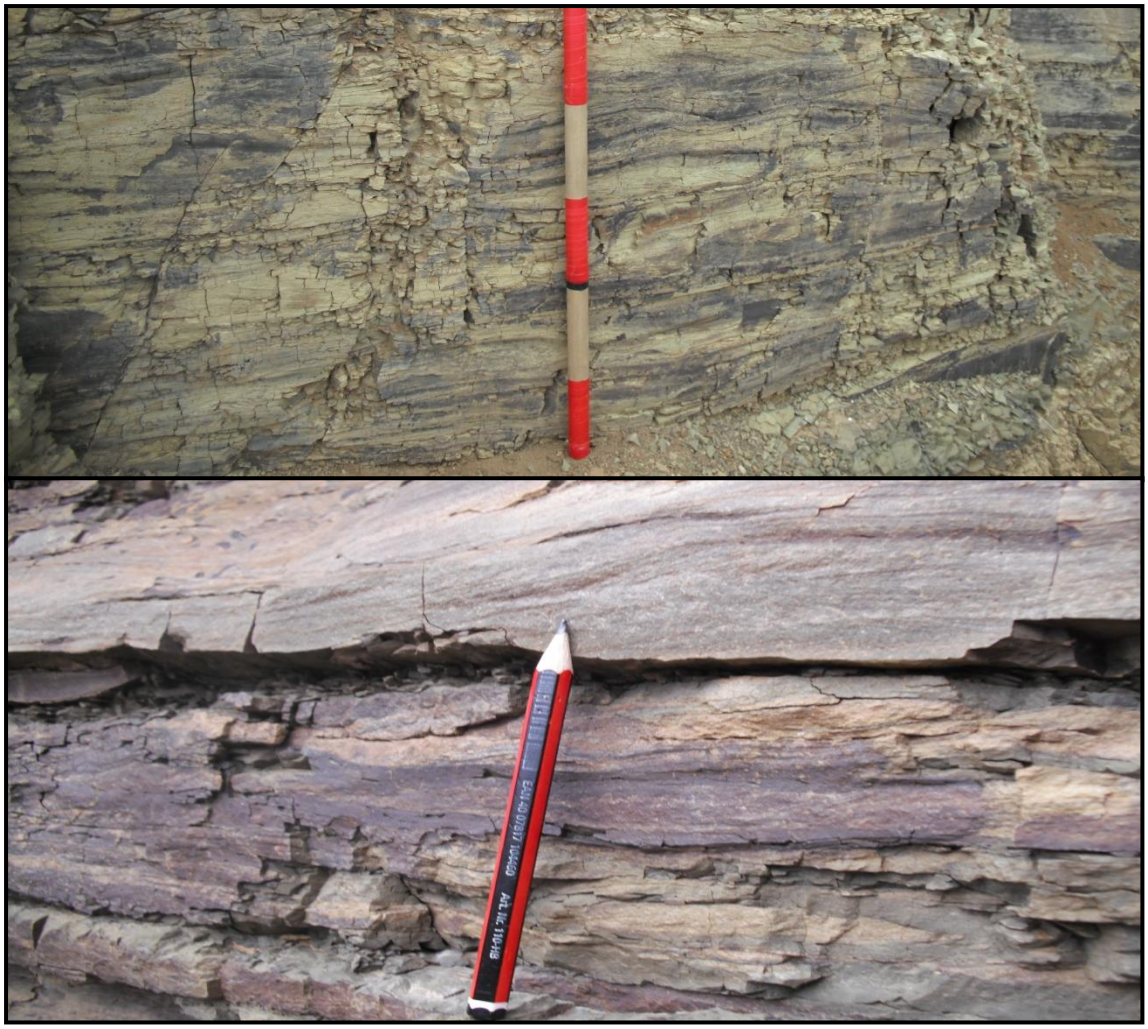

Depofacies 4- Interbedded very fine to fine-grained sandstones and siltstones: Unidirectional current ripples with occasional parallel lamination with moderate bioturbation. Bedding varies from very thin to thin while bed contacts vary from sharp to gradational. Facies thickness varies from 4.5 m to 8.8 m. Sand to silt ratio is approximately 60% to 40%. Processes are same as for depofacies 2 and 3 but with more reworking by current ripples and organic activities.

Depofacies 5- Interbedded very fine to fine-grained sandstones and siltstones: Current to wave ripple lamination with small-scale swaley cross-stratification with moderate bioturbation. Bedding varies from very thin to thin while bed contacts vary from sharp to gradational. Facies thickness varies from 2.6 m to 14.25 m. Sand to silt ratio is approximately 60% to 40%. This succession represents distal delta front sedimentation with variable reworking by current and wave ripples as well as organic activities; sand deposition is by gravity-driven hyperpycnal flow.

Depofacies 6- Fine-grained sandstones with siltstones: Current to wave ripple lamination with low-angle planar lamination and small-scale swaley cross-stratification (SCS) with moderate bioturbation. Bedding varies from thin to medium while facies thickness varies from 2.7 m to 5.95 m. Sand to silt ratio is approximately 70% to 30%. This succession represents mid-delta front sedimentation at or above wave base. The variation in wave amplitude and sinuosity on different bed surfaces (i.e. alternating sharp and rounded/broad crests) is interpreted to be due to variation in wave energies.

Depofacies 7- Fine-grained sandstones with siltstones: Planar cross-stratification with wave to current ripples and occasional parallel lamination and swaley cross-stratification. Bedding varies from very thin to thin while facies thickness varies from 0.8 m to 30.7 m. Sand to silt ratio is approximately 65% to 35%. This succession represents mid-delta front sedimentation at or above wave base. The variation in wave amplitude and sinuosity on different bed surfaces (i.e. alternating sharp and rounded/broad crests) is interpreted to be due to variation in wave energies.

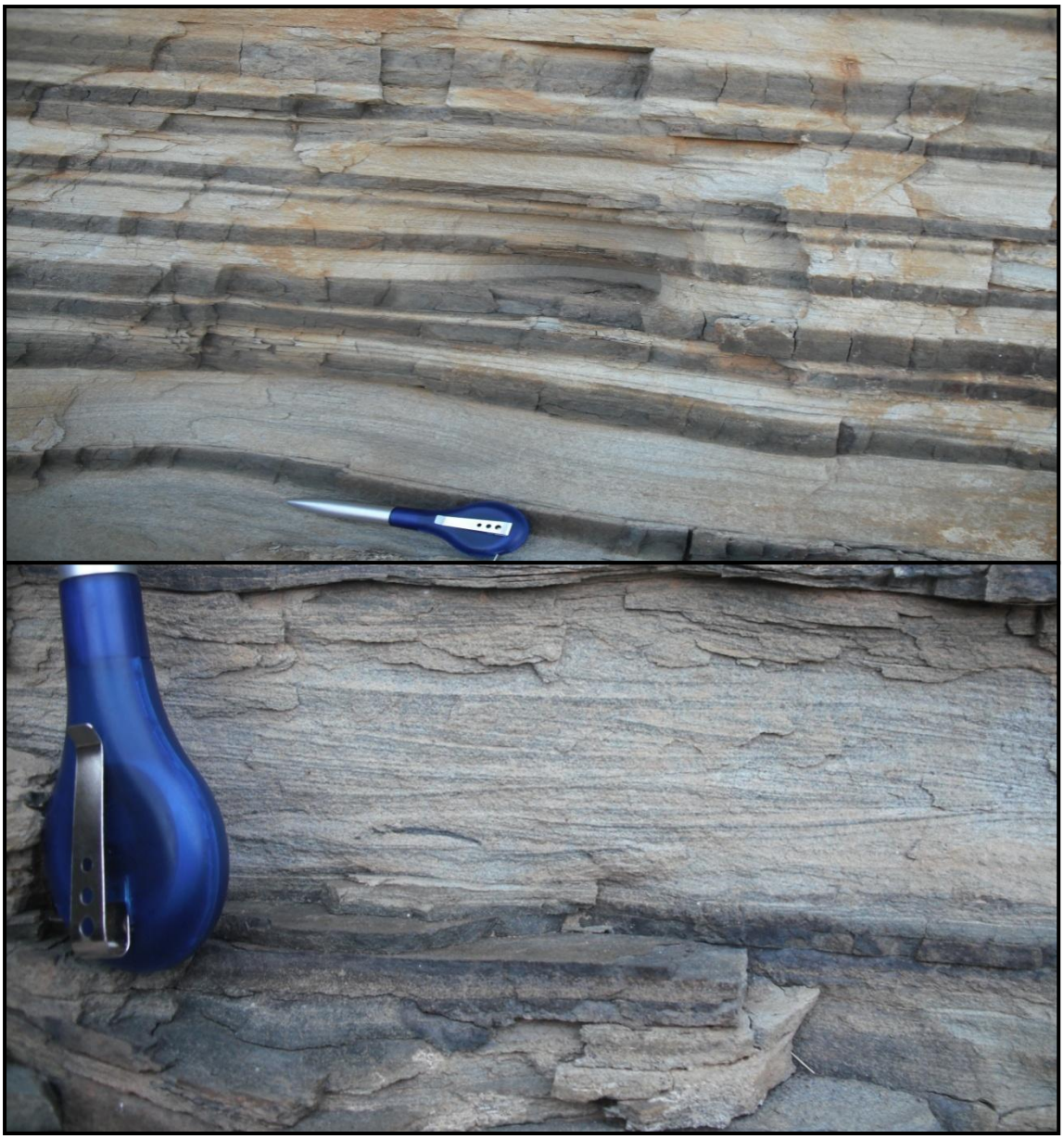

Depofacies 8- Fine to medium-grained sandstones with siltstones: Low-angle planar lamination with wave ripples and very rare current ripple cross-lamination. Bedding varies from thin to medium while facies thickness varies from 1.5 m to 5 m. Sand to silt ratio is approximately 80% to 20%. This succession represents mid-delta front sedimentation at or above wave base. The variation in wave amplitude and sinuosity on different bed surfaces (i.e. alternating sharp and rounded/broad crests) is interpreted to be due to variation in wave energies.

Depofacies 9- Soft-sediment deformed sandstones and siltstones (slumps and dewatered structures): Homogenous fine sand and silt with load cast and flame structures as well as slump folds. Facies thickness varies from 3.35 m to 18.2 m. Sand to silt ratio is approximately 60% to 40%. This facies succession represents product of intense soft-sediment deformation due to delta slope instability and gravity-driven mass transport of sediments over the shelf edge.

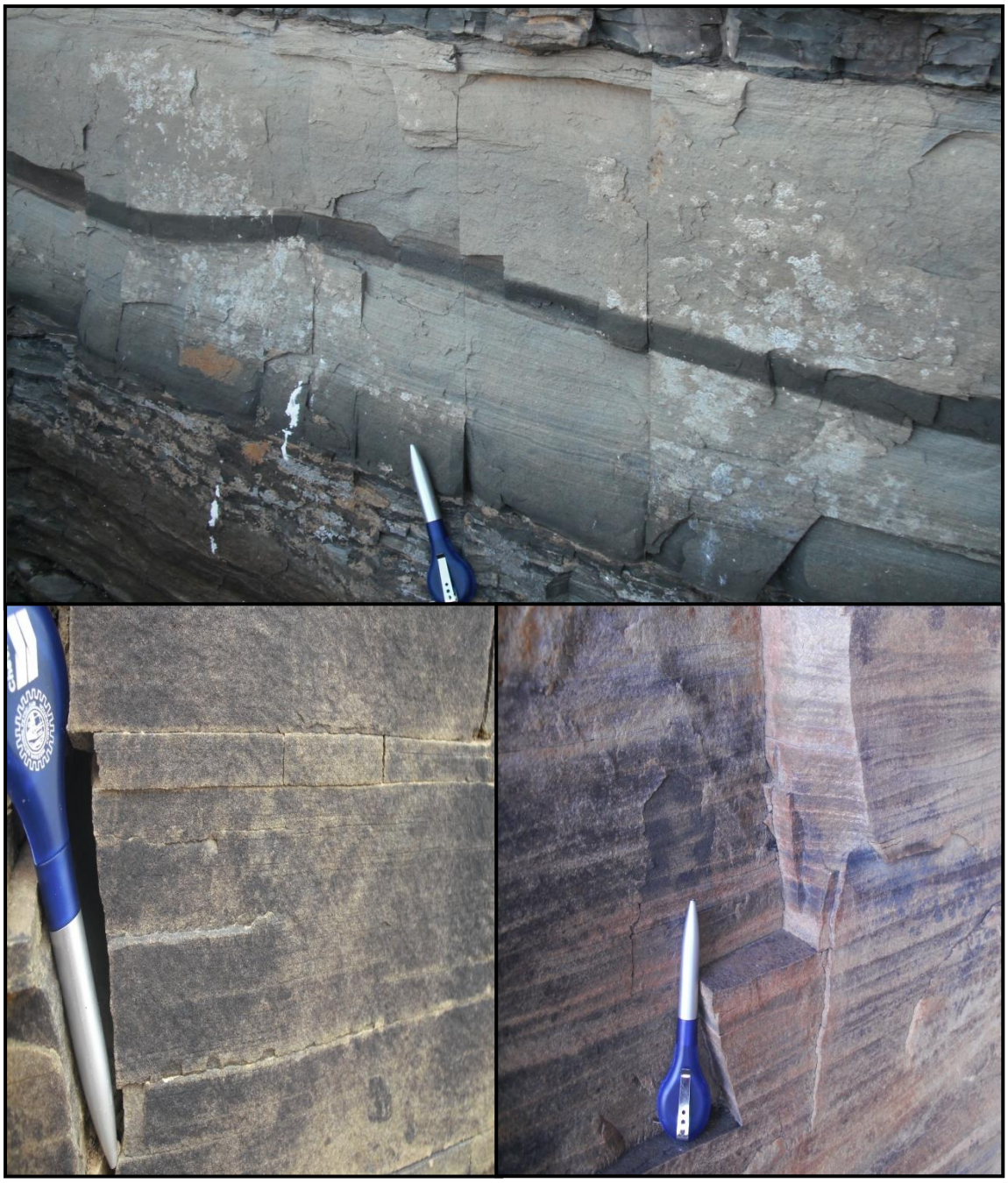

Depofacies 10- Fine to medium-grained bedded sandstones: Low-angle planar cross-stratification with wave bedforms. Bedding thickness varies from medium to thick while facies thickness varies from 0.51 m to 1.55 m. Sand to silt ratio is approximately 90% to 100%. This succession represents delta front sandstones deposited probably by gravity-driven hyperpycnal flow above fair weather wave base.

Depofacies 11- Medium-grained amalgamated bedded sandstones: Massive to planar cross-bedding with wave bedforms and very rare horizontal lamination with very rare bioturbation. Bedding thickness varies from thick to very thick while facies thickness varies from 3 m to 6.2 m. Sand to silt ratio is approximately 90% to 100%. This succession represents proximal mouthbar sandstones probably deposited as bedloads also sediments are being reworked by wave ripples

Depofacies 12- Medium-grained amalgamated sandstones interbedded with sand/silt interbeds: Massive to planar cross-bedding with wave bedforms, moderate bioturbation and very rare horizontal lamination. Bed thickness varies from thick to very thick which facies thickness varies from 3.15 m to 12 m. Sand to silt ratio is approximately 90% to 100%. This succession represents proximal river-dominated mouthbar sandstones probably deposited as bedloads; also sediments are being reworked variably by wave ripples.

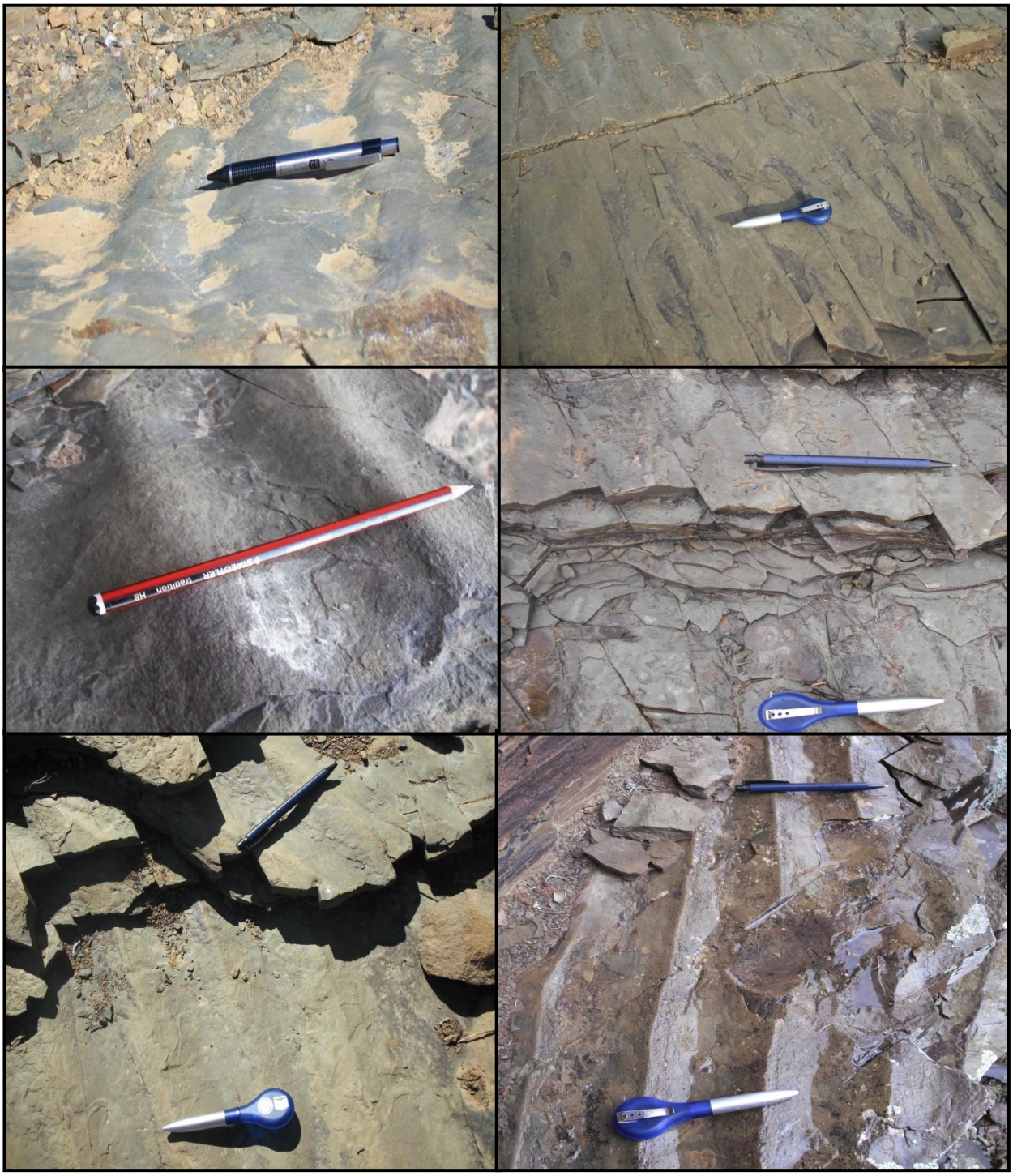

Wave ripples: Different wave bedforms observed on bed tops in the study area (Kookfontein Formation deltaic sequence). Wave amplitude, sinuosity, orientation and crest-form are widely variables. Wave ripple crest varies from sharp to more rounded indicating variations in wave energies and possibly water depths.

Appendix C – Sample photomicrographs

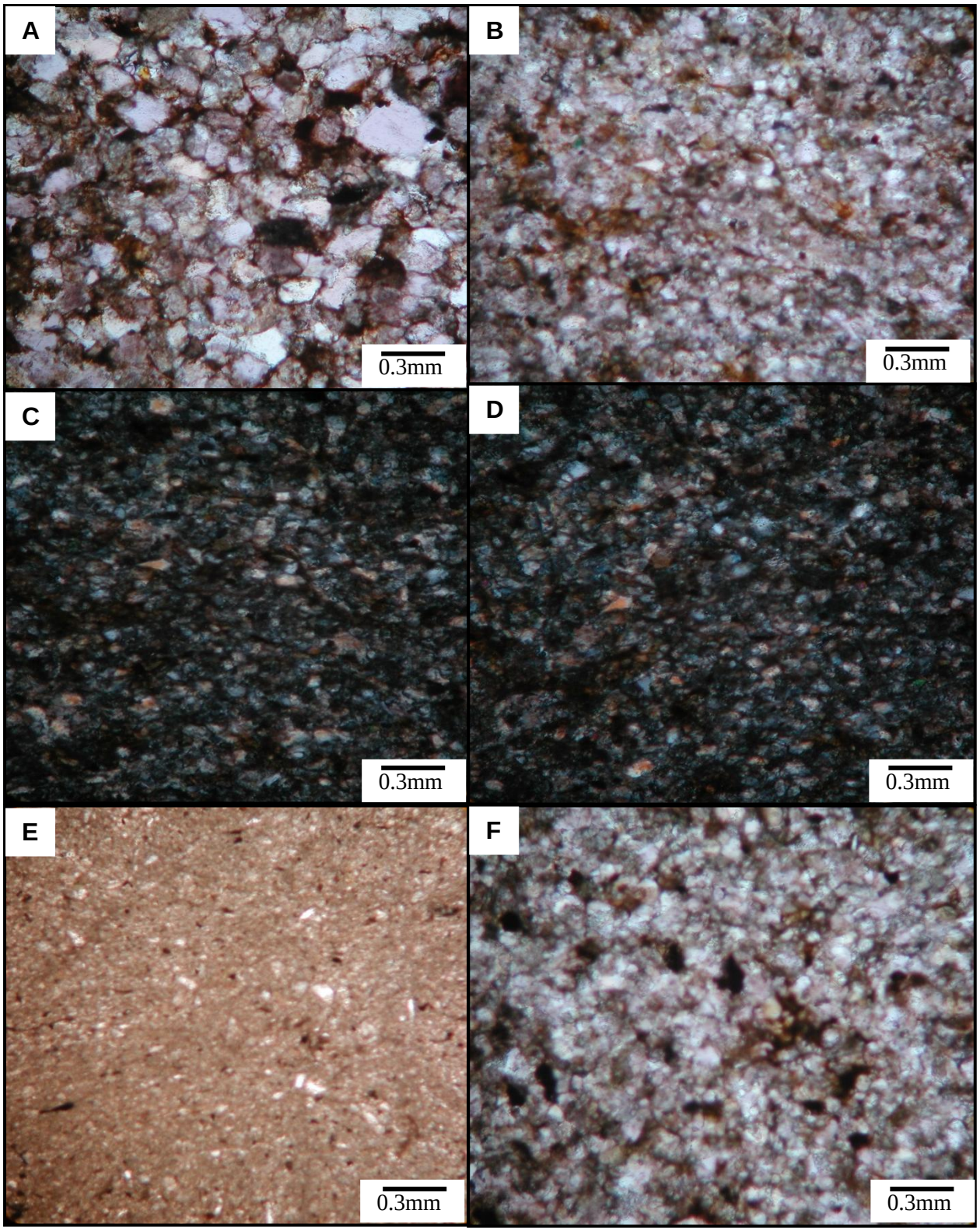

Photomicrograph description: (A) Sample SGSR: Lithofeldspathic sandstone under PL; (B) Sample SWA6: Lithofeldspathic sandstone under plane under PL; (C) Sample SWA6: Lithofeldspathic sandstone under XN; (D) Sample SWA17: Lithofeldspathic sandstone under XN; (E) Sample SWA7: Feldspathic wacke under PL; (F) Sample SWA17: Lithofeldspathic sandstone under PL.

PL: Plane-polarised light; XN: Crossed nicols

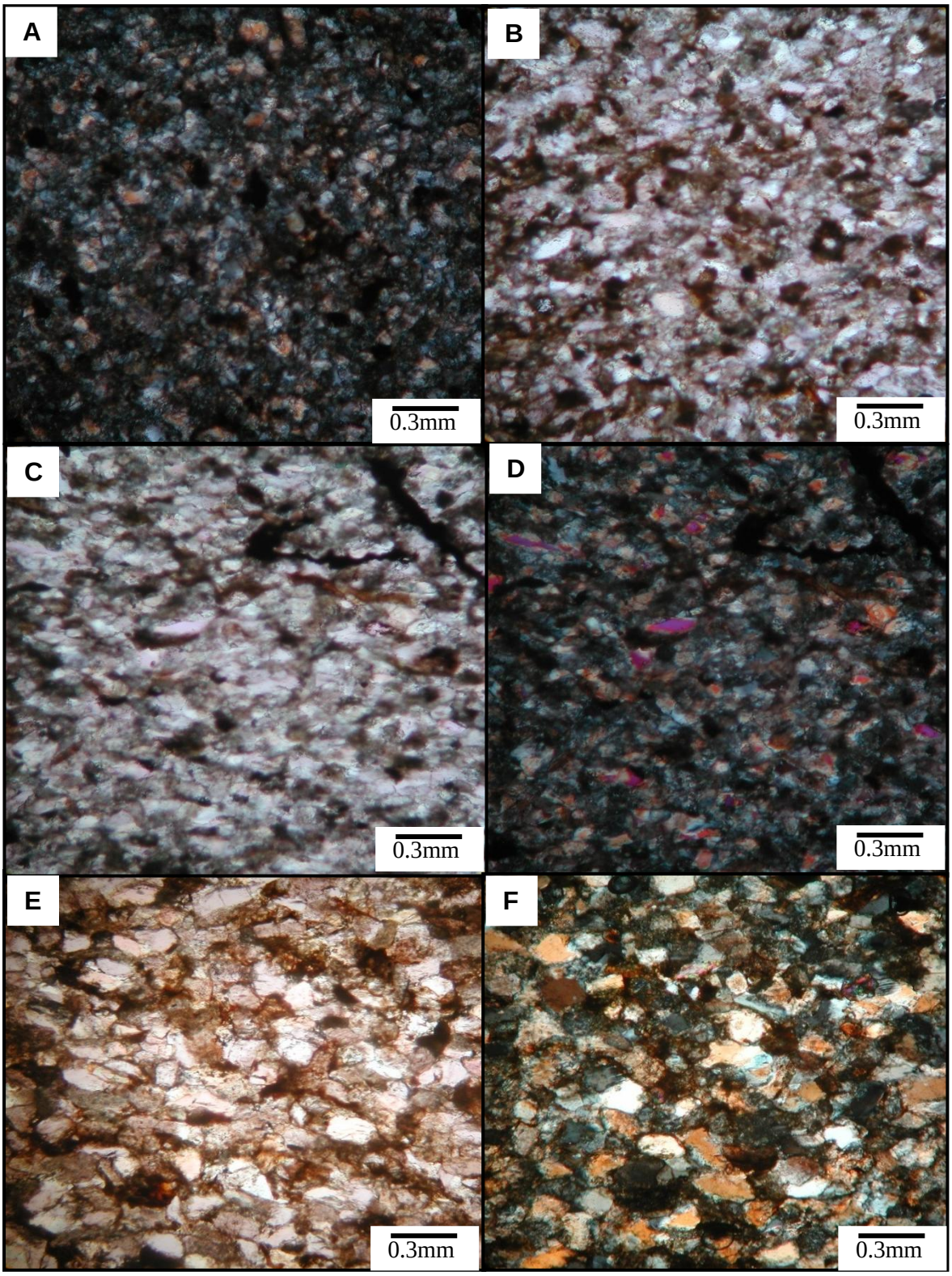

Photomicrograph description: (A) Sample SWA16: Lithofeldspathic sandstone under XN; (B) Sample SWA16: Lithofeldspathic sandstone under plane under PL; (C) Sample SWA15.2: Lithofeldspathic wacke under PL; (D) Sample SWA15.2: Lithofeldspathic wacke under XN; (E) Sample SWA20: Subfeldspathic sandstone under PL; (F) Sample SWA20: Subfeldspathic sandstone under XN.

PL: Plane-polarised light; XN: Crossed nicols

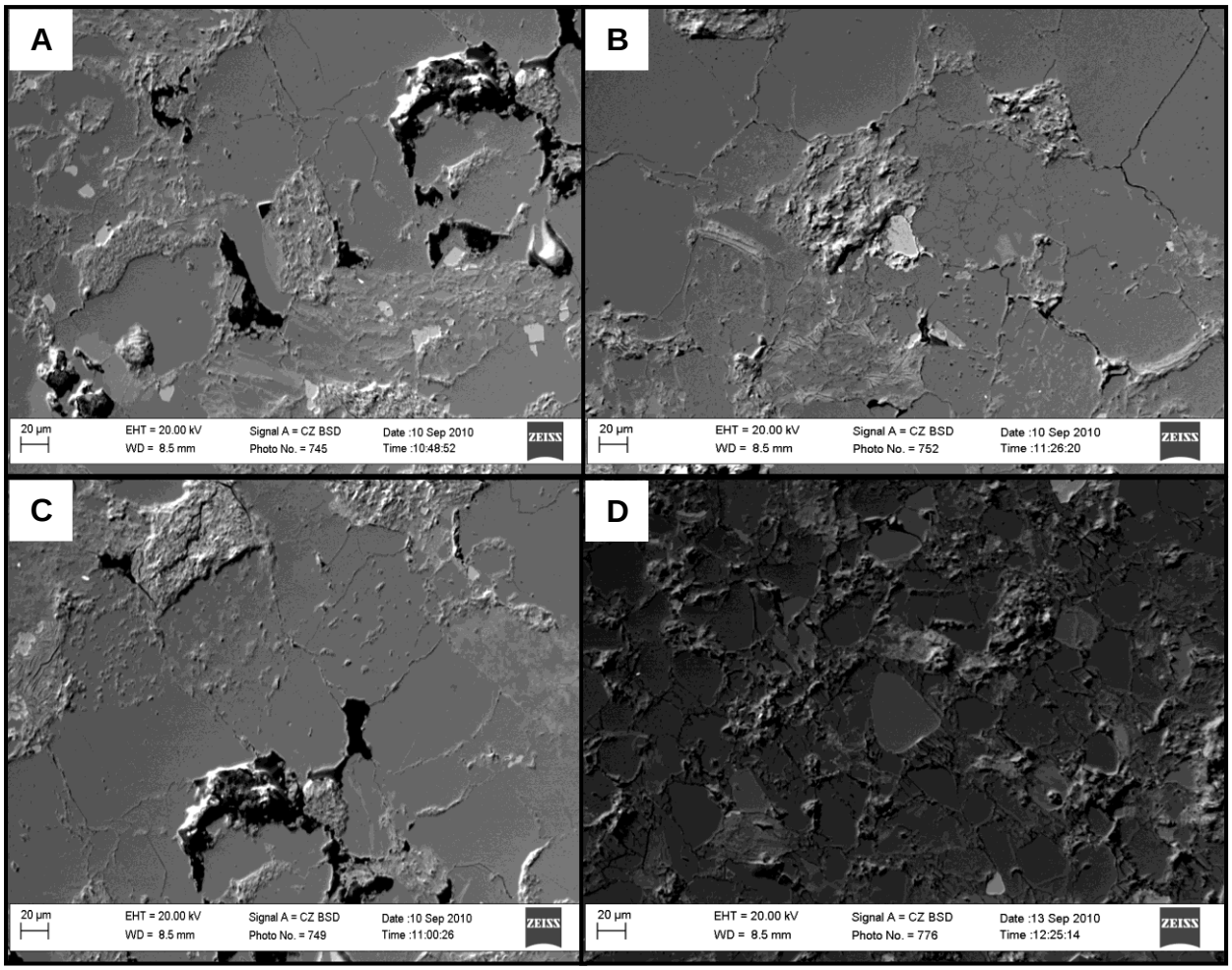

SEM carbon-coated samples: (A) Sample SGSR3: Lithofeldspathic sandstone; (B) Sample SGSR5: Feldspathic sandstone; (C) Sample SWA22: Lithofeldspathic sandstone; (D) Sample SWA6: Lithofeldspathic sandstone.

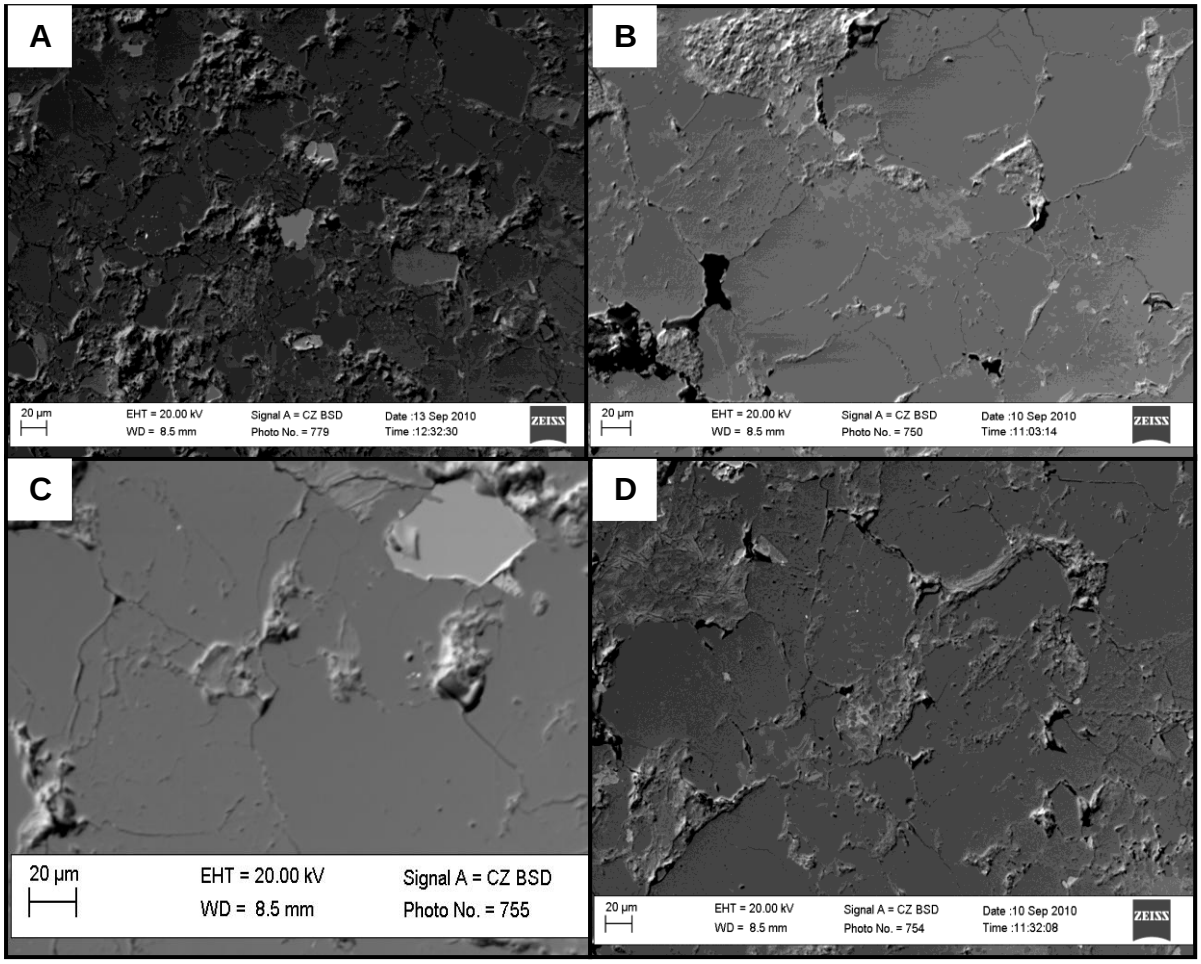

SEM carbon-coated samples: (A) Sample 15.2: Lithofeldspathic wacke; (B) Sample SWA16: Lithofeldspathic sandstone; (C) Sample SWA14: Subfeldspathic sandstone; (D) Sample SWA20: Subfeldspathic sandstone.